5-2014

Cost-Benefit Analyses for Load Resistance Factor Design (LRFD) of Drilled Shafts in Arkansas

Sarah Michelle Bey
University of Arkansas, Fayetteville

Cost-Benefit Analyses for Load Resistance Factor Design (LRFD) of Drilled Shafts in Arkansas

Cost-Benefit Analyses for Load Resistance Factor Design (LRFD) of Drilled Shafts in Arkansas

A thesis submitted in partial fulfillment
of the requirements for the degree of
Master of Science in Civil Engineering

By

Sarah M. Bey
Missouri University of Science and Technology
Bachelor of Science in Civil Engineering, 2012

May 2014
University of Arkansas

This thesis is approved for recommendation to the Graduate Council.

Dr. Richard A. Coffman
Thesis Director

Dr. Norman D. Dennis
Committee Member

Dr. Micah W. Hale
Committee Member

Abstract

To achieve more cost efficient transportation infrastructure within the state of Arkansas, a series of cost-benefit analyses were performed. The analyses, specifically developed for load resistance factor design (LRFD) designed drilled shaft foundations, were designed to compare the fiscal impacts of the drilling and sampling, in-field and laboratory testing, full-scale load testing, and concrete mixing techniques utilized by the University of Arkansas (UofA), the Arkansas Highway and Transportation Department (AHTD), and the Missouri Department of Transportation (MODOT). The methodologies were compared at three test site locations within the state of Arkansas: Siloam Springs, AR, Turrell, AR, and Monticello, AR. These sites were selected to represent the predominant geological deposits within the state. Three drilled shaft foundations (two four-foot diameter drilled shafts and one six-foot diameter drilled shaft) were each constructed at the Siloam Springs Arkansas Test Site (SSATS) and the Turrell Arkansas Test Site (TATS). A drilled shaft database was developed containing soil properties, and predicted and measured results of the full-scale load tests performed upon each drilled shaft. Cost-benefit analyses for each methodology were compared by means of predicted and measured static axial capacity. Values of predicted axial capacity were generated for each methodology using the Bridge Software Institute FB-Deep, Ensoft SHAFTv2012, and Microsoft Excel® spreadsheet programs. Based on the results of the full-scale load testing, the FB-Deep program utilizing the data from the UofA sampling and testing method was selected as the best methodology for predicting the axial capacity values for drilled shaft foundations in the state of Arkansas. Results of the cost-benefit analyses indicated a potential savings of $262,800 (32 percent) for drilled shaft foundations in rock. A potential savings of $323,800 for performing full-scale drilled shaft load tests in rock were attained. Unit cost per ton of resistance values of

$24.11 and $82.70, and $75.47 and $141.57 were determined for the UofA and AHTD sampling and testing methods at the SSATS and TATS, respectively. Drilled shaft foundations tested in liquefiable soil were concluded to cost $137,500 (8.7%) more than driven pile foundations, but provided the benefit of additional lateral resistance.

Acknowledgements

This research project would not have been possible without the help and support of many. First, I would like to thank Dr. Richard Coffman for his mentoring and guidance throughout this comprehensive learning process, as well as providing the opportunity to assist with this research project. I would like to thank the additional members of my committee, Dr. Norman Dennis and Dr. Micah Hale, for their support and guidance throughout my educational career at the University of Arkansas as a graduate student. I would like to thank Morgan Race for her inexhaustible assistance, as well as her help in collecting and analyzing the data associated with this project. I would also like to thank all the organizations who made this project a success. These organizations include but are not limited to: the Arkansas Highway Transportation Department, Loadtest Inc., the International Association of Foundation Drilling, the Missouri Department of Transportation, McKinney Drilling Company, Aldridge Construction Company, and Hayes Drilling Company. Lastly, special thanks to all the students who also assisted with this project or with peer reviewing. These people include but are not limited to Cyrus Garner, Mike Deschenes, Yi Zhao, Elvis Ishimwe, and Sean Salazar.

Table of Contents

List of Figures

Figure 7.7. Values of a) interpreted soil profile and ultimate axial capacity with respect to depth for spreadsheet b) four-foot and c) six-foot diameter shafts for the UofA and AHTD testing and sampling methods.

Figure 7.8. Values of a) interpreted soil profile and ultimate axial capacity as a function of depth for SHAFT a) four-foot and b) six-foot diameter shafts for the UofA and AHTD testing and sampling methods.

Figure 7.9. Values of a) interpreted soil profile and axial capacity using the b) mean, c) mean plus one standard deviation, and d) mean minus one standard deviation data values as a function of depth for four-foot diameter shafts utilizing FB-Deep, SHAFT, and a spreadsheet.

Figure 7.10. Values of a) interpreted soil profile and axial capacity using the b) mean, c) mean plus one standard deviation, and d) mean minus one standard deviation data values as a function of depth for six-foot diameter shafts utilizing FB-Deep, SHAFT, and a spreadsheet.

Figure 7.11. Values of a) interpreted soil profile and ultimate axial capacity as a function of depth for b) four-foot and c) six-foot diameter shafts for the UofA and AHTD testing/sampling methods.

Figure 7.12. Values of a) interpreted soil profile b) mean, c) mean plus one standard deviation, and d) mean minus one standard deviation side friction resistance as a function of depth for a four-foot diameter shaft utilizing a spreadsheet.

Figure 7.13. Differences in side friction resistance with respect to differences in unconfined compressive strength.

Figure 7.14. Values of a) interpreted soil profile and end bearing resistance for b) mean, c) mean plus one standard deviation, and d) mean minus one standard deviation as a function of depth for a four-foot diameter shaft utilizing a spreadsheet.

Figure 7.15. Differences in values of a & b) side friction resistances, and c & d) end bearing resistances with respect to differences in RQD% and uniaxial unconfined compressive strength input values, respectively.

Figure 7.16. The a) interpreted profile and differences in values of b) corrected blow count, c) total unit weight, d) undrained shear strength, and e) correlated friction angle, as a function of depth, as gathered during the UofA, AHTD, and MODOT geotechnical investigations at the Turrell Arkansas Test Site (modified from Race and Coffman, 2013).

Figure 7.17. Comparison of values from a standard split spoon sampler and a California split spoon sampler in adjacent boreholes at the TATS, from Race and Coffman (2013).

Figure 7.18. Differences in axial load with respect to various soil engineering properties inputs for a) four-foot diameter and b) six-foot diameter shafts at the TATS.

List of Tables

Table 8.10. Comparisons between mean predicted and measured axial capacities and subsequent data ranges at the given constructed depth of each test shaft.

Chapter 1: Introduction

1.1. Background

In 2007, load resistance factor design (LRFD) was specified as the mandatory practice by the U.S. Department of Transportation (USDOT) for all infrastructure projects that receive funding through the Federal Highway Administration (FHWA) or other USDOT funding vehicles (Lwin, 2007). LRFD methods, compared to the previously utilized allowable stress design (ASD) methods, incorporate a unified measure of reliability for superstructure and substructure, with the ultimate goal of developing cost efficient designs. Due to the influence of federal funding for construction of transportation infrastructure, the FHWA LRFD requirement has become an obligation for state highway authorities to implement in all new transportation infrastructure construction. Extensive research has been conducted for implementation of the new design methodology for substructure design, as well as developing regional soil specific resistance factors.

In the state of Arkansas, the Arkansas State Highway and Transportation Department (AHTD) primarily employs the use of standard penetration testing (SPT) blow count data to estimate the engineering properties of soils. AHTD also currently utilizes overly conservative, nationalized American Association of State Highway and Transportation Officials (AASTHO) recommended LRFD resistance factors. The use of these resistance factors is the result of current AASHTO LRFD resistance factors being either a) back-calculated from historically employed ASD factors of safety, or b) calculated using reliability theory from outdated methods. As a result, the current design practices employed by the AHTD fail to benefit from the potential advantages of advanced sampling techniques, advanced in-situ testing, advanced laboratory testing, and advanced full-scale load tests. Therefore, the fiscal advantages associated with the

implementation of LRFD are not realized. In order to achieve more cost efficient infrastructure within the state of Arkansas, researchers at the University of Arkansas (UofA) are developing regionally calibrated resistance factors through the means of advanced sampling, advanced in-situ testing, advanced laboratory testing, and advanced full-scale load testing.

1.2. Significance to the Geotechnical Engineering Community

This research project will benefit the geotechnical design community by providing engineers with regionally calibrated resistance factors to use in LRFD drilled shaft design, ultimately yielding a more cost efficient design. Within the scope of the work described in this document, this research project will contribute to the expanding knowledge base concerning advanced full-scale load testing and cost analyses. Specifically relationships obtained through full scale load testing between the predicted and measured skin friction and end bearing resistances of drilled shafts embedded into clay, sand, and competent limestone shall be evaluated. The research will investigate the discrepancies between two available commercial software programs widely used to evaluate drilled shaft axial capacity. As a benefit to the general public, this project will increase the knowledge base contributing to more sustainable and fiscally beneficial infrastructure design.

1.3. Project Overview

The Arkansas State Highway and Transportation Department's (AHTD) current design practices incorporate an overly-conservative amount of uncertainty and bias, potentially increasing the fiscal burden incurred by the state and public. Savings from less overly-conservative designs based on locally calibrated LRFD resistance factors may be obtained through the means of advanced sampling, in-situ testing, laboratory testing, and full-scale load tests.

Geotechnical site investigations were conducted at three locations within the state of Arkansas: Siloam Springs, Turrell, and Monticello. The locations of each project site are presented in Figure 1.1. Siloam Springs, situated within the Northwestern portion of the state geology, consists of a competent limestone overlain by approximately sixteen feet of cherty clay. Turrell, located near the Mississippi River, exhibits floodplain characteristics and is composed of a sand base overlain by ten feet of low plasticity silt, overlain by ten feet of high plasticity clay. Monticello, situated within the Southeastern portion of the state, consists of sand, overlain by approximately twenty feet of stiff clay, overlain by ten feet of sand, overlain by thirty feet of desiccated clay. The site stratigraphy at each of the three sites obtained from subsurface investigation borings and recovered samples is presented in Figure 1.2.

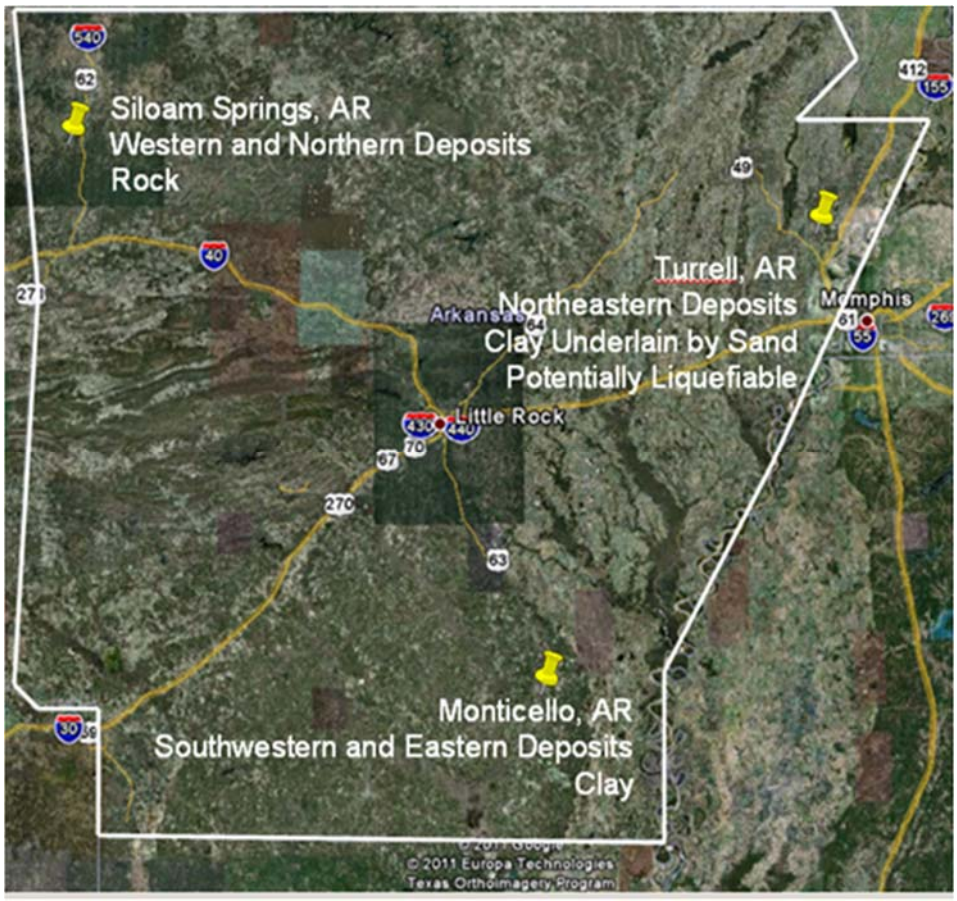

Figure 1.1. Site vicinity map of site investigations (modified from Google Earth, 2012).

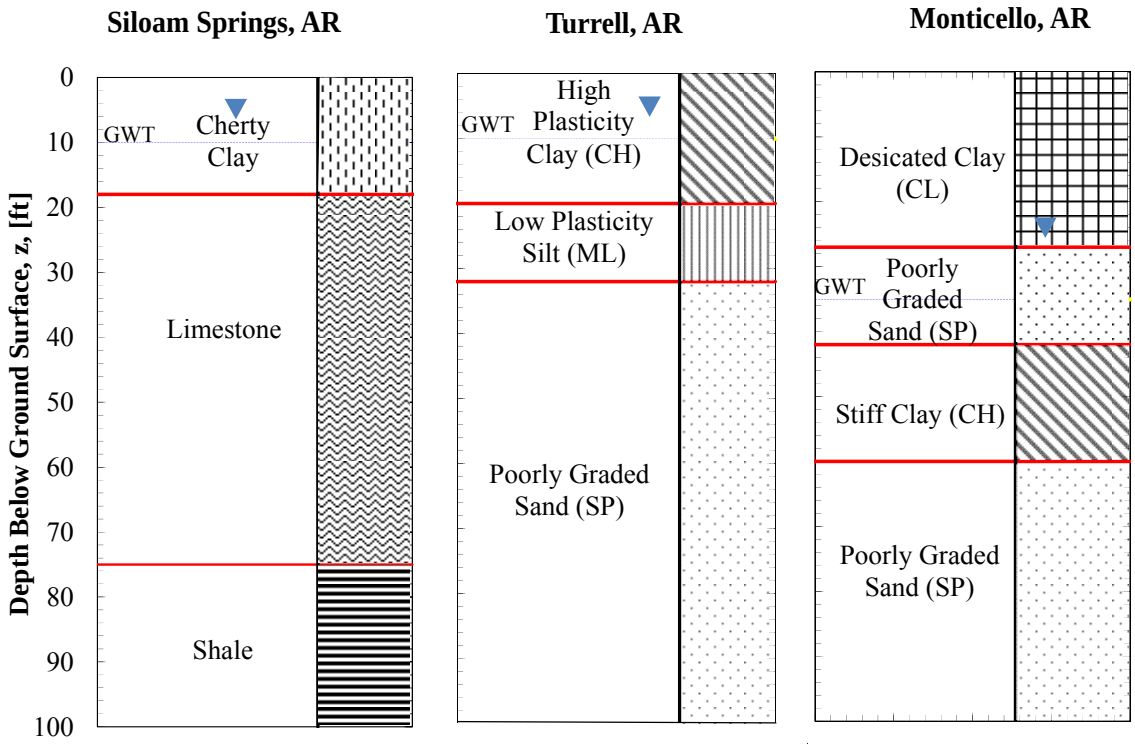

Figure 1.2. Interpreted soil profiles at Siloam Springs, Turrell, and Monticello Arkansas Test Sites.

The geotechnical site investigations performed by the University of Arkansas (UofA) (in conjunction with MODOT) and AHTD consisted of respectively advanced and conventional sampling and testing procedures. UofA samples were obtained every 2.5 feet (using SPT in sands, Osterberg hydraulic fixed-piston sapling in clay, Pitcher barrel sampling in stiff clay or soft rock, and double swivel core barrel in hard rock). AHTD samples were obtained (using a split barrel sampler, Shelby tube sampler, and core-barrel sampler) every 2.5 feet to 20 feet depth, then every five feet till termination of the boring. Each UofA and AHTD boring was terminated at either 100 feet depth or after 15 feet of continuous rock core had been obtained. Samples collected from the AHTD boreholes were placed in cardboard core boxes prior to transport. Samples collected from UofA boreholes were saved in sealed, expandable packers that

were waxed, and maintained prior to transport. CPT tests were conducted at each site on behalf of the UofA by MODOT personnel (with the exception of rock sites) after the UofA and AHTD boreholes were completed.

The University of Arkansas (UofA) conducted conventional laboratory testing on all samples and advanced laboratory testing only on select samples. Conventional laboratory testing included the following: Atterberg limits, moisture content, unit weight, grain size analysis, specific gravity, and calcium carbonate content. Advanced laboratory testing consisted of unconsolidated-undrained triaxial compression. AHTD conventional testing included Atterberg Limits, moisture content, and unit weight.

Engineering properties of the geomaterial encountered during the investigations preformed at each site were compared for the various sampling and testing methods. From these properties, predictions of ultimate axial capacity and load settlement curves utilizing the various sampling and testing methods and prediction programs were performed and compared. Cost predictions for each shaft were also determined. From capacity predictions, length determinations for each of the test drilled shaft foundations were performed. Based on each determination, the test shafts (three for each site consisting of two four-foot diameter shafts and one six-foot diameter shaft) were further designed and constructed. The cost of construction for each shaft was recorded. Full-scale load tests were performed at the Siloam Springs and Turrell Arkansas Test Sites to compare the predicted and measured capacities of each constructed drilled shaft foundation. From the measured capacities and the recorded costs associated with each shaft, a unit cost per ton of capacity for the UofA and AHTD testing and sampling methods were determined. These unit values were then utilized to determine the cost implications of each testing and sampling method at various levels of infrastructure. Further future data analysis shall

enable the determination of regionally-calibrated resistance factors, aiding designers in the State of Arkansas.

1.4. Thesis Overview

This document is divided into nine chapters. Chapter 1 includes an introduction, a brief overview of the project, and an overview of this thesis. Chapter 2 contains a literature review on LRFD practice, axial design capacity methods, drilled shaft capacity predictive technologies, and full-scale Osterberg Cell (O-Cell®) testing. The literature review also encompasses drilled shaft advanced load testing case studies. A detailed site description along with a description of the methods and procedures used to conduct the geotechnical site investigations at each site are discussed in Chapter 3. The predictive methods and procedures used to determine a scope for the advanced full-scale load tests are discussed in Chapter 4. The procedures discussed include developing a determination length and capacity for each shaft, and evaluating the variances in predicted capacities using different sampling techniques, testing techniques, and predictive technologies. Chapter 4 also contains a description of the methods utilized to perform the cost-benefit analyses. The construction processes associated with the Siloam Springs Arkansas Test Site, along with the quantitative and qualitative characteristics of each advanced full-scale load test are discussed in Chapter 5. Likewise, the construction processes associated with the Turrell Arkansas Test Site, along with the quantitative and qualitative characteristics of each advanced full-scale load test are discussed in Chapter 6. The results of the predictive technology evaluation in regard to different sampling and testing techniques are evaluated and discussed in Chapter 7. Results contained in Chapter 8 specifically include an evaluation of O-Cell® output data, a discussion between predicted vs measured ultimate axial capacities, predicted vs measured unit end bearing resistances, and predicted vs measured skin frictions, a discussion on the differences

between predictive technologies, as well as a discussion evaluating the overall effects of advanced sampling, and testing methods. Chapter 8 also contains the results of the cost-benefit analyses. Chapter 9 contains conclusions developed from a culmination of the literature review as well as the collected results. From the conclusions, recommendations for countering the potential fiscal deficits associated with the results of overly-conservative, conventional designs in the state of Arkansas are addressed through suggested sampling methods, testing methods, and predictive technologies. Recommendations for future testing are also included in Chapter 9.

Chapter 2: Literature Review

2.1. Introduction

A broad body of research exists regarding the cost-benefits of LRFD by using Osterberg load cell tests; however no research specifically addresses the potential fiscal benefits associated with this type of testing in the state of Arkansas. This literature review is composed of the following sections, a discussion of the relevance of LRFD and the application of LRFD to drilled shaft design (Sections 2.2. and 2.3., respectively). A summary of the methods of axial capacity estimation is presented in Section 2.4. Detailed discussions on Osterberg load cell testing and Osterberg load cell case studies are presented in Section 2.5. Cross-hole sonic logging is addressed in Section 2.6. The variability and uncertainty introduced from sample size in LRFD are discussed in Section 2.7., while commercially available drilled shaft axial capacity prediction software programs are presented in Section 2.8. The last item discussed in this chapter is concrete admixtures (Section 2.9.).

2.2. Historical Background of Load Resistance Factor Design (LRFD)

Fundamental structural reliability theory was first introduced by Fredenthal (1956) and Pugsley (1955), which advocated probability theory over absolute reliability theory. A process for developing the design criteria to ensure a small probability of failure was discussed in each publication (Phoon, 2004). In Cornell (1969), the concept of a reliability index (β) was introduced, how this reliability index was be used to calculate load and resistance factors was then addressed in Lind (1971). According to Phoon (2004), the reliability method was first implemented in Ravindra and Galambos (1978) for steel structures, and is still utilized in the structural community. As discussed in Section 2.3., the use of the reliability method in geotechnical applications began in 1965, and was implemented following a federal mandate in

2007. The research that led to this mandate and the acquired resistance factors are discussed in sections 2.2.2 and 2.2.3, respectively.

2.3. Historical Background of Load Resistance Factor Design (LRFD) for Geotechnical Applications

One of the first LRFD efforts for geotechnical applications involving foundation design is found in Hansen (1965). Hansen (1965) advocated the separation of ultimate and serviceability limit state checks, as well as partial load factors and soil parameters (Phoon, 2004). As a result, modified partial factors of safety were implemented in the Danish Code of Practice for Foundation Engineering (1985), and the Canadian Foundation Engineering Manual, CFEM, 3rd Ed. (Canadian Geotechnical Scociety, 1992). In the United States, the transition to LRFD calibrated factors from a semi-analytical reliability-based approach (as opposed to ASD fitted calibration) was retarded due to a lack of statistical data and funding until research was performed by Rojiani et al. (1991) and Yoon and O'Neill (1997). According to Phoon (2004), reliability indexes (using an extensive range of procedures including rational, semi-empirical, and in-situ methods) were developed from risk levels. In Paikowsky and Stenersen (2000), differences between the AASHTO (1997) specifications and the NCHRP Report 343 (Barker et al., 1991) were discussed. A target reliability index of 3.5 for bridge superstructures was recommended in AASHTO (1997), yet reliability indices ranging from 2.5 to 3.5 for drilled shafts, and 2.0 to 2.5 for driven piles were recommended in NCHRP Report 343 (Barker et al., 1991). This difference negates one of the chief principals behind LRFD practice – uniting the bridge superstructure and substructure. In response, NCHRP Project 24-17 (Paikowsky, 2002) was initiated to revise the driven pile and drilled shaft portions of Section 10 of the AASHTO (1997) Specifications, and to specify a resistance factor calibration procedure. Currently, in

AASTHO (2012), a design target reliability of 2.3 (with an approximate probability of failure of 0.01) is specified for redundant foundations systems based on recommendations in Zhang et al. (2001), Allen et al. (2005), and Paikowsky (2004).

2.3.1. Load Resistance Factor Design (LRFD) in Drilled Shaft Design

Because protecting the safety of the general public is the the primary objective of all drilled shaft design approaches, the design load (Q_{des}) is specified not to exceed the available capacity (Q_{ult}) for allowable stress design (ASD). As presented in Equation 2.1, the use of a pre-determined global factor of safety (FS) is utilized to prevent failure and ensure the safety of the general public.

$$Q_{des} \leq Q_{all} = \frac{Q_{ult}}{FS} \qquad \text{(Brown et al., 2010)} \qquad \textbf{Equation 2.1}$$

Where: Q_{des} = applied design load,

Q_{all} = allowable load,

Q_{ult} = ultimate load capacity,

FS = global factor of safety (≥1).

The aforementioned global factor of safety is used to assess the potential for adverse performance. Factors such as construction quality, material and load anomalies, or unexpected subsurface conditions are all accounted for in a single variable (Brown et al., 2010). Because the ASD methodology does not identify all possible failure modes, the approach has been replaced with limit state design. Partial factors to modify loads and resistances (the smaller the partial factor applied, the more uncertain the quantity) are utilized in load resistance factor design. LRFD is viewed as an improvement in design methodology because individual factors of safety

can be applied to each quantity rather than lumped together at the end of the design process (Brown et al., 2010). By utilizing LRFD, all limiting components of a structure are individually evaluated, resulting in a more cost-effective design. As presented in Table 2.1, thirteen (13) potential limit states are identified in Article 3.4 of the AASHTO LRFD Bridge Design Specifications (2012) for bridge design evaluation.

Table 2.1. Limit states for bridge design (after AASHTO, 2012).

Limit State	Case	Load Combination Description
Strength	I	Basic Load Combination, normal vehicular use without wind
	II	Owner-specified special design values, without wind
	III	Bridge exposed to wind velocity exceeding 55 mph
	IV	Very high dead load to live load force effect ratios
	V	Normal vehicular use with wind of 55 mph
Service	I	Normal operational use with 55 mph wind and all loads taken at nominal values
	II	Control yeilding of steel structures, slip-critical connections
	III	Longitudinal analysis
	IV	Tension in prestressed concrete columns with crack control
Extreme Event	I	Load combination including earthquake
	II	Ice load, vehicle and vessel collisions, certian hydraulic events
Fatigue	I	Infinite repetative vehicular live loads and dynamic responses
	II	Finite repetative vehicular live loads and dynamic responses

The equations used to calculated LRFD strength limit state of a drilled shaft is presented in Equation 2.2. For each limit state, the sum of factored force effects (including axial loads, shear forces, or moments) may not exceed the sum of factored resistances.

$$\sum \eta_i \gamma_i Q_i \leq \sum \phi_i R_i \qquad \text{(Brown et al., 2012)} \qquad \textbf{Equation 2.2}$$

Where: η_i = load modifier (to accommodate for group effects),

γ_i = load factor (applied to force effect i),

Q_i = nominal value of force effect i,

ϕ_i = resistance factor (applied to resistance component i),

R_i = nominal value of resistance component i.

Examples of commonly utilized load factors from AASHTO (2012) are presented in Tables 2.2 and 2.3. Specifically, each table accounts for the various loading combinations associated with each limit state.

Table 2.2. Load combinations and load factors (after AASHTO, 2012).

Load Combination State	DC DD DW EH EV ES EL PS CR SH	LL IM CE BR PL LS	WA	WS	WL	FR	TU	TG	SE	Use One at a Time				
										EQ	BL	IC	CT	CV
Strength I	γp	1.75	1.00	-	-	1.00	0.50/1.20	γTG	γSE	-	-	-	-	-
Strength II	γp	1.35	1.00	-	-	1.00	0.50/1.20	γTG	γSE	-	-	-	-	-
Strength III	γp	-	1.00	1.4	-	1.00	0.50/1.20	γTG	γSE	-	-	-	-	-
Strength IV	γp	-	1.00	-	-	1.00	0.50/1.20	-	-	-	-	-	-	-
Strength V	γp	1.35	1.00	0.4	1.0	1.00	0.50/1.20	γTG	γSE	-	-	-	-	-
Service I	1.00	1.00	1.00	0.3	1.0	1.00	1.00/1.20	γTG	γSE	-	-	-	-	-
Service II	1.00	1.30	1.00	-	-	1.00	1.00/1.20	-	-	-	-	-	-	-
Service III	1.00	0.80	1.00	-	-	1.00	1.00/1.20	γTG	γSE	-	-	-	-	-
Service IV	1.00	-	1.00	0.7	-	1.00	1.00/1.20	-	1.0	-	-	-	-	-
Extreme Event I	γp	γEQ	1.00	-	-	1.00	-	-	-	1.00	-	-	-	-
Extreme Event II	γp	0.50	1.00	-	-	1.00	-	-	-	-	1.00	1.00	1.00	1.00
Fatigue I (LL, IM, CE only)	-	1.50	-	-	-	-	-	-	-	-	-	-	-	-
Fatigue II (LL, IM, CE only)	-	0.75	-	-	-	-	-	-	-	-	-	-	-	-

Table 2.3. Load factors for permanent loads (after AASHTO, 2012).

Type of Load, Foundation Type, and Method Used to Calculate Downdrag		Load Factor	
		Maximum	Minimum
DC: Component and Attachments		1.25	0.90
DC: Strength IV only		1.50	0.90
DC: Downdrag	Drilled Shafts, O'Neill and Reese (1999) Method	1.25	0.35
DW: Wearing Surfaces and Utilities		1.50	0.65
EH: Horizontal Earth Pressure			
Active		1.50	0.90
At-Rest		1.35	0.90
AEP for Anchored Walls		1.35	N/A
EL: Locked-in Construction Stresses		1.00	1.00
EV: Vertical Earth Pressure			
Overall Stability		1.00	N/A
Retaining Walls and Abutments		1.35	1.00
Rigid Buried Structure		1.30	0.90
Rigid Frames		1.35	0.90
Flexible Buried Structures			
+ Metal Box Culverts and Structural Plate Culverts with Deep Corrugations		1.50	0.9
+ Thermoplastic Culverts		1.3	0.9
+ All Others		1.95	0.9
ES: Earth Surcharge		1.50	0.75

Where: Permanent loads

CR = force effects due to creep,

DD = downdrag force,

DC = dead load of structural components and nonstructural components,

DW = dead load of wearing surfaces and utilities,

EH = horizontal earth pressure load,

EL = miscellaneous locked-in force effects from the construction process,

ES = earth surcharge load,

EV = vertical pressure from dead load of earth fill,

PS = secondary forces from post-tensioning,

SH = force effects due to shrinkage,

Transient loads

BL = blast loading,

BR = vehicular braking force,

CE = vehicular centrifugal force,

CT = vehicular collision force,

CV = vessel collision force,

EQ = earthquake load,

FR = friction load,

IC = ice load,

IM = vehicular dynamic load allowance,

LL = vehicular live load,

LS = live load surcharge,

PL = pedestrian live load,

SE = force effect due to settlement,

TG = force effect due to temperature gradient,

TU = force due to uniform temperature,

WA = water load and stream pressure,

WL = wind on live load,

WS = wind load on structure.

The aforementioned empirically derived methods used to evaluate drilled shaft capacity are determined from the principals of static forces acting on the surfaces of the shaft. The methods involve the summation of resistance from both the side friction and end resistance. As presented in Figure 2.1, the probability of failure, a function of loading conditions (Q) and

resistance conditions (R), increases when load (Q) exceeds resistance (R). Prior to the implementation of LRFD, the methodology in O'Neill and Reese (1999) was used in ASD to calculate axial shaft resistance (undrained shear strength in clay, friction angle in sand, and uniaxial compressive strength in rock and in intermediate geomaterials). The O'Neill and Reese (1999) method is also used to calculate shaft resistance in LRFD framework by utilizing a probability of failure instead of a factor of safety. Resistance conditions are a function of soil type, sampling procedure, laboratory testing, and full-scale load tests, while loading conditions are determined from initial design criteria (Allen et al., 2005). The reliability index (β) represents the number of standard deviations between the mean safety margin and the failure limit, and decreases as the probability of failure increases (Allen et al., 2005).

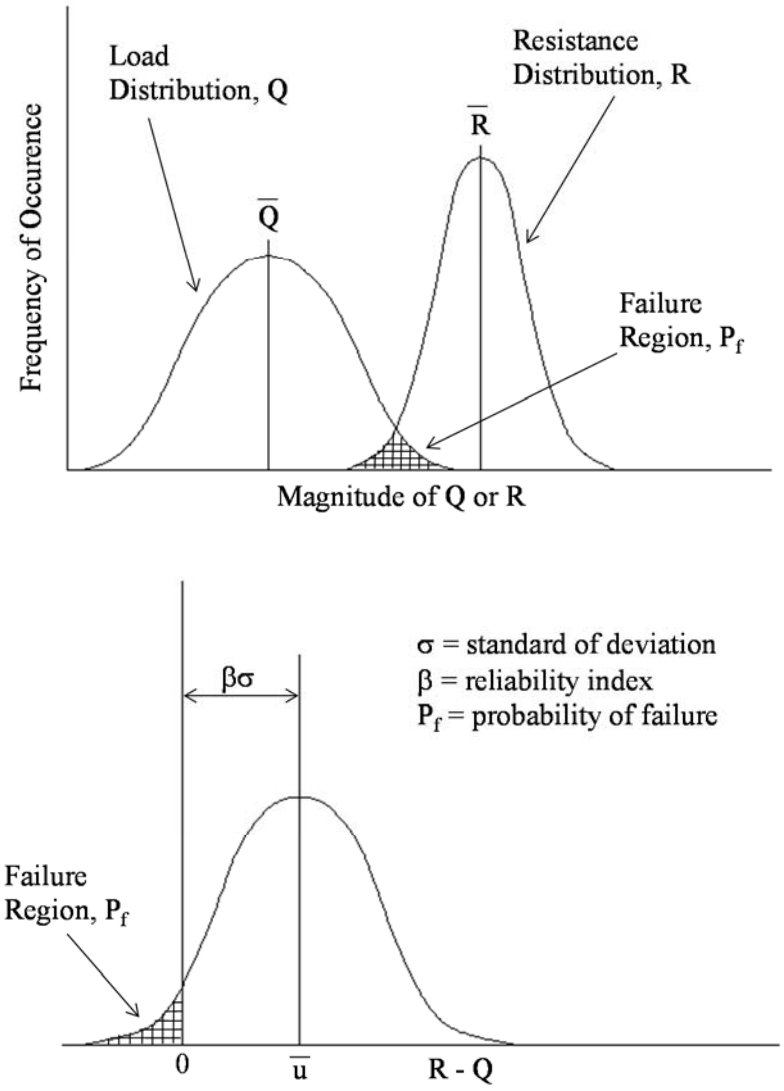

Figure 2.1. Schematic of LRFD load and resistance parameters (after Withiam et al., 1998).

2.3.1.1. Resistance Factors

In practice, a design engineer may not need to conduct reliability analyses on data acquired from field and laboratory testing, to apply LRFD to drilled shaft design. Resistance factors for routine design as published in AASHTO (2012) are presented in Table 2.4. These factors are developed from reliability theory and statistical analyses of full-scale load tests or are fitted from ASD methods (Paikowsky, 2004). Calibration by reliability theory and fitting to ASD is further discussed in Sections 2.3.1.1 and 2.3.1.2, respectively. Although resistance

factors for drilled shaft design are published for routine design (AASHTO, 2012), the limitations of the presented values are based on the calibration characteristics. Each resistance factor value is only valid for a particular range of parameters and should only be utilized if the parameters of the design criteria coincide with the parameters of the original calibration. These parameters include design equations, load factors, geomaterial type, and geomaterial properties (Allen et al., 2005).

Table 2.4. Resistance factors for geotechnical resistance of drilled shafts (after AASHTO, 2012).

Method/Soil/Condition			Resistance Factor
Nominal Axial Compressive Resistance of Single Drilled Shafts, ϕ_{stat}	Side resistance in clay	α-method O'Neill and Reese, (1999)	0.45
	Tip resistance in clay	Total Stress O'Neill and Reese, (1999)	0.40
	Side resistance in sand	β-method O'Neill and Reese, (1999)	0.55
	Tip resistance in sand	O'Neill and Reese, (1999)	0.50
	Side resistance in IGMs	O'Neill and Reese, (1999)	0.60
	Tip resistance in IGMs	O'Neill and Reese, (1999)	0.55
	Side resistance in rock	Horvath and Kenny, (1979) O'Neill and Reese, (1999)	0.55
	Side resistance in rock	Carter and Kulway, (1988)	0.50
	Tip resistance in rock	Canadian Geotechnical Scociety, (1985) Pressuremeter method Canadian Geotechnical Scociety, (1985) O'Neill and Reese, (1999)	0.50
Uplift Resistance of Single Drilled Shafts, ϕ_{up}	Clay	α-method O'Neill and Reese, (1999)	0.35
	Sand	β-method O'Neill and Reese, (1999)	0.45
	Rock	Horvath and Kenny, (1979) Carter and Kulway, (1988)	0.40
Horizontal Geotechnical	All materials		1.0
Static Load Test (compression), ϕ_{load}	All materials		0.70

2.3.1.2. Calibration to Fit Method

The "calibration to fit method" is usually performed after a design philosophy change (e.g., ASD to LRFD) and results from a lack of statistical data. Using the calibration to fit method (Equation 2.3), resistance factors used in LRFD specifications are adjusted to produce designs similar to the ASD specifications. Because the calibration is developed by fitting to ASD method, and because the ASD method uses the historic factor of safety, the uncertainty (or actual margin of safety) of the load and resistance is NOT considered (Allen et al., 2005). A means to back-calculate a necessary resistance factor magnitude from a pre-determined factor of safety is provided in the design method.

$$\phi_R = \frac{\frac{\gamma_{DL}\, DL}{LL} + \gamma_{LL}}{FS\left(\frac{DL}{LL} + 1\right)} \qquad \text{(Allen et al., 2005)} \qquad \textbf{Equation 2.3}$$

Where: γ_{DL} = dead load factor,

γ_{LL} = live load factor,

DL = dead load,

LL = live load,

FS = global factor of safety.

2.3.1.3. Calibration Using Reliability Theory

Calibration by means of the use of reliability theory involves the development of load and resistance factors from a targeted probability of failure, where the force effect (Q) and available resistance (R) are treated as random variables. The general steps for calibration of resistance factors, using reliability theory, as described in Allen et al. (2005) are presented below.

- Determine the statistical parameters (e.g. mean, standard of deviation, and coefficient of variation [COV]) that characterize the force effects and resistances.

- Estimate the reliability inherent in the currently available design procedures.
- Given the currently implied margin of safety, and noting the reliability levels applied throughout literature and the AASHTO (2012) specification, select a target level of reliability.
- Calculate resistance factors using load factors specified by AASHTO (2012) for the given evaluated limit state.

Resistance factors may be calculated using normal load and resistance distributions using Equation 2.4. Resistance factors may be calculated using lognormal load and resistance distributions using Equation 2.5.

$$\beta = \frac{\mu_R - \mu_Q}{\sqrt{\sigma_R^2 + \sigma_Q^2}}$$ (Allen et al., 2005) **Equation 2.4**

Where: β = the reliability index,

μ_R = mean value of the resistance,

μ_Q = mean value of the load,

σ_R = standard of deviation value of the resistance, and

σ_Q = standard of deviation value of the load.

$$\beta = \frac{\ln\left[\frac{\lambda_R FS\left(\frac{Q_D}{Q_L}+1\right)}{\lambda_D \frac{Q_D}{Q_L}+\lambda_{LL}} \sqrt{\frac{1+COV_R^2+COV_{QD}^2+COV_{QL}^2}{1+COV_R^2}}\right]}{\sqrt{\ln\left[\left(1+COV_R^2\right)\left(1+COV_{QD}^2+COV_{QL}^2\right)\right]}}$$ (Whithiam et al., 1998) (Nowak, 1999) **Equation 2.5**

Where: β = the reliability index,

Q_D = nominal value of the dead load,

Q_L = nominal value of the live load,

λ_R = mean value of the bias values (measured / predicted) for resistance,

λ_D = mean value of the bias values (measured / predicted) for the dead load,

λ_{LL}= mean value of the bias values (measured / predicted) for the live load,

FS = the factor of safety used in ASD,

COV_{QD} = the coefficient of variation value of the bias values for the dead load,

COV_{QL} = the coefficient of variation value of the bias values for the live load, and

COV_R = the coefficient of variation value of the bias values for the resistance.

2.3.1.3.1. Reliability Calibration by Barker et al. (1991)

For the calibration of resistance factors for drilled shafts as reported in Barker et al. (1991), statistical data was obtained from 76 load tests as reported in Reese and O'Neill (1988) and Horvath and Kenney (1979). For Barker et al. (1991), normal distributions of dead and live loads, lognormal distributions of resistances, a dead to live load ratio of 3.0, and the load statistics presented in Table 2.5 were utilized. Based on results, the factor of safety from previously utilized ASD had a significant influence on final resistance factor selection (Allen, 2005). Despite the AASHTO specified structural bridge reliability index of 3.5, the β value calculated from previous ASD factors of safety were found to be typically less in Barker et al. (1991), especially with redundant foundations. A recommended β value ranging from 2.5 to 3.0 for drilled shafts was specified in Barker et al. (1991).

Table 2.5. Load statistics and factors utilized (after Barker et al., 1991).

Load Type	Mean of Bias	Coefficent of Variation	Load Factor Used
Dead Load	$\lambda_D = 1.05$	$COV_{QD} = 0.09$	$\gamma_{DL}=1.3$
Live Load	$\lambda_L = 1.05 - 1.22$	$COV_{QL} = 0.11$	$\gamma_{LL}= 2.17$

2.3.1.3.2. Reliability Paikowsky et al. (2004)

Calibrations in Paikowsky et al. (2004) were performed on 338 pile load tests and 256 drilled shaft load tests that focused on the strength limit state. Unlike Barker et al. (1991), the database was gathered under the assumption that the full-scale field installations addressed sources of uncertainty including spatial variability, design model error, and systematic error. For the analysis conducted, load statistics from Nowak (1999) and load factors from AASHTO (2007) were utilized (Table 2.6). In Paikowsky et al. (2004), lognormal distributions of dead and live loads, a dead load to live load ratio of 2.0, and predominately lognormal distributions of resistances were assumed. Results obtained from the use of the reliability theory developed by Hasofer and Lind (1974), and none from previous ASD factors of safety, were used to determine resistance factors (unlike Barker et al., 1991). In Paikowsky et al. (2004), it was concluded that a target reliability index of 3.0 should be used for shaft and pile groups less than 5. For shaft and pile groups greater than 5, a target reliability index of 2.3 should be used. A summary of calibration results from Barker et al. (1991) and Paikowsky et al. (2004) are presented in Table 2.7.

Table 2.6. Load statistics and factors utilized (after Paikowsky et al., 2004).

Load Type	Mean of Bias	Coefficent of Variation	Load Factor Used
Dead Load	$\lambda_D = 1.05$	$COV_{QD} = 0.1$	$\gamma_{DL}=1.25$
Live Load	$\lambda_L = 1.15$	$COV_{QL} = 0.2$	$\gamma_{LL}= 1.75$

Table 2.7. Summary of Barker et al. (1991) and Paikowsky et al. (2004), after Allen et al. (2005).

Strength Limit State	Condition and Location	Design Method	ASD FS Used	ϕ from Calibration by Fitting to ASD (Barker et al., 1991)	ϕ from Reliability Theory (Barker et al., 1991)	ϕ Recommended (Barker et al., 1991)	ASD FS Practice	ϕ from Calibration by Fitting to ASD	ϕ from Reliability Theory Updated (Barker et al., 1991)	ϕ from Reliability Theory Recommended (Paikowsky et al., 2004)	New Recommended ϕ
Bearing	Side Resistance in Clay	α-method (Reese and O'Neill,	2.5	0.61	0.72	0.65	2.5	0.55	0.6	0.30	0.45
Bearing	Base Resistance in Clay	Total Stress (Reese and O'Neill,	2.75	0.55		0.55	2.75	0.50		0.30	0.40
Bearing	Side Resistance in Sand	β-method (Reese and O'Neill,	2.5	0.61	-	-	2.5	0.55	-	0.40	0.55
Bearing	Base Resistance in Sand	Reese and O'Neill, (1988)	2.75	0.55		-	2.75	0.5		0.40	0.50
Bearing	Side and Base Resistance in Mixed	Reese and O'Neill, (1988)	-	-	-	-	2.5	0.55	-	0.5 - 0.7	0.55 for Side, 0.50 for Base
Bearing	IGM's	O'Neill and Reese, (1999)	-	-	-	-	2.5	0.55	-	0.57 - 0.65	0.60 for Side, 0.55 for Base
Bearing	Side Resistance in Rock	Carter and Kulhawy (1988)	2.5	0.61	0.43	0.55	2.5	0.55	0.4	0.45 - 0.49	0.50
Bearing	Side Resistance in Rock	Horvath and Kenney (1979)	2.5	0.61	0.73	0.65	2.5	0.55	0.55	-	0.55

2.4. *Existing Methods of Axial Capacity Estimation*

Empirically determined methods (methods derived from the results of full-scale load testing) for predicting axial drilled shaft resistance using AASHTO (2007, 2012) design procedures are presented in this section. The ultimate axial capacity for the LRFD strength limit state may be evaluated as the sum of two major resistance components: side friction resistance (f_s) and end bearing resistance (q_b), as presented in Equations 2.6 through 2.8.

$$\sum \phi_i R_i = \sum_{i=1}^{n} \phi_{S,i} R_{SN,i} + \phi_B R_{BN} \quad \text{(Brown et al., 2010)} \quad \textbf{Equation 2.6}$$

$$R_{SN} = \pi B \, \Delta z_i \, f_s \quad \text{(Brown et al., 2010)} \quad \textbf{Equation 2.7}$$

$$R_{BN} = \frac{\pi B^2}{4} q_b \quad \text{(Brown et al., 2010)} \quad \textbf{Equation 2.8}$$

Where: $\phi_{s,i}$ = resistance factor for side resistance in layer *i*,

$R_{SN,i}$ = nominal side resistance for layer *i*,

n = number of geomaterial layers providing side resistance,

R_{BN} = nominal end bearing resistance,

ϕ_b = resistance factor for base resistance,

B = shaft diameter,

Δ_{zi} = thickness of geomaterial layer *i*,

f_s = nominal unit side resistance, and

q_b = nominal unit base resistance.

Nominal side resistance ($R_{SN,i}$) is a function of the surface area of the drilled shaft in contact with a given geomaterial layer. Nominal base resistance ($R_{BN,i}$) is a function of the cross-sectional area of the base of a shaft. Methods for determining unit side and base resistance are presented

in Sections 2.4.1. through 2.4.6. for cohesive, non-cohesive, and rock geomaterial layers, respectively. Axial capacity prediction methods are based largely on the research described in Reese and O'Neill (1988) and O'Neill and Reese (1999). The O'Neill and Reese (1999) method produces shaft resistances within 10 to 20 percent of the original Reese and O'Neil (1988) method, however the O'Neill and Reese (1999) method more clearly separates the strength and service limit states by excluding base diameter settlement correction factors for strength limit state design (Allen et al., 2005). The primary differences between the Reese and O'Neill (1988) and the O'Neill and Reese (1999) methods are outlined in Allen et al. (2005) and are presented in Table 2.8.

Table 2.8. Differences between Reese and O'Neill (1988) and O'Neill and Reese (1999), from Allen et al. (2005).

Resistance Condition	Difference
Side Friction in Clay	At shear strengths (c_u) greater than 3 ksf (150 kPa), the O'Neill and Reese (1999) method is approximatley 10% more conservative than Reese and O'Neill (1988) method.
End Bearing in Clay	O'Neill and Reese (1999) method excludes base diameter correction factor, the O'Neill and Reese (1999) method is less conservative than the Reese and O'Neill (1988) method.
Side Friction in Sand	In loose to medium dense sands (N60 ≤ 15 blows/ft), the O'Neill and Reese (1999) method is more conservative by a ratio of N60/15 than the Reese and O'Neill (1988) method.
End Bearing in Sand	If N60 ≤ 50 blows/ft, the O'Neill and Reese (1999) method is 5% more conservative. The O'Neill and Reese (1999) method excludes base diameter correction factor, the O'Neill and Reese (1999) method is less conservative than the Reese and O'Neill (1988) method.
Rock	The O'Neill and Reese (1999) method and the Reese and O'Neill (1988) method are significantly different (not comparable).

2.4.1. Side Friction Resistance in Cohesive Soils

The O'Neill and Reese (1999) method for predicting the unit side shear resistance of drilled shafts is one of the most widely utilized methods for computing deep foundation capacity for cohesive soils. To determine the unit side shear resistance (f_s) in cohesive soils, the undrained shear strength of the soil (c_u) is multiplied by alpha (α) to account for the variability in side resistance, as presented in Equation 2.9 (Reese and O'Neill, 1988). Alpha is a dimensionless correlation coefficient, and is limited to a value of 1.0 (Equations 2.10 and 2.11). From O'Neill and Reese (1999), an average alpha value of 0.55 is recommended, except along the top five feet (1.5 m) of the shaft and the bottom one diameter of the shaft ($\alpha = 0$). The reduction factor is used to account for uncertainties in the strength of the cohesive material due to differing construction techniques and/or inadequate soil/concrete bonds.

$$f_s = \alpha\, c_u \qquad \text{(O'Neill and Reese, 1999)} \qquad \textbf{Equation 2.9}$$

$$if\ \frac{c_u}{P_a} < 1.5\,, \alpha = 0.55 \qquad \text{(O'Neill and Reese, 1999)} \qquad \textbf{Equation 2.10}$$

$$if\ \frac{c_u}{P_a} \geq 1.5\,, \alpha = 0.55 - 0.1\left(\frac{c_u}{P_a - 1.5}\right) \qquad \text{(O'Neill and Reese, 1999)} \qquad \textbf{Equation 2.11}$$

Where: f_s = unit skin friction (ksf),

α = empirical cohesion factor,

c_u = undrained shear strength (ksf), and

P_a = atmospheric pressure (2.12 ksf).

2.4.2. End Bearing Resistance in Cohesive Soils

The O'Neill and Reese (1999) method for calculating load transfer from tip resistance in cohesive soils is subject to less uncertainty than load transfer due to skin friction (O'Neill and

Reese, 1999). Unit end bearing resistance (q_b) for drilled shafts in clay is a function of the average undrained shear strength of the clay (c_u) over a depth of two diameters below the base and the bearing resistance factor (N^*_c) as presented in Equations 2.12 through 2.14. Values of N^*_c are presented in Table 2.9, and should be linearly interpolated for values between those tabulated. If the undrained shear strength of the soil is less than one ton per square foot (tsf) and the depth of the base is greater than three times the diameter of the shaft, the rigidity index (I_r) is included as a function of the maximum end bearing resistance. The rigidity index is directly related to soil stiffness and inversely related to shear strength (O'Neill and Reese, 1999).

$$if\ c_u > 1\ tsf\ (96\ kPa), and\ D_b \geq 3B,$$

$$q_{bmax} = 9\ c_u$$

(O'Neill and Reese, 1999) **Equation 2.12**

$$if\ c_u < 1\ tsf\ (96\ kPa), and\ D_b \geq 3B,$$

$$q_{bmax} = \frac{4}{3}\ [\ln(I_r + 1)]\ c_u$$

(O'Neill and Reese, 1999) **Equation 2.13**

$$if\ D_b < 3B,$$

$$q_{bmax} = \frac{2}{3}\left[1 + \frac{1}{6}\left(\frac{D_b}{B}\right)\right] N_c^*\ c_u$$

(O'Neill and Reese, 1999) **Equation 2.14**

Where: c_u = undrained shear strength,

D_b = depth of shaft base,

B = diameter of shaft base,

q_{bmax} = maximum unit end bearing resistance,

I_r = "rigidity" index, and

N^*_c =bearing capacity factor ≤ 9.0.

Table 2.9. Values of $I_r = E_s / 3c_u$ and N^*_c, (after O'Neill and Reese, 1999).

c_u	$E_s / 3\ c_u$	N^*_c
500 lb/ft^2 (24 kPa)	50	6.5
1000 lb/ft^2 (48 kPa)	150	8.0
2000 lb/ft^2 (≥ 96 kPa)	250-300	9.0

2.4.3. Side Friction Resistance in Non-Cohesive Soils

The beta method presented in O'Neill and Reese (1999) is utilized for calculating unit side resistance in non-cohesive soils. Unit side resistance (f_{smax}) is a function of the effective normal stress and the interface friction angle of the shaft and borehole, as presented in Equations 2.15 through 2.17. Beta (β), a dimensionless correlation factor between the vertical effective stress (σ'_v) and unit side friction resistance (f_{smax}) for a given layer of soil, is back-calculated from full-scale static load tests. This correlation factor is not be confused with the previously discussed coefficient of variation (β). The value of the correlation factor decreases solely as a function of depth and is bounded between the depths of 5 and 86 feet. According to O'Neill and Reese (1999), after 86 feet, friction angle values approach a common magnitude from the high shearing strains induced by drilling at the wall of the borehole.

$$f_{smax} = \beta\ \sigma'_v \leq 4.0 \frac{kip}{ft^2}\ for\ 0.25 \leq \beta \leq 1.2 \quad \text{(O'Neill and Reese, 1999)} \quad \textbf{Equation 2.15}$$

$$if\ N_{60} \geq 15, \beta = 1.5 - 0.135\sqrt{z}\ (ft) \quad \text{(O'Neill and Reese, 1999)} \quad \textbf{Equation 2.16}$$

$$if\ N_{60} < 15, \beta = \frac{N_{60}}{15}\left(1.5 - 0.135\sqrt{z}\ (ft)\right)$$ (O'Neill and Reese, 1999) **Equation 2.17**

Where: β = load transfer coefficient,

f_{smax} = maximum unit skin friction resistance,

σ'_v = vertical effective stress (ksf),

z = depth below ground surface (ft), and

N_{60} = average corrected blow count (corrected for hammer efficiency only).

2.4.4. End Bearing Resistance in Non-Cohesive Soils

The calculation of unit end bearing resistance (q_{bmax}) is a function of uncorrected blow count values (N). When an excavation is drilled into sand, there is a tendency for the sand at the bottom of the excavation to loosen upon drilling. As settlement occurs, the previously loosened sand beneath the tip of the drilled shaft densifies (Reese and O'Neill, 1988). Because of this phenomenon, a limiting values for end bearing was established (Equation 2.18) in Reese and O'Neill (1988). If the base of the shaft exceeds 50 inches in diameter, a modified value of unit end bearing resistance (q_{br}) may be utilized, as presented in Equation 2.19.

$$if\ 0 \le N \le 50, q_{bmax} = 0.6\ N \le 30\ tsf$$ (O'Neill and Reese, 1999) **Equation 2.18**

$$if\ B \ge 50\ in\ , q_{br} = \frac{50}{B} q_{bmax}$$ (O'Neill and Reese, 1988) **Equation 2.19**

Where: q_{bmax} = maximum unit end bearing resistance,

N = uncorrected blowcount,

q_{br} = reduced unit end bearing resistance,

z = depth below ground surface (ft), and

N_{60} = average corrected blow count (corrected for hammer efficiency only).

2.4.5. Side Friction Resistance in Rock

Until a total shaft movement of 0.4 inches occurs, it is recommended that the axial compressive load is solely supported by shaft side friction resistance (AASTHO, 2012). In AASHTO (2012), two methods for calculating side friction resistance in rock are presented, the O'Neill and Reese and (1999) method and the Horvath and Kenney (1979) method. According to the O'Neill and Reese (1999) method, unit side friction resistance is a function of the unconfined rock compressive strength (q_u), the atmospheric pressure (P_a), and the concrete compressive strength (f'_c). Depending on the condition of the rock socket, smooth or rough, equations may be utilized to analyze unit side resistance (Equations 2.20 and 2.21, respectively). For rock that is stronger than concrete, unit side friction may be governed by the strength of the concrete rather than the strength of the rock mass.

For smooth socket:

$$f_{smax} = 0.65\, P_a \left[\frac{q_u}{P_a}\right]^{0.5} \leq 0.65 P_a \left[\frac{f_c'}{P_a}\right]^{0.5}$$ (O'Neill and Reese, 1999) **Equation 2.20**

For rough socket:

$$f_{smax} = 0.8 \left[\frac{\Delta r}{r}\left(\frac{L'}{L}\right)\right]^{0.45} q_u$$ (O'Neill and Reese, 1999) **Equation 2.21**

Where: f_{smax} = maximum unit skin friction resistance,

P_a = atmospheric pressure (2.12 ksf),

q_u= unconfined uniaxial compressive strength of rock $\leq 0.75\ f'_c$,

f'_c = 28-day compressive strength of concrete, and

r, Δr, L, L'= geometric terms associated with rock socket (Figure 2.2).

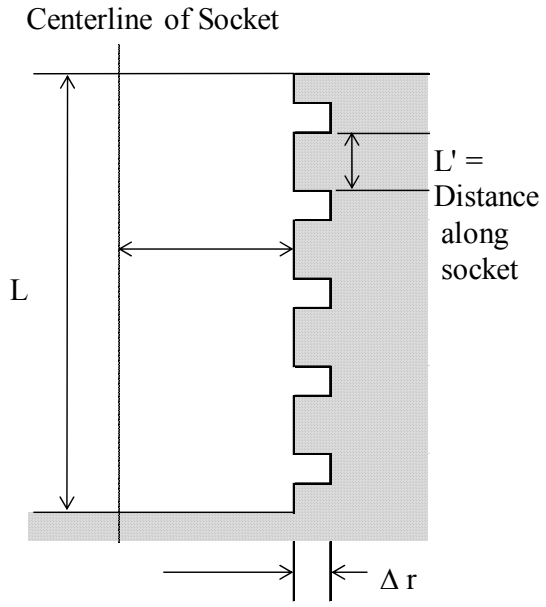

Figure 2.2 Geometric terms associated with Equation 2.21 (after O'Neill and Reese, 1999).

In Horvath and Kenney (1979), rock joint spacing must also be considered as a function of unit side friction. To account for rock joint spacing, the reduction factor (α_e) is utilized (Equation 2.22) as presented in AASHTO (2012). Values of α_e are presented in Table 2.11. This reduction factor (α_e), estimated from O'Neill and Reese (1999), is determined from the ratio of the rock mass modulus (E_m) to intact rock modulus (E_i) as correlated from RQD values (Table 2.12).

$$f_{smax} = 0.65\alpha_e\, P_a \left[\frac{q_u}{P_a}\right]^{0.5} \leq 7.8\, P_a \left[\frac{f'_c}{P_a}\right]^{0.5} \qquad \text{(AASHTO, 2012)} \qquad \textbf{Equation 2.22}$$

Where: f_{smax} = maximum unit skin friction resistance,

P_a = atmospheric pressure (2.12 ksf),

q_u = unconfined uniaxial compressive strength of rock $\leq 0.75\, f'_c$,

f'_c = 28-day compressive strength of concrete, and

α_e = rock joint reduction factor (Table 2.8).

Table 2.10. Estimated values of α_e (after O'Neill and Reese, 1999).

E_m/E_i	α_e
1.0	1.0
0.5	0.8
0.3	0.7
0.1	0.55
0.05	0.45

Table 2.11. Estimated values of E_m / E_i based on RQD, (after O'Neill and Reese, 1999).

RQD (Percent)	E_m/E_i	
	Closed Joints	Open Joints
100.0	1.00	0.60
70.0	0.70	0.10
50.0	0.15	0.10
20.0	0.05	0.02

The Carter and Kulhawy (1988) method for predicting unit side friction resistance in rock, a method that is similar to the O'Neill and Reese (1999) method, is presented in Equation 2.23. Although designers prefer the direct relation of unconfined compressive strength to unit side shear resistance, the simplified relationship may be misleading (Carter and Kulhawy, 1988). It is difficult to correlate a simple rock property to the overall mechanical behavior of a shaft/rock system. Consequently, the equation is applicable to uniform, sound rock constructed for smooth

wall sockets. Additional methods to evaluate unit skin friction resistance in rock are presented in Table 2.10.

$$f_{smax} = 0.63\, P_a \left[\frac{q_u}{P_a}\right]^{0.5} \qquad \text{(Carter and Kulhawy, 1988)} \qquad \textbf{Equation 2.23}$$

Where: f_{smax} = maximum unit skin friction resistance,

P_a = atmospheric pressure, and

q_u = unconfined uniaxial compressive strength of rock.

Table 2.12. Additional methods for evaluating skin friction resistance.

Soil Type	Condition	Method	Equation
Rock	Skin Friction	Gupton and Logan (1984)	$f_s = 0.20\ (q_u)$
		Reynolds and Kaderabek (1980)	$f_s = 0.30\ (q_u)$
		Rowe and Armitage (1987) - smooth	f_s [Mpa] $= 0.45\ (q_u)^{0.5}$
		Rowe and Armitage (1987) - rough	f_s [Mpa] $= 0.6\ (q_u)^{0.5}$

2.4.6 End Bearing Resistance in Rock

Three methods for calculating unit end bearing resistance in rock are included in AASHTO (2012). These methods include the O'Neill and Reese (1999) method, the Canadian Geotechnical Society (1985) method, and the Pressuremeter method, also from the Canadian Geotechnical Society (1985). According to O'Neill and Reese (1999), unit end bearing resistance (q_{bs}) is a function of rock joint spacing parameters (s and m), and unconfined uniaxial compressive strength (q_u). If no compressible material or gouge-filled seams exist up to two diameters below the base of the shaft (intact, high quality rock with RQD values of 100 percent), and the depth of the socket extends below the ground surface by greater than 1.5 times the shaft diameter, then unit end bearing resistance may be determined using Equation 2.24. If jointed rock (e.g. shale or a limestone shale mix) exists up to two diameters below the base of the

socket, the values of unconfined compressive strength are smaller than 5.2 tsf, and all joints are closed and generally horizontal, then Equation 2.25 should be utilized to determine the unit end bearing resistance. If joints up to two diameters below the base of the shaft are randomly orientated and can be evaluated from cuts in the excavations, then Equation 2.26 should be utilized. In highly fractured rock, the joint parameters *s* and *m*, based on rock type descriptions from Hoek and Brown (1988), are used; values of s and m parameters are presented in Table 2.13. Additional methods to evaluate unit end bearing resistance in rock are presented in Table 2.14.

$$if\ RQD = 100\%\ up\ to\ 2B, and\ D_b \geq 1.5B$$
$$q_{bmax} = 2.5 q_u$$

(O'Neill and Reese, 1999) **Equation 2.24**

$$if\ 70\% < RQD < 100\%\ up\ to\ 2B, q_u > 5.2\ tsf$$
$$q_{bmax} = 4.83[10.44\ q_u]^{0.51}$$

(O'Neill and Reese, 1999) **Equation 2.25**

$$if\ RQD \leq 70\%\ up\ to\ 2B$$
$$q_{bmax} = [s^{0.5} + (ms^{0.5} + s)^{0.5}]\ q_u$$

(O'Neill and Reese, 1999) **Equation 2.26**

Where: q_{bsmax} = maximum unit end bearing resistance,

RQD = rock quality designation,

q_u= unconfined uniaxial compressive strength of rock,

B = shaft diameter, and

s, m = fractured rock mass parameters (Table 2.11).

Table 2.13. Approximate relationship between rock mass quality, material constants, and nonlinear strength (after Hoek and Brown, 1988).

Rock Quality	Constants	Rock Type				
		A = Carbonate rocks with well-developed crystal cleavage - *dolomite, limestone, and marble*				
		B = Lithified agrillaceous rocks - mudstone, siltstone, shale, and slate (normal to cleavage)				
		C = Arenaceous rocks with strong crystals and poorly developed crystal cleavage - *sandstone and quartzite*				
		D = Fine-grained polyminerallic igneous crystalline rocks - *andesite, dolerite, diabase and rhyolite*				
		E = Coarse grained polyminerallic igneous and metamorphic crystalline rocks - *amphibolite, gabbro gniess, granite, norite, quartz-diorite*				
		A	B	C	D	E
INTACT ROCK SAMPLES Laboratory size specimens free from discontinuities	s m	7.00 1.00	10.00 1.00	15.00 1.00	17.00 1.00	25.00 1.00
VERY GOOD QUALITY ROCK MASS: Tightly interlocking undisturbed rock with unweathered joints at 3-10 ft.	s m	2.40 0.082	3.43 0.082	5.14 0.082	5.82 0.082	8.567 0.082
GOOD QUALITY ROCK MASS Fresh to slightly weathered rock, slightly disturbed joints at 3-10 ft.	s m	0.575 0.00293	0.821 0.00293	1.231 0.00293	1.395 0.00293	2.052 0.00293
Fair QUALITY ROCK MASS Several sets of moderately weathered joints spaced at 1-3 ft.	s m	0.128 0.00009	0.183 0.00009	0.275 0.00009	0.311 0.00009	0.458 0.00009
POOR QUALITY ROCK MASS Numerous weathered joints at 2-12 in., some gouge. Clean compacted waste rock.	s m	0.029 3X10-6	0.041 3X10-6	0.061 3X10-6	0.069 3X10-6	0.102 3X10-6
VERY POOR QUALITY ROCK MASS: Numerous heavily weathered joints spced <2 in. with gouge. Waste rock with fines.	s m	0.007 1x10-7	0.010 1x10-7	0.015 1x10-7	0.017 1x10-7	0.025 1x10-7

Table 2.14. Additional methods for evaluating unit end bearing resistance.

Rock	Zhang and Einstien (1998)	Qt = 4.83*(qu^.51)*(A)
	Reese and O'Niell (1999)	Qt = 2.5(qu)
	Kulhawy and Prakoso (2006)	Qt=3.38(qu)
	Rowe and Armitage (1987)	Qt=2.5(qu)

2.5. Full-Scale Load Testing

The ultimate capacity and deformation behavior of a drilled shaft foundation may be difficult to predict using standardized design methods. Local geology and construction procedures can affect the behavior of a drilled shaft, making full-scale load testing desirable. Load tests are used to determine the load-transfer characteristics or lateral performance of a drilled shaft (O'Neill and Reese, 1999). Failure of a drilled shaft may be defined as either "plunging" (large movements) under extremely small increments of load, or a total movement equal to five percent of the diameter of the drilled shaft (O'Neill and Reese, 1999). A typical load test setup is instrumented to identify the internal load distribution within the shaft, enabling an analysis of the end bearing and skin friction resistances. From the information obtained during a load test, data may then be used to improve the design efficiency of drilled shaft foundations for the area. Potential benefits and limitations associated with full-scale load testing performed in the design phase are presented in Table 2.15.

Table 2.15. Summary of benefits and limitations associated with load tests, (after Brown et al., 2010).

Benefits	Limitations
1. Results can be readily implemented for econmony and constructablility 2. Alternative foundation systems can be compared. 3. Mitigation of constructability issues 4. May reduce construction time.	1. Requires extra time and effort. 2. Can extenuate design time. 3. Separate permitting issues may arise. 4. Success dependent upon construction procedures.

2.5.1. Osterberg Load Cell Testing

The Osterberg load cell (O-Cell^{TM}), developed by Jori Osterberg, was first used in 1984, and is presently utilized to determine drilled shaft resistance (Zhang, 2004; Yu et al., 2012). Compared to a conventional top-down load test, which requires a static load frame, anchor system, and conventional hydraulic jack, O-Cell testing may be performed by applying load from a hydraulic jack that was cast within the shaft during construction. An advantage of O-Cell testing over top-down load testing (with appropriate instrumentation) is the ability to differentiate between side friction and end bearing resistance values. Utilizing an O-Cell, side friction resistance and end bearing resistance can be separated by applying a bi-directional load upon a drilled shaft as presented in Figure 2.3 (Zhang, 2004).

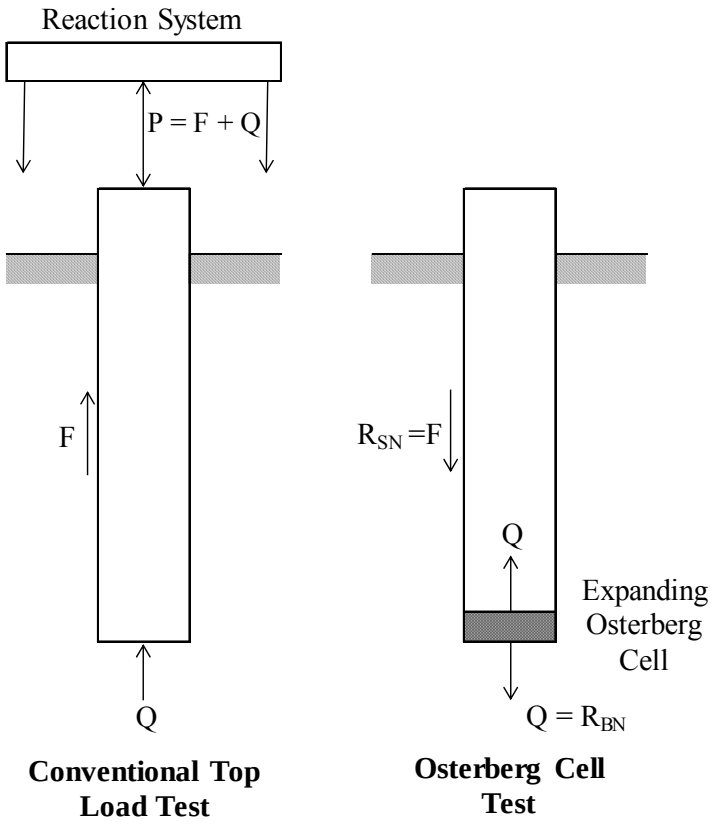

Figure 2.3. Comparison of O-Cell™ and conventional tests (modified from Schmertmann and Hayes, 1997).

The O-Cell has large pistons, allowing for the application of large loads with comparatively low jack pressures (Zhang, 2004). Available O-Cell sizes and respective capacities are presented in Table 2.15. As the O-Cell expands, the side friction resistance (R_{SN}) developed above the O-cell serves as the reaction force against which the end bearing resistance (R_{BN}) below the cell reacts (Miller, 2003). Conversely, end bearing resistance (R_{BN}) is developed at the same time and serves as the reaction force against which side friction resistance (R_{SN}) above the O-Cell reacts. O-Cells normally reach the ultimate load for only one of the two resistance components. To ensure adequate information, the O-Cell should be placed in an optimum location in which the predicted forces below and above the cell are equivalent (Schmertmann and Hayes, 1997). O-Cell load tests are performed in accordance with ASTM

D1143 (2013) in which increments equivalent to five percent of the anticipated failure load are applied at least every four minutes. Instrumentation utilized to measure strains and displacements along the shaft during testing (mechanical and electronic) may include those listed in Table 2.17. O-Cells are sacrificial, and are usually considered expendable upon completion of the test. A schematic of a typical Osterberg cell load test setup is presented in Figure 2.4.

Table 2.16. Available O-Cell sizes and capacities (Zhang, 2004).

Nominal Diameter		Nominal Capacity		Total Test Capacity	
(in)	(mm)	(kips)	(MN)	(kips)	(MN)
9	230	450	1.8	900	3.6
13	330	870	3.6	1740	7.2
21	540	2000	8.9	4000	17.8
26	660	3640	16	7280	32
34	870	6150	27	12300	54

Table 2.17. Possible instrumentation summary of an O-Cell load test (after Miller, 2003).

Type of Instrumentation	Load Test Location	Measurment Component
Linear Vibrating Wire Transducers (LVWT)	Bottom plate of Osterberg cell	Extension between the two plates of the O-Cell
Linear Voltage Displacement Transducers	Reference beam or telltale at top of shaft	Vertical/horizontal movement of the top of the shaft
Strain Gauges	Various locations along shaft	Stress/strain within the shaft
Dial Gauges	Reference beam or telltale at top of shaft	Vertical/horizontal movement of the top of the shaft
Telltales	Extend from the bottom and/or top plate of the O-cell to the top of the	Vertical movement of the O-Cell and compression of the shaft

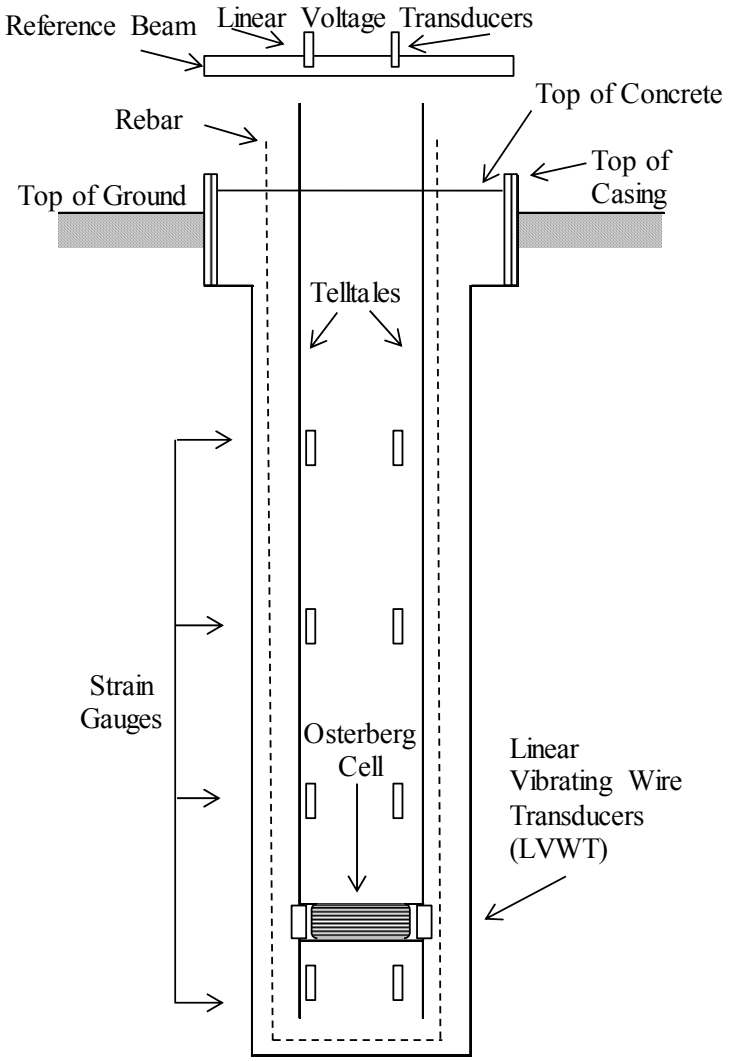

Figure 2.4. Schematic of an example Osterberg cell load test setup (modified from Miller, 2003).

A method for constructing a load-displacement curve equivalent to applying the load at the top of the shaft was developed in Osterberg (1998). The method was based upon the following assumptions: a) the shaft is considered rigid, b) the base resistance curve obtained from the O-Cell test is the same as the curve obtained from a conventional load test, and c) the friction resistance curve obtained from the O-Cell test is the same as the curve obtained from a conventional load test. By adding the side resistance and base resistance at the same displacement point on the curve (Figure 2.5a) for several displacement points, the equivalent

load displacement curve, as would have been measured from the top of the shaft, is obtained (Figure 2.5b).

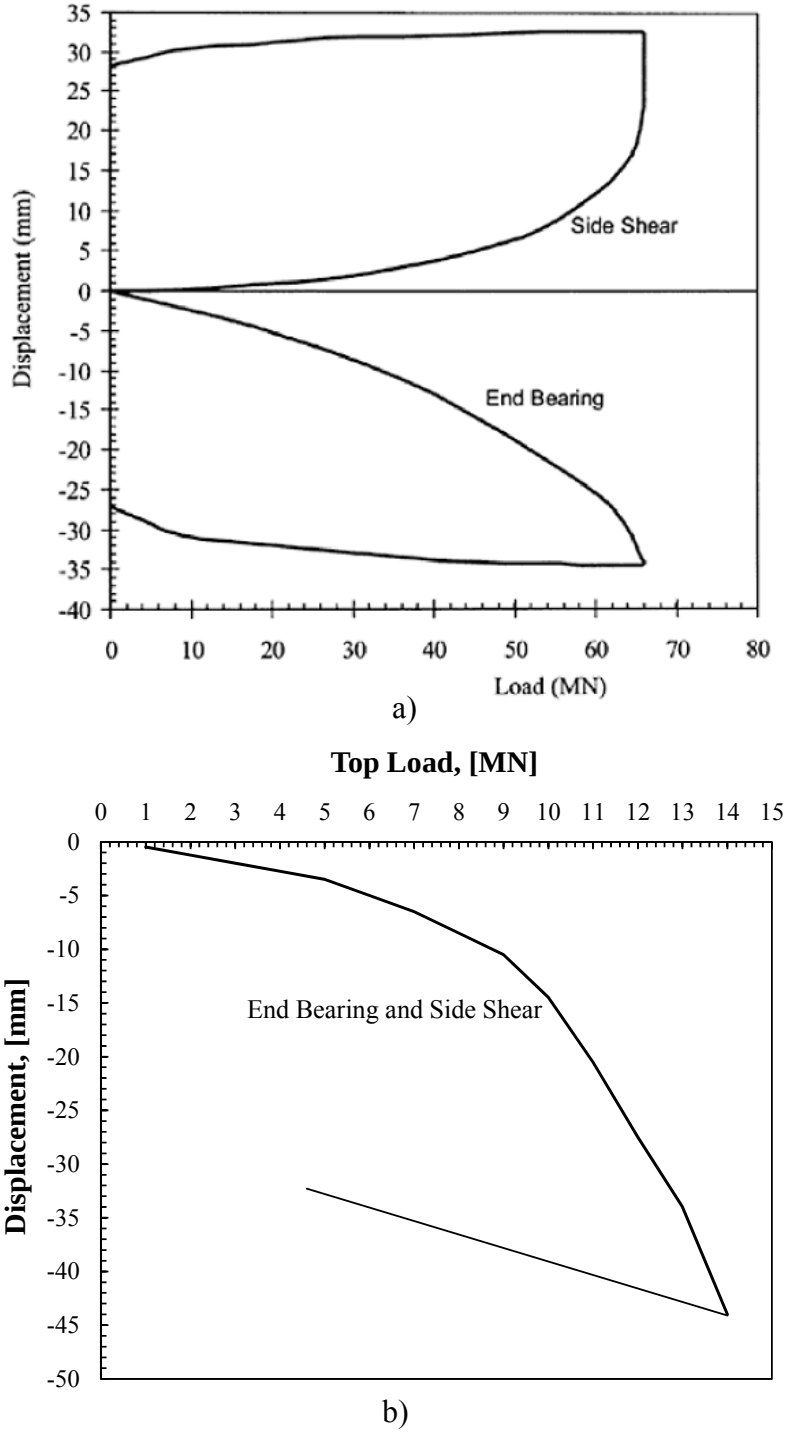

Figure 2.5. Example of a load displacement curve from a) an O-Cell (Osterberg, 1998), and b) a top-down load displacement test.

2.5.2. Osterberg Load Cell Case Studies

O-Cell load tests are commonly utilized to aid in the determination of locally calibrated LRFD resistance factors (Yu et al., 2012). An overview of select case studies utilizing O-Cell load testing to determine LRFD resistance factors is presented. These case studies include testing performed in Louisiana and Mississippi as found in Yu et al. (2012) as discussed in Section 2.5.2.1, in the Midwest as presented by Yang et al. (2008) and discussed in Section 2.5.2.2, in Florida as presented in Kuo et al. (2002) and discussed in Section 2.5.2.3, and in Missouri as presented in Vu (2013) and discussed in Section 2.5.2.4.

2.5.2.1. Louisiana

O-Cell testing was utilized to calibrate the LRFD resistance factors for drilled shafts in Louisiana (Yu et al., 2012). Twenty-two (22) drilled shafts located in Louisiana and Mississippi were tested using Osterberg load cells in soils consisting of clay, silt, sand, and gravel. The ultimate nominal resistance was specified using the criteria provided in O'Neill and Reese (1999). In some cases, where the failure criterion was not met, an estimated load at failure was extrapolated for select load-settlement curves; settlements requiring a large amount extrapolation were rejected (Yu et al., 2012). Based on the results of statistical comparisons between the predicted and measured drilled shaft resistances, as obtained using the Monte-Carlo simulation method, the current FHWA/AASTHO method (O'Neill and Reese, 1999) underestimated shaft resistance by an average of 17 percent. Yu et al. (2012) calculated total resistance factors and recommended a value of 0.6 to be used by the Louisiana Department of Transportation and Development (LADOTD) engineers. However, this value (17 percent underestimation and, resistance factor of 0.60) may fail to include the amount of uncertainty from soil sampling and testing methods used to obtain the evaluated soil properties (Race et al., 2013). Race et al. 2013

recommended that the variability in soil sampling and testing methods must also be evaluated prior to developing a load test database to determine local resistance factors.

2.5.2.2. Midwest

O-Cell test data was utilized to calibrate LRFD side friction resistance factors for drilled shafts in weak rock in Missouri, Kansas, and Colorado in Yang et al. (2008). In O'Neill and Reese (1999) "weak rock" is defined as intermediate geomaterials (IGMs) having an unconfined compressive strength between 0.5 and 5 MPa. Examples of the weak rock encountered within the Yang et al. (2008) study included shale, sandstone, claystone, siltstone, fossiliferous limestone, and ammonite. Calibrations were performed using the Monte Carlo simulation method on data collected from 19 O-Cell tests on drilled shafts designed using the FHWA/AASHTO method (O'Neill and Reese, 1999). Although the FHWA/AASTHO method significantly underestimated side resistance, the calibrated resistance factors were found to be comparable with current AASTHO LRFD Bridge Design Specifications (Yang et al., 2008).

2.5.2.3. Florida

Load test data was utilized to calibrate LRFD resistance factors for drilled shafts in sand, gravel, and rock in Florida by Kuo et al. (2002). Calibrations were performed using the first-order second-moment method on data collected from 185 static load tests on drilled shafts designed using the O'Neill and Reese (1988) and Reese and Wright (1977) methods. From the data, calculated resistance factors were generally within the range of 0.3 to 0.6. Resistance factors obtained from the Reese and O'Neill (1988) method were higher than that of the Reese and Wright (1977) method for most soils. It was concluded, in Kuo et al. (2002), that the cased-hole method of construction had the highest resistance in sand and clay layers, but dry-hole construction had the highest resistance factors for shafts constructed in rock. For clay and sand

deposits, skin friction resistance factors were higher than the combined skin and tip resistance factors. This trend was reversed for shafts constructed in rock (Kuo et al., 2002).

2.5.2.4. Missouri

Data from O-Cell testing was utilized to calibrate LRFD service limit resistance factors for drilled shafts in Missouri shales (Vu, 2013; Ding, 2013). Tests were performed on twenty-one (21) instrumented drilled shafts, located at two sites. Vu (2013) concluded that ultimate capacity may not be mobilized until larger displacements (up to 11 percent of the shaft diameter) occur. This 11 percent ultimate mobilized displacement is much larger than the current assumption of an ultimate mobilization displacement of five percent of the shaft diameter. Vu (2013) also noted the wide range in results. Ranges in data were significantly larger than the range of results in Reese and O'Neill (1999). Based on the increased range, if the Reese and O'Neill (1999) range of variability was later utilized for analysis, the results will be unconservative. Calibrated resistance factors were determined for shafts in which both skin friction resistance and end bearing resistance were considered (Equation 2.27), as well as special cases in which only end bearing resistance or skin friction resistance was utilized (Table 2.18). It is important to note that for the special cases, resistance factors may not be used separately for side friction and tip resistances.

$$\phi = \left[\frac{(5 - COV)(\theta - COV)}{10} + c_{pf}\right] c_{L/D} \qquad \text{(Vu, 2013)} \qquad \textbf{Equation 2.27}$$

Where: COV = coefficient of variation of uniaxial compressive strength,

θ = normalized load over capacity,

c_{pf} = coefficient for different probability of failure (p_f), and

$c_{L/D}$ = coefficient for different shaft length over shaft diameter (L/D).

Table 2.18. Special case calibrated resistance factors (Vu, 2013).

	Shaft Diameter (Shaft Length = 30ft.)			Shaft Length (Shaft Diameter = 3 ft.)		
	2 ft.	4 ft.	6 ft.	10 ft.	20 ft.	30 ft.
Side Resistance Factor	0.165	0.165	0.017	0.165	0.165	0.165
Tip Resistance Factor	0.275	0.280	0.280	0.280	0.280	0.280

2.6. Cross-Hole Sonic Logging

During and after the construction process of large diameter drilled shafts, anomalies in the shaft may be introduced from a variety of sources including the improper handling of slurry, concrete, casings, and/or reinforcement. These anomalies can have negative effects on shaft performance and include voids, honeycombing, necking, cracks, soil inclusions, and/or exposed rebar (Li et al., 2005). To ensure the safety of the drilled shaft foundation, anomalies should be identified as soon as possible, making non-destructive evaluation testing after drilled shaft construction attractive. According to Chernauskas and Paikowsky (2000), one of the most common non-destructive testing techniques utilized to assess the structural integrity of a drilled shaft is cross-hole sonic logging (CSL). The CSL system includes lowering a pair of piezoelectric transducers into diametrically opposing vertical PVC or steel tubes that have been filled with water (as a coupling agent). One transducer is used to generate sound compression waves (10 pulses per second) that propagate through the shaft, while the other transducer is used to receive the signals (Chernauskas and Paikowsky, 2000). A typical CSL test setup is presented in Figure 2.7. The transducers are placed at the bottom of each diametrically opposing pipe such that they are in the same horizontal plane and are then raised at a rate of one foot per second (Figure 2.6). The assembly is raised till it reaches the top of the shaft, and the process is repeated

for each tube-pair combination. As the probability of encountering an anomaly decreases with the increase of shaft diameter (if the size of the anomaly remains constant), larger shaft diameters require a larger number of tubes to accurately assess the integrity of the shaft (Li et al., 2005). In quality, homogenous concrete, the stress/sound wave speed (C) is a function of the elastic modulus, bulk density, and unit weight of the concrete (Equation 2.28). According to Chernauskas and Paikowsky (2000), values of C typically range between 12,000 and 13,000 feet per second.

$$C = \sqrt{\frac{E\ g}{\gamma}}$$ (Chernauskas and Paikowsky, 2000) **Equation 2.28**

Where: C = stress/sound wave speed (ft/sec),

E = modulus of concrete (lb/ft^2),

γ = unit weight of concrete (lb/ft^3), and

g = gravitational coefficient (ft/sec^2).

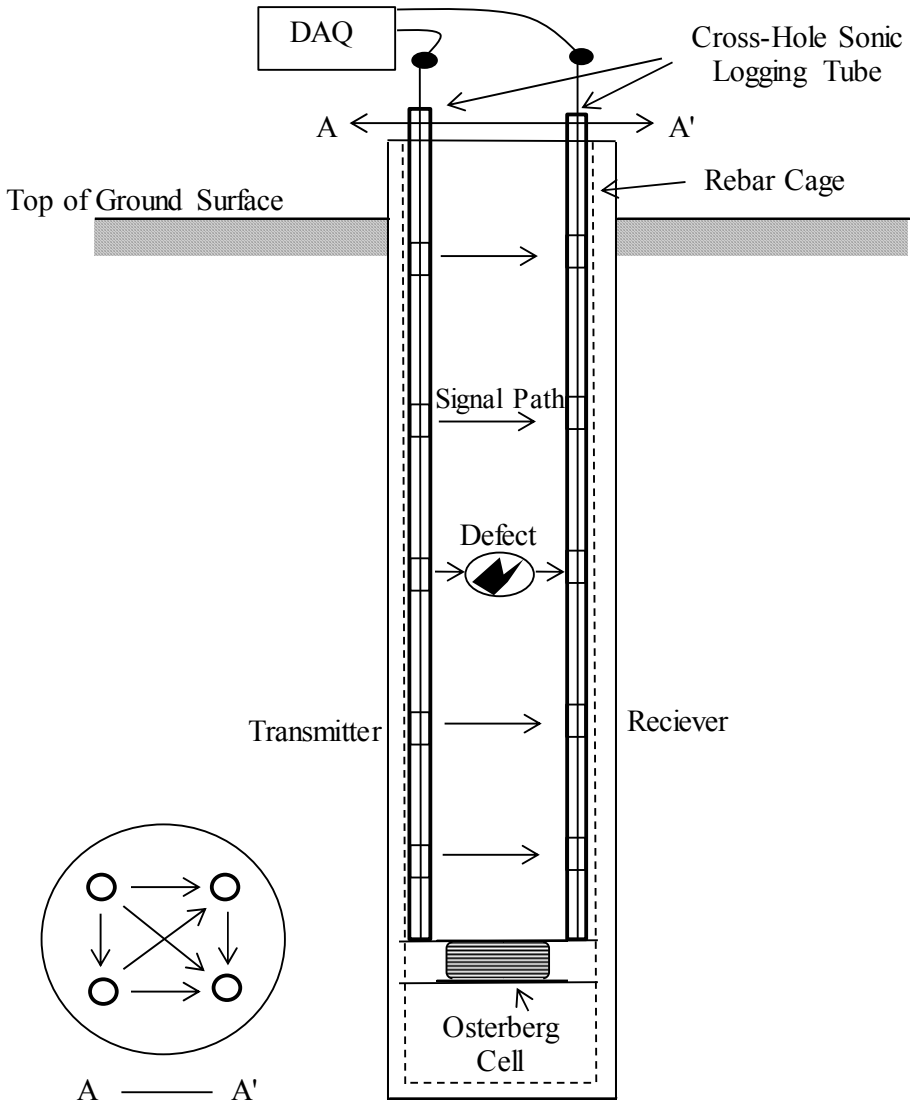

Figure 2.6. Typical CSL test setup showing transmitter and receiver at various depths, and a plan view of possible test combinations (after Chernauskas and Paikowsky, 2000).

The CSL method allows for a direct, timely assessment of pile integrity, however the method is limited in that detection of anomalies is bounded only between the tubes, and testing can only be performed on shafts for which the tubes were previously installed during construction. Debonding between the concrete and tubes may also present an issue if testing is delayed.

2.7. Uncertainty and Variability in LRFD from Number Samples

Mathematical and statistical models exist to interpret soil parameters obtained from soil samples. However, when the number of samples obtained for interpretation is small (due to site conditions, time constraints, and budget constraints), large amounts of uncertainty may be present in the collected soil property data. This uncertainty may result in either over-conservative and costly designs or failure-prone designs. The effects of sample populations on the uncertainty and variability of LRFD spread footings was evaluated in Ding (2013). Ding (2013) also developed a method to account for the negative effects of limited sample numbers. Samples from four sites in Missouri were selected and analyzed to determine the effects of sample size on foundation capacity. Results indicated that with an increasing number of samples, the percentage of over-conservative cases decreased from 90 percent to less than 20 percent. The percentage of under-conservative designs decreased as the sample size increased from three (3) to six (6) samples, but failed to decrease again until the number of samples exceeded 40. It was concluded in Ding (2013) that to reduce the incidence of a failure prone case, a very large sample population size is necessary. Regardless of the intended target probability of failure, it was found that foundations designed at the same site conditions, at the same depths have similar occurrences of under-conservative, over-conservative cases. To account for the effects of sample population size on a given confidence interval (CI), factors d and d_c were developed for lognormal linear regression models (Figure 2.7) and lognormal constant regression models (Figure 2.8), respectively (Ding, 2013).

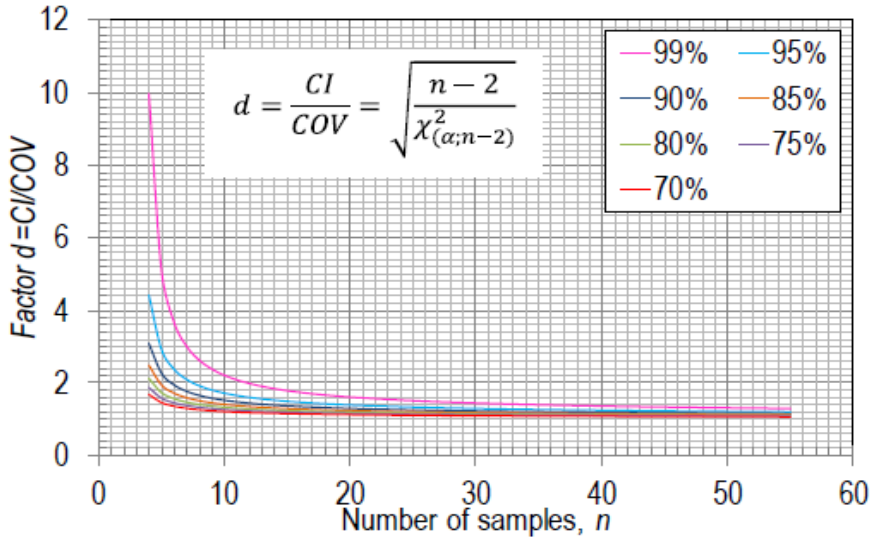

Figure 2.7 Factor d for various confidence bounds and number of samples for lognormal linear regression models (Ding, 2013).

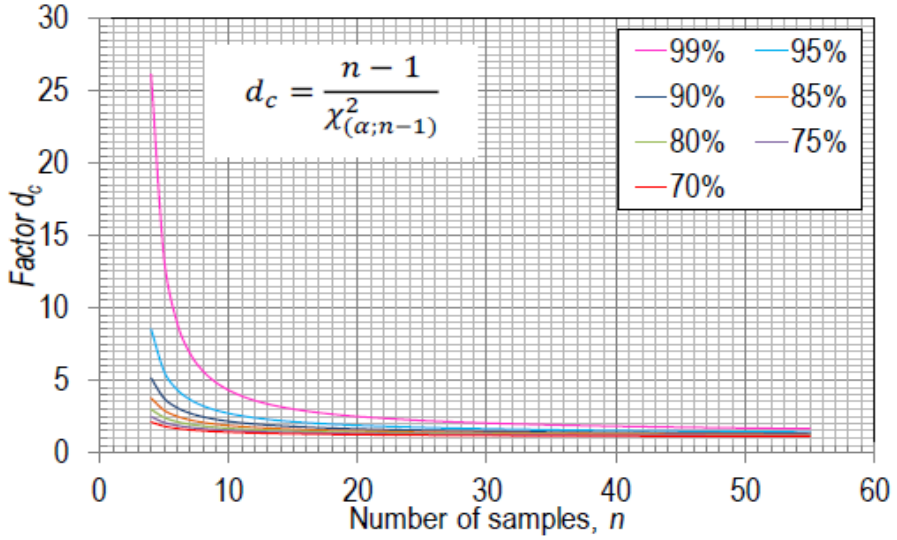

Figure 2.8 Factor d_c for various confidence bounds and number of samples for lognormal constant regression models (Ding, 2013).

Utilizing the Upper Confidence Interval of COV (CI) method on only extremely small sample population sizes (n<5), the occurrence of failure prone cases can be reduced to less than 15 percent (Ding, 2013). Because the uncertainty associated with smaller sample sizes is too great, Ding (2013) recommends using a population size of at least three soil samples to estimate

soil parameters. Although the research specifically addressed the uncertainty with spread footings, the CI-method may be applied to other engineering practices like deep foundation systems (Ding, 2013).

2.8. Static Axial Capacity Estimation Programs

Two static axial capacity estimation programs exist that can be utilized to predict the ultimate axial capacity for drilled shaft foundation systems and the load settlement curves for drilled shaft foundation systems. The programs, Bridge Software Institute FB-Deep (2012) and Ensoft SHAFT (2012), are presented in Sections 2.8.1 and 2.8.2, respectively. These sections also include program specific evaluation methodologies which deviate from AASHTO (2012).

2.8.1. Bridge Software Institute FB-Deep

Bridge Software Institute FB-Deep (FB-Deep 2012, Townsend 2003a, Townsend 2003b) is a commercially available static axial capacity estimation program developed by the Bridge Software Institute at the University of Florida. The program may be used to evaluate the static axial capacity of either driven piles or drilled shafts. Using FB-Deep, axial capacity is predicted by utilizing methods contained in FHWA report FHWA-NHI-10-016 (Brown et al., 2010) and AASHTO LRFD Bridge Design Specification (AASTHO, 2007). Site specific soil parameters obtained from standard penetration testing (SPT) or cone penetration testing (CPT) are utilized in the FB-Deep program to predict static axial capacity. Using SPT input data, empirical relationships based on Floridian soils between SPT and CPT data (Schmertmann, 1967; Bloomquist et al., 1992) are used to predict axial capacity based on the relationships developed in Schmertman (1978), Bustamante and Gianeselli (1982), and Bloomquist et al. (1992).

2.8.1.1. FB-Deep Side Friction Resistance in Cohesive Soil

In accordance with AASHTO (2007), the α Method to is utilized in FB-Deep to calculate ultimate friction resistance (Q_s). Following the recommendations of O'Neill and Reese (1999), the alpha value is neglected along the top five feet of clay along the shaft, as well as one diameter from the base of the shaft. However, unlike O'Neill and Reese (1999), the alpha value is set to equal 0.55, rather than the value being a function of undrained shear strength and atmospheric pressure (Equation 2.29).

$$f_s = \alpha\, c_u \leq 2.75\ tsf \qquad \text{(AASHTO, 2007)} \qquad \textbf{Equation 2.29}$$

Where: f_s = unit skin friction ≤ 2.75 tsf,

α = empirical cohesion factor 0.55, and

c_u = undrained shear strength (ksf).

2.8.1.2. FB-Deep End Bearing Resistance in Cohesive Soil

The O'Neill and Reese (1999) method is used in the FB-Deep program to determine the unit end bearing resistance for drilled shafts in clay (as presented previously in Equations 2.12 through 2.14). The program interpolates or extrapolates undrained shear strength values at depths one diameter below the shaft base. If the base of the shaft is located at the top of a clay layer, FB-Deep utilizes weighted averages of the undrained shear strength values at depths two diameters below the shaft base in the calculation of capacity. According to Lai (2012), in instances where the clay located at the base of the shaft is soft, the undrained shear strength value may be reduced by one-third to account for high strain-bearing failure.

2.8.1.3. FB-Deep Side Friction Resistance in Non-Cohesive Soil

The β Method from O'Neill and Reese (1999) is used in the FB-Deep program to determine ultimate side friction resistance (as previously presented in Equations 2.15 through 2.17). For soil layers larger than five feet thick, the program subdivides the layer into one foot increments in which to calculate β values. Besides this deviation from O'Neill and Reese (1999), the methods are otherwise similar.

2.8.1.4. FB-Deep End Bearing Resistance in Non-Cohesive Soil

The equations and theory introduced by Reese and O'Neill (1988) are used in the FB-Deep program to calculate unit end bearing resistance in sand (as presented previously in Equations 2.18 and 2.19). Weighted average modified blowcount values are also utilized at depths between 1.5 to 2 diameters below the base of the shaft. If modified blowcount (N_{60}) values exceed a value of 50, the material is classified and evaluated as an intermediate geomaterial (IGM).

2.8.1.5. FB-Deep Side Friction Resistance in Rock

Utilizing FB-Deep, a user may select one of two methods for calculating frictional resistance in limestone. The UF-Method from McVay et al. (1992), developed particularly for limestone (Equation 2.30), enables the unit frictional resistance to be calculated as a function of unconfined compressive strength (q_u) and tensile strength (q_t). Also associated with the UF-method is a general correlation of unconfined compressive strength to unit skin friction resistance. The correlation (Equation 2.31) allows the user to input empirical parameters based on engineering judgment from the geological area associated with the design. The correlation is a required input parameter when using FB-Deep with smooth rock sockets. Values of previously determined a and b coefficients as utilized by various researchers are presented in Table 2.19.

$$f_{su} = 0.5\sqrt{q_u}\sqrt{q_t}$$ (McVay et al., 1992) **Equation 2.30**

$$f_{su} = a\, q_u^b$$ (McVay et al., 1992) **Equation 2.31**

Where: f_{su} = unit skin friction resistance (tsf),

q_u = unconfined compressive strength (tsf),

q_t = tensile strength (tsf), and

a and *b* = empirical geological parameters (Table 2.19).

Table 2.19. Previous empirical geological values (a & b) for Equation 2.32 (after McVay et al., 1992).

Author	a [tsf]	b [tsf]
Williams et al., (1980)	1.842	0.367
Rowe and Armitage, (1987) [smooth sockets]	1.45	0.50
Rowe and Armitage, (1987) [rough sockets]	1.94	0.50
Horvath and Kenny, (1979)	0.21	0.50
Carter and Kulhawy, (1988)	0.2	0.50
Reynoldds and Kaderabek, (1980)	0.3	1.0
Gupton and Logan, (1984)	0.2	1.0
Reese and O'Neill, (1988)	0.15	1.0

2.8.1.6. FB-Deep End Bearing Resistance in Rock

A user defined unit end bearing capacity value is required for FB-Deep. If the value is not input, a value of one-half of the uniaxial unconfined compressive strength of the rock is utilized (Equation 2.32).

$$q_{bu} = 0.5\, q_u$$ (FB-Deep, 2012) **Equation 2.32**

Where: q_{bu} = unit end bearing resistance,

q_u = unconfined compressive strength.

2.8.2. SHAFTv2012

Ensoft SHAFT (Reese 2012a, 2012b, SHAFT 2012), a widely used axial capacity estimation program, was commercially released in 1987 under the direction of Dr. Lymon C. Reese. Since 1978, seven versions of SHAFT have been distributed by ENSOFT. The predictive methods utilized in SHAFT are also based on methods obtained from Brown et al. (2010) and AASHTO (2007). The settlement of the drilled shaft, as a function of load, and the distribution of load along the shaft are predicted using SHAFT. Additionally, LRFD reduction factors for side friction and tip resistance in each soil layer may be specified for each geostrata layer. Using the SHAFT program, axial capacity values are predicted based on the analysis methods presented in Table 2.20.

Table 2.20. SHAFTv2012 analysis methods.

Soil Type	Resistance Type	Basic Approach
Cohesive Soil	Side Resistance	α-method (O'Neill and Reese, 1999)
	Bearing Capacity	(Skempton, 1951)
		(Sheikh and O'Neill, 1986)
Non-Cohesive Soil	Side Resistance	β-method (O'Neill and Reese, 1999)
	End Bearing	(Meyerhof, 1976)
		(Quiros and Reese, 1977)
Rock	Side Resistance	(Hovarth and Kenney, 1979)
	Bearing Capacity	(Canadian Geotechnical Society, 1978)
		(Bieniawski, 1984)
Non-Cohesive Intermediate GeoMaterials (IGMs)	Side Resistance	(Mayne and Harris, 1993)
		(O'Neill et al., 1996)
	Bearing Capacity	(Mayne and Harris, 1993)
		(O'Neill et al., 1996)
Cohesive Intermediate GeoMaterials (IGMs)	Side Resistance	(O'Neill et al., 1996)
	Bearing Capacity	(O'Neill et al., 1996)
Gravelly Sand and Gravel	Side Resistance	(O'Neill and Reese, 1999)
		(Rollins et al., 2005)
	Bearing Capacity	(Meyerhof, 1976)
		(Quiros and Reese, 1977)

2.9. Concrete Admixtures

Concrete admixtures are ingredients added to concrete, before placement, which are not the main constituents of concrete that include water, aggregates, cement, or fibers. The use of admixtures can provide the following beneficial properties:

- acceleration or retardation of set time,
- enhanced chemical resistance,
- enhanced freeze/thaw resistance,
- enhanced strength,
- enhanced workability, and
- and enhanced finishability.

In 2011, the Federal Highway Administration (FHWA) reported an estimated 80 percent of the concrete produced in North America contains one or more admixtures. Many perform multiple

functions, further forwarding the ultimate goals of public safety and cost-savings. The two types of commonly utilized admixtures are mineral (Section 2.9.1) and chemical (Section 2.9.2).

2.9.1. Mineral Admixtures

Mineral admixtures include fly ash (Section 2.9.1.1), silica fume (Section 2.9.1.2), and blast furnace slag (2.9.1.3). These admixtures are usually added in large amounts to allow for a reduction in cement. However, additional benefits of mineral admixtures include alkali-silica reaction (ASR) resistance, sulfate attack resistance, and thermal cracking resistance.

2.9.1.1. Fly Ash

Fly ash is a finely ground (finer than cement), glassy, end-product of coal combustion which has been used in the U.S. to supplement cement since the early 1930's (Davis et al., 1937). Along with the environmental and fiscal benefits associated with the re-use of coal combustion products, fly ash can also improve the workability, segregation potential, bleeding potential, heat generation, and ASR susceptibility of concrete. Two classes of fly ash are Class C and Class F. Class C fly ash is produced from burning subbitumous coal and lignite, and possesses cementitious and pozzolanic properties (Halstead, 1986). Class F fly ash is produced from burning anrthracite or bituminous coal, and is rarely cemetitious (Halstead, 1986). Currently in the U.S., a maximum substitution rate of 15 to 25 percent fly ash replacement is required, as specified in ASTM C618 (2012).

2.9.1.2. Silica Fume

Silica fume is a byproduct of the coal combustion process which is also purposed for cement replacement. Silica fume consists of fine (up to 100 times finer than cement) vitreous particles with strong pozzolanic properties (Luther, 1990). This mineral admixture improves

compressive strength, bond strength, abrasion resistance, and density. According to the Luther (1989), a maximum substitution rate of up to 15 percent silica fume replacement is currently specified for projects completed in the United States, as addressed in ASTM C1240 (2012).

2.9.1.3. Blast Furnace Slag

Blast furnace slag is a granular, semi-crystalline product of molten iron being quenched with water. It is highly cementitious, and is classified into three grades: 80, 100, and 120 (Lewis, 1981). The use of grade 80 blast furnace slag should be generally avoided as a concrete admixture. However, according to the FHWA (2011), grade 100 and 120 blast furnace slag will yield equal or greater seven-day compressive strengths, and may be substituted for cement on a one to one basis, as addressed in ASTM C989 (2012). The mineral admixture improves early strength gain potential, permeability, and ASR resistance.

2.9.2. Chemical Admixtures

Chemical admixtures include water reducing agents (Section 2.9.2.1), air entraining agents (Section 2.9.2.2), set retarders (Section 2.9.2.3), accelerators (Section 2.9.2.4), and superplasticizers (2.9.2.5). These admixtures are usually added in very small amounts to perform a variety of functions.

2.9.2.1. Water Reducing Agents

Water reducing admixtures are added to concrete to: improve workability, achieve a given slump at a lower water/cement ratio, or achieve a specified strength at lower cement contents than those used in standard concrete. Water reducers are commonly utilized in bridge deck construction, low-slump overlays, and patching applications (Rixom and Mailvaganam, 1986). A reduction in water demand of seven to ten percent is usually achieved utilizing a water

reducer, as well as an increase in compressive strength of up to 25 percent, as compared to standard concrete (Mindess and Young, 1981).

2.9.2.2. Air Entrainment

Air entrainment is the uniform incorporation of small air bubbles into the cement paste matrix of a concrete. Most air entraining agents are categorized as organic additives such as wood resin salts, synthetic detergents, petroleum acid salts, or fatty/resinous acids and salts (Edmeades and Hewlett, 1986). According to the FHWA (2011), specifications of air entraining agents in concrete are located in ASTM C260 (2010). Adding air entraining agents can improve the freeze/thaw resistance, workability, bleed potential, and segregation potential of concrete.

2.9.2.3. Set Retarders

Set retarders are used to delay cement hydration without impacting the long-term mechanical properties of the concrete mixture. Retarders delay hydration by offsetting the heat of hydration; enabling more time for hauling, placing, and/or texturing (Mindess and Young, 1981). The formation of cold joints, and crack formation from form deflection are also minimized utilizing retarders. Because of these benefits, retarders are widely utilized on bridge decks, and are considered the second most commonly utilized admixture (U.S. Dept. Trans., 1990).

2.9.2.4. Accelerants

Accelerating agents are utilized in concrete to promote early compressive and flexural strength gain as well as a shortened setting time. Calcium chloride is the most common and economical concrete accelerant despite the potential for steel corrosion from the calcium chloride (Ramachandran, 1984a). Because of the potential for corrosion, allowable dosage rates of

calcium chloride are limited to two percent of the cement content, and chloride free accelerants including sulfates, formates, nitrates, and triethanolamines have been researched (Ramachandran, 1984b). All accelerants should meet the specifications required, as described in ASTM C494 (2013). Despite the corrosion potential, calcium chloride is noted to improve the workability, water demand, and bleed potential of freshly placed concrete.

2.9.2.5. Superplasticizers

Superplasticizers (or high range water reducers) are linear polymers which belong to one of four families. According to Mindess and Young (1981), these families include:

1) sulfonated melamine-formaldehyde condensates (SMFs),
2) sulfonated naphthalene-formaldehyde condensates (SNFs),
3) modified lignosulfonates, and
4) polycarboxylate derivatives.

Superplasitcers neutralize the surface charges on cement particles, releasing the water in the cement particle agglomerations, and reducing the viscosity of the paste (Mindess and Young, 1981). Superplasticizers can produce high flowing concrete with slumps ranging from seven to nine inches, and high strength concrete at water cement rations from 0.3 to 0.4 (Ramachandran and Malhorta, 1984). Due to the admixture reducing water demands from 12 to 15 percent without hindering workability, compressive strength values greater than 14,000 pounds per square inch at 28 days have been achieved, as well as reduced concrete permeability values (Malhorta, 1989). Specifications for superplasticizers are presented in ASTM C494.

2.10. Conclusion

This literature review discussed LRFD and its relevance to drilled shaft design in Sections 2.2. and 2.3., highlighting the calibration to fit method (ASD) and the calibration based on reliability method. Previous calibrations performed by Barker et al. (1991) and Paikowsky

(2004) were compared. Barker et al. (1991) used both fitting and reliability theory to recommend resistance factors, while Paikowsky et al. (2004) only used reliability theory. The issue of current resistance factors used with O'Neill and Reese (1999) from AASHTO (2012) to have been selected based on calibrations performed on Reese and O'Neill (1988) was also presented.

As a result of current methods utilizing outdated resistance factors, the differences between O'Neill and Reese (1999) and Reese and O'Neill (1988) were discussed in Section 2.4 along with methods of axial capacity estimation. For cohesive and non-cohesive soils, the methodology by O'Neill and Reese (1999) was reported. However, in rock, various methods for calculating shaft axial capacity including O'Neill and Reese (1998), Carter and Kulhawy (1988), Horvath and Kenney (1979), and Zhang and Einstin (1999) were discussed. The major property from which most predictive methods in rock are based upon is uniaxial compressive strength, although rock joint spacing should also be considered.

To validate the predictive methods in Section 2.4, full-scale load tests should be performed. Section 2.5 discussed Osterberg load cell testing, specifically the benefits of separating side friction resistances and end bearing resistances with O-Cell testing versus conventional top-down testing was discussed, as well as previous Osterberg load cell case studies. Previous O-Cell load tests results were used to calibrate resistance factors in soils in Louisiana, weak rock in the Midwest, granular media and rock Florida, and shales in Missouri. In Louisiana, the effects of uncertainty in regard to sample collection and testing were not addressed when generating a load test database, undermining the claim of AASHTO (2012) methods being 17 percent overconservative in this geologic region.

CSL testing, and how piezoelectric transducers may be utilized to determine the structural integrity of a drilled shaft was discussed in Section 2.6. The test should be performed raising the transmitter and receiver in unison at one foot per second. Competent concrete is reported to have a sonic/stress velocity around 12,000 to 13,000 feet per second. The variability and uncertainty introduced from sample size in LRFD was addressed by Ding (2013), and concluded that a sample population of at least three should always be utilized in determining soil properties (Section 2.7).

Current commercially available drilled shaft axial capacity prediction software programs Bridge Software Institute and Ensoft were introduced in Section 2.8. Bridge Software Institute FB-Deep is developed by researchers in Florida, and can utilize both CPT and SPT input to determine static axial capacity. In limestone specifically, the program utilizes predictive methods by McVay et al. (1992), but also allows the user to input rock parameters based on local geology. Ensoft SHAFT is developed by researchers in Texas, and can utilize friction angle input as well as blow count input. In rock, the program requires rock joint spacing input. Concrete admixtures are presented in Section 2.9. Physical descriptions, dosage rates, and effects on concrete of common mineral and chemical admixtures are discussed, as well their current specifications.

Chapter 3: Test Sites and Investigations

3.1. Introduction

A general description of the Siloam Springs, Turrell, and Monticello Arkansas Test Sites are presented in this chapter (Figure 1). Specifically, site access considerations and the geological formations specific to each test site are addressed in Section 3.2. Descriptions of the geotechnical investigations performed to acquire engineering properties at each test site are discussed in Section 3.3. The sampling and testing methods performed by UofA, AHTD, and MODOT personnel are compared in Section 3.4.

(a) (b) (c)

Figure 3.1. Photographs of the (a) Siloam Springs, (b) Turrell, and (c) Monticello Arkansas Test Sites.

3.2. Test Site Descriptions

Each test site, located within the State of Arkansas (Figure 3.2), was selected represent typical geologic profile that matched one of the typical geological profiles found within the state of Arkansas. Thereby, the results of this study could supplement most regional projects. The Siloam Springs Arkansas Test Site, located in the Northwestern region of the state, exemplifies the Ozark karst topography (Section 3.2.1). The Turrell Arkansas Test Site, situated near the Mississippi River, exhibits floodplain characteristics and is prone to liquefaction (Section 3.2.2). The Monticello Arkansas Test Site, situated within the Southeastern portion of the state, exemplifies gulf coastal plain characteristics (Section 3.2.3).

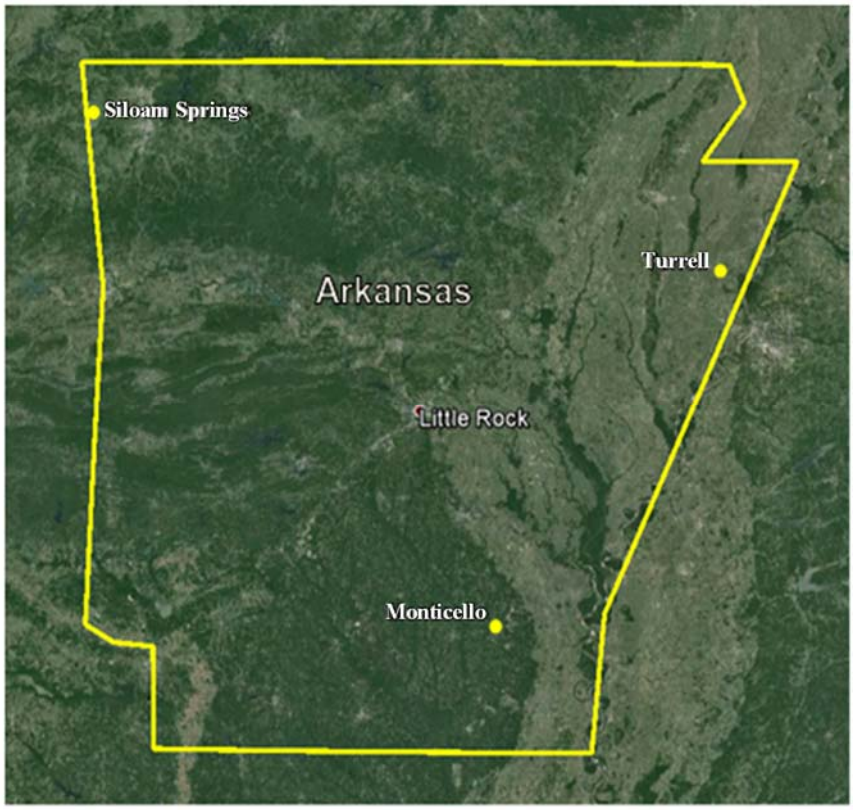

Figure 3.2. Site vicinity map of test site locations (modified from Google Earth, 2013).

3.2.1. Siloam Springs Site Description

The Arkansas Highway and Transportation Department (AHTD) is in the process of designing a new bridge across the Illinois River near Siloam Springs, Arkansas. The town of Siloam Springs is located in the Northwestern region of the state. The Siloam Springs Arkansas Test Site is located on County Road 16 (AR-16) approximately 1.4 miles southeast of the city limits of Siloam Springs (Township 17 North Range 33 West). The site utilized for this research project is located to the north of the exiting bridge (Figure 3.3a). The soil conditions at the site consist of approximately 16-feet of cherty clay below ground surface underlain by 59-feet of competent limestone, underlain by dark grey shale to a depth of 100-feet, the termination of most

borings (Figure 3.3b). Site access considerations included a steep access road, an existing superstructure located 22-feet above the ground surface, and river flood stage periods.

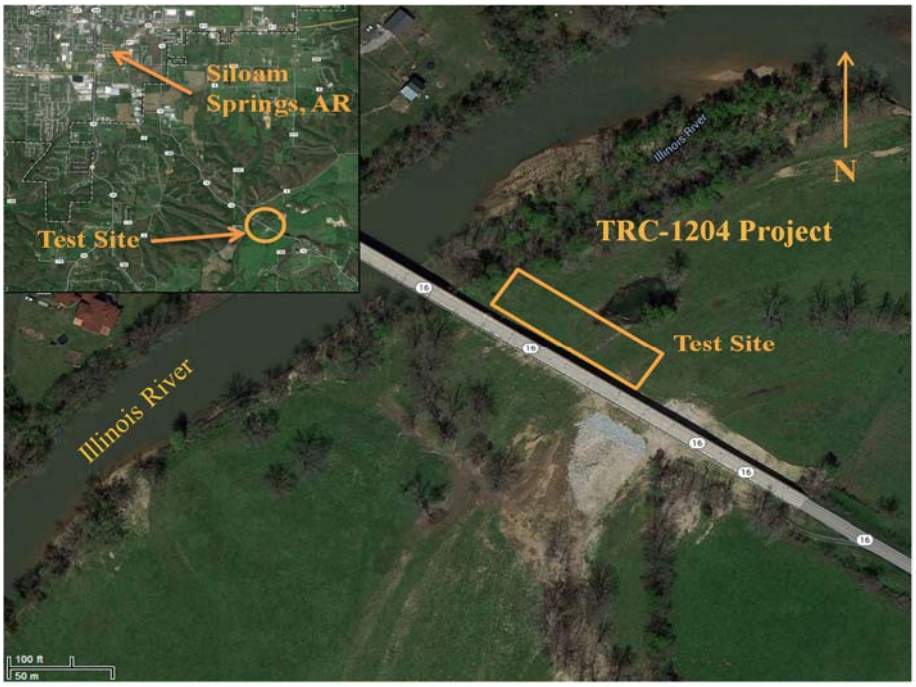

(a)

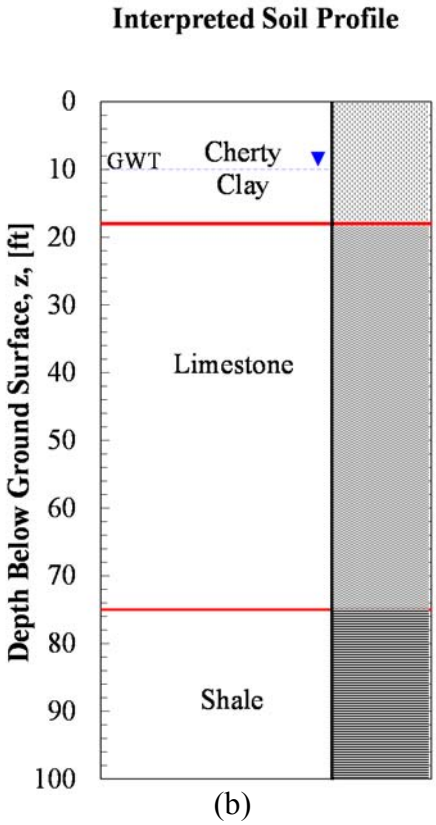

(b)

Figure 3.3 Location and layout of Siloam Springs Arkansas Test Site (a) relative to city of Siloam Springs (modified from Google Earth, 2013), and (b) interpreted test site soil profile as obtained from geotechnical investigation.

3.2.1.1. Geology of Area

The underlying rock formation at the Siloam Springs Arkansas Test Site (SSATS) is located near to two major characteristic formations: the Pitkin Limestone/Fayetteville Shale Formation and the Boone Formation (Figure 3.4). These formations are located along the Springfield Plateau and exhibit normal faulting, with displacement to the southern side (McFarland, 2004). As associated with many Ozark geological formations, each formation is known for dissolutional features including large fissures, caves, and sinkholes. According to the Arkansas Geological Survey (AGS), the SSATS is located less than one mile southeast of a normal fault (Figure 3.4).

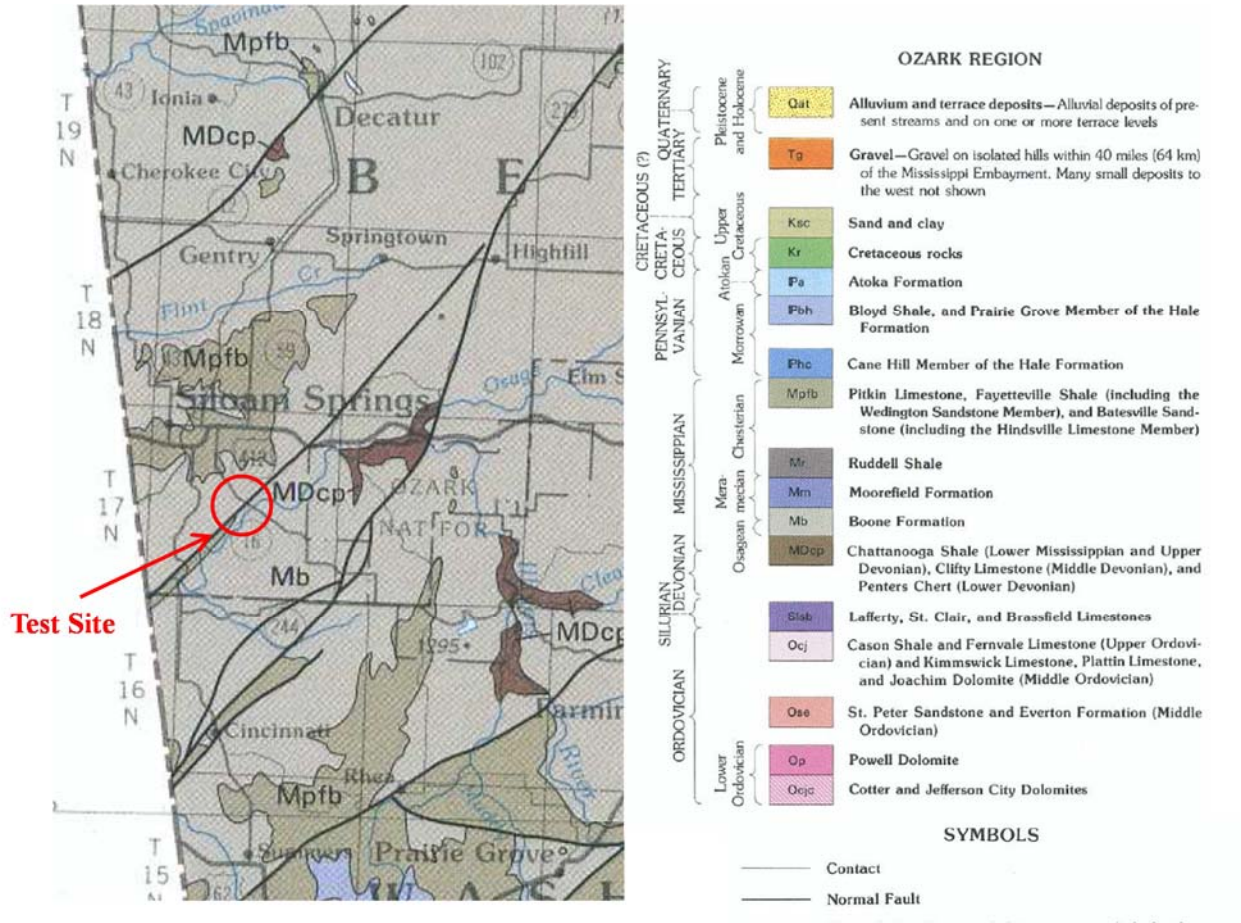

Figure 3.4. Geological formations associated with Siloam Springs Arkansas Test Site location (modified from USGS, 2013)

3.2.1.1.1. Pitkin Limestone/Fayetteville Shale

The Pitkin Limestone Formation (named for outcrops near the Pitkin post office of Washington County, AR) is of the late Mississippian period, and is located throughout the Ozark Plateaus of northern Arkansas, and eastern Oklahoma. The Pitkin Limestone Formation is characterized as fine to course grained, oolitic, lioclastic limestone with sequences of interbedded black shale, and/or chert located throughout the formation (McFarland, 2004). The average thickness of the Pitkin Limestone Formation ranges from about 50 feet in the Western Ozarks to about 200 feet in the Eastern Ozarks (McFarland, 2004).

The Fayetteville Shale Formation, also deposited in late Mississippian period, is a black, fissile, concretionary clay shale that is commonly inerbedded with fine grained limestone (McFarland, 2004). The thicknesses of the Fayetteville Shale Formation typically range between 10 and 400 feet (McFarland, 2004). The formation is located in north-central Arkansas, and is underlain by the Batesville Sandstone Formation. A photograph of a typical outcrop of the Pitkin Limestone Formation underlain by the Fayetteville Shale Formation, near Marshall, AR, is presented in Figure 3.5.

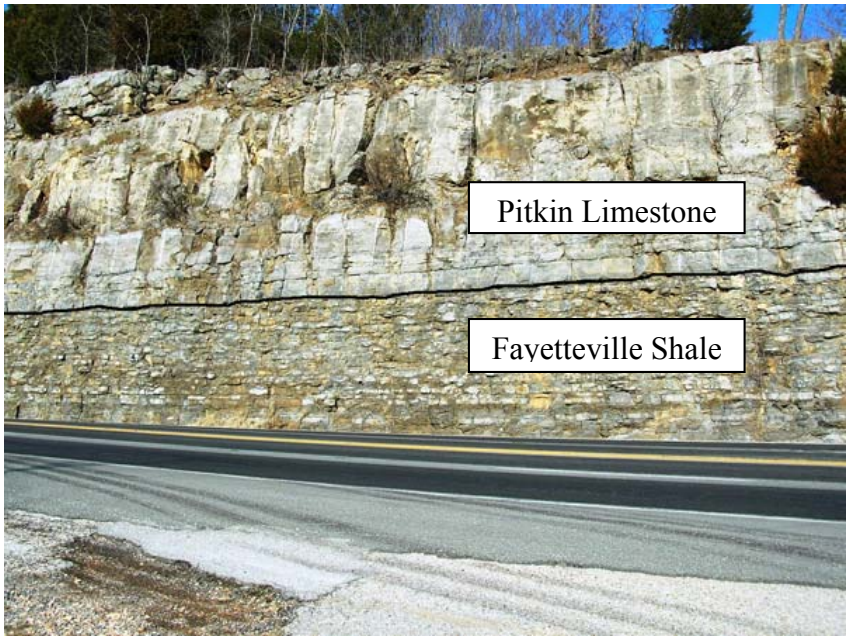

Figure 3.5. Photograph of an outcrop of the Pitkin Limestone Formation underlain by Fayetteville Shale Formation along Highway 65 near Marshall, AR (modified from USGS, 2013).

3.2.1.1.2. Boone Formation

The Boone Formation (named after the extensive features found throughout Boone County, AR) was formed in the middle Mississippian geologic period, and is located throughout the Ozark plateau of northern Arkansas, Southwestern Missouri, and Eastern Oklahoma. The Bonne Formation is composed of fine to course grained fossiliferous limestone with chert intrusions (McFarland, 2004). Lower zones of the formation are suggested to abut the Chattanooga Shale Formation at depths ranging from 300 to 350 feet (McFarland, 2004). A photograph of an exposed outcrop of the Boone Formation, near Marshall, AR, is presented in Figure 3.6.

Figure 3.6. Photograph of Boone Formation along Highway 65 at Marshall, AR (from USGS, 2013).

3.2.1.1.3. Siloam Springs Formation Determination

An investigation of collected rock core samples recovered from depths ranging from 15 to 102 feet below ground surface was performed by UofA personnel to determine the geologic formation and depth of the underlie at the Siloam Springs Arkansas Test Site (Figure 3.7). The limestone cores recovered at depths ranging from 1 to 38 feet were found to consist of fine to course grained limestone interbedded with sequences of dark grey to black chert throughout the material. At the Siloam Springs Arkansas Test Site, the shale interface was located at a depth of approximately 75 feet. No fine grained limestone intrusions were observed in rock core samples recovered at the Siloam Springs Arkansas Test Site, as would be expected from the Fayetteville Shale Formation.

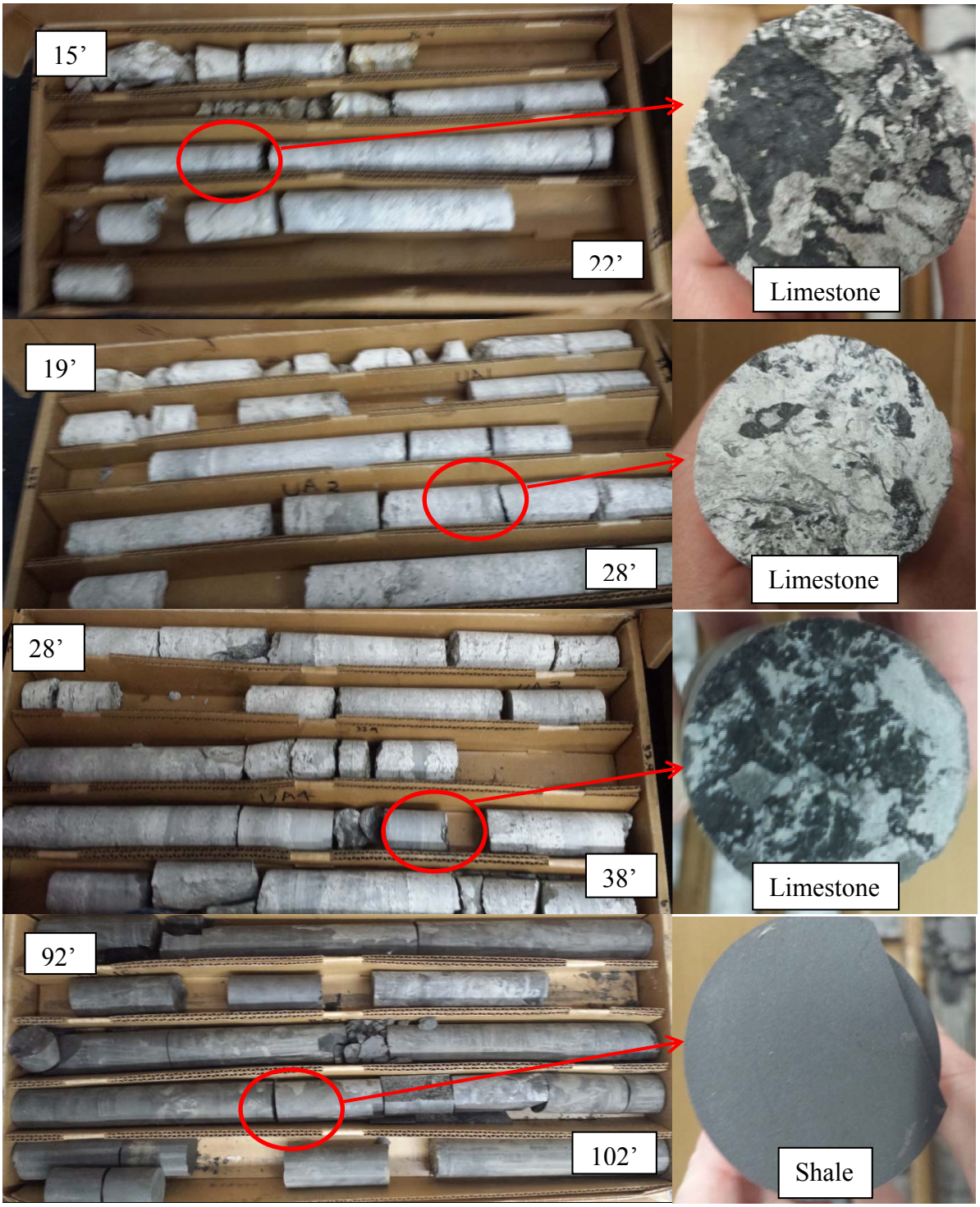

Figure 3.7. Examples of the cores of limestone and shale as collected and stored by researchers at the University of Arkansas.

3.2.2. Turrell Site Description

In the Arkansas Highway and Transportation Department (AHTD) constructed a new overpass for US Highway 63 across Interstate 55 (I-55) within Crittenden County near the town of Turrell, Arkansas. Turrell is located in the Eastern region of the state, approximately 5.3 miles east of the Mississippi River. The test site is located within the city limits of Turrell (Township 9 North Range 8 East), within the clover leaf connecting southbound US 63 traffic with northbound Interstate 55 traffic. The site is Southwest of the existing overpass spanning I-55 (Figure 3.8) and consists of approximately twenty-feet of high plasticity clay below the ground surface underlain by twelve feet of low plasticity silt, underlain by poorly graded sand (Figure 3.9). Site access considerations included on-coming traffic safety and wetland depressions.

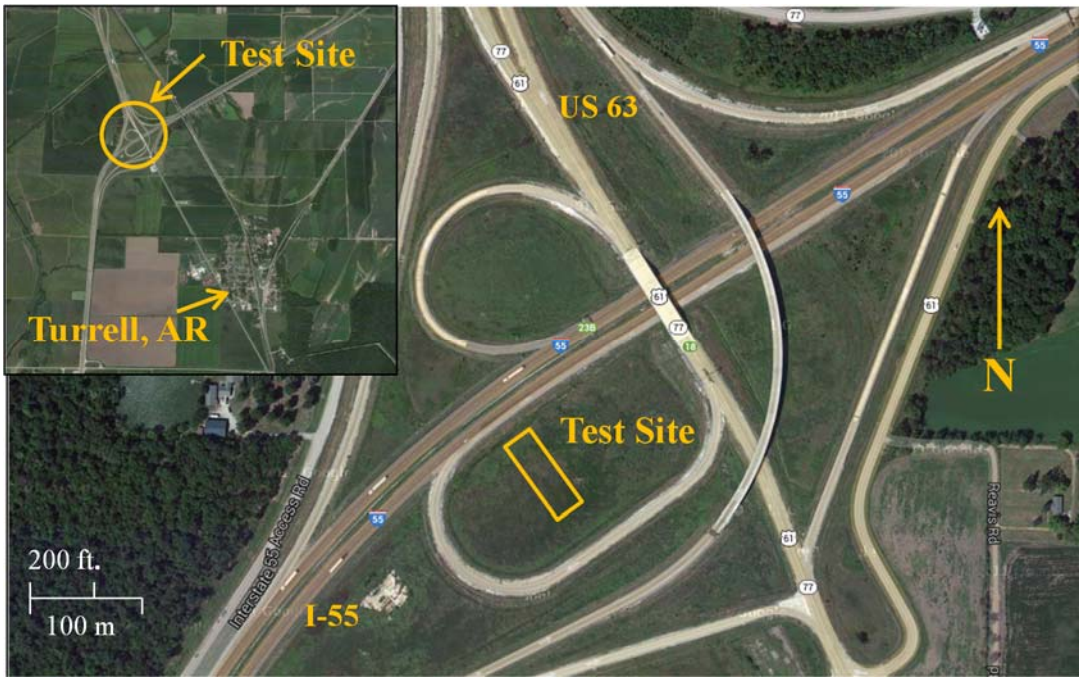

Figure 3.8. Location and layout of Turrell Arkansas Test Site relative to the town of Turrell (modified from Google Earth, 2013).

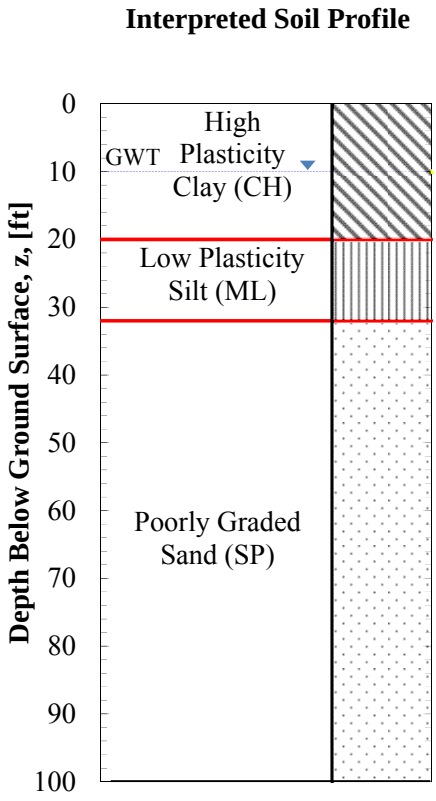

Figure 3.9. Turrell Arkansas Test Site subsurface stratigraphy as obtained from geotechnical investigations.

3.2.2.1. Site Geology

Topographically, the Eastern and North Eastern area of Arkansas range from low hills to essentially flat terrain. The area is widely dominated by Quaternary terrace and alluvial deposits with minimum exposure of Tertiary units (AGS, 2013). Due to the being within the Mississippi Embayment, the area exhibits a North-South erosional characteristic (from Crowley's Ridge), which is generally capped by Quaternry loess, preventing the exposures of the Tertiary deposits (AGS, 2013). The site geology at the Turrell Arkansas Test Site is based widely on geomorphic considerations rather than lithology or age (AGS, 2013), and is largely comprised of alluvium and dune sand (Figure 3.10).

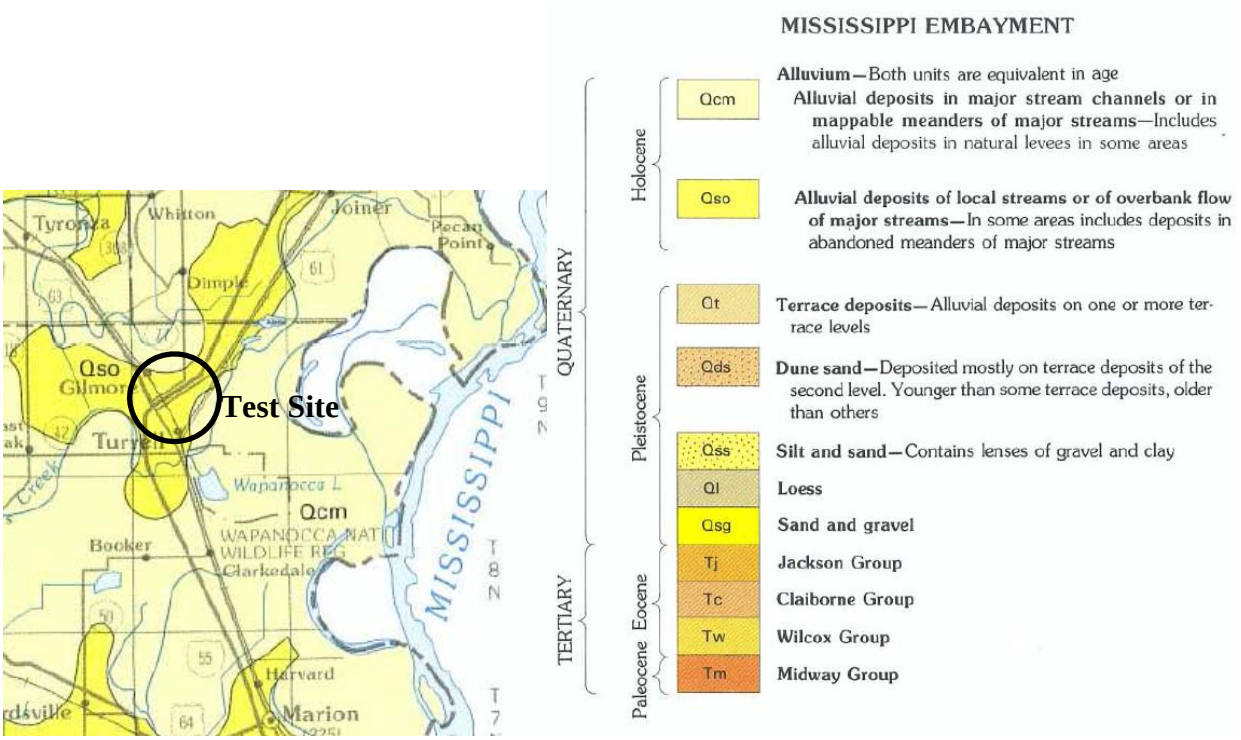

Figure 3.10. Geological formations associated with Turrell Arkansas Test Site (modified from AGS, 2013).

3.2.2.1.1. Alluvium

The alluvium (located up to approximately 32 feet below ground surface at the Turrell Arkansas Test Site) is deposited from major and local stream channels, meanders, natural levees, and/or overbank flows. According to AGS (2013), these deposits date from the Quaternary Period, Holocene Epoch and are distributed throughout the Mississippi River Embayment and Eastern Arkansas (Figure 3.10). The stratigraphy is known for highly variable layer thicknesses, variable lower contact zones, and a scarce amount of fossils (AGS, 2013).

3.2.2.1.2. Crowley's Ridge Sand

Underlying the alluvial deposits of the Mississippi Embayment (located approximately at 32 feet below ground surface at the Turrell Arkansas Test Site), homogenous, poorly-graded, tan to buff-grayish sand was encountered. According to AGS (2013), the material is thought to be

derived from glacial outwash originally deposited along major drainage channels during the initial states of the interglacial times. These deposits date from the Quaternary Period, Holocene Epoch and are distributed east of Crowley's Ridge (Figure 3.10). The northern portion of Crowley's Ridge is capped by intervals of unconsolidated silt and sand with lenses of clay and gravel (AGS, 2013). However, this unit has never been thoroughly studied in the state of Arkansas.

3.2.2.2. Earthquake Hazards

The Turrell Arkansas Test Site is located within the New Madrid Seismic Zone. Due to the stratigraphic makeup of the site (loose cohesionless deposits less than 50 feet below ground surface and a high water table), and the proximity of the site to the New Madrid Seismic Zone, the site is classified as being very highly susceptible to liquefaction (Figure 3.12). The area has been recorded to have experienced numerous seismic events of ranging magnitudes since 1811 (Figure 3.11). As a result, seismic effects were considered in the design process at the Turrell Arkansas Test Site location, as further discussed in Chapter 6.

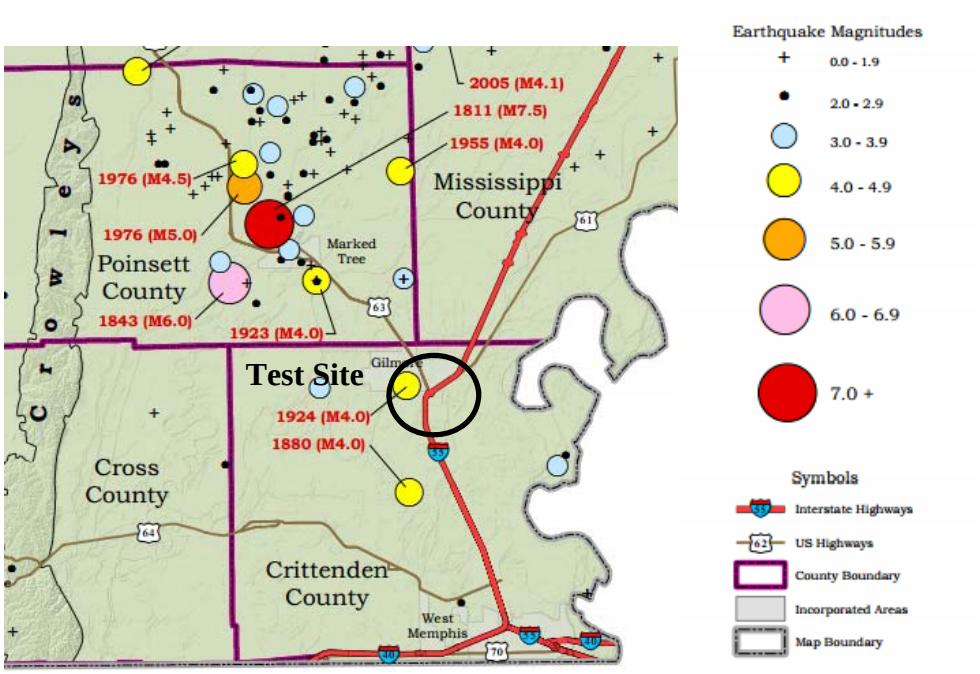

Figure 3.11. Recorded seismic events in the New Madrid Seismic Zone (after AGS, 2013).

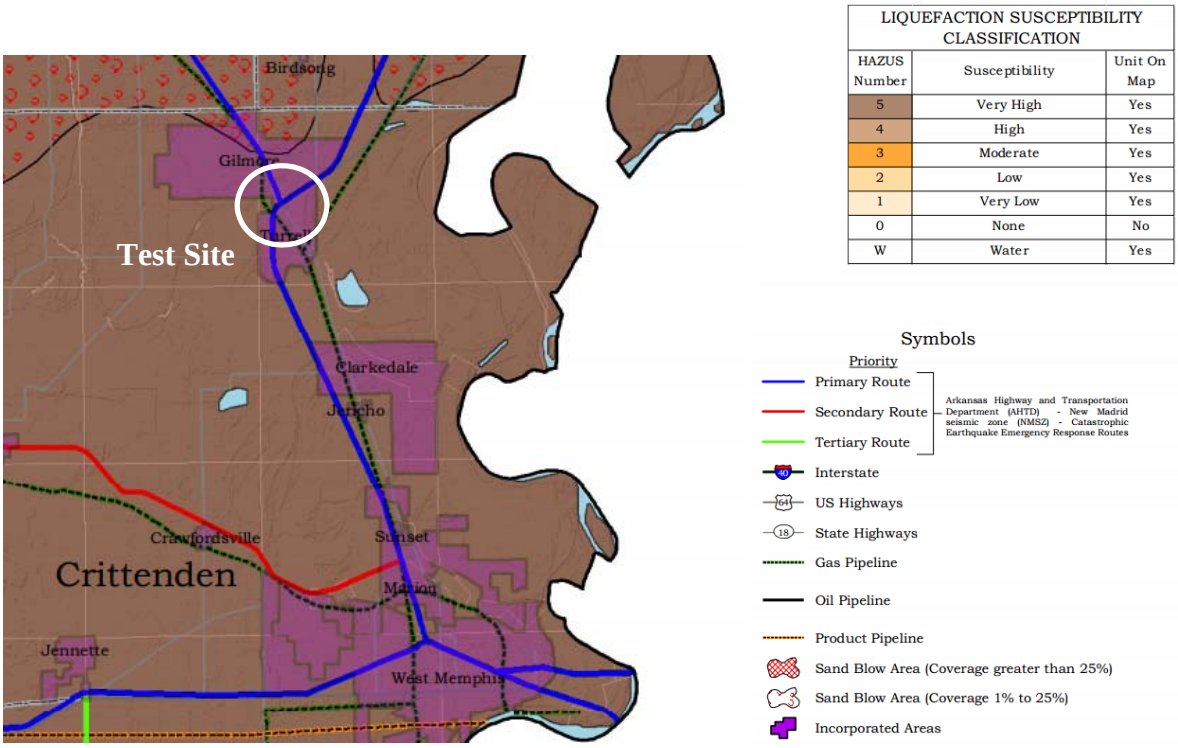

Figure 3.12. Liquefaction susceptibility of the Turrell Arkansas Test Site (after AGS, 2013).

3.2.3. Monticello Site Description

The Arkansas Highway and Transportation Department (AHTD) is planning to construct a new overpass spanning a railroad in Drew County near the town of Monticello, Arkansas. The overpass is part of the new US-69 corridor (Figure 3.13). The town of Monticello is located in the southeast region of the state. The test site is located approximately 1.9 miles Southeast of the city limits of Monticello (Township 13 South Range 6 West), along the eastern side of the railway. The site consists of approximately twenty-seven feet of desicated clay below the ground surface underlain by fifteen feet of poorly graded sand, underlain by eighteen feet of stiff clay, underlain by poorly graded sand (Figure 3.14). Site access considerations include airport proximity, railroad safety, and consistency of the topmost desiccated clay layer.

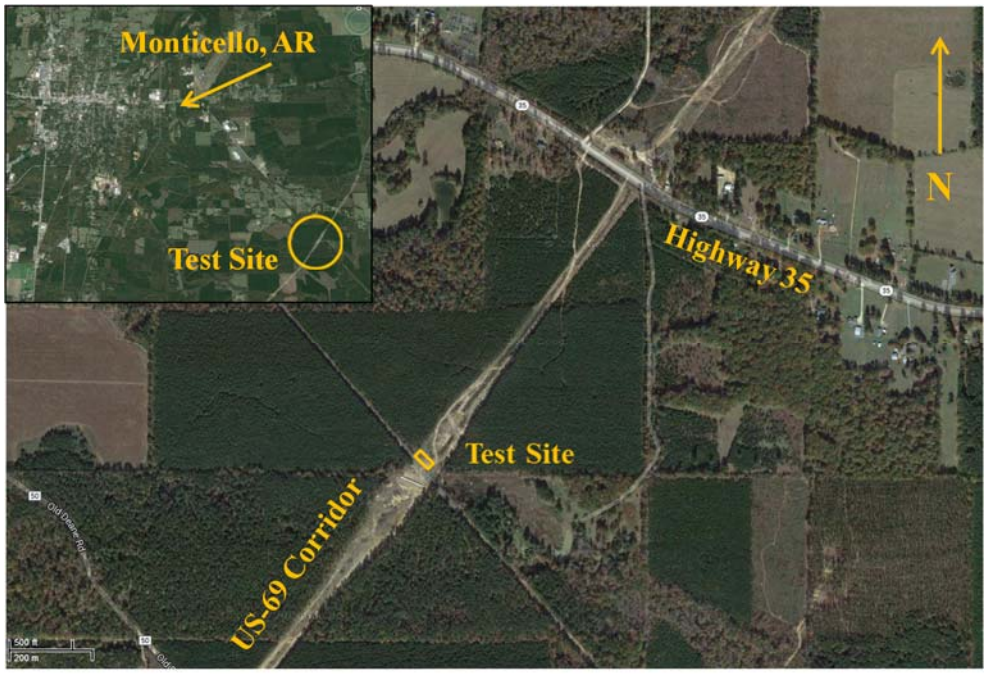

Figure 3.13. Location and layout of the Monticello Arkansas Test Site relative to the city of Monticello (modified from Google Earth, 2013).

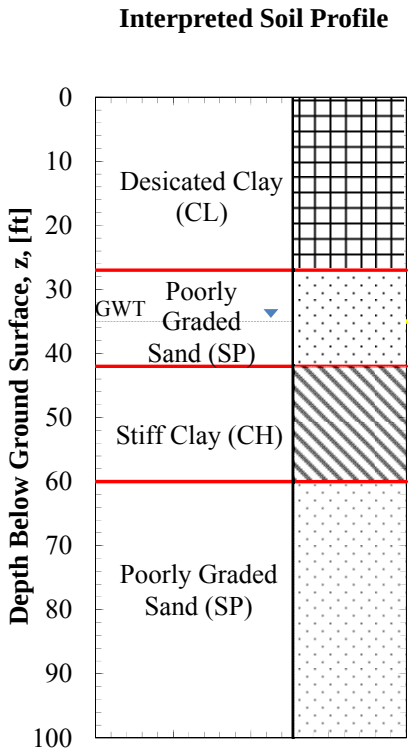

Figure 3.14. Monticello Arkansas Test Site interpreted soil profile as obtained from geotechnical investigation.

3.2.3.1. Site Geology

The major underlying geological formations encountered at the Monticello Arkansas Test Site are Terrace deposits (Figure 3.15). As typically exemplified in Southeastern Arkansas, the area is dominated by Tertiary Marginal Marine and Coastal Plain deposits, including a layer of Quaternary Terrace and Alluvial deposits (AGS, 2013). The features encountered at the Monticello Arkansas Test Site are identified as Gulf Coastal Plain and Mississippi Embayment deposits by AGS (2013), and exhibit generally normal faulting, with displacement to the Southern side (3.13).

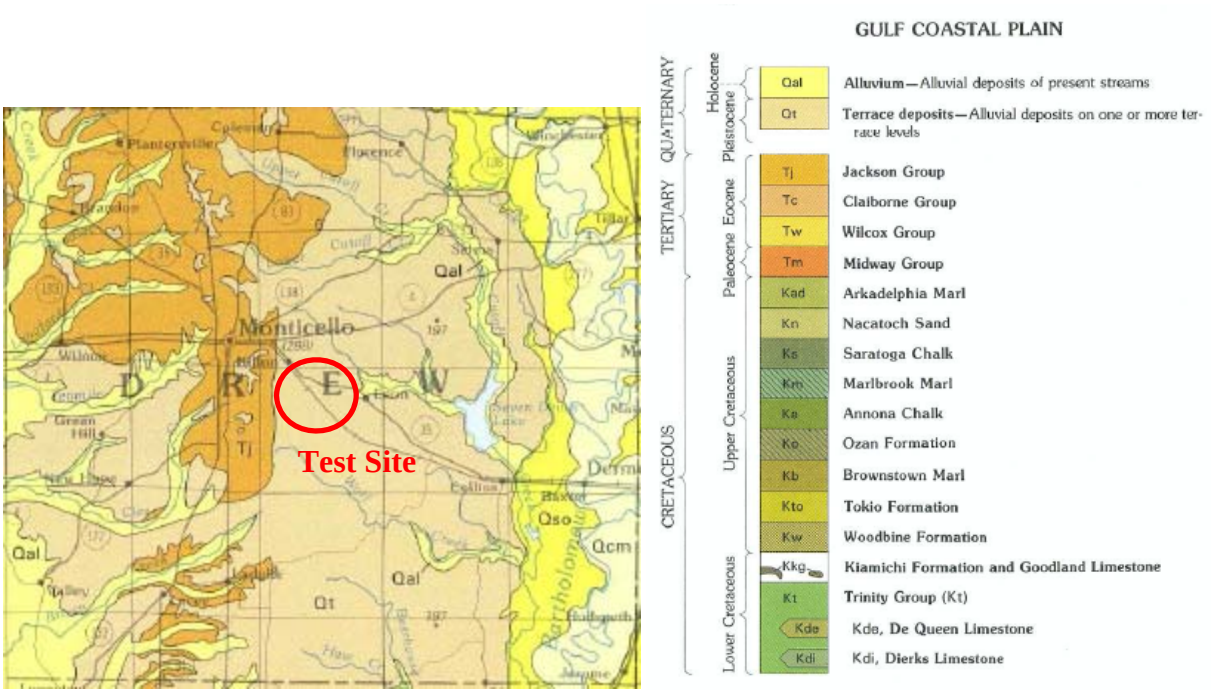

Figure 3.15. Geological formations associated with Monticello Arkansas Test Site (after AGS, 2013).

3.2.3.1.1. Terrace Deposits

Terrace deposits, from the Qauternary Period, Pleistocene Epoch, are located in Eastern and Southern Arkansas, the Mississippi Embayment, and the Gulf Coastal Plain. These deposits include a vibrational sequence of gravels, sands, silts, and clays, with individual deposits being lenticular and discontinuous. Fossils are rare in Terrace deposits, and several terrace levels are recognized with the lowest stratigraphic layer being the youngest. The thickness and lower contact areas of these layers are variable.

3.3. Site Investigations

Geotechnical site investigations were conducted at all three test site locations (Siloam Springs, Turrell, and Monticello) within the state of Arkansas. The geotechnical investigations included field and laboratory testing on samples obtained from AHTD boreholes, University of Arkansas (UofA) boreholes, and cone penetration test (CPT) soundings. The geotechnical site

investigations were performed by personnel from the UofA (in conjunction with personnel from the Missouri Department of Transportation [MODOT] and AHTD) and consisted of advanced and conventional sampling and testing procedures.

UofA samples were obtained every 1.5 feet in sand and every two (2) feet in clay, or every five (5) feet (using SPT [60 mm diameter] in sands, Osterberg hydraulic fixed-piston sampling in soft to stiff clay, Pitcher barrel sampling in stiff clay, and double swivel core barrel in hard rock). AHTD samples were obtained (using a standard split barrel sampler [30 mm diameter] in sands and clays or a core-barrel sampler in rock) every five (5) feet to the termination of each boring. In general, UofA and AHTD borings were terminated at either 100 feet depth or after 15 feet of continuous rock core had been obtained. Clay samples collected from UofA boreholes were saved in wax-sealed Shelby tubes with expandable packers prior to transport. Sand samples were saved in sealed plastic bags. Rock core samples were stored in waxed cardboard boxes. CPT tests were conducted at each site on behalf of the UofA by MODOT personnel simultaneously as UofA and before AHTD boreholes were completed at the Turrell and Monticello Arkansas Test Sites. UofA in-field tests performed on collected samples included unconsolidated undrained triaxial compression, minivane, torvane, and pocket penetrometer readings. All necessary equipment for conducting in-filed testing was housed in a mobile lab facility as presented in Figure 3.16.

Figure 3.16. Photograph of the UofA mobile lab facility.

3.3.1. Siloam Springs Investigations

UofA geotechnical investigations were performed at the Siloam Springs Arkansas Test Site (SSATS) from October 3 through October 6, 2011, and included field and laboratory testing on samples obtained from six (6) UofA boreholes and 13 AHTD boreholes (Figure 3.17a). The UofA field testing in conjunction with MODOT was performed on November 10, 2011, and included field testing at five (5) cone penetration test (CPT) soundings. Each sounding extended to a minimum depth below ground surface of 13.5 feet. A photograph of the stored samples from the SSATS is presented in Figure 13.7b.

(a) (b)

Figure 3.17. Photograph of (a) geotechnical investigations performed by UofA in conjunction with AHTD at Siloam Springs Arkansas Test Site, and (b) UofA stored rock cores and soil samples.

3.3.2. Turrell Investigations

UofA geotechnical investigations were performed at the Turrell Arkansas Test Site (TATS) from November 7 through November 9, 2011, and included field and laboratory testing on samples obtained from six (6) UofA boreholes and six (6) AHTD boreholes. A photograph of bulk sample collection from a Shelby tube is presented in Figure 3.18a. The UofA field testing in conjunction with MODOT was performed from October 19 through October 20, 2011, and included field testing at five (5) cone penetration test (CPT) soundings. Each sounding extended to a minimum depth below ground surface of 53 feet. A photograph of the MODOT CPT rig is presented in Figure 3.18b.

(a) (b)

Figure 3.18. Photograph of (a) bulk sample collection performed by UofA personnel at the TATS, and (b) MODOT CPT rig.

3.3.3. Monticello Investigations

UofA geotechnical investigations were performed at the Monticello Arkansas Test Site (MATS) from January 31st through February 1, 2012, and included field and laboratory testing on samples obtained from five (5) UofA boreholes and five (6) AHTD boreholes (Figure 3.19a). The UofA field testing in conjunction with MODOT was performed from October 8 through October 9, 2011, and included field testing at three (3) cone penetration test (CPT) soundings. Each sounding extended to a minimum depth below ground surface of 70 feet. A photograph of a typical UU triaxial compression sample acquired from the MATS is presented in Figure 3.19b.

(a) (b)

Figure 3.19. Photograph of (a) geotechnical investigations performed by UofA in conjunction with AHTD at Monticello Arkansas Test Site, and (b) UofA UU triaxial compression test sample.

3.4. Laboratory Testing

UofA personnel conducted conventional laboratory testing on all samples and advanced laboratory testing on select samples. Conventional laboratory testing included: Atterberg limits, moisture content, unit weight, grain size analysis, and specific gravity tests. Uniaxial unconfined compression testing was also performed on rock core samples at depths every five feet. Advanced laboratory testing consisted of unconsolidated-undrained (UU) triaxial compression testing on clay and consolidated drained (CD) triaxial compression testing on sands. Raw California split spoon sampler blow count values were correlated to standard blow count values utilizing the empirical transfer function presented in Figure 3.20.

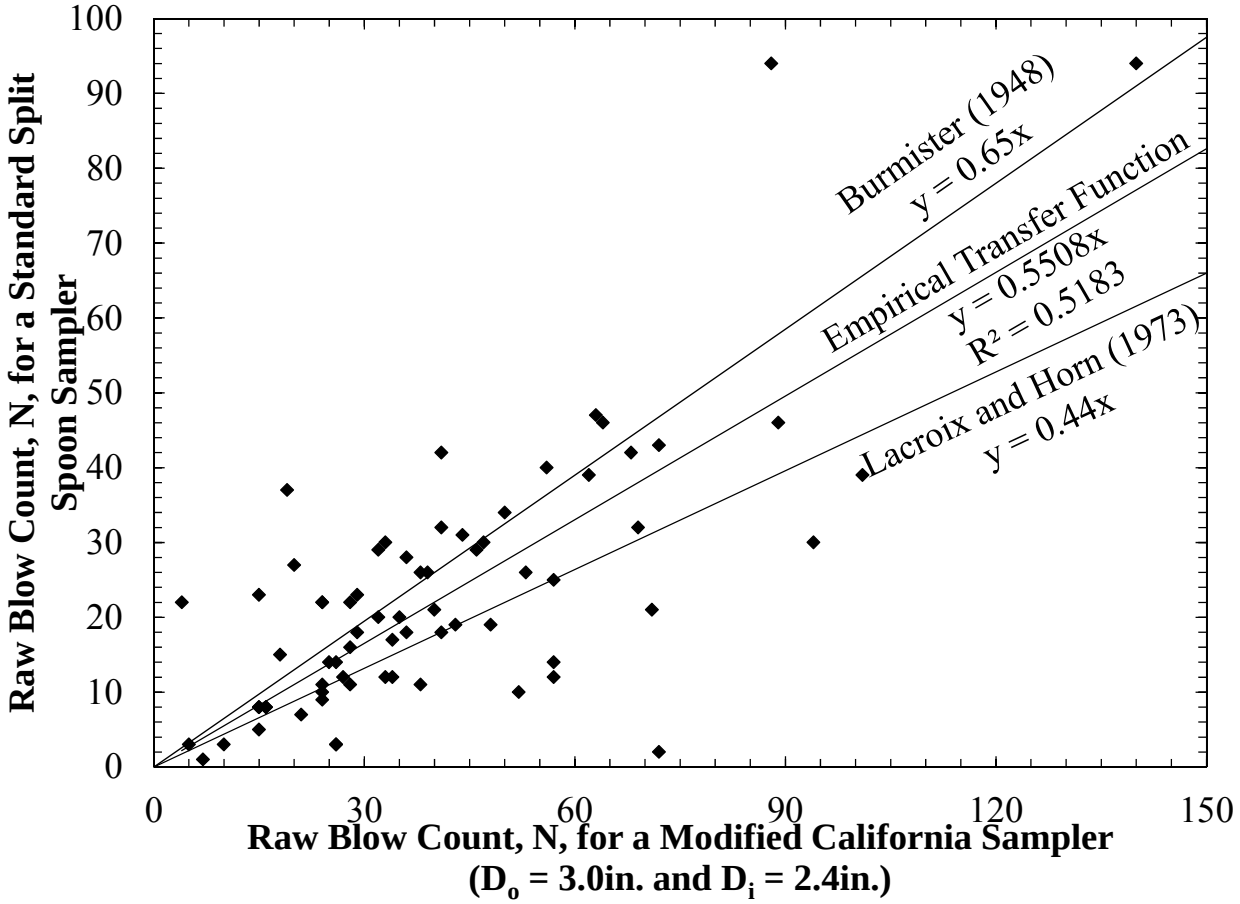

Figure 3.20. Empirical transfer function for raw blow count values utilized by UofA.

AHTD determined Atterberg limits and moisture contents in the laboratory, and unit weights from correlations described in Bowles (1977) with SPT standard split spoon blowcount values (Table 3.1). A summary of the combined sampling and testing methods conducted by both UofA and AHTD personnel is presented in Table 3.1.

Table 3.1. AHTD empirically correlated values for unit weight from blow count (from Bowles, 1977).

DESCRIPTION	VERY LOOSE	LOOSE	MEDIUM	DENSE	VERY DENSE
Relative Density Dr	0	0.15	0.35	0.65	0.85 1.00
Corrected Standard penetration no. "N'"		4	10	30	50
		28°	30°	36°	41°
Approx. angle of internal friction ϕ*	25-30°	27-32°	30-35°	35-40°	38-43°
Approx. range of moist unit weight (γ) pcf	70-100	90-115	110-130	110-140	130-150

Table 3.2. Sampling and testing methods performed by UofA and AHTD personnel.

Organization	Testing/Sampling Method	Geomaterial	ASTM
University of Arkansas (UofA)	Standard Penetration Testing (62 mm)		D1586
	California Spilt Spoon Sampler	Sand	
	Osterberg Hydraulic Fixed-Piston Sampler	Clay	
	Shelby Tube Sampler	Clay	
	Pitcher Barel Sampler	Stiff Clay/Soft Rock	
	Double Swivel Core Barrel Sampler	Rock	
	Cone Penetration Testing	Sand/Silt/Clay	D5778
	Unconsolidated Undrained Triaxial	Sand/Silt/Clay	D2850
	Consolidated Drained Triaxial Compression	Sand/Silt/Clay	D7181
	Grain Size Analysis	Sand/Silt/Clay	D422
	Wet and Dry Sieve	Sand/Silt/Clay	
	Hydrometers	Silt/Clay	
	Atterberg Limits	Silt/Clay	D4318
Arkansas State Highway and Transportation Department (AHTD)	Standard Penetration Testing (30 mm)		D1586
	Standard Split Spoon Sampler	Sand	
	Core Barrel Sampler	Rock	
	Atterberg Limits	Silt/Clay	D4318

3.5. Conclusion

The site conditions and geotechnical investigations performed at each test site were discussed. The Siloam Springs Arkansas Test Site was determined to be located in the alluvial plain of the Illinois River, underlain by the Boone Formation underlain by the Chattanooga Shale Formation. The Turrell Arkansas Test Site was determined to be located in the depositional plain of the Mississippi Embayment, underlain by alluvium and Crowley's Ridge sand. The stratigraphy at the Turrell Arkansas Test Site was additionally identified as being susceptible to liquefaction due to its proximity to the New Madrid Fault Zone. The Monticello Arkansas Test Site was determined to be located within the Gulf Coastal Plain of the Mississippi Embayment, underlain by Terrace deposits.

Geotechnical investigations were performed at each test site location by personnel from the UofA, AHTD, and MODOT. UofA in-situ testing/sampling methods consisted of SPT testing with a California split spoon in cohesionless soils. An Osterberg hydraulic fixed piston, Shelby tube sampler, and pitcher barrel sampler were utilized in cohesive soils. Additionally, a double swivel core barrel sampler was utilized in rock. AHTD in-situ testing/sampling methods consisted of SPT testing with a standard split spoon in all soils, and double swivel core barrel sampler in rock. MODOT in-situ testing (on behalf of the UofA) was performed using a CPT apparatus for cohesive and cohesionless soils. Soil properties (i.e. unit weight, moisture content, friction angle, percent fines, plasticity index, shear strength, and uniaxial compressive strength) were determined from conventional and advanced laboratory testing following the UofA sampling method. Select AHTD soil engineering properties (i.e. moisture content, plasticity index, and percent fines) were determined from conventional laboratory testing. All other AHTD

soil engineering properties were determined utilizing Bowles (1977) by correlating values of SPT blow-counts.

Chapter 4: Predictive and Cost-benefit Methods

4.1. Introduction

Discussions of the predictive methods utilized to determine drilled shaft ultimate axial capacity for each site are presented in this chapter. Prior to performing the predictions, a database was developed that contained the engineering soil properties that were obtained from the UofA, AHTD, and MODOT methods (Section 4.2). Ultimate axial capacities were then predicted by inputting these values [including mean, mean plus one standard of deviation (mean +1 SD), and mean minus one standard of deviation (mean -1 SD)] into predictive software programs (Ensoft SHAFTv2012, Bridge Software Institute FB-Deep, and in Microsoft Excel®), as discussed in Section 4.3. From the generated outputs, ultimate axial capacities were then compared, as a function of depth, to determine the effects of each predictive software program.

Included within Section 4.3 is a discussion of the methodology utilized to compare methods for predicting the ultimate axial capacity in rock. Empirically determined methods, including O'Neill and Reese (1999), Horvath and Kenney (1979), Rowe and Armitage (1987), etc., for predicting unit side friction and end bearing resistance in rock were compared utilizing a spreadsheet, for the Siloam Springs Arkansas Test Site (SSATS). Ultimate axial capacities were then compared as a function of depth to determine the effects of each predictive method and input range (mean, mean +1 SD, and mean -1 SD). Results of these comparisons are discussed in Chapter 7.

A description of the methodology utilized to perform the cost-benefit analysis for UofA and AHTD sampling and testing methods is presented in Section 4.5. Also included within this section is a discussion regarding the methodology utilized to perform the fiscal impact analysis associated with each sampling and testing method for different levels of infrastructure.

4.2. Engineering Properties Database

Prior to the prediction of the ultimate axial capacities for each of the proposed drilled shafts, an engineering properties database was developed for each site. This database contained the mean, mean +1 SD, and mean -1 SD engineering property values, as a function of depth, for each sampling method at each site. Depending on the site, these engineering properties included some or all of the following:

a) corrected blow count (N_{60}),
b) total unit weight (γ_t),
c) undrained shear strength (c_u),
d) friction angle (ϕ),
e) CPT tip resistance (q_c),
f) shear wave velocity measurements (V_s),
g) uniaxial unconfined compressive strength (q_u) [only for Siloam Springs],
h) uniaxial tensile strength (q_b) [only for Siloam Springs],
i) modulus of elasticity (E_m) [only for Siloam Springs], and
j) rock quality designation (RQD%) [only for Siloam Springs].

To simplify the input process, engineering properties were compiled in units specific to each technology. Values of uniaxial tensile strength of rock at a given depth were calculated as being one-half of the value of the uniaxial unconfined compressive strength of the rock. In some instances, the values for a given depth were unavailable (as indicated by red text). As a result, the value was determined from the average of the nearest top and bottom value. Water content and other soil index properties were also utilized to help identify strata. A screen-shot of a portion of the complied database is presented in Figure 4.1.

Monticello	Depth	N60			Unit Weight			FB Cu-DIR		
		Mean	1+	-1	Mean	1+	-1	Mean	1+	-1
	[ft]	[blows]	[blows]	[blows]	[pcf]	[pcf]	[pcf]	[tsf]	[tsf]	[tsf]
	5.5	48	75	21	148.00	152.47	143.53	2.350	3.661	1.039
	11.5	36	43	29	148.00	152.47	143.53	1.750	2.087	1.413
	16.5	31	42	20	144.00	149.48	138.52	1.525	2.056	0.994
	21.5	34	56	12	144.00	152.94	135.06	1.675	2.740	0.610
	26.5	32	46	19	140.00	147.07	132.93	1.328	1.721	0.935
	31.5	33	38	27	122.00	138.43	105.57	1.625	1.625	1.625
	36.5	37	49	26	120.00	127.07	112.93			
	41.5	16	20	11	134.00	139.48	128.52	0.775	0.999	0.551
	46.5	14	17	10	132.00	136.47	127.53	0.675	0.843	0.507
	51.5	22	33	10	138.00	146.37	129.63	1.063	1.614	0.511
	56.5	22	25	18	140.00	140.00	140.00	1.050	1.206	0.894
	61.5	37	52	23	120.00	127.07	112.93			
	66.5	41	65	18	118.00	126.37	109.63			
	71.5	38	53	23	120.00	127.07	112.93			
	76.5	40	47	32	118.00	122.47	113.53			
	81.5	41	54	29	120.00	127.07	112.93			
	86.5	38	50	26	120.00	127.07	112.93			
	91.5	37	42	33	120.00	120.00	120.00			
	96.5	48	61	35	124.00	129.48	118.52			
	101.5	48	53	42	122.00	126.47	117.53			
Source		From Field Data 2012 Tab : California vs Standard			From Field Data 2012 Tab: AHTD Data			From Field Data 2012 Tab: California vs Standard		

Figure 4.1. Screenshot of engineering properties database utilized for AHTD drilled shaft axial capacity prediction at the Monticello Arkansas Test Site.

4.2.1. Siloam Springs Rock Engineering Properties

Rock properties of interest at the Siloam Springs Arkansas Test Site included q_u, q_b, RQD%, and E_m, as obtained following the UofA drilling and sampling method to a depth of 100 feet below ground surface. Following the AHTD drilling and sampling methodology, RQD values were only collected to a depth of 38 feet below ground surface. Below 38 feet engineering properties were assumed to be constant for values obtained from the AHTD method. Due to the nature of CPT testing, rock engineering property values were not obtained following the MODOT drilling and sampling procedures.

4.2.2. MODOT Acquired Soil Engineering Properties at the Turrell Arkansas Test Site

MODOT obtained values of soil engineering properties at the Turrell Arkansas Test Site (TATS) were assumed to be constant below a depth of 71.5 feet below ground surface. These constant values were attributed to a maximum CPT sounding depth of 71.5 feet. The sounding was terminated prematurely to prevent equipment damage that was possible due to the dense sand strata encountered at that depth.

4.3. Predictive Technologies

Values injested into the Ensoft SHAFTv2012 software program, Bridge Software Institute FB-Deep software program, and the Microsoft Excel® spreadsheet were acquired from the aforementioned generated engineering properties database (Section 4.3.3). For completeness, a general background of the Ensoft SHAFTv2012 and Bridge Software Institute FB-Deep was previously presented in Chapter 2. Selected data from the generated output file from each program/spreadsheet, for each site, and from each geotechnical investigation methodology (UofA, MODOT, AHTD) were then compiled (Section 4.3.4) and compared (Section 4.3.5). A matrix illustrating the different combinations of inputs required for the calculations of ultimate axial capacity for each of the drilled shafts, and comparisons between the different methods, is presented in Table 4.1.

Table 4.1. Input combinations for SHAFTv2012, FB-Deep, and the developed spreadsheet for each four and six foot diameter drilled shaft.

For Each Four-foot and Six-foot Diameter Shaft							
FB-Deep				SHAFT - Friction Angle			
Test Site	Monticello	Siloam	Turrell	Test Site	Monticello	Siloam	Turrell
UofA	Mean	Mean	Mean	UofA	Mean	Mean	Mean
	1	1	1		1	1	1
	-1	-1	-1		-1	-1	-1
AHTD	Mean	Mean	Mean	AHTD	Mean	Mean	Mean
	1	1	1		1	1	1
	-1	-1	-1		-1	-1	-1
ODOT - c_u direct in	Mean	Mean	Mean	MODOT	Mean	Mean	Mean
	1	1	1		1	1	1
	-1	-1	-1		-1	-1	-1
MODOT - c_u q_c inp	Mean	Mean	Mean	SHAFT - Blow Count			
	1	1	1	Test Site	Monticello	Siloam	Turrell
	-1	-1	-1	UofA	Mean	Mean	Mean
Spreadsheet					1	1	1
Test Site	Monticello	Siloam	Turrell		-1	-1	-1
UofA	Mean	Mean	Mean	AHTD	Mean	Mean	Mean
	1	1	1		1	1	1
	-1	-1	-1		-1	-1	-1
AHTD	Mean	Mean	Mean	MODOT	Mean	Mean	Mean
	1	1	1		1	1	1
	-1	-1	-1		-1	-1	-1
MODOT	Mean	Mean	Mean				
	1	1	1				
	-1	-1	-1				

4.3.1. Data Entry

The data entry process for each of the predictive methods is presented in this section. Discrepancies between each program/spreadsheet are noted. Additionally, special requirements, assumptions, and proprietary omissions noted during the data entry process for each program/spreadsheet are discussed.

4.3.1.1. SHAFTv2012

Utilizing SHAFTv2012, the ultimate axial capacity predictions for drilled shafts were calculated in English units. In noncohesive soils, the SHAFT program utilized a linear interpolation from zero values at ground surface to the maximum values at ten pile diameters below ground surface. In cohesive soils, a five foot upper exclusion zone was specified, as recommended in O'Neill and Reese (1999). At the Siloam Springs, Turrell, and Monticello Arkansas Test Sites, a water table elevation of ten, ten, and thirty-five feet below ground surface, respectively, was input for each prediction. SHAFTv2012 enables the user to specify a corrected blow count (N_{60}) or friction angle (ϕ) value to determine the axial capacity for a given drilled shaft. As a result, two predictions (one based on N_{60} values and one based on ϕ values) for each site were performed.

Upon creating a new file in within the SHAFT program, a soil profile was created and values were entered. The soil layer data window (as indicated by the layered icon presented in Figure 4.2) first requires a soil type selection. The dropdown window allowed for the selection of nine possible soil types using the SHAFT program. At the Siloam Springs Arkansas Test Site, "clay (FHWA Spec.)" was selected to a depth of 16 feet below ground surface. Below a depth of 16 feet, "strong rock (side friction + end bearing)" was selected to a depth of 50 feet. At the Turrell Arkansas Test Site, "clay (FHWA Spec.)" was selected to a depth of 30 feet below ground surface. Below a depth of 30 feet, "sand (FHWA Spec.)" was selected to a depth of 99.5 feet. At the Monticello Site, "clay (FHWA Spec.)" was selected to a depth of 27 feet below ground surface. From 27 feet to 37 feet, "sand (FHWA Spec.)" was selected, and from 37 to 56 feet, "clay (FHWA Spec.)" was selected. Below a depth of 56 feet, "sand (FHWA Spec.)" was selected as the soil type to a depth of 100.5 feet.

Following the layer selection, the depth of the bottom of each of the selected soil layers was then entered. Ror the UofA testing results, the geomaterial layer depths were designated at increments of five feet (exempting geomaterial interface layers). For the AHTD testing results, geomaterial layer depths were also designated at increments of five feet in soil. In rock however, the geomaterial layer depths for the AHTD testing results were variable. For the MODOT testing results, the soil layers at the Siloam Springs Arkansas Test Site were designated at increments of 1.5 feet, while soil layers at the Turell and Monticello Arkansas Test Sites were designated at increments of five feet. A screenshot of the soil layer data entry interface (for the Siloam Springs Site with the mean values of the UofA data) is presented in Figure 4.2.

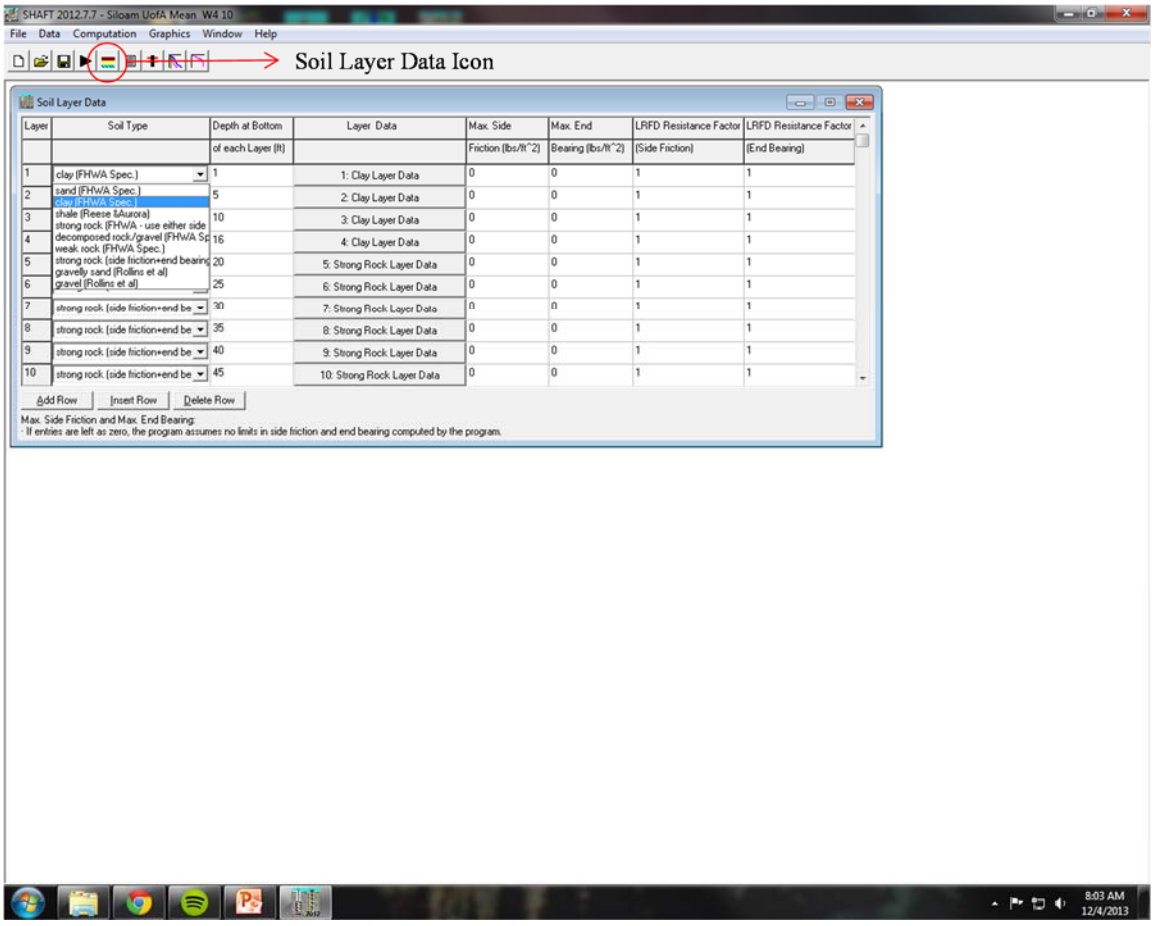

Figure 4.2. Screenshot of the SHAFT soil layer data entry interface for the Siloam Springs UofA mean testing and sampling method.

Following the selection of the depth of each layer, the individual soil layer data was then entered. For clay layers, values of total unit weight, and cohesion were required. Blow count values, alpha factors, and bearing capacity coefficients were not entered due to alpha values and bearing capacity coefficients being internally generated by the program. Due the presence of cohesion values, blow count values were not required for analysis. A screenshot of the clay layer data entry interface window (for the SS-W4 shaft at the Siloam Springs site using the UofA data) is presented in Figure 4.3.

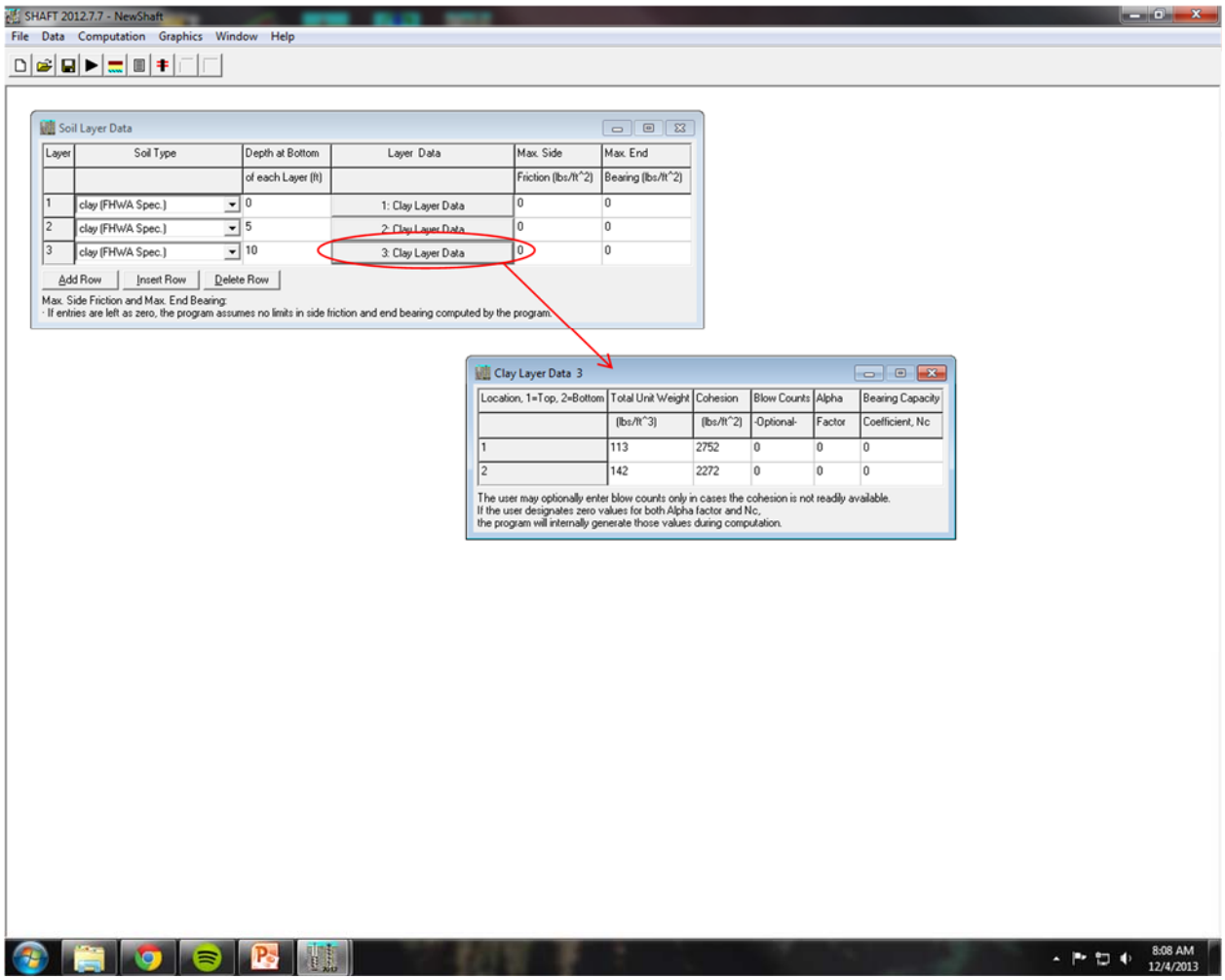

Figure 4.3. Screenshot of the SHAFT clay layer data entry interface for the Siloam Springs UofA mean sampling and testing program.

For sand layers, values of total unit weight, and friction angle or blow count, were entered. Values of K_o and beta were not entered, because they were internally generated by the program. Two separate files (one with entered blow count values and one with entered friction angle values) were generated for the Turrell and Monticello Arkansas Test Sites for each drilling and sampling method and each statistical sampling of the data. A screenshot of the sand layer data entry interface window (for the four-foot diameter shaft at the Monticello site for the UofA drilling and statistical sampling method) is presented in Figure 4.4.

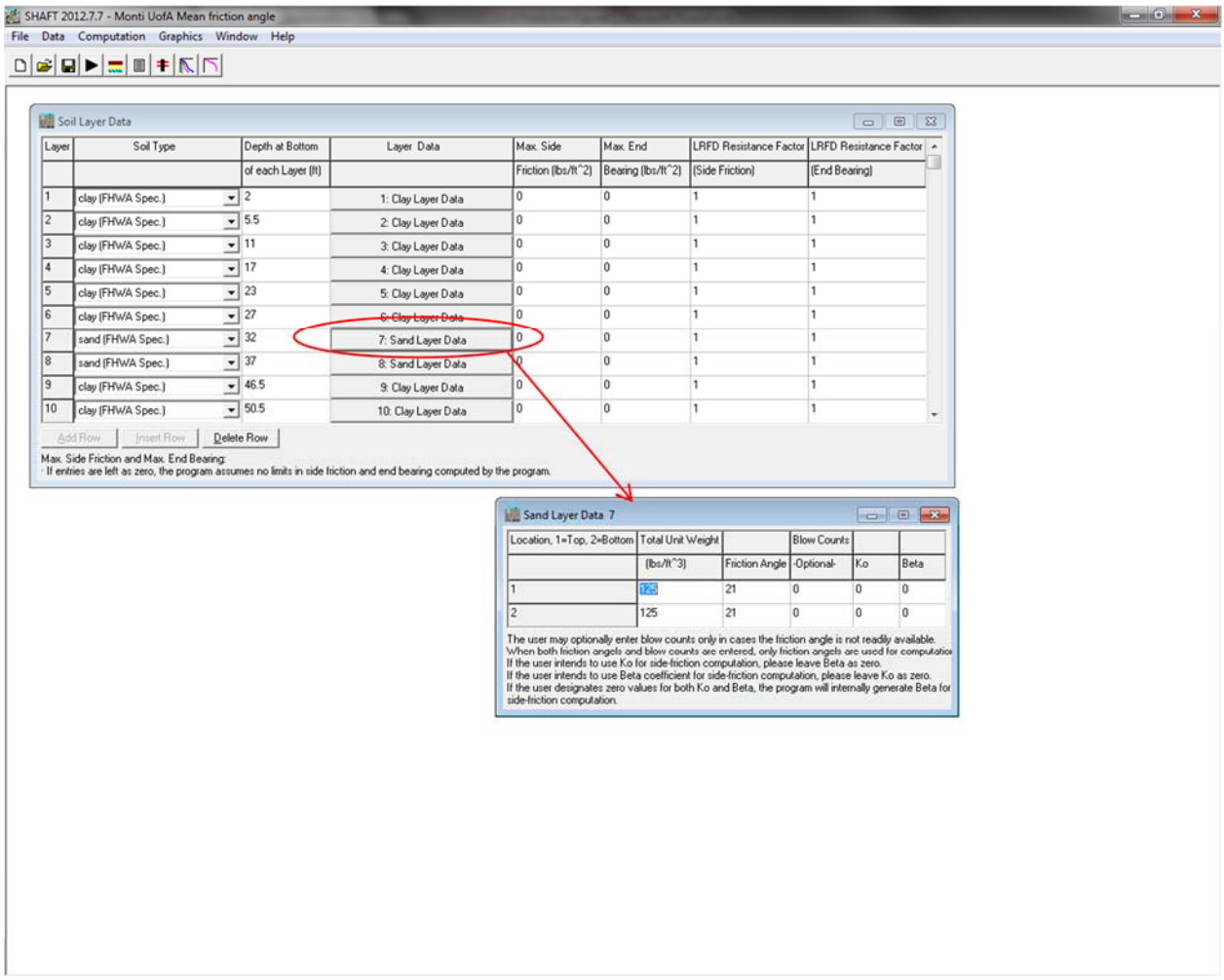

Figure 4.4. Screenshot of the SHAFT sand layer data entry interface for the Monticello UofA mean drilling and sampling method.

For rock layers encountered at the Siloam Springs Site, input parameters of uniaxial unconfined compressive strength, concrete compressive strength, rock joint discontinuity spacing, rock joint discontinuity thickness, elastic modulus, socket diameter, and RQD% were entered. All of the concrete compressive strength values were input as the minimum AHTD required value of 504000 psf. Values of rock joint discontinuity spacing and thickness were not determined by personnel during any of the testing/sampling programs. To acquire values for this necessary input field, a sensitivity analysis was performed. Values of six feet and 0.0001 feet for rock joint discontinuity spacing and rock joint discontinuity thickness, respectively, were selected to be entered for among the values obtained from each drilling and sampling program. Additionally, a socket diameter of 4 feet and 6 feet was entered for each four- and six-foot diameter shaft setup, respectively. An example screenshot of the SHAFT rock layer input interface for mean values of the UofA obtained data at the Siloam Springs Arkansas Test Site for the SS-W4 shaft is presented in Figure 4.5.

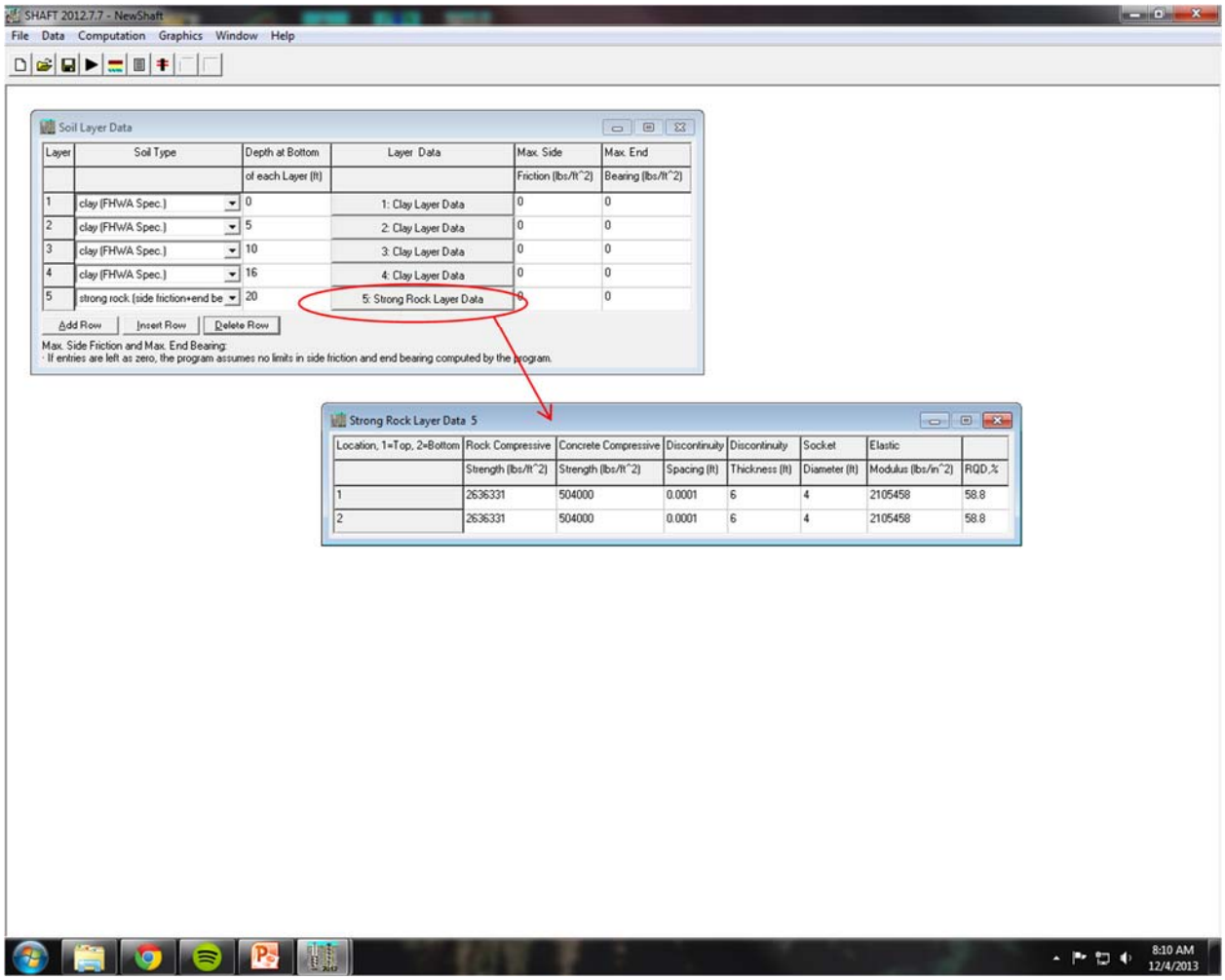

Figure 4.5. Screenshot of the SHAFT rock layer data entry for mean values of the UofA obtained data at the Siloam Springs Arkansas Test Site.

Upon the creation of a given soil profile, the boundary conditions of the drilled shaft were defined. The drilled shaft properties entry window (as navigated to from the data tab in Figure 4.6) enables the user to enter the geometric characteristics of the shaft, as well as input a shaft modulus of elasticity. For each case, a straight shaft was selected with a minimum and maximum diameter equal to either four or six feet. An upper exclusion zone of five feet was entered for each case, as well as a modulus of elasticity of 3372165 psi. This values was selected as a function of the input concrete compressive strength. A screenshot of the SHAFT drilled-shaft properties screen with the UofA obtained mean values at the Siloam Springs Arkansas Test Site

is presented (Figure 4.6). A summary of the input SHAFT geometries for each site is presented (Table 4.2). Two predictions were completed at the Siloam Springs and Turrell Arkansas Test Sites – the first prediction with as-designed lengths, and the second prediction with as-constructed lengths.

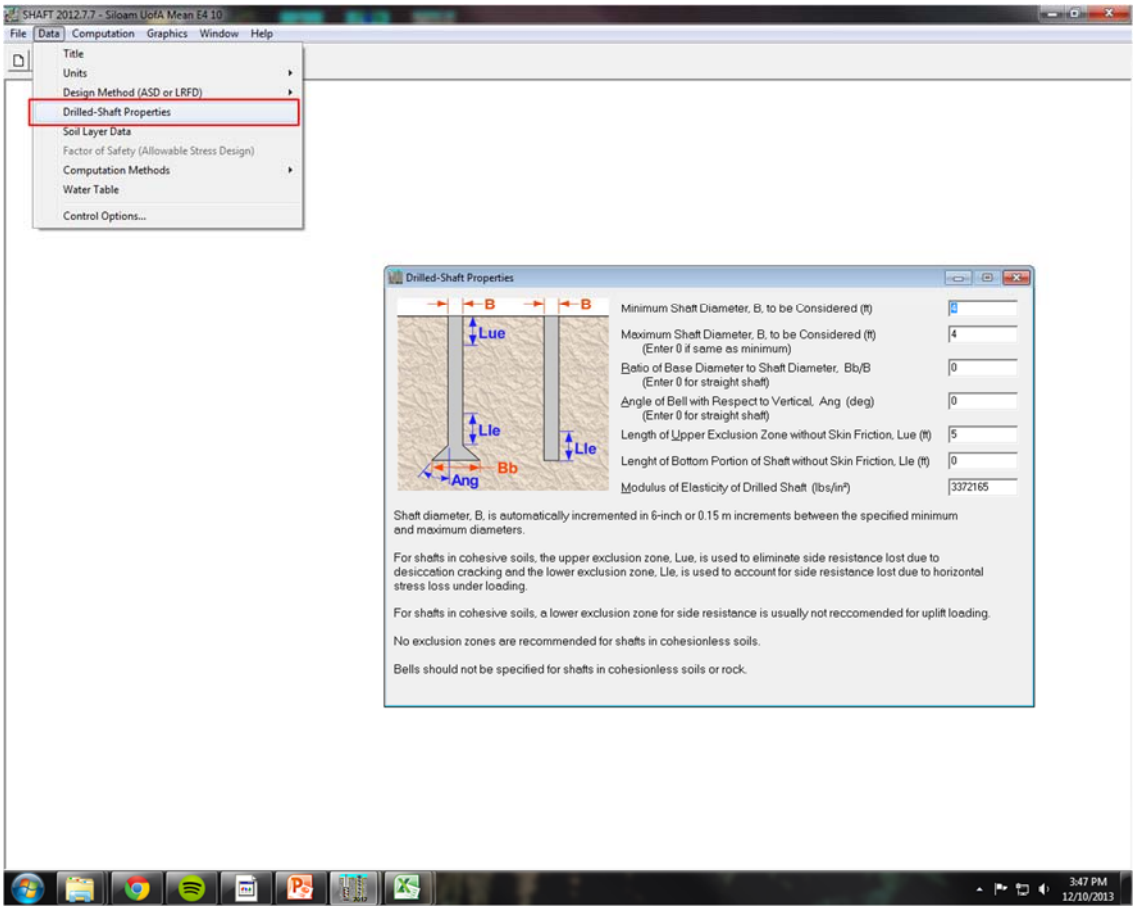

Figure 4.6. Screenshot of the SHAFT drilled-shaft properties screen for the UofA obtained mean values for a four-foot diameter shaft at the Siloam Springs Arkansas Test Site.

Table 4.2 SHAFT entered shaft geometries for the Siloam Springs, Turrell, and Monticello Arkansas Test Sites.

Test Site	Shaft ID	Total Length [ft]	Diameter [in]	Increments [ft]
Siloam Springs	SS-E4	23*	48	1
	SS-W4	26*	48	1
	SS-C6	21*	72	1
Turrell	T-N4	88.0*	48	1
	T-S4	86.5*	48	1
	T-C6	61.5*	72	1
Monticello	M-?4	91.5	48	1
	M-?4	91.5	48	1
	M-C6	72	72	1

*Pending on Construction

Following the entry of the drilled-shaft properties and soil layer data, values were validated and an "elevation view" of the shaft geometry within the soil profile was generated. This elevation view was utilized to further identify errors in the data entry. The drilled shaft geometry, as illustrated in relation to the designated soil profile, is presented in the "elevation view" window, and is designated by the icon indicated in Figure 4.7.

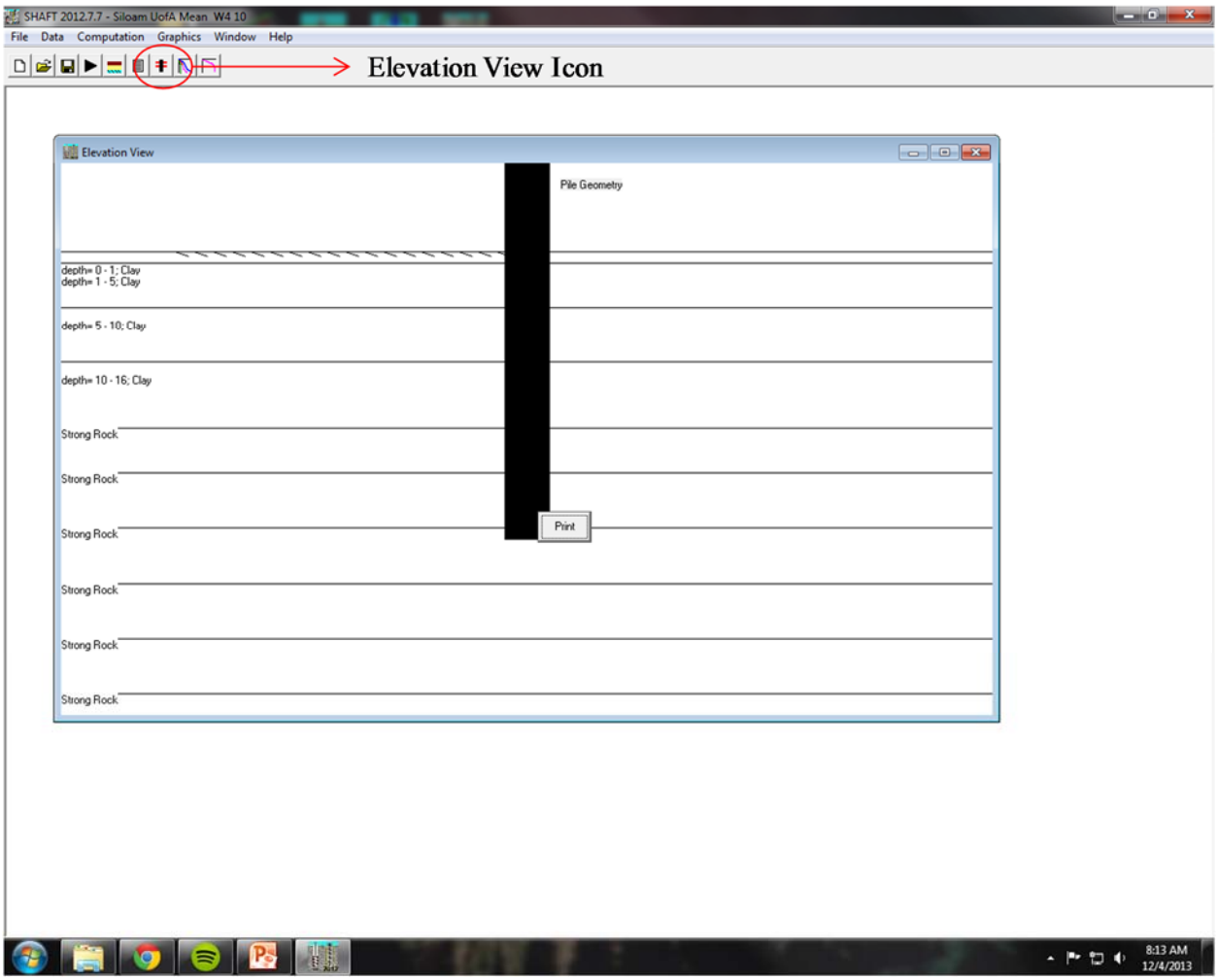

Figure 4.7. Screenshot of the SHAFT "elevation view" window for the UofA data for a four-foot diameter shaft at the Siloam Springs Arkansas Test Site.

Following data entry in SHAFT, the output capacity for each drilled shaft configuration was generated by clicking on the computation icon shown in Figure 4.8. Upon a successful completion of the computational analysis, the message presented in Figure 4.8 is displayed in SHAFT. Major errors in data entry prevented an output file from being generated. Minor errors were directly addressed in the output file. Specifically, if the previously entered soil property values were outside the pre-determined range of acceptable values for a given soil type, it was noted in the output file. At the Siloam Springs Site in particular, values of unit weight at the clay/rock interface were selected as being higher than the maximum accepted value for the clay

soil type. This error was ignored, because the values that were entered were directly measured and deemed suitable for unit weights at that given interface.

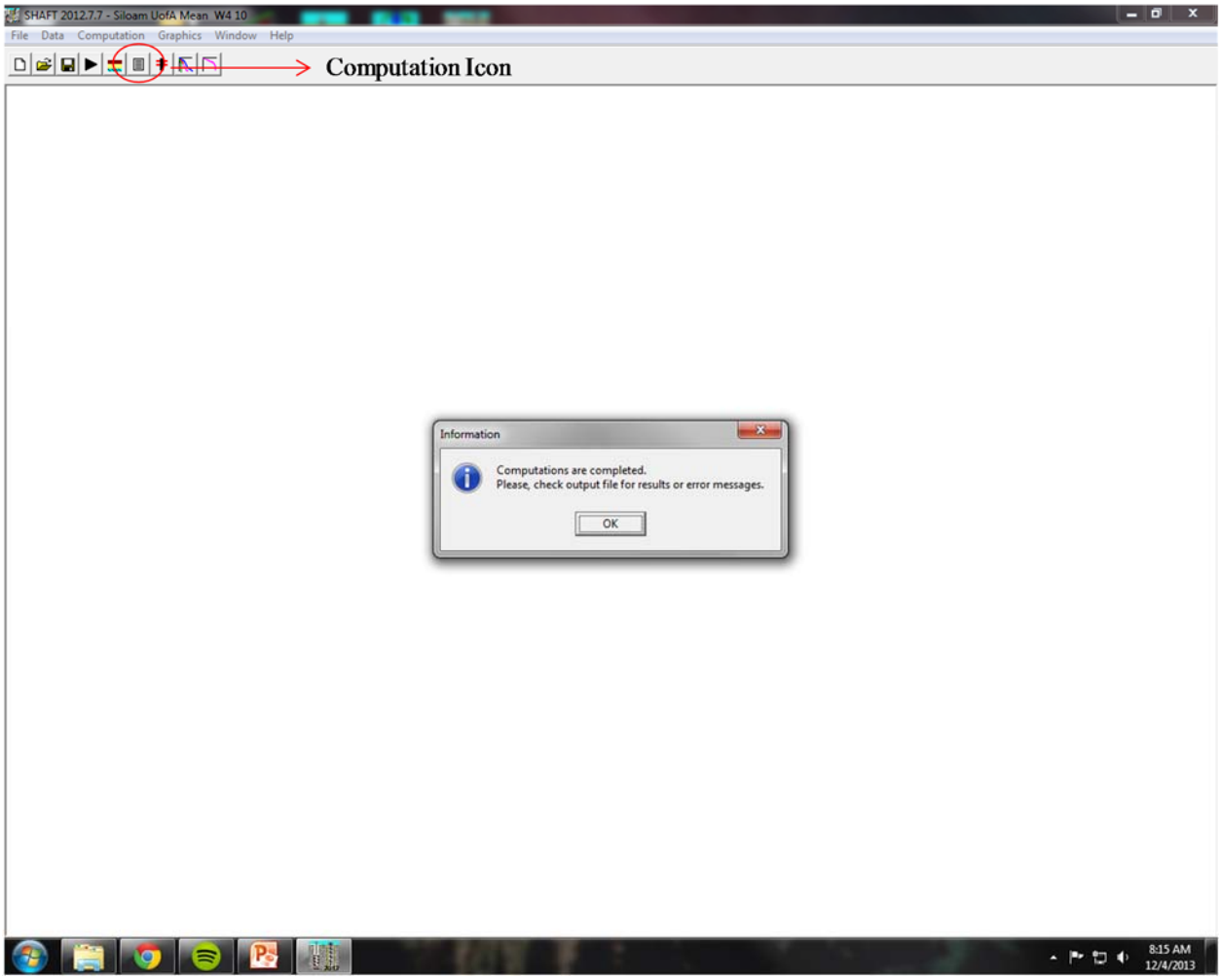

Figure 4.8. Screenshot of an example of a SHAFT successful computational output message.

Following acquisition of measured displacement values, utilizing iterations from the SHAFT program, modified predicted values of axial capacity were generated using load-settlement plots, as presented in Figure 4.9. At a displacement of 0.15 percent, a value of predicted axial capacity was selected following the regression of the load-settlement curve for each shaft. Note this selected value was significantly smaller than the original value generated for a displacement of 5 percent of the drilled shaft diameter.

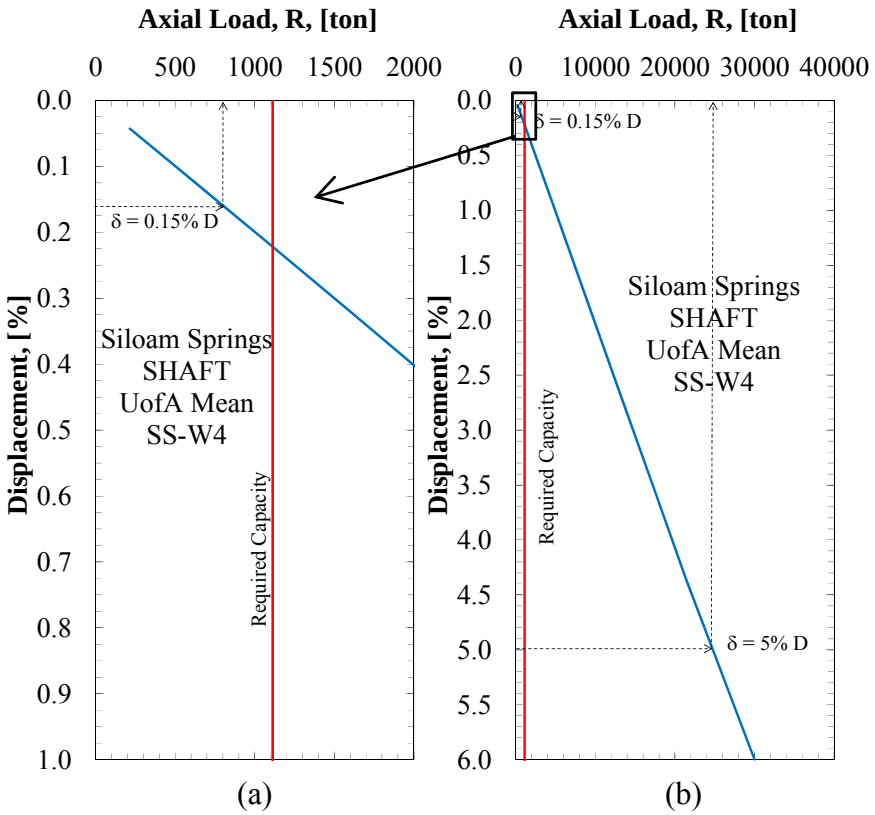

Figure 4.9. SHAFT-generated values of axial capacity from a load-settlement curve for Test Shaft SS-W4 at the SSATS at (a) 0.15 percent shaft diameter and (b) 5 percent shaft diameter.

4.3.1.2. FB-Deep

Utilizing FB-Deep, ultimate axial capacity predictions of the drilled shafts were calculated in English units. Upon creating a new file in FB-Deep, a soil profile was entered. The boring log entry window (as indicated by the layered icon shown in Figure 4.10) required the addition of a new soil layer. New soil layers were added by clicking "Insert Layer" within the boring log screen, as presented in Figure 4.11. The depth below the ground surface corresponding to the bottom of each newly created soil layer was then entered. The same soil layer thicknesses that were utilized in SHAFT (Section 4.3.1.1) were also utilized in FB-Deep.

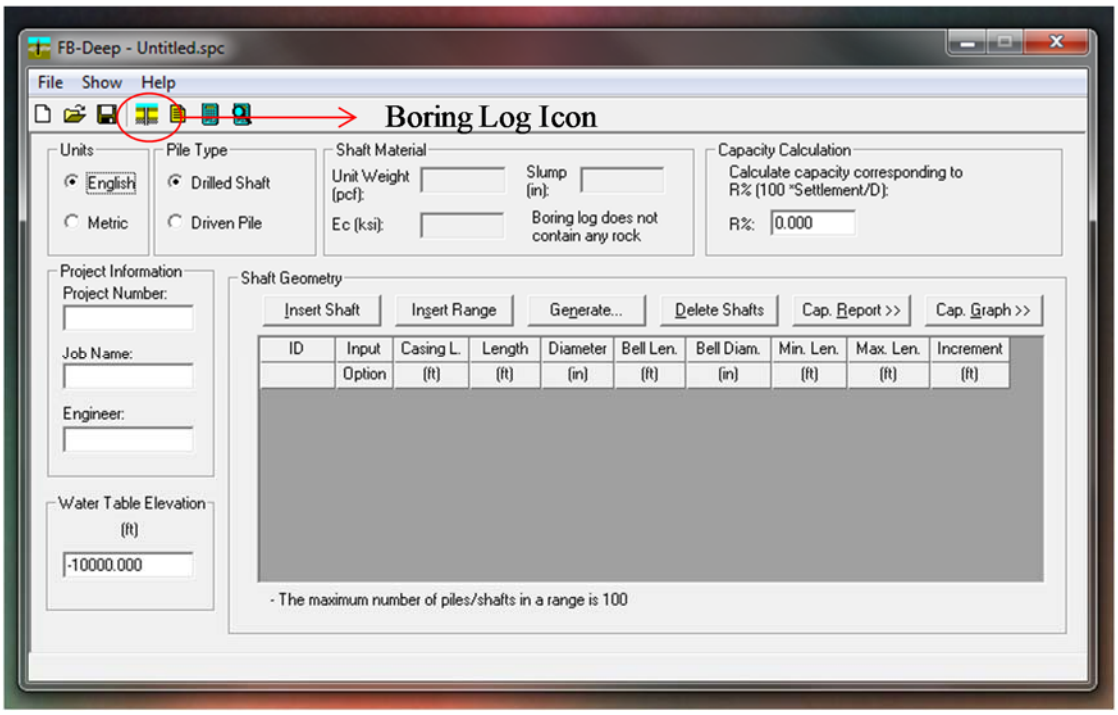

Figure 4.10. Screenshot of the FB-Deep user interface.

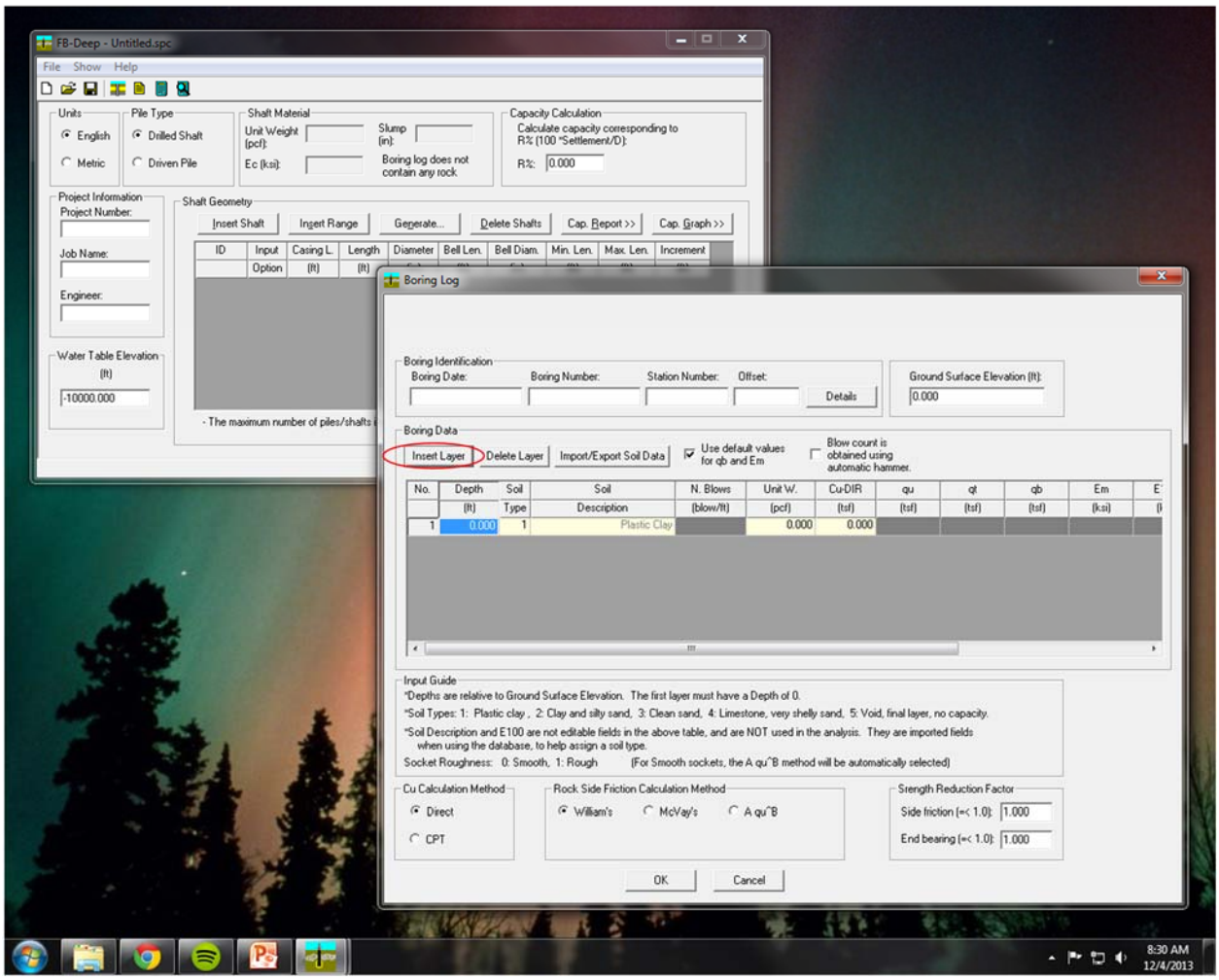

Figure 4.11. Screenshot of the FB-Deep boring log user interface.

Following input of the layer thickness, the soil description was then selected. Five possible soil types were available for selection within FB-Deep. Plastic clay, clean sand, and limestone strata were designated as soil types 1, 3, and 4, respectively. However, in FB-Deep, soil type 4 was classified as "Limestone, very shelly sand". This classification indicates predicted capacities for the limestone may be conservative..

A ground surface elevation of zero feet was specified for all predictions. At the Siloam Springs Arkansas Test Site, Soil Type 1 "plastic clay" was selected to a depth of 16 feet below ground surface. Below a depth of 16 feet, Soil Type 4 "limestone, very shelly sand" was selected

to a depth of 100 feet. At the Turrell Arkansas Test Site, Soil Type 1 "plastic clay" was selected to a depth of 30 feet below ground surface. Below a depth of 30 feet, Soil Type 3 "clean sand" was selected to a depth of 99.5 feet. At the Monticello Site, Soil Type 1 "plastic clay" was selected to a depth of 27 feet below ground surface. From 27 to 37 feet, Soil Type 3 "clean sand" was selected, and from 37 to 56 feet, Soil Type 1 "plastic clay" was selected. Below a depth of 56 feet, Soil Type 3 "clean sand" was selected to a depth of 100.5 feet.

Following entry of the soil type, individual soil layer data was entered. For clay layers, the method of undrained shear strength calculation was designated (c_u calculation method) within a box located in the boring log entry window (Figure 4.12). Utilizing the direct undrained shear strength (c_u) calculation method, values of total unit weight, and cohesion were entered. Utilizing the CPT c_u calculation method, values of unit weight and CPT tip resistance (q_c) were required. Two predictions for the MODOT sampling and testing method were performed at each site (one prediction utilized the calculated c_u values, and one prediction utilized the measured q_c values). A screenshot of the clay layer data entry interface for the direct c_u calculation method is presented in Figure 4.12. For the MODOT testing and sampling method, calculated c_u values were obtained from Robertson (2012) utilizing values of q_c and effective vertical stress.

$$c_u = \frac{q_c - \sigma'_{vo}}{N_k} \qquad \text{(Robertson, 2012)} \qquad \textbf{Equation 4.1}$$

Where: c_u = undrained shear strength (ksf),

q_c = CPT tip resistance (ksf),

σ'_{vo} = effective vertical stress for a given depth (ksf), and

N_k = 14 for normally consolidated clays, 18 for over consolidated clays.

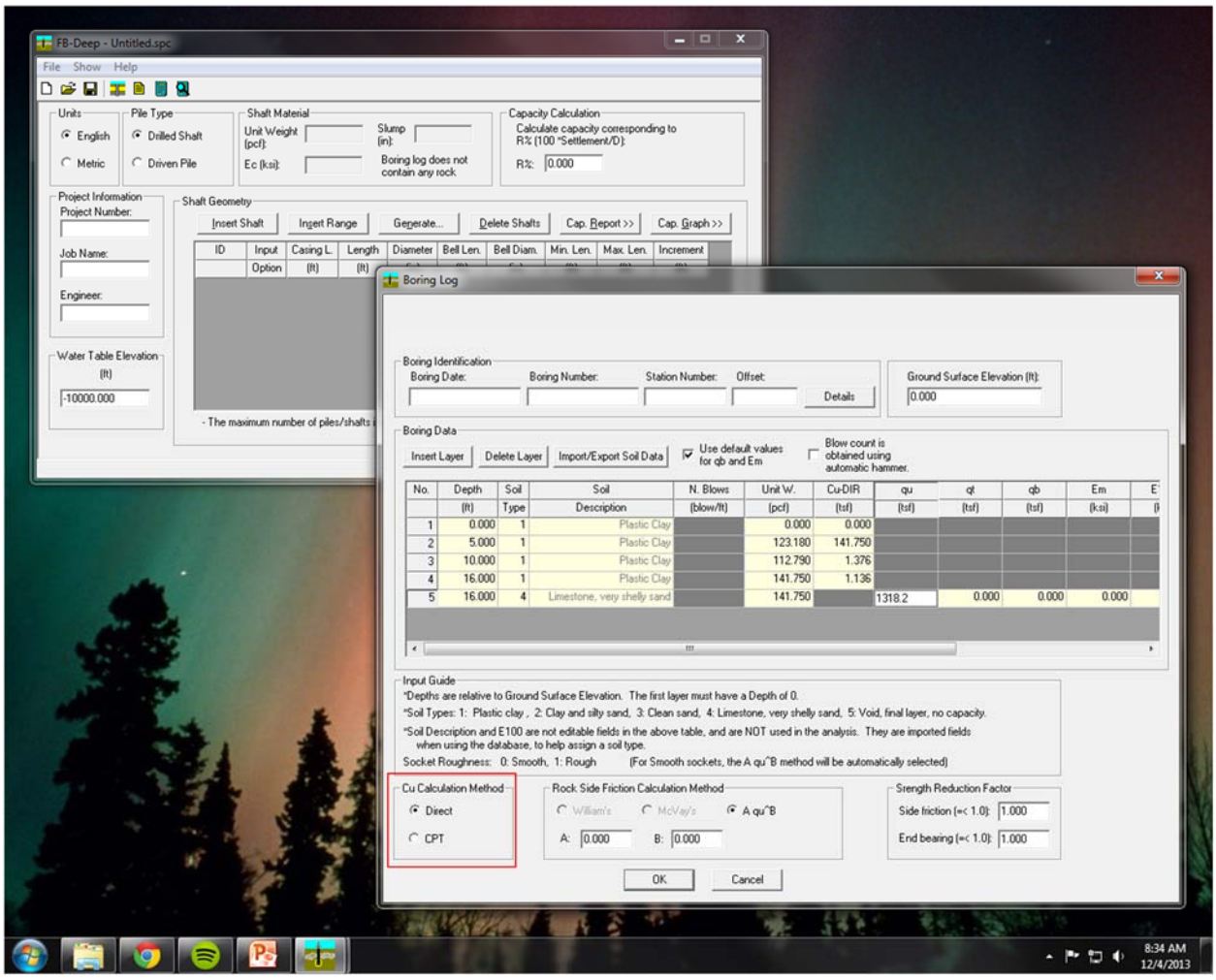

Figure 4.12. Screenshot of the FB-Deep plastic clay, via direct c_u calculation method, entry fields.

For the rock layers encountered at the Siloam Springs Site, input parameters of uniaxial unconfined compressive strength (qu), elastic modulus (E_m), RQD%, and socket roughness were entered. A selection of a rock side friction calculation method was also required. All shaft socket roughnesses were entered as smooth. As a result, all rock side friction calculation methods were pre-specified as "A qu^B" by the program. Values of A and B were input as 0.670 and 0.50, respectively, in accordance with O'Neill and Reese (1999) and Horvath and Kenney (1979). The "A qu^B" method was selected as being the most similar to the modified method specified in AASHTO (2012). In AASTHO (2012), a reduction factor (α) which varies with

RQD% is applied to the value of unit skin friction resistance that is otherwise calculated using O'Neill and Reese (1999), and Horvath and Kenney (1979). However, because the FB-Deep program is proprietary and it is unknown how the program utilizes required input values of RQD%, the AASTHO (2012) method was not selected. An example screenshot of the FB-Deep rock layer input interface for the mean values obtained by the UofA drilling and sampling procedures at the Siloam Springs Arkansas Test Site is presented in Figure 4.13.

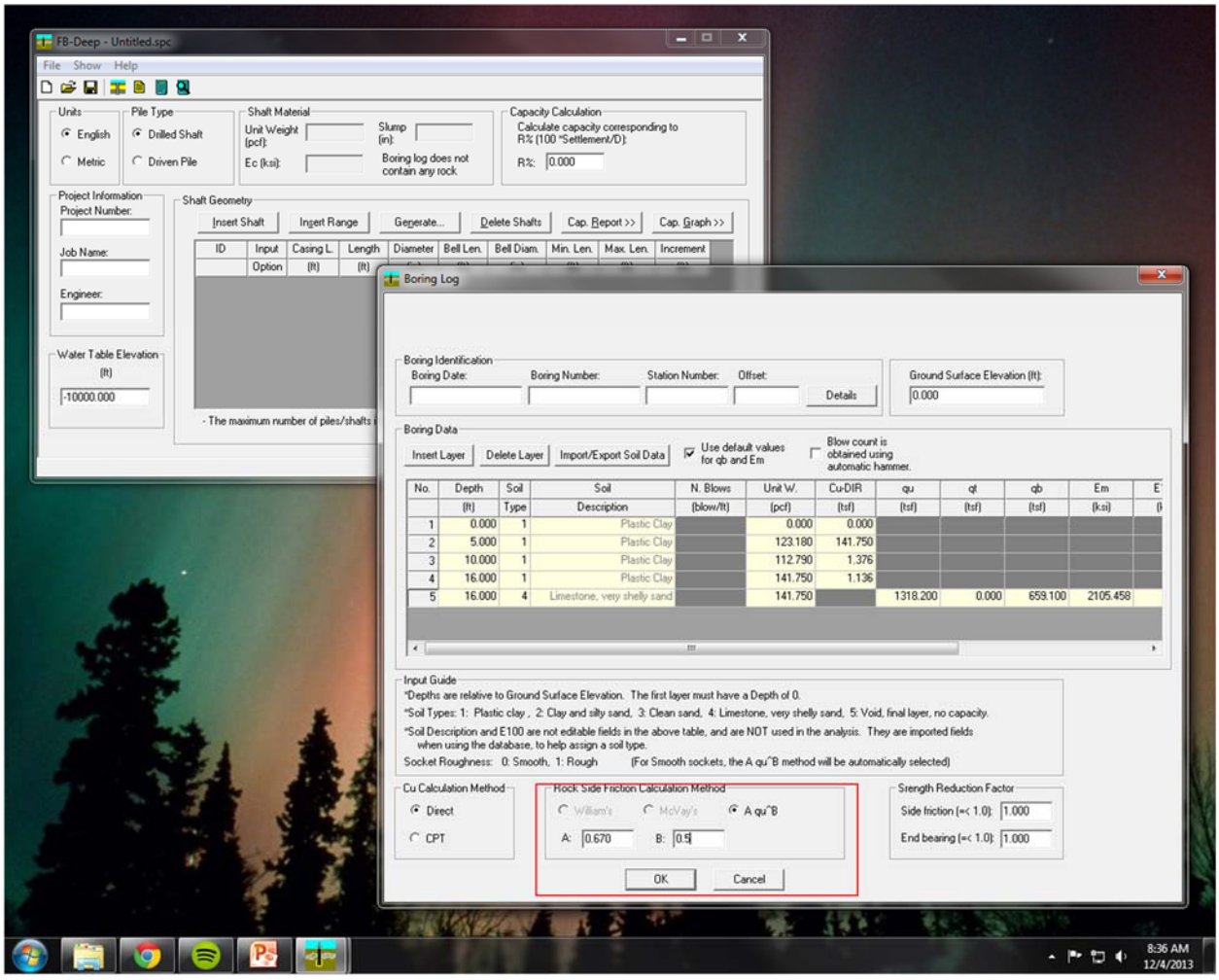

Figure 4.13. Screenshot of the FB-Deep Soil Type 4 "limestone, very shelly sand" entry fields and rock side friction calculation method designation.

For sand layers, values of total unit weight and blow count were entered. All of the blow count values entered were indicated to have been obtained using an automatic hammer (Figure

4.14). However, a blow count modification factor of 1.0 was selected, as the previously entered blow counts were already corrected by a factor of 1.28 for hammer and energy efficiency (Race and Coffman, 2013). A screenshot of the boring log screen with input data for sasnd is presented in Figure 4.14.

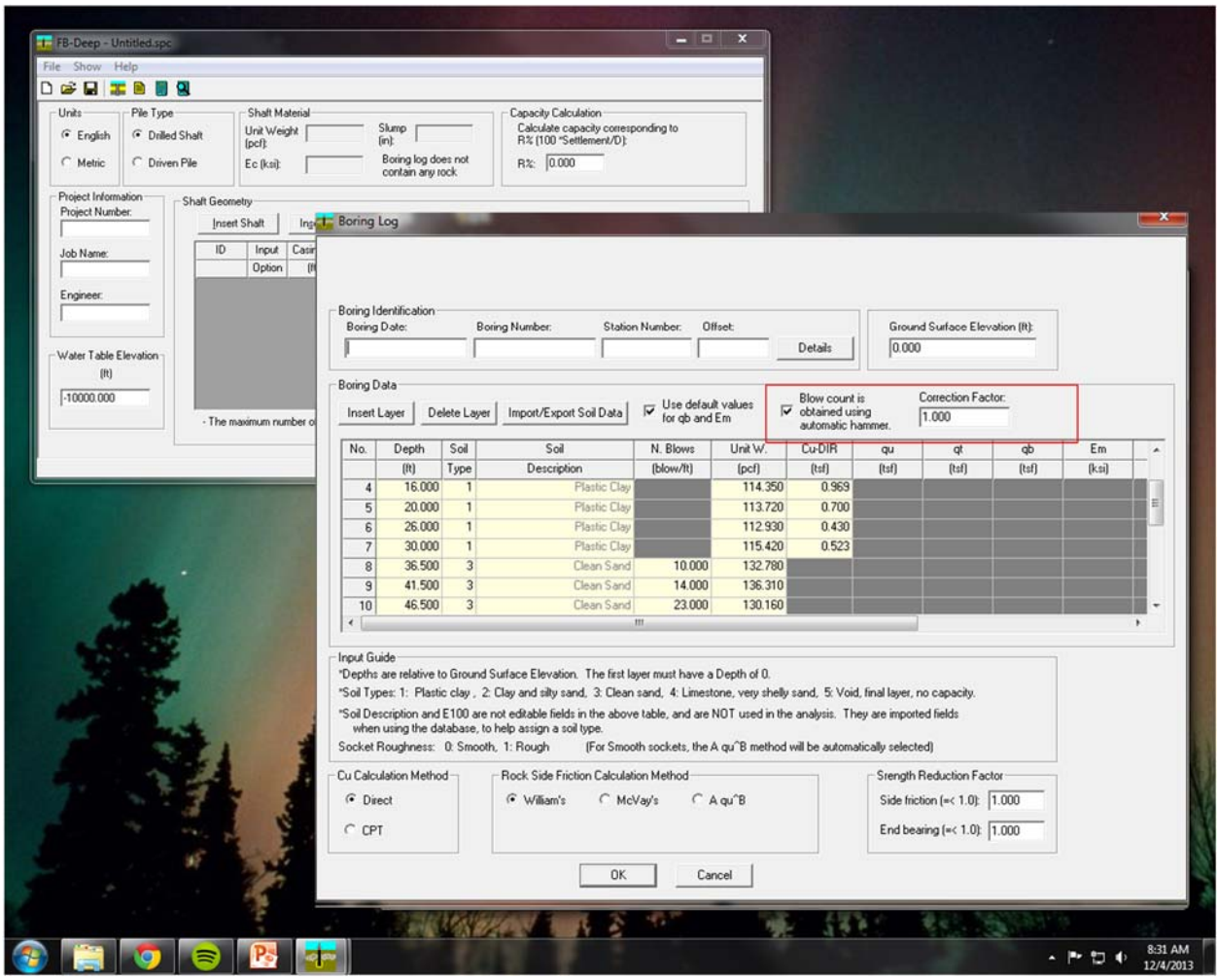

Figure 4.14. Screenshot of the FB-Deep Soil Type 3 "clean sand" entry fields and blow count modification factor.

Upon the creation of a soil profile, the boundary conditions of the drilled shaft were defined. The drilled shaft property entry fields were located in the main FB-Deep interface (as shown in Figure 4.15). This interface enables the user to enter geometric characteristics and material properties of the shaft. For all cases, a concrete unit weight of 150 pcf, a concrete

elastic modulus of 3372000 psi (selected as a function of the input concrete compressive strength), and a concrete slump of seven inches were entered (Figure 4.15). A capacity calculation corresponding to a vertical settlement of five percent of the shaft diameter was also entered for each case, as recommended by AASHTO (2012). At the Siloam Springs and Turrell Arkansas Test Sites, a water table elevation of ten feet below ground surface was entered. At the Monticello Arkansas Test Site, a water table elevation of 35 feet below ground surface was entered.

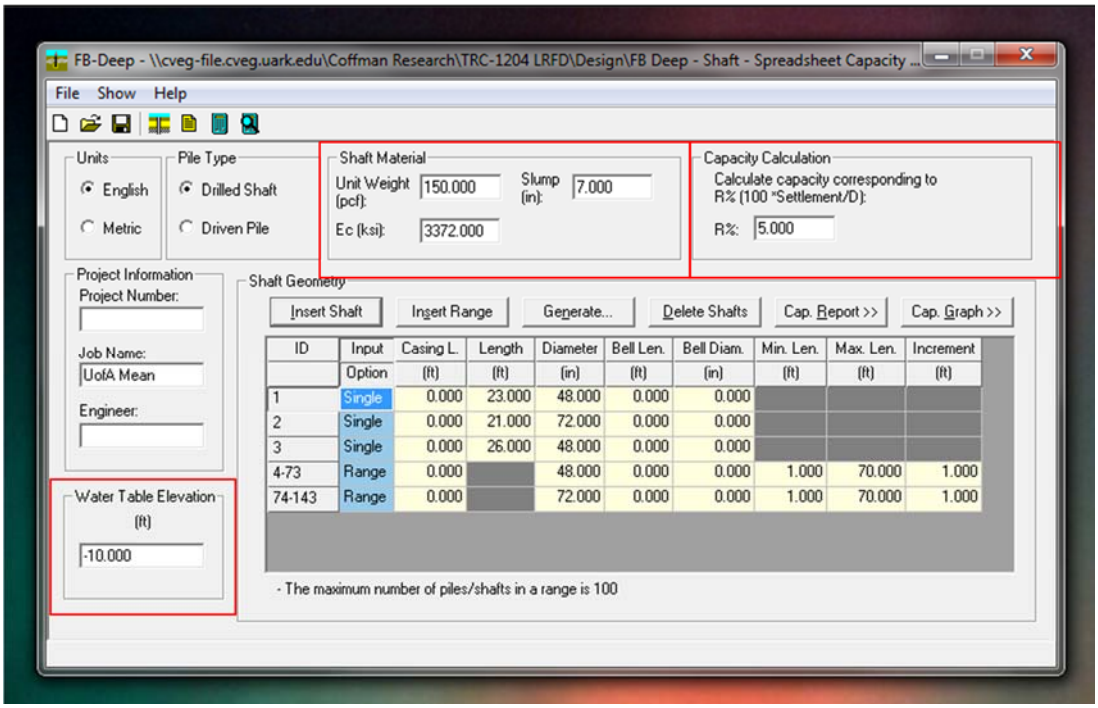

Figure 4.15. Screenshot of the Siloam Springs Arkansas Test Site boundary conditions entry fields.

The "Insert Shaft" button was selected to create a new fixed-length shaft. To create a shaft which enabled the user to evaluate a range of lengths, the "Insert Range" button was selected. For the Siloam Springs and Turrell Arkansas Test Sites, a fixed length shaft for each as-constructed shaft was inserted, as well as a range of shaft lengths for both the four- and six-foot diameter shafts. For the Monticello Arkansas Test Site, the as-designed lengths and range

of lengths were inserted for both the four-and six-foot diameter shafts. A summary of each of the shafts generated at each site is presented in Table 4.3.

Table 4.3. FB-Deep entered shaft geometries for the Siloam Springs, Turrell, and Monticello Arkansas Test Sites.

Test Site	Shaft ID	Input Option	Total Length [ft]	Diameter [in]	Minimum Length [ft]	Maximum Length [ft]	Increments [ft]
Siloam Springs [as-constructed]	SS-W4	Single	26	48			1
	SS-E4	Single	23	48			1
	SS-C6	Single	21	72			1
		Range		48	1	70	1
		Range		72	1	70	1
Turrell [as-constructed]	T-N4	Single	86.5	48			1
	T-S4	Single	86.5	48			1
	T-C6	Single	61.5	72			1
		Range		48	1	100	1
		Range		72	1	100	1
Moticello [as-designed]	M-N4	Single	91.5	48			1
	M-S4	Single	91.5	48			1
	M-C6	Single	72	72			1
		Range		48	1	100	1
		Range		72	1	100	1

Following the entry of drilled-shaft properties and soil layer data, values were validated and an "input echo" of the data was generated. This "input echo" report was utilized to further identify errors in the data entry. Drilled shaft material and geometric properties were tabulated in relation to the designated soil profile (Figure 4.16). This report, generated prior to the computational analysis, was designated by the icon indicated in Figure 4.16.

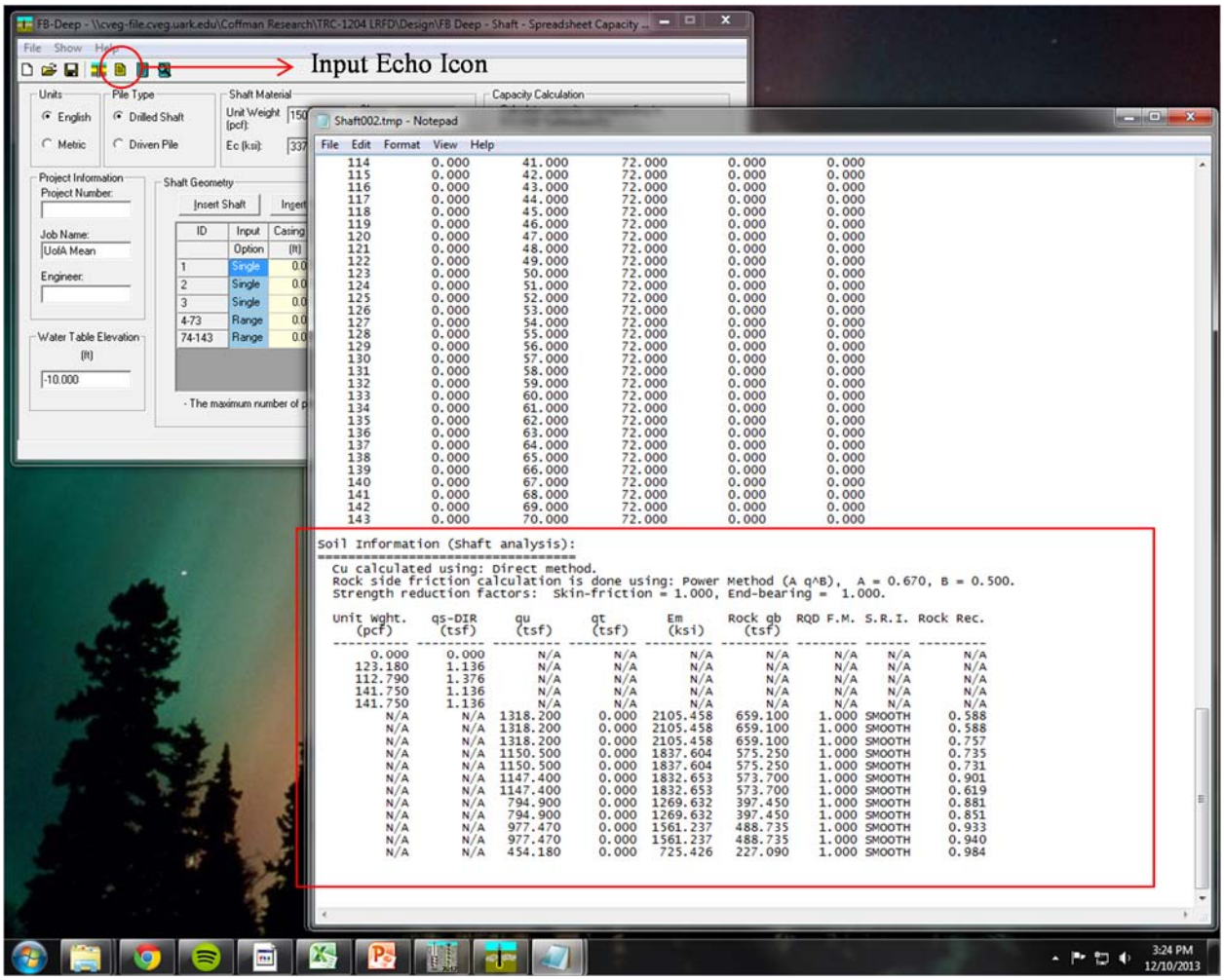

Figure 4.16. Screenshot of FB-Deep input echo report generated prior to computation.

Following data entry and the "input echo" validation, an output capacity for each given drilled shaft configuration was generated by selecting the Shaft ID of interest within the shaft geometry window, and clicking the "Cap. Report > >" button, as shown in Figure 4.17.

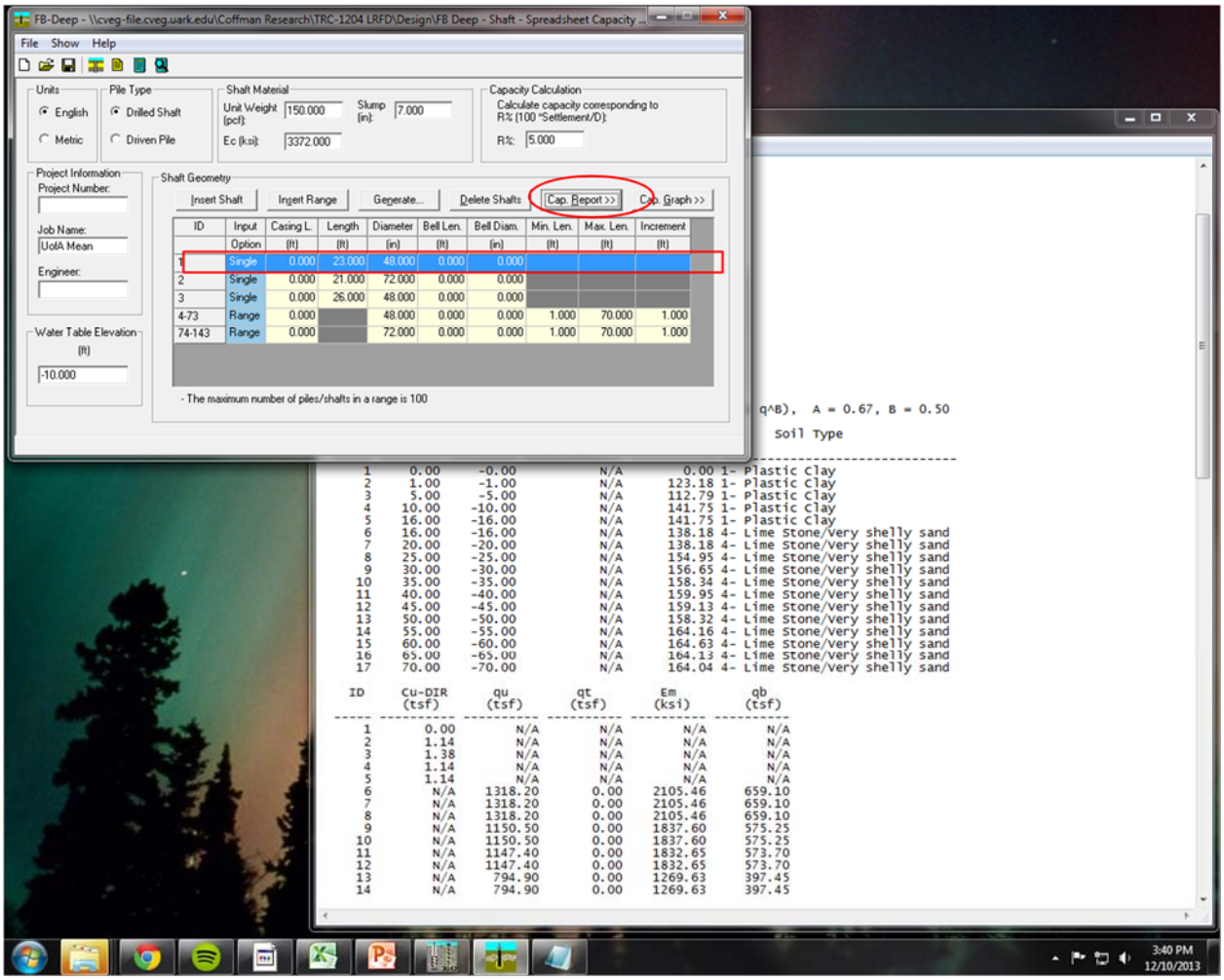

Figure 4.17. Screenshot of example FB-Deep computation procedure for Test Shaft SS-E4.

4.3.1.3. Spreadsheet

Utilizing an Excel® spreadsheet, ultimate axial capacity predictions for drilled shafts was calculated, in English units, in a manner consistent with a failure criteria based on a vertical displacement of five percent of the drilled shaft diameter. The methods used to determine ultimate axial capacity in soil were selected to model the AASTHO (2012) design process, with one exception. As specified in Reese and O'Neill (1988), an end bearing resistance reduction factor for shaft diameters greater than 50 inches was applied to end bearing resistance values. The methods used to determine ultimate axial capacity in rock were selected to model the AASTHO (2012) design process utilizing O'Neill and Reese (1999). Drilled shaft concrete

compressive strength values were required to predict ultimate resistances in rock. For all predictions incorporating rock, a concrete compressive strength of 4000 pounds per square inch was input. At the Siloam Springs, Turrell, and Monticello Arkansas Test Sites, a water table elevation of ten-, ten-, and thirty-five feet below ground surface, respectively, was utilized for each prediction. Resistance values for four- (D1) and six-foot (D2) diameter shafts were investigated. A screenshot of the spreadsheet user interface for UofA mean values at the Turrell Arkansas Test Site is presented in Figure 4.18.

Layer [Δ]	Depth [z]	Unit Weight	N60	Su	ϕ	U	σ'z	Method	Reese and O'niell 1988 Side Friction - Granular					Reese and O'niell 1988 Side Friction - Cohesive				
(ft)	(ft)	(pcf)	[blow/ft]	(ksf)	(deg)	(ksf)	(ksf)		β	Qs (ksf)	D1 (t)	D2 (t)	D3 (t)	α	Qs (ksf)	D1 (t)	D2 (t)	D3 (t)
0.0	0	0	0	0.000		0	0.00		-	-	-	-	-	0.00	0.00	0.00	0.00	0.00
2.0	2	113.07		4.260		0	0.226		-	-	-	-	-	0.00	0.00	0.00	0.00	0.00
4.0	6	112.30		3.796		0	0.675		-	-	-	-	-	0.55	2.09	13.12	19.68	26.24
4.0	10	113.12		1.435		0	1.128		-	-	-	-	-	0.55	0.79	32.96	49.44	65.92
6.0	16	114.54		1.919		-0.3744	1.441		-	-	-	-	-	0.55	1.06	72.74	109.12	145.49
4.0	20	112.68		1.401		-0.624	1.642		-	-	-	-	-	0.55	0.77	92.10	138.15	184.21
6.0	26	113.23		0.848		-0.9984	1.947		-	-	-	-	-	0.55	0.47	109.69	164.53	219.37
4.0	30	115.49	10	0.796	28.680	-1.248	2.159		-	0.00	0.00	0.00	0.00	0.55	0.44	120.70	181.04	241.39
6.5	36.5	132.78	10		28.890	-1.6536	2.617		0.68	1.79	73.14	109.71	146.27	-	-	-	-	-
5.0	41.5	136.31	14		29.580	-1.9656	2.986		0.63	1.88	132.27	198.40	264.54	-	-	-	-	-
5.0	46.5	130.16	23		29.350	-2.2776	3.325		0.58	1.93	192.79	289.19	385.59	-	-	-	-	-
5.0	51.5	136.74	20		29.300	-2.5896	3.697		0.53	1.96	254.48	381.73	508.97	-	-	-	-	-
5.0	56.5	140.30	18		30.110	-2.9016	4.086		0.49	1.98	316.78	475.16	633.55	-	-	-	-	-
5.0	61.5	148.02	33		29.900	-3.2136	4.514		0.44	1.99	379.36	569.04	758.72	-	-	-	-	-
5.0	66.5	141.16	28		29.740	-3.5256	4.908		0.40	1.96	440.90	661.35	881.80	-	-	-	-	-
5.0	71.5	145.66	26		30.030	-3.8376	5.324		0.36	1.91	500.86	751.29	1001.72	-	-	-	-	-
5.0	76.5	149.21	31		29.650	-4.1496	5.758		0.32	1.84	558.61	837.92	1117.23	-	-	-	-	-
5.0	81.5	141.15	27		29.790	-4.4616	6.152		0.28	1.73	612.97	919.46	1225.95	-	-	-	-	-
5.0	86.5	145.54	26		30.290	-4.7736	6.568		0.25	1.64	664.56	996.84	1329.11	-	-	-	-	-
5.0	91.5	144.69	39		30.180	-5.0856	6.979		0.25	1.74	719.37	1079.06	1438.74	-	-	-	-	-
5.0	96.5	153.38	49		30.970	-5.3976	7.434		0.25	1.86	777.76	1166.64	1555.52	-	-	-	-	-
3.0	99.5	143.67	56		30.970	-5.5848	7.678		0.25	1.92	813.94	1220.91	1627.88	-	-	-	-	-

Figure 4.18. Screenshot of Excel® spreadsheet data entry field and predictive computations.

4.3.2. Exported Data

Output files generated by SHAFT and a spreadsheet enabled the user to predict the ultimate axial capacity for both four- and six-foot diameter shaft foundations. Output files generated by FB-Deep were computed separately for the four- and six-foot diameter shafts. A screenshot of the utilized output values collected from SHAFTv2012, FB-Deep, and a spreadsheet for UofA mean values at the Turrell Arkansas Test Site are presented in Figures 4.19, 4.20, and 4.21, respectively.

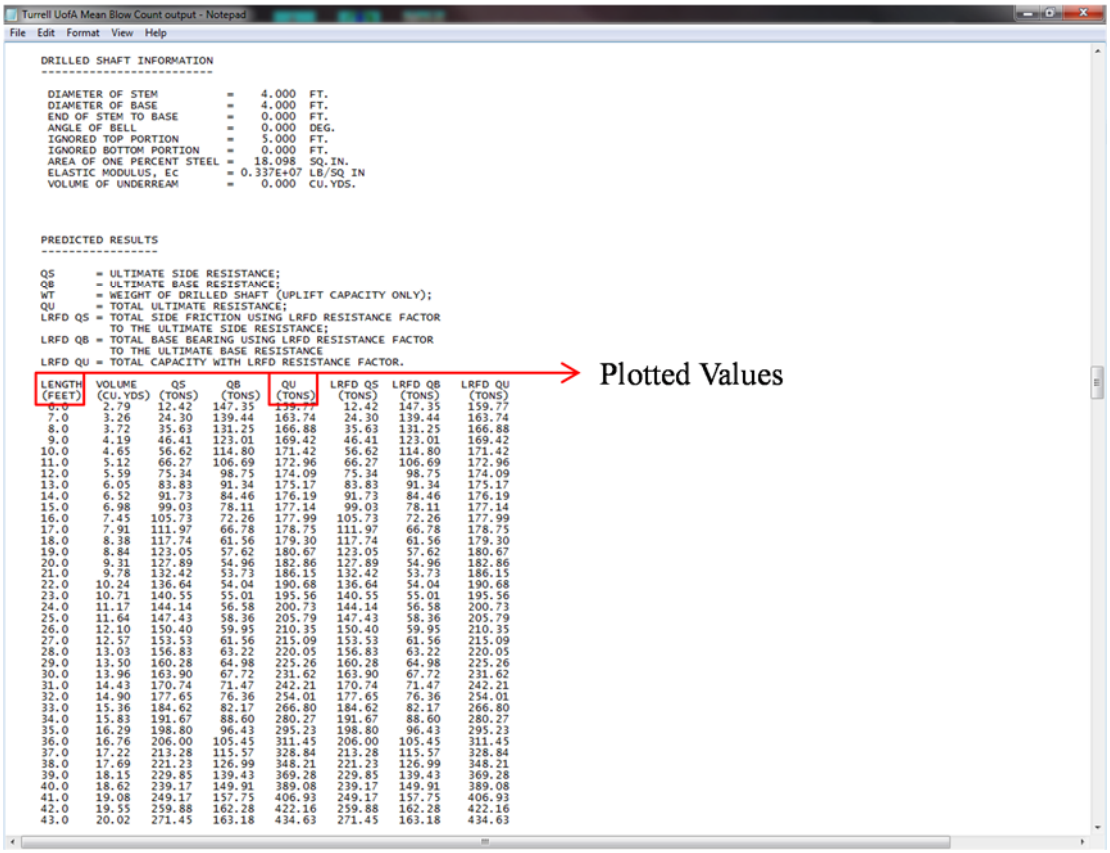

Figure 4.19. Screenshot of SHAFT output data for UofA mean values at the Turrell Arkansas Test Site for a four foot diameter shaft.

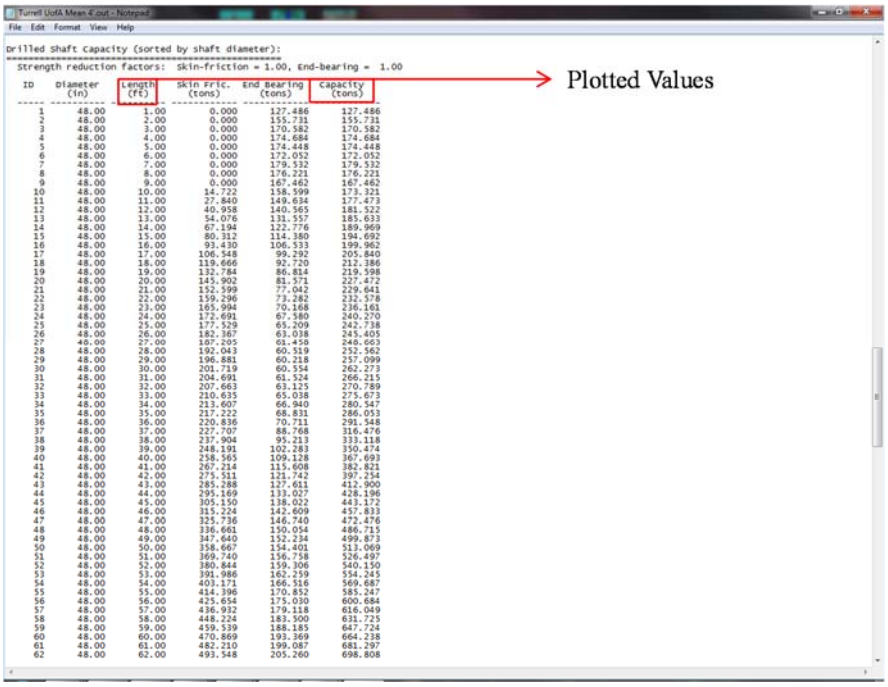

Figure 4.20. Screenshot of FB-Deep output data for UofA mean values at the Turrell Arkansas Test Site for a four-foot diameter shaft.

Depth [z]	Turrell Length Determination - Unfactored Strength					
	D1 = 4 ft			D2 = 6 ft		
(ft)	Side (ton)	Tip (ton)	Ultimate (ton)	Side (ton)	Tip (ton)	Ultimate (ton)
0	0	0	0	0	0	0
2	0	125.664	125.6637061	0	282.743	282.7433388
6	13.11934	116.811	129.9307207	19.67902	242.608	262.2872603
10	32.96023	89.6218	122.5819906	49.44035	179.244	228.6838646
16	72.74343	78.5509	151.2943464	109.1151	176.74	285.8547053
20	92.10303	57.3966	149.4996313	138.1545	129.142	267.2968965
26	109.6864	46.4957	156.1821572	164.5297	104.615	269.1450243
30	120.6954	76.5511	197.2464592	181.0431	119.611	300.6541295
36.5	193.8327	76.5511	270.3837588	290.7491	119.611	410.360079
41.5	252.9651	102.068	355.0331987	379.4477	159.481	538.9290523
46.5	313.4895	173.303	486.792584	470.2343	270.786	741.0203183
51.5	375.1789	148.849	524.0281499	562.7683	232.577	795.3453041
56.5	437.4711	136.091	573.5618721	656.2067	212.642	868.8484806
61.5	500.0568	247.728	747.7845337	750.0852	387.075	1137.159782
66.5	561.596	213.705	775.3009931	842.394	333.914	1176.308053
71.5	621.5576	192.441	813.9983896	932.3363	300.689	1233.025137
76.5	679.3087	231.78	911.0882845	1018.963	362.156	1381.11865
81.5	733.6687	203.073	936.7416307	1100.503	317.301	1417.804504
86.5	785.2525	196.694	981.9461843	1177.879	307.334	1485.212631
91.5	840.0677	297.699	1137.766234	1260.102	465.154	1725.255509
96.5	898.4558	369.997	1268.452587	1347.684	578.12	1925.803677
99.5	934.6376	423.157	1357.794813	1401.956	661.183	2063.139545

Figure 4.21. Screenshot of spreadsheet output data for UofA mean values at the Turrell Arkansas Test Site for a four- and six-foot diameter shaft.

4.3.3. Comparisons

From the text output files generated by SHAFTv2012 and FB-Deep, as well as spreadsheet results, the predicted ultimate axial capacity values of each of the drilled shaft foundations were implemented into a new spreadsheet to expedite the comparative process. The predicted axial capacity values, at given depths, were plotted for the Turrell and Monticello Arkansas Test Sites. The predicted values were determined by utilizing pertinent values as obtained from the UofA, AHTD, and MODOT sampling and testing methods. Specifically, the values obtained from SHAFT, FB-Deep, and a spreadsheet were compared (Table 4.4). A total of 202 summarizing plots were developed. The predicted ultimate predicted drilled shaft ultimate capacity values as obtained from the various software programs are presented in each of the plots. For the Siloam Springs Arkansas Test Site, values of axial capacity, at a given depth were not plotted for the MODOT sampling and testing method, because the properties of the rock were not determined using this method. For each test site, plots were generated comparing the following:

a) sampling and testing methods with respect to software program,

b) software program with respect to data range, and

c) data range with respect to sampling and testing method were generated.

Table 4.4. Quantity of comparisons summary.

Test Site	Sampling and Testing w.r.t Technology	Technology w.r.t Data Range	Data Range w.r.t. Sampling and Testing	Total
Siloam Springs	12 (4 ft. dia.)	8 (4 ft. dia.)	9 (4 ft. dia.)	58
	12 (6 ft. dia.)	8 (6 ft. dia.)	9 (6 ft. dia.)	
Turrell	12 (4 ft. dia.)	12 (4 ft. dia.)	12 (4 ft. dia.)	72
	12 (6 ft. dia.)	12 (6 ft. dia.)	12 (6 ft. dia.)	
Monticello	12 (4 ft. dia.)	12 (4 ft. dia.)	12 (4 ft. dia.)	72
	12 (6 ft. dia.)	12 (6 ft. dia.)	12 (6 ft. dia.)	

4.3.3.1. Additional comparisons in Rock

The predictive methods used to determine unit side friction and end bearing resistance in rock socketed drilled shafts at the Siloam Springs Arkansas Test Site were compared. The mean, mean +1 SD, and mean -1 SD values of the unconfined compressive strength for the rock were utilized to compare seven methods for predicting unit side friction resistance, and five methods for predicting end bearing resistance. Values of end bearing resistance and unit side friction resistance were also compared for each of the testing and sampling methods.

4.3.3.1.1. Methodology Selection

The predictive methods that were utilized to determine unit side friction and end bearing resistances were selected based on the following criteria:

a) the AASTHO LRFD Bridge Design Specifications (2012),
b) geologic regions comparable to the state of Arkansas, and/or
c) drilled shaft design literature.

The selected methods for calculating unit side friction and end bearing resistance are listed in Table 4.5. For this research project, McVay et al. (1992) was omitted from unit side friction resistance predictions due to a lack of rock tensile strength data. Additionally, Reese and O'Neill (1988) was omitted from end bearing resistance predictions due to a lack of rock joint spacing data.

Table 4.5. Selected rock socketed drilled shaft axial capacity prediction methods.

Method		Equation
Unit Side Friction Resistance		
Reese and O'Niell (1999)		f_s [Mpa] = 0.65 $(q_u/P_a)^{0.5}$ < 7.8 P_a $(f'_c/P_a)^{0.5}$
Rowe and Armitage (1987)		f_s [tsf] = 1.45 $q_u^{0.5}$
Carter and Kulhawy (1988)		f_s [tsf] = 0.63 $(q_u / P_a)^{0.5}$
AASHTO (2012) Modified From: Horvath and Kenney (1979) O'Niell and Reese (1999)		f_s [ksf] = 0.65 α $(q_u/P_a)^{0.5}$ < 7.8 P_a $(f'_c/P_a)^{0.5}$
Reynolds and Kaderabek (1980)		f_s [tsf] = 0.3 q_u
Horvath and Kenney (1979)		f_s [tsf] = 0.67 $q_u^{0.5}$
Gupton and Logan (1984)		f_s [tsf] = 0.2 q_u
Unit End Bearing Resistance		
AASHTO (2012) From: O'Niell and Reese (1999)		qb [tsf] = 2.5 qu
Hoek and Brown (1988) Reese and O'Niell (1988)	Good Quality Rock s = 0.00293 , m = 0.575	q_b [ksf] = [$s^{0.5}$ + (m ($s^{0.5}$)+ s)$^{0.5}$] q_u
Hoek and Brown (1988) Reese and O'Niell (1988)	Very Good Quality Rock s = 0.082 , m = 2.40	q_b [ksf] = [$s^{0.5}$ + (m ($s^{0.5}$)+ s)$^{0.5}$] q_u
Zhang and Einstien (1998)		q_b [Mpa] = 3.38 $q_u^{0.5}$
Kulhawy and Prakoso (2006)		q_b [tsf] = 3.38 q_u
Rowe and Armitage (1987)		q_b [tsf] = 2.5 q_u

4.3.3.1.2. Rock Comparisons

From the spreadsheet results, values of drilled shaft predicted axial capacity with depth were implemented into a new spreadsheet to expedite the comparative process. Values of axial capacity at one-foot increments of depth were plotted at the Siloam Springs Arkansas Test Site for UofA, AHTD, and MODOT sampling and testing methods (Table 4.6). A total of 24 plots were developed comparing the following:

a) mean sampling and testing regime with respect to methodology,

b) mean +1 SD sampling and testing regime with respect to methodology, and

c) mean -1 SD sampling and testing regime with respect to methodology.

Table 4.6. Quantity of comparisons summary for values of axial capacity at the Siloam Springs Arkansas Test Site.

Test Site	Side Friciton Resistance w.r.t Methodology	End Bearing Resistance w.r.t Methodology	Total
Siloam Springs	6 (4 ft. dia.)	6 (4 ft. dia.)	24
	6 (6 ft. dia.)	6 (6 ft. dia.)	

4.4. Cost-benefit Analyses

The methods utilized to perform the cost-benefit analyses for the Siloam Springs (Section 4.4.1) and Turrell (Section 4.4.2) Test Sites are presented in this Section. Two analyses were performed for each site: one to establish a unit cost per ton of resistance utilizing the UofA and AHTD sampling and testing methods, and one to evaluate the cost implications of UofA and AHTD sampling and testing methods on various types of infrastructure. Due to time scope, a cost-benefit analyses for the Monticello Arkansas Test Site was not performed.

4.4.1. Siloam Springs Arkansas Test Site

Methods utilized to perform the cost-benefit analyses at the SSATS are presented in this Section. The methods utilized to develop values of unit cost per ton of resistance for AHTD and UofA sampling and testing methods are presented in Section 4.4.1.1. The methods utilized to develop the cost implications of UofA and AHTD sampling and testing methods upon various levels of infrastructure at the Siloam Springs Site are discussed in Section 4.4.1.2. As the SSATS cost-benefit analysis for the UofA sampling and testing method was developed utilizing measured load test values, the proposed cost savings associated with the SSATS were expected to be conservative estimates. Savings reported were calculated utilizing capacities measured at settlements ranging between 0.02 and 0.18 percent. Note that values of maximum measured capacity were intended to be reported at settlements of five percent, however due to scheduled lateral load testing, displacements during testing were minimalized.

4.4.1.1. Unit Cost of the UofA and AHTD Sampling and Testing Methods in Rock

The methods utilized to develop values of unit cost per ton of resistance utilizing the UofA and AHTD testing and sampling methods presented in this Section. For the UofA testing and sampling method, upon development of the top down load settlement curve for the western oriented four-foot diameter drilled shaft (SS-W4), centrally oriented six-foot diameter drilled shaft (SS-C6), and eastern oriented four-foot diameter drilled shaft (SS-E4), values of maximum capacity at respective settlements were recorded. For the AHTD testing and sampling method, a maximum axial design load value (as previously provided by AHTD) was utilized. The as-built cost for each shaft was then determined utilizing typical current practice. As-built costs for shafts constructed utilizing the UofA sampling and testing method were developed utilizing the following:

a) estimates from AHTD (geotechnical investigation plus rock strength testing),
b) materials take-offs,
c) estimates from Aldridge Construction Co. (shaft construction), and
d) estimates from Loadtest Inc. (load testing).

Communal fees, such as those for equipment rentals and labor, were divided according to duration of construction for each shaft. As-built costs for shafts to be constructed utilizing the AHTD sampling and testing method were developed utilizing the following:

a) estimates from AHTD (geotechnical investigation),
b) materials take-offs, and
c) estimates from Aldridge Construction Co. (shaft construction).

Costs associated with the construction for each UofA constructed shaft, as well as a typical AHTD constructed shaft within the same test site profile are presented in Table 4.7.

Table 4.7. Costs associated with the construction of each UofA constructed shaft and typical AHTD shaft.

SSATS		ID	Dia. [ft]	Depth of Shaft [ft]	Cost of Concrete	Cost of Steel	Cost of Labor / Equiptment	Cost of Mobilization /	Cost of Geotechnical Investigation	Cost of Load Test
Measured	UofA	W4	4	26	$ 2,520.00	$ 4,474.45	$ 29,805.65	included	$ 6,173.62	$ 75,000.00
		E4	4	23	$ 1,929.60	$ 4,474.45	$ 15,223.59	included	$ 6,174.62	$ 75,000.00
		C6	6	21	$ 4,100.40	$ 7,623.14	$ 20,911.09	included	$ 6,175.62	$ 75,000.00
Designed	AHTD	N/A	4	26	$ 2,520.00	$ 4,474.45	$ 29,805.65	included	$ 10,186.68	$ -
	UofA	N/A	4	26	$ 2,520.00	$ 4,474.45	$ 29,805.65	included	$ 6,175.62	$ -

*Load test cost based upon Brown (2008)

Upon determination of the cost associated with each shaft, unit cost per ton of resistance was determined. For the UofA sampling and testing method, the three values of unit cost per ton of resistance were determined. From these three values, the most suitable shaft (SS-E4) was selected using engineering judgment. The unit cost per ton value for this shaft was later utilized to perform the cost implication. As the design length for all shafts utilizing the AHTD sampling and testing method were specified at 26 feet, only one unit cost per ton of resistance value was required, and was subsequently selected to perform the cost implication.

4.4.1.2. Cost Implications for Infrastructure in Rock

The methods utilized to calculate the cost implications of UofA and AHTD testing and sampling methods upon various levels of infrastructure are presented in this Section. Fiscal impacts utilizing the UofA and AHTD testing and sampling methods at the Siloam Springs Arkansas Test Site were evaluated and for the AHTD-provided load condition and for three additional hypothetical load conditions. The three hypothetical load conditions evaluated included the following:

a) A heavy building,
b) A large structure with less concentrated loads, and
c) A medium structure with moderate loads.

Each load condition (exempting the AHTD-provided condition) was taken from discussions found within Brown (2008), and descriptions for each load condition are presented in Table 4.8. All load conditions were evaluated utilizing the SSATS soil profile, specifically. Utilizing the unit cost per ton of resistance factors (as previously discussed in Section 4.4.1.1.) generated for the UofA and AHTD sampling and testing methods, the total cost of foundations for each load condition was calculated and then compared.

Table 4.8. Summary of the SSATS AHTD-provided and hypothetical load condition descriptions.

Load Condition	Description	No. of Shafts [n]	Max Axial Load [tons]
AHTD - Provided	Single-lane Bridge Superstructure	22	445
Hypothetical 1	Heavy Building with Concentrated Loads	50	1700
Hypothetical 2	Large Stucture with Less Concentrated Loads	150	850
Hypothetical 3	Medium Structure with Moderate Loads	40	500

Values were calculated by multiplying the unit cost per ton of resistance by the max axial load and number of shafts associated with each load condition. The costs of the geotechnical investigations and load testing for each sampling and testing method were then added to this value to generate a project cost. Project costs were evaluated for the following methods:

a) the UofA measured method (utilizes the benefits of UofA full-scale load testing and UofA advanced sampling and testing methods at settlements of 0.18%),
b) the AHTD method (includes the AHTD geotechnical investigation only at settlements of 5%), and
c) the UofA designed method (utilizes only the benefits of the UofA advanced sampling and testing methods at settlements of 5%).

4.4.2. Turrell Arkansas Test Site

The methods utilized to perform the cost-benefit analyses at the TATS are presented in this Section. The methods utilized to develop values of unit cost per ton of resistance for the AHTD, MODOT, and UofA sampling and testing methods are presented in Section 4.4.2.1. The methods utilized to develop the cost implications of UofA and AHTD sampling and testing methods upon various levels of infrastructure at the Turrell Arkansas Test Site are discussed in Section 4.4.2.2. As with the SSATS, the TATS cost-benefit analysis for the UofA sampling and testing method was developed utilizing measured load test values. As a result, proposed cost savings associated with the TATS were expected to be conservative estimates. Savings reported

were calculated utilizing capacities measured at settlements ranging between 1.02 and 3.06 percent. Note that values of maximum measured capacity were intended to be reported at settlements of five percent, however due to scheduled lateral load testing, displacements during testing were minimalized.

4.4.2.1. Unit Cost of the UofA, MODOT, and AHTD Sampling and Testing Methods in Soil

The methods utilized to calculate values of unit costs per ton of resistance utilizing the UofA, MODOT, and AHTD testing and sampling methods at the TATS are presented in this Section. For the UofA testing and sampling method, upon development of the top down load settlement curve for the southern oriented four-foot diameter drilled shaft (T-S4), centrally oriented six-foot diameter drilled shaft (T-C6), and northern oriented four-foot diameter drilled shaft (T-N4), values of maximum capacity at respective settlements were recorded. The MODOT sampling method only utilized values of maximum capacity from test shaft T-S4. For the AHTD testing and sampling method, a maximum axial design load value (as previously provided by AHTD) was utilized. The as-built cost for each shaft was then determined utilizing typical current practice. As-built costs for shafts constructed utilizing the UofA and MODOT sampling and testing methods were developed utilizing the following:

a) estimates from AHTD (geotechnical investigation plus advanced testing),
b) materials take-offs,
c) estimates from MODOT,
d) estimates from McKinney Drilling Co. (shaft construction), and
e) estimates from Loadtest Inc. (load testing).

Communal fees, such as those for equipment rentals and labor, were divided according to duration of construction for each shaft. As-built costs for shafts to be constructed utilizing the AHTD sampling and testing method were developed utilizing the following:

a) estimates from (geotechnical investigation),
b) materials take-offs, and
c) analysis of bids from AHTD (piling construction).

The costs associated with the construction of each shaft for the UofA and MODOT testing and sampling methods, as well as a pile group for the AHTD sampling and testing method for the TATS soil profile are presented in Table 4.9.

Table 4.9. Costs associated with the construction of each UofA constructed shaft and AHTD pile group utilizing the TATS soil profile.

TATS		ID	Dia. [ft]	Depth of Shaft [ft]	Cost of Concrete	Cost of Steel	Cost of Labor / Equiptment	Cost of Mobilization	Cost of Geotechnical	Cost of Load Test
Measured	UofA	S4	4	86.5	$ 5,903.87	$ 12,330.06	$ 99,483.51	$ -	$ 8,927.98	$ 75,000.00
		N4	4	88	$ 7,590.69	$ 11,910.54	$ -	$ -	$ 8,928.98	$ 75,000.00
		C6	6	62.5	$ 7,590.69	$ 15,878.27	$ -	$ -	$ 8,929.98	$ 75,000.00
	MODOT	S4	4	86.5	$ 5,903.87	$ 12,330.06	$ -	$ -	$ 14,060.63	$ 75,000.00
Designed	AHTDa	N/A	1.5	85	Not Available	Not Available	Not Available	Not Available	$ 7,014.84	$ -
	AHTDb	N/A	1.5	85	Not Available	Not Available	Not Available	Not Available		
	AHTDc	N/A	1.5	85	Not Available	Not Available	Not Available	Not Available		
	UofA	N/A	4	86.5	$ 653.70	$ 41,925.00	$ 7,656.54	$ -	$ 8,927.98	$ -

*Load test cost based upon Brown (2008)

4.4.2.2. Cost Implications for Infrastructure in Soil

The cost implications of utilizing the UofA, MODOT, and AHTD testing and sampling methods upon various levels of infrastructure are presented in this Section. Fiscal impacts utilizing the UofA, MODOT, and AHTD testing and sampling methods at the Turrell Arkansas Test Site were evaluated and for the AHTD-provided load condition and for three additional hypothetical load conditions (as previously described in Section 4.4.1.2). Each load condition (exempting the AHTD-provided condition) was taken from discussions found within Brown (2008), and descriptions for each load condition are presented in Table 4.10. All load conditions were evaluated utilizing the TATS soil profile, specifically.

Table 4.10. Summary of the TATS AHTD-provided and hypothetical load condition descriptions.

Load Condition	Description	No. of Shafts	Max Axial Load
		[n]	[tons]
AHTD - Provided	Principal Arterial Bridge for On-Ramp Approach	28	395
Hypothetical 1	Heavy Building with Concentrated Loads	50	1700
Hypothetical 2	Large Stucture with Less Concentrated Loads	150	850
Hypothetical 3	Medium Structure with Moderate Loads	40	500

Utilizing values of unit cost per ton of resistance (as previously discussed in Section 4.4.2.1.) the total cost of each load condition for the UofA and AHTD sampling and testing methods were calculated and then compared. These values were calculated by multiplying the unit cost per ton of resistance by the max axial load and number of shafts associated with each load condition. The costs of the geotechnical investigations and load testing for each sampling and testing method were then added to this value to generate a project cost. Project costs were evaluated for the following methods:

a) the UofA measured method (utilizes the benefits of UofA full-scale load testing and UofA advanced sampling and testing methods at settlements of 1.19%),

b) the MODOT method (utilizes benefits of MODOT CPT geotechnical investigation and UofA full-scale load testing),
c) the AHTD method (includes the AHTD geotechnical investigation only at settlements of 5%), and
d) the UofA designed method (utilizes only the benefits of the UofA advanced sampling and testing methods at settlements of 5%).

4.5. Conclusion

The predictive methods that were utilized to estimate the ultimate axial capacity for drilled shaft foundations associated with this research project were discussed in Chapter 4. The results The predictive software programs utilized to compare values of capacity included Ensoft SHAFT, Bridge Software Institute FB-Deep, and an Excel® spreadsheet. Results of these comparisons are discussed in Chapter 7. To optimize the predictive process, an engineering properties database was developed containing relevant soil and rock properties (as determined by geotechnical investigations). Property values that were missing were obtained by averaging values from the nearest surrounding depths. Rock engineering property values obtained from the AHTD method at the Siloam Springs Arkansas Test Site were assumed to be constant below a depth of 38 feet below ground surface. Soil engineering property values obtained from the MODOT method at the Turrell Arkansas Test Site were assumed to be constant below a depth of 71.5 feet below ground surface.

From the engineering properties database, the values were entered into Ensoft SHAFTv2012, Bridge Software Institute FB-Deep, and the Excel® spreadsheet. A sensitivity analysis was performed to acquire additional necessary input values for rock utilizing the SHAFT program. At the Siloam Springs, Turrell, and Monticello Arkansas Test Sites, a water table elevation of ten-, ten-, and thirty-five feet below ground surface, respectively, was utilized

for each prediction. Utilizing FB-Deep, an energy correction factor of 1.0 was applied to all input N_{60} values. Furthermore, FB-Deep soil type 4 is classified as "Limestone, very shelly sand", which could possibly yield conservative estimates. Utilizing a spreadsheet, methods for determining values of ultimate axial capacity were selected to model the AASTHO (2012) design process, with one exception. As specified in Reese and O'Neill (1988), an end bearing resistance reduction factor for shaft diameters greater than 50 inches was applied to end bearing resistance values.

Output files generated by SHAFT and the spreadsheet enabled the user to predict drilled shaft ultimate axial capacity for both the four- and six-foot diameter drilled shaft foundations. Output files generated by FB-Deep for the four- and six-foot diameter shaft foundations were computed separately. From the text output files and spreadsheet results, predicted axial capacity values for the respective foundations were plotted for each test site corresponding to the data obtained from the UofA, AHTD, and MODOT sampling and testing methods as obtained using SHAFT, FB-Deep, and the spreadsheet. A total of 202 summarizing plots for predicted drilled shaft ultimate capacity were generated.

Predictive methods for determining the unit side friction and end bearing resistance for the rock socketed drilled shaft foundations at the Siloam Springs Arkansas Test Site were also analyzed. Utilizing mean, mean +1 SD, and mean -1 SD values of the unconfined compressive strength for the rock, seven methods for predicting unit side friction resistance and five methods for predicting end bearing resistance were selected, computed in a spreadsheet, and compared. McVay et al. (1992) was omitted from unit side friction resistance predictions due to a lack of rock tensile strength data. Additionally, Reese and O'Neill (1988) was omitted from end bearing

resistance predictions due to a lack of rock joint spacing data. A total of 24 summarizing plots for predicted drilled shaft ultimate capacity were generated.

The cost-benefit analyses performed for the SSATS and TATS each consisted of two parts. The first part included establishing a unit cost per ton of resistance for each UofA (and MODOT) constructed shaft and the originally designed UofA and AHTD shafts/pile groups. Values of unit cost per ton of resistance for the SSATS were determined from estimates from Aldridge Construction Co., AHTD, materials take-offs, and Loadtest Inc. Values of unit cost per ton of resistance for the TATS were determined from estimates from McKinney Drilling Co., AHTD, materials take-offs, MODOT, and Loadtest Inc. Using engineering judgment, a most suitable unit cost per ton of resistance value was selected for each method. The second part of the cost-benefit analyses consisted of utilizing values of unit cost per ton of resistance to evaluate the fiscal implication of each sampling and testing method upon various levels of infrastructure. Total project foundation costs for UofA Measured, MODOT, AHTD, and UofA Designed methods were calculated and compared for three hypothetical load conditions (provided from Brown, 2008), as well as the original site load condition (provided from AHTD).

Chapter 5: Construction and Testing at the Siloam Springs Arkansas Test Site

5.1. Introduction

To develop more economical designs for the proposed drilled shaft foundations, Osterberg load cell tests (O-Cell) were performed at Siloam Springs, Turrell, and Monticello. For the Siloam Springs Site, design considerations (Section 5.2) are presented in this chapter as well as a discussion on the construction process for each shaft (Section 5.3). Concrete testing and cross hole sonic logging were performed prior to testing, and are addressed in Sections 5.4 and 5.5, respectively. The full scale load testing setup and procedures for each shaft at Siloam Springs are discussed (Section 5.6), as well as an explanation of the data interpretation process for evaluating load transfer characteristics (Section 5.7).

5.2. Foundation Design

Three drilled shafts, two measuring four feet in diameter, and one measuring six feet in diameter were designed to a depth which would support a design load of 1112.5 tons. The West four foot diameter shaft (hereinafter referred to as SS-W4), the East four foot diameter shaft (hereinafter referred to as SS-E4), and the central six foot diameter shaft (hereinafter referred to as SS-C6) were designed using the O'Neill and Reese (1999) methods of predicting drilled shaft resistance in cohesive materials and rock as found in AASHTO (2012). Both skin friction resistances and end bearing resistances were utilized to determine ultimate shaft capacity. Ultimate side friction resistance was determined by using equations 2.22 and 2.23, as presented previously in Chapter 2. Ultimate end bearing resistance was determined by using equation 2.24 also presented in Chapter 2. Based on the geotechnical investigation (discussed in Chapter 3) the cherty clay is underlain by limestone, with the top of the limestone at a depth of 18 feet below the ground surface. Based on the results from predictive equations, the design requirements were

met when the tips of the shafts constructed reached a depth of 20 feet. However, to ensure adequate data collection and embedment length of each shaft into limestone, the drilled shafts were each designed with a seven-foot rock socket (the tips of the shafts were specified for 25-feet below the ground surface). This seven foot rock socket length was specified even though current AHTD drilled shaft design practices require a minimum rock socket depth of ten feet. From the specified depths, additional drilled shaft properties including rebar quantities and configurations, spacer quantities and locations, CSL tubing quantities and locations, and mix design considerations were developed using ACI 318 (2008), AASHTO (2012), and O'Neill and Reese (1999). A typical schematic for the four-foot and six-foot diameter test shaft designs is presented in Figure 5.1 and Figure 5.2, respectively.

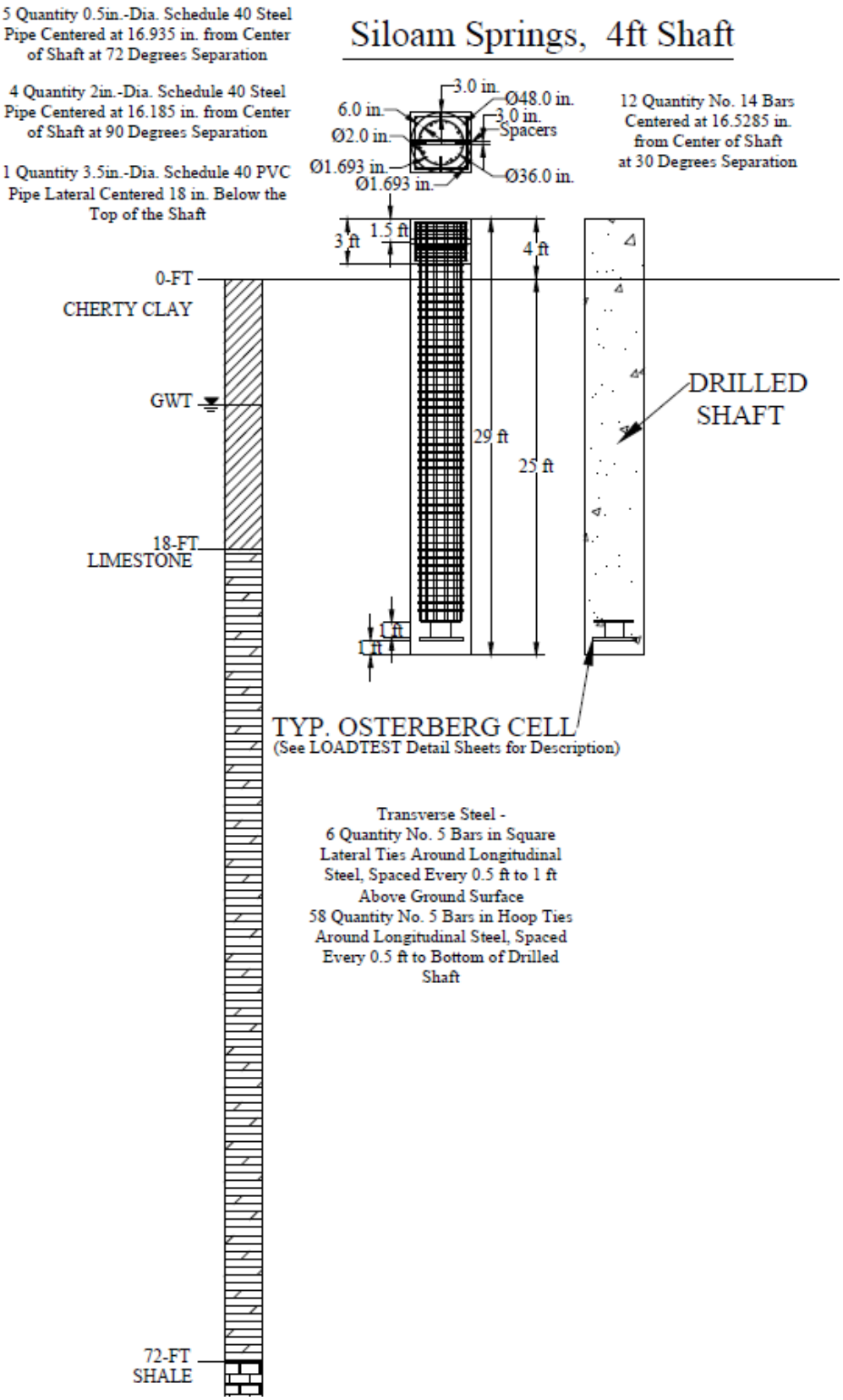

Figure 5.1. Schematic of four-foot diameter shaft design.

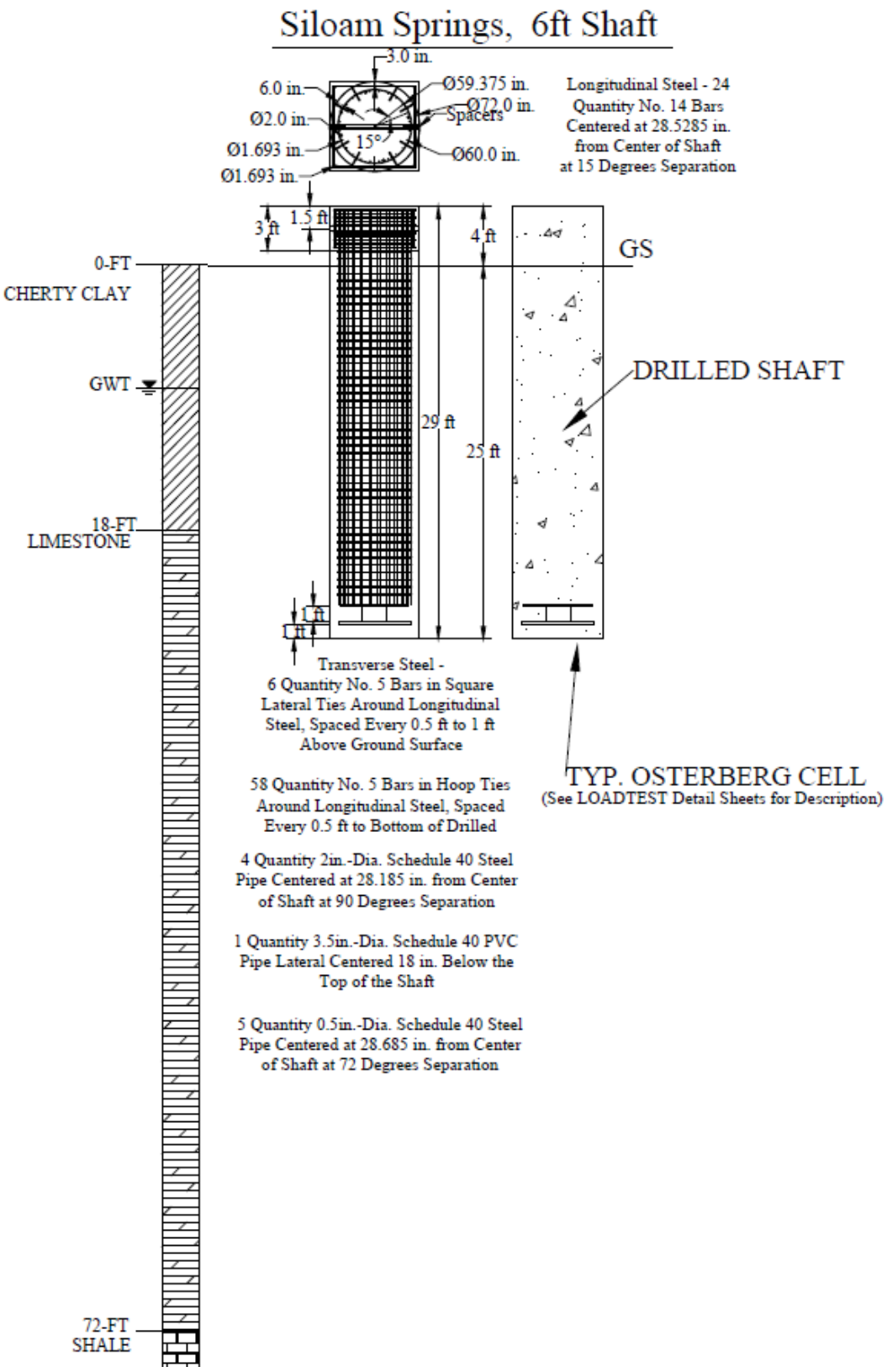

Figure 5.2. Schematic of six-foot diameter shaft design.

5.2.1. Test Shafts SS-W4 and SS-E4

Test shaft SS-W4 (measuring four feet in diameter and oriented furthest West on the test site) and test shaft SS-E4 (measuring four feet in diameter and oriented furthest East on the test site) were designed to extend 25 feet below the ground surface, and have a reveal length of four feet, equaling a total shaft length of 29 feet. The longitudinal steel of each shaft was chosen to equal less than 1.5 percent of the gross cross-sectional area of the shaft with 12 (quantity) Number 14 bars of Grade 60 steel centered at 16.53 inches from the center of the shaft (separated at 30 degrees), as presented in Figure 5.3. Transverse reinforcement within each of the SS-W4 and SS-E4 shafts included tied Grade 60 steel hoops consisting of 58 (quantity) Number 5 bars spaced from every 0.5-feet from 0.25-feet below the top of the shaft to the bottom of the drilled shaft (Figure 5.3). The tubing for cross hole sonic logging consisted of four (quantity), two inch diameter, Schedule 40 steel pipe centered 28.19 inches from the center of the shaft (separated at 90 degrees), as presented in Figure 5.3.

(a) (b)

Figure 5.3. Photograph of a four-foot diameter shaft reinforcement cage from the (a) end, and (b) side views.

Plastic spacers, attached to the transverse steel, were specified at eight foot increments to provide six inches of clearance between the outer transverse steel and the edge of the concrete. The top four feet of reveal of each shaft consisted of a four foot cubic block of concrete. This block contained extra reinforcement including four (quantity) Number 14 longitudinal bars and six

(quantity) Number 5 transverse bars. A photograph of the reinforcement utilized within the top block is presented in Figure 5.4. A four foot long piece of 3.5 inch diameter Schedule 40 polyvinylchloride pipe was also specified to be installed across the center of the shaft and located eighteen inches below the top of each block (oriented East to West). This pipe (located at the same vertical elevation in each shaft) was included to enable future lateral load testing.

Figure 5.4. Photograph of extra reinforcement for the top block reinforcement cage.

Linear vibrating wire displacement transducers (LVWDTs) were specified to monitor strains within the shaft at given locations to better understand the load transfer characteristics of the construction. Pairs of diametrically opposing linear vibrating wire displacement transducers (LVWDTs) were specified to be installed (utilizing zip ties and welded mounts) within each four-foot diameter shaft at three locations. Displacement transducers were located at depths below ground surface of 14.7, 20.7, and 24.7-feet within test shaft SS-W4. Within test shaft SS-E4, displacement transducers were located at depths below ground surface of 12.8, 16.8, and 21.5-feet. A photograph of a linear vibrating wire transducer is presented in Figure 5.5a. Also specified within each shaft were five 0.5-inch diameter Schedule 40 black steel telltale casings.

Each casing was specified to house one 0.125-inch diameter stainless steel telltale. Within test shaft SS-W4, three telltale casings were specified to rest upon the side of the bottom O-Cell steel plate at a depth below ground surface of 23.5-feet, and two telltale casings were specified to rest upon the side of the top O-Cell plate at a depth of 24.7-feet. Within test shaft SS-E4, three telltale casings were specified to rest upon the side of the bottom O-Cell steel plate at a depth below ground surface of 21.5-feet, and two telltale casings were specified to rest upon the side of the top O-Cell plate at a depth of 20.3-feet. A photograph of the telltale casings installed is presented in Figure 5.5b.

(a) (b)

Figure 5.5. Photograph of (a) linear vibrating wire displacement transducers and (b) telltale casings utilized in each shaft.

5.2.2. Test Shaft SS-C6

Test Shaft SS-C6 (measuring six feet in diameter and centrally oriented on the test site) was also designed to extend 25 feet below the ground surface, and have a reveal length of four feet, equaling a total shaft length of 29 feet. The longitudinal steel of the shaft was chosen to equal less than 1.33 percent of the gross cross-sectional area of the shaft with 24 (quantity) Number 14 bars of Grade 60 steel centered at 28.53 inches from the center of the shaft (separated at 15 degrees), as presented in Figure 5.6. Transverse reinforcement within the SS-C6 test shaft

included tied Grade 60 steel hoops consisting of 58 (quantity) Number 5 bars spaced every 0.5-feet from 0.25-feet between the top of the shaft to the bottom of the drilled shaft (Figure 5.6). The tubing for cross hole sonic logging consisted of four (quantity), two-inch diameter, Schedule 40 steel pipe centered 28.19 inches from the center of the shaft (separated at 90 degrees). Tied, plastic spacers were specified at eight foot increments to provide six inches of clearance between the outer transverse steel and the edge of the concrete. The top four feet of reveal of the shaft consisted of a four foot by six foot by six foot block of concrete. This block contained extra reinforcement including four (quantity) Number 14 longitudinal bars and 6 (quantity) Number 5 transverse bars. A six foot long piece of 3.5-inch diameter Schedule 40 polyvinylchloride pipe was also specified to be installed across the center of the shaft and loaded 18 inches below the top of the block (oriented East to West). This pipe (located at the same vertical elevation as the pipes in Test Shafts SS-W4 and SS-E4) was included to enable future lateral load testing.

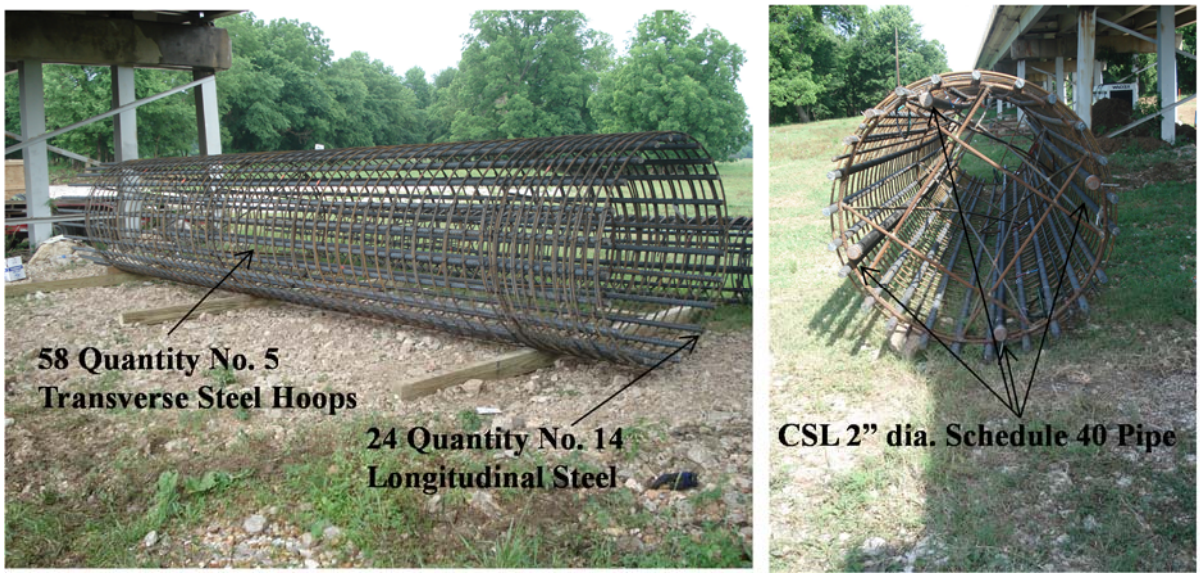

(a) (b)

Figure 5.6. Photograph of a six-foot diameter shaft reinforcement cage from the (a) side, and (b) end views.

Linear vibrating wire displacement transducers (LVWDTs) were also specified to monitor strains within test shaft SS-C6 at given locations to better understand the load transfer characteristics of the construction. Pairs of diametrically opposing linear vibrating wire displacement transducers (LVWDTs) were specified to be installed (utilizing zip ties and welded mounts as presented in Figure 5.7) within the six-foot diameter shaft at three locations. Displacement transducers were located at depths below ground surface of 7.3, 13.3, and 19.8-feet within test shaft SS-C6. Also specified within this shaft were five 0.5-inch diameter Schedule 40 black steel telltale casings. Each casing was specified to house one 0.125-inch diameter stainless steel telltale. Within test shaft SS-C6, three telltale casings were specified to rest upon the side of the bottom O-Cell steel plate at a depth below ground surface of 19.8-feet, and two telltale casings were specified to rest upon the side of the top O-Cell plate at a depth of 18.6-feet.

Figure 5.7. Photograph of installed vibrating wire strain gauge utilizing welded mount and zip ties.

5.3. Construction of Test Shafts

In Section 5.3 the materials and equipment utilized to construct the test shafts are described. The construction process of SS-W4 (Section 5.3.1), SS-C6 (Section 5.3.2), and SS-C6 (Section 5.3.3) is also discussed (including the excavation, reinforcement cage and O-Cell

assembly, placement, concrete pouring, and formwork). The errors associated with the construction of test shafts SS-C6 and SS-E4, and the solutions to these errors are addressed.

Each test shaft was constructed, by personnel from Aldridge Construction, at 53 feet center to center spacings using a Caterpillar AF 240 drill rig. The rig was selected for having a vertical clearance of 22 feet, enabling site access under the existing bridge (Figure 5.8). The steel utilized to construct the reinforcement cages for each shaft was provided by Aldridge Construction, while the concrete utilized to pour each shaft was provided by GCL and Midcontinent. Additionally, the spacers utilized to center each shaft were provided by Foundation Technologies.

(a) (b)

Figure 5.8. Photograph of Caterpillar AF 240 drill rig (a) mobilizing at the Siloam Springs site, and (b) in full operation at the Siloam Springs Site.

The concrete mix utilized to pour each shaft was specified to contain a water cement ratio of 0.45, a slump of eight inches (plus or minus one inch), an entrapped air content of 2 percent, a maximum aggregate size of one inch, and a unit weight of 146.7 pounds per cubic foot. Constituents of the concrete mix are presented in Table 5.1. Water reducing admixtures and hydration stabilization admixtures (provided by Grace Concrete Products) were introduced in

accordance with ASTM C494 (2013). Each shaft was poured utilizing a Mantex R-232 concrete pump truck (Figure 5.9a) and a 4-inch diameter, tremie pipe supplied by Western Concrete Pumping (Figure 5.9b). To verify the concrete quality, UofA personnel cast 10 four-inch diameter cylinders composed of concrete obtained from each concrete truck to perform uniaxial compressive strength and modulus of elasticity testing. (A minimum required uniaxial compressive strength of 3500 psi is specified by current AHTD regulations.) UofA personnel also performed slump and air content testing on a portion of the concrete from each truck (Figure 5.10). Each sample was obtained from samples that had been previously ran through the pump truck (not directly from the concrete truck). An as-built schematic of each test shaft is presented in Figure 5.11.

Table 5.1. Concrete mix constituents.

Material Type	Description	Specific Gravity	Design Quantity
Cement	ASTM C-150 Type I/II Cement	3.15	452 lb
Fly Ash	ASTM C-618 Class C Fly Ash	2.65	192 lb
Coarse Aggregate	ASTM C-33 #57 Limestone	2.65	1765 lb
Fine Aggregate	ASTM C-33 Natural Sand	2.63	1260 lb
Water	Water (35 gal)	1.00	292 lb
Admixture	ASTM C-494 Type A/D Water Reducer	-	-
Admixture	ASTM C-494 B Recover	-	-

(a) (b)

Figure 5.9. Photograph of the concrete placement equipment utilized during construction including the (a) Mantex R-232 concrete pump truck, and (b) tremie pipe.

(a) (b)

Figure 5.10. Photograph of concrete quality assurance testing including (a) slump and cylinder casting, and (b) air content testing.

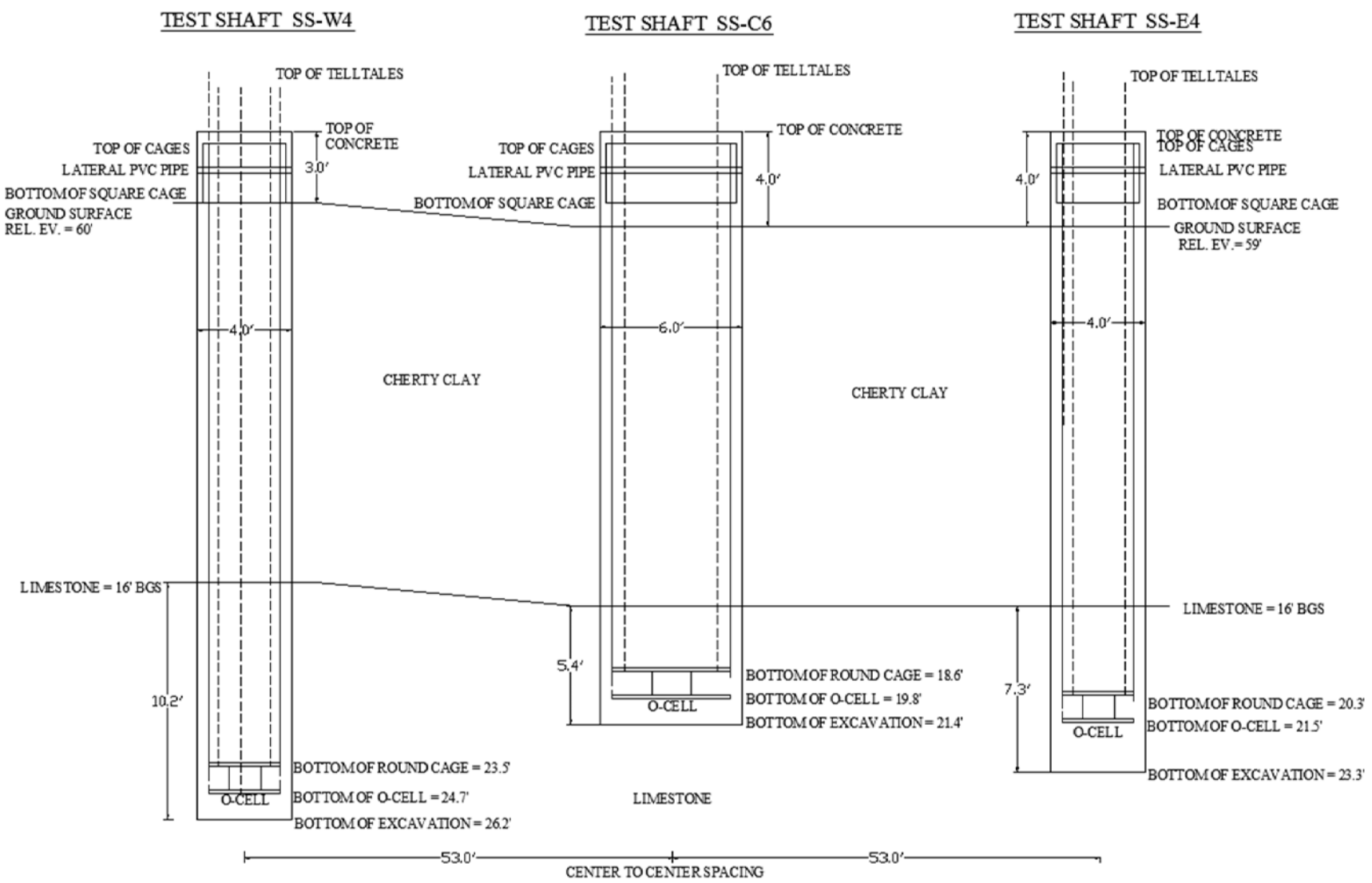

Figure 5.11. Schematic of the cross-section of the SSATS after completion of construction.

5.3.1. Test Shaft SS-W4

Section 5.3.1 describes the construction process associated with test shaft SS-W4. This shaft, situated closest to the Illinois River, had the largest rock socket depth of 10.2 feet. The equipment utilized and the excavation process involved with test shaft SS-W4 is described (Section 5.3.1.1). Assembly of the steel reinforcement cage and O-Cell are discussed in Section 5.3.1.2. Additionally addressed in Section 5.3.1.2 are the placement of the completed cage within the excavation, the concrete placement, and cap formation of test shaft SS-W4.

5.3.1.1. SS-W4 Excavation

Personnel from Aldridge Construction excavated soil and rock at the location of Test Shaft SS-W4 from June 16th through June 19th, 2013, using the previously mentioned Caterpillar AF-240 drill rig. To prevent caving, upon an excavation depth of five feet, a five-foot ten-inch inner diameter, ten-foot temporary steel casing was inserted into the top of the cherty-clay top soil. Upon reaching an excavation depth of 15-feet, a second temporary casing measuring 20-foot long four-foot inner diameter steel casing was inserted. Water percolation in the bottom of the excavation was noted at a depth of 8.8 feet below the ground surface. Limestone was encountered at a depth of approximately 16 feet, upon which the flight auger (Figure 5.12a) was exchanged for a rock core barrel (Figure 5.12b). Due to the strength of the limestone (around 18,000 pounds per square foot between depths of 16 and 30 feet), the rock socket excavation of 10 feet extended for a duration of four days. This time was furthered due to the need for frequent teeth replacement on the rock core barrel excavator. Because of the extenuated excavation time encountered with Test Shaft SS-W4, the excavation depths for Test Shafts SS-C6 and SS-E4 were reduced.

(a) (b)

Figure 5.12. Photographs of Caterpillar AF-240 drill rig utilized to excavate Test Shaft SS-W4 with (a) a flight auger, and (b) a rock core barrel.

5.3.1.2. SS-W4 Rebar Cage and Concrete Placement

Upon completion of the 26-foot deep excavation, the rebar and concrete for Test Shaft SS-W4 were placed on June 20, 2013, in conjunction with Aldridge Construction and Loadtest, Inc. The O-Cell, composed of a ten inch tall hydraulic jack encompassed by a two-inch thick steel plate mounted on the top and bottom of the assembly, was then welded to the bottom of the reinforcement cage (Figure 5.13).

Figure 5.13. Photograph of installed O-Cell on bottom of SS-W4 reinforcement cage.

The cage, measuring 27 feet in length after installation of the O-Cell, was lowered into the excavation using the Caterpillar AF-240 and a Builtrite 2200-TM material handler (Figure 5.14a)

. Following concrete placement within the excavation, a shaft reveal length of three feet was formed by placing a pre-constructed four foot wide by four foot long wooden form over the poured shaft. Upon lowering the additional reinforcement (as outlined in the previous section) and placing the lateral polyvinylchloride pipe to elevation, concrete was poured within the assembly (Figure 5.14b). Upon setting of the concrete within the block, the wooden forms were removed.

(a) (b)

Figure 5.14. Photograph of Test Shaft SS-W4 (a) poured excavation casing removal and prior to placement of the square cap, and (b) three foot reveal placing form work for square cap.

Twenty-seven cubic yards of concrete was utilized to complete the construction of this shaft. Exempting the following, all other as-built features met the design specifications outlined in Section 5.2.1:

1) an increase in shaft excavation depth from 25 feet to 26.2 feet due to the installation of the O-Cell,

2) a decrease in the reveal length of the shaft from 4 feet to 3 feet to align the vertical elevations of all shafts for potential future lateral load capacity testing, and

3) an increase in telltale pipe length for the bottom O-Cell plate.

The total length of Test Shaft SS-W4 measured 29.2 feet from the bottom of the excavation to the top edge of the three-foot tall concrete block reveal. A photograph of the finished shaft is presented in Figure 5.15.

Figure 5.15. Photographs of Test Shaft SS-W4 (a) rebar cage, and (b) finished construction.

5.3.2. Test Shaft SS-C6

Section 5.3.2 describes the construction process associated with test shaft SS-C6. Test Shaft SS-C6 was constructed from June 21th through June 25th, 2013, and was situated centrally between SS-W4 and SS-E4. This shaft had a rock socket depth of 5.5 feet. Along with reducing the time of construction, the rock socket depth of Test Shaft C6 was reduced to aid in data collection regarding rock/socket load transfer relationships. The equipment utilized and the

excavation process involved with test shaft SS-C6 is described (Section 5.3.2.1). Assembly of the steel reinforcement cage and O-Cell are discussed in Section 5.3.2.2. Additionally described in Section 5.3.2.2 are the placement of the completed cage within the excavation, the concrete placement, and cap formation of test shaft SS-C6.

5.3.2.1. SS-C6 Excavation

Test Shaft SS-C6 was excavated by personnel from Aldridge Construction from June 21 through June 24, 2013. To prevent caving, upon an excavation depth of six feet, a seven-foot ten-inch inner diameter, 10-foot long temporary steel casing was inserted into the top of the cherty-clay top soil. Upon reaching an excavation depth of 16 feet, a second temporary casing with measurements of six-foot ten-inch inner diameter by 15-foot long was inserted (Figure 5.16). Water percolation in the bottom of the excavation was noted at a depth of 12.5 feet. Limestone was encountered at a depth of 16 feet, upon which the flight auger was exchanged for a rock core barrel. The rock socket excavation extended a depth of 5.5 feet below the cherty clay/limestone interface, and required approximately two days of drilling. Upon completion of the 21.5-foot deep excavation on June 24, the hole was covered with lumber and left open overnight.

(a) (b)

Figure 5.16. Photographs of Test Shaft SS-C6 (a) during the 15 foot length casing installation, and (b) after completed casing installation.

5.3.2.2. SS-C6 Rebar Cage and Concrete Placement

The rebar and concrete for Test Shaft SS-C6 were placed on June 25, 2013, in conjunction with Aldridge Construction, and Loadtest, Inc. The rebar cage, measuring 24 feet in length after installation of the O-Cell on the bottom of the rebar cage, was lowered using the Caterpillar AF-240. During installation of the O-Cell tell-tale mounts to the rebar cage, a construction error was made. All three tell-tale mounts originally intended to be welded to the side of the bottom O-Cell steel plate were welded to the side of the top O-Cell steel plate (Figure 5.17). This error inhibited the measurement of the displacement of the bottom O-Cell plate (a crucial measurement in determining the load/displacement relationships of the construction). Actions taken to resolve this problem are presented in Section 5.6.2. Concrete was placed using a Manitex R-232 pump truck and a 4-inch diameter tremie. A shaft reveal length of four-feet was formed by placing a pre-constructed six-foot wide by six-foot long wooden form over the poured shaft (Figure 5.18). Soil was placed around the outsides of the wooden form to reinforce the shape while the concrete hydrated.

(a) (b)

Figure 5.17. Photograph of Test Shaft SS-C6 (a) rebar cage and (b) tell-tale mount installation error.

Figure 5.18. Photograph of Test Shaft SS-C6 four-foot reveal construction.

Forty-four cubic yards of concrete was utilized to complete the construction of this shaft. Exempting the following, all other as-built features met the design specifications outlined in Section 5.2.2:

1) a decrease in rebar cage length from 25 feet to 22.5 feet due to drilling time and load transfer considerations,
2) a decrease in excavation depth from 25 feet to 21.5 feet due to load transfer considerations, and
3) telltale pipe length for bottom plate

The total length of Test Shaft SS-C6 measured 25.5 feet from the bottom of the excavation to the top edge of the 4 foot tall concrete block reveal. Photographs of the a) poured excavation and b) finished shaft are presented in Figure 5.19.

Figure 5.19. Photograph of the Test Shaft SS-C6 finished construction.

5.3.3. Test Shaft SS-E4

Test Shaft SS-E4 was constructed from June 21 through June 25, 2013. This shaft, located furthest East from the Illinois River was embedded to create a rock socket depth of eight feet. Similar to Test Shaft SS-C6, the rock socket depth of Test Shaft SS-E4 was reduced to aid in data collection regarding rock/socket load transfer relationships. Section 5.3.3 describes the

construction process associated with test shaft SS-E4. Test Shaft SS-E4 was constructed from June 21th through June 25th, 201, and had a rock socket depth of 5.5 feet. The equipment utilized and the excavation process involved with test shaft SS-E4 is described (Section 5.3.3.1). Assembly of the steel reinforcement cage and O-Cell are discussed in Section 5.3.3.2. Additionally described in Section 5.3.3.2 are the placement of the completed cage within the excavation, the concrete placement, and cap formation of test shaft SS-E4.

5.3.3.1. SS-E4 Excavation

Test Shaft SS-E4 was excavated by Personnel from Aldridge Construction June 21 and June 22, 2013. To prevent caving, upon an excavation depth of five-feet, a temporary steel casing with measurements of a five-foot ten-inch inner diameter by 10-foot long was inserted into the top of the cherty-clay top soil. Upon reaching an excavation depth of 15 feet, a second temporary steel casing with measurements of a five-foot four-inch inner diameter by 20-foot long was inserted. Water percolation in the bottom of the excavation was noted at a depth of 12 feet. Limestone was encountered at a depth of 16 feet, upon which the flight auger was exchanged for a rock core barrel. The rock socket excavation extended a depth of 5.5 feet below the cherty clay/limestone interface, and required approximately 18 hours of drilling. Upon completion of the 23-foot excavation on June 22nd, the hole was covered with lumber and left till June 25th.

5.3.3.2. SS-E4 Rebar Cage and Concrete Placement

The rebar and concrete for Test Shaft SS-E4 were placed on June 25, 2013 in conjunction with Aldridge Construction and Loadtest, Inc. The rebar cage, measuring 25-feet in length after installation of the O-Cell to the bottom of the reinforcement cage, was lowered using a Caterpillar AF-240. During installation of the O-Cell tell-tale mounts to the rebar cage of Test

Shaft SS-E4, a construction error was made. All three tell-tale mounts originally intended to be welded to the side of the bottom O-Cell steel plate were welded to the side of the top O-Cell steel plate (Figure 5.20). Actions taken to resolve this problem are presented in Section 5.6.3.

Figure 5.20. Photograph of Test Shaft SS-E4 rebar cage and tell-tale mount installation error.

Concrete was placed using a Manitex R-232 pump truck and a 4-inch diameter tremie. A shaft reveal length of four feet was formed by placing a pre-constructed four-foot wide by four-foot long wooden form over the poured shaft (Figure 5.21). Soil was placed around the block form to reinforce the mold, and was removed upon hydration of the concrete.

Figure 5.21. Photograph of Test Shaft SS-E4 four foot reveal construction.

Twenty-three cubic yards of concrete were poured to complete the construction of Test Shaft SS-E4. Exempting the following, all other as-built features of the shaft met the design specifications outlined in Section 5.2.1:

1) a decrease in rebar cage length from 25 feet to 24 feet due to drilling time and load transfer considerations, and
2) a decrease in excavation depth from 25 feet to 23 feet due to load transfer considerations.

The total length of Test Shaft SS-E4 measured 27-feet from the bottom of the excavation to the top edge of the four-foot tall concrete block reveal. Photographs of the a) poured excavation with square cap formwork and b) finished shaft are presented in Figure 5.22.

(a) (b)

Figure 5.22. Photographs of the Test Shaft SS-E4 (a) rebar cage and pipe for lateral load testing, and (b) finished construction.

5.4. Concrete Testing

Concrete testing, including uniaxial compressive strength and modulus of elasticity, were performed on the cylinders (four-inches in diameter and eight-inches in height) that were cast in the field. Four trucks of concrete were required to pour Test Shaft SS-W4 (resulting in four batches of ten cylinders). Three trucks of concrete were required to pour Test Shaft SS-E4 (resulting in three batches of ten cylinders). From the remains of the contents of the last truck used to pour Test Shaft SS-E4, the pour for Test Shaft SS-C6 commenced. Including this last truck, six trucks of concrete were required to pour Test Shaft SS-C6 (resulting in six batches of ten cylinders). The cylinders from every batch were transported in water-containing coolers or plastic sheeting-lined boxes to the laboratory at the University of Arkansas, and stripped of their forms after seven days. The cylinders were then submerged in a water bath until testing was performed. The designated testing regiment for each batch is presented in Table 5.2.

Table 5.2. Designated concrete testing regiment per batch.

Test Performed	Number of Tests Performed Per Batch
Seven-Day Uniaxial Compressive Strength	3
Fourteen-Day Uniaxial Compressive Strength	3
Twenty-Eight Day Uniaxial Compressive Strength	3
Modulus of Elasticity	1

5.4.1. Uniaxial Compressive Strength

Uniaxial compressive strength testing was performed in accordance with ASTM C39 (2012) was performed after seven, fourteen, and twenty-eight days from the date of the construction of the cylinders. A Forney F Series standard compression machine was utilized to complete the testing (Figure 5.23a). Each batch of cylinders, for each shaft was tested at a rate of 35 +/- 7 pounds per square inch (psi) per second.

5.4.2. Modulus of Elasticity

Modulus of elasticity testing was performed after 28 days in accordance with ASTM 469 (2010). The test was performed on one cylinder per batch using a Forney F Series standard compression machine and a compressometer (Figure 5.23b). Load was applied to each cylinder at a rate of 35 +/- 7 psi per second, and the modulus of elasticity was calculated using Equation 5.1.

$$E = \frac{(S_1 - S_2)}{(\varepsilon_2 - 0.000050)} \qquad \text{(ASTM C469, 2010)} \qquad \textbf{Equation 5.1}$$

Where: E = chord modulus of elasticity of concrete (psi),

S_1 = stress corresponding to a longitudinal strain, ε_1, of 50 millionths (psi),

S_2 = stress corresponding to 40% of ultimate load (psi), and

ε_2 = longitudinal strain produced by stress S_2.

(a) (b)

Figure 5.23. Photographs of (a) uniaxial compression testing, and (b) compressometer used for modulus of elasticity testing.

5.5. Cross-Hole Sonic Logging

On Thursday, September 12, 2013, personnel from GEI, performed cross-hole sonic logging on each drilled shaft. Following calibration, two piezoelectric probes were inserted in multiple sequences into the aforementioned four diametrically opposed, two-inch diameter CSL tubes. The sequence utilized on each shaft (composed of six soundings) is presented in Figure 5.24, and commenced from the Northern-most oriented CSL tube.

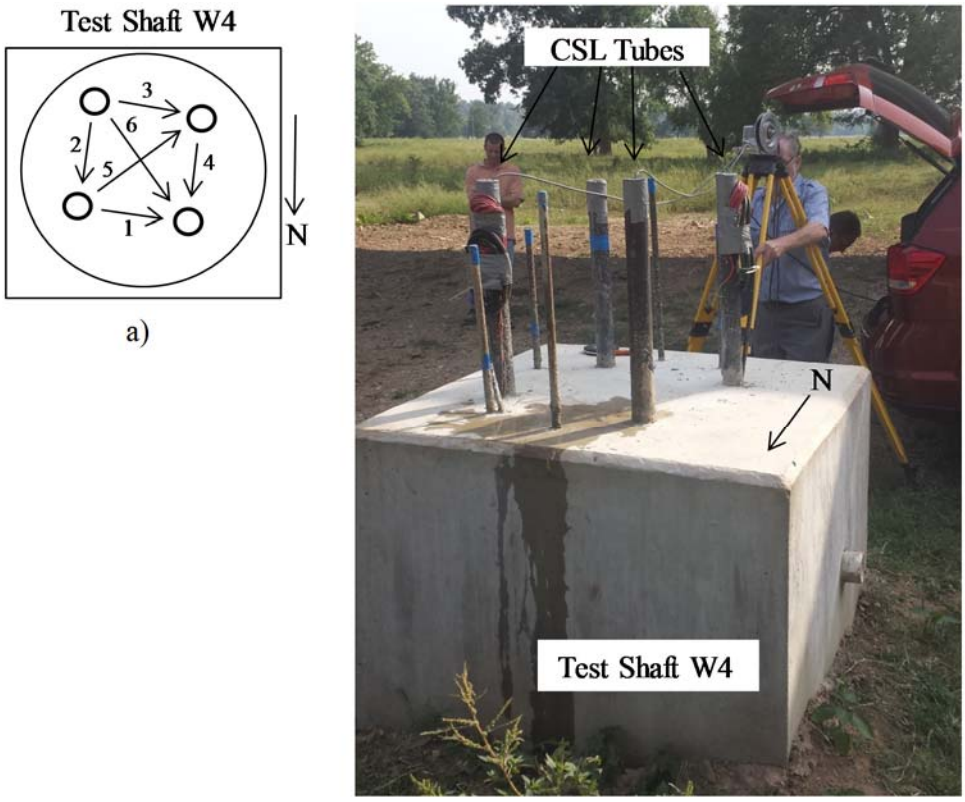

Figure 5.24. Summary of (a) plan view of six-step CSL testing sequence commencing from the north, and (b) photograph of testing performed on Test Shaft SS-W4.

The probes were lowered to rest upon the bottom cap of the water-filled tubes, located directly above the two inch thick steel plate attached to the top of the O-Cell in each shaft. Upon commencement of the test, the probes were simultaneously extracted at a rate of about one foot per second. A photograph of the piezoelectric probes utilized to transmit and receive the sonic waves through the length of the shaft is presented in Figure 5.25. A photograph of the CSL test in progress on Test Shaft SS-E4 is presented in Figure 5.26.

Figure 5.25. Photograph of piezoelectric probes utilized for CSL testing.

Figure 5.26. Photograph of CSL testing performed on Test Shaft SS-E4.

5.6. Load Test Setup and Procedures

From Tuesday, September 17, through Friday September 20, 2013, in conjunction with personnel from Loadtest Inc., Osterberg load Cell (O-Cell) testing was performed on each drilled shaft. Upon individual setup, each test consisted of the following general procedure:

1) calibration of the hydraulic pump,
2) separation of O-Cell tell-tale bonds,
3) the loading stage,
4) the unloading stage, and
5) monitoring of shaft while at rest.

While performing the O-Cell tests, an automatic pressure regulator (Figure 5.28) was utilized to maintain a constant pressure for each load increment. Displacement of the 1/8- inch tell-tale rods that were positioned within the ½-inch pipe connected to the top and bottom plates of the O-Cell were monitored using linear variable displacement transducers (LVDTs) (Figure 5.27a). The displacement of the top of the shaft was monitored using automated surveying levels (Figure 5.27b) taking readings on an Invar sight that was clamped to one of the cross-hole sonic tubes. Strain within the strain gauges that were previously installed within sonic tubes were monitored using an automated data acquisition system. All measurements were recorded using the automated data acquisition system.

(a) (b)

Figure 5.27. Photographs of (a) LVDT displacement instrumentation that was attached to the top of each telltale, and (b) survey levels used to record the shaft head displacement.

(a) (b)

Figure 5.28. Photographs of (a) data acquisition system, and (b) automated pressure regulator and hydraulic pump utilized to perform the O-Cell testing.

5.6.1. Test Shaft SS-W4

On September 17, 2013, full-scale l load testing was performed on Test Shaft SS-W4. The shaft was loaded every eight minutes at increments of 1000 psi for fifteen intervals (peaking

at 15,000 psi). The shaft was then unloaded using four minutes increments, decreasing the pressure by 3000 psi for each of the five intervals (reducing pressure back to zero pounds psi). Following unloading, the shaft was monitored at rest for a period of eight minutes. Displacement readings were acquired for the top of the shaft, and for the top and bottom of the O-Cell (two within the piped mounted to the top plate of the O-Cell, and three within the piped mounted to the bottom plate of the O-Cell. A photograph of the testing setup and the test in progress are presented in Figure 5.29.

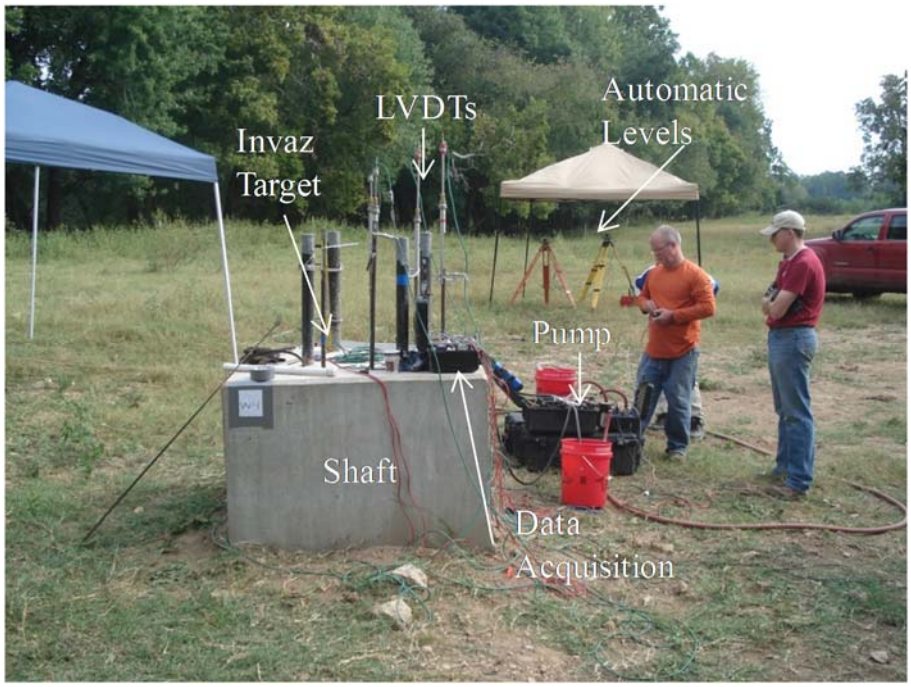

Figure 5.29. Photograph of the Test Shaft SS-W4 O-Cell test in progress.

5.6.2. Test Shaft SS-C6

O-Cell load testing for Test Shaft SS-C6 was originally scheduled to be performed on September 17, 2013. However due to an error that occurred during construction, testing was delayed (as previously discussed in Section 5.3.2.2). In the design plans, five (quantity) 0.25-inch diameter telltales were specified to measure O-Cell displacements. Each telltale (installed immediately before testing) required a 0.5-inch diameter access housing and mount to be

installed during construction. The housing for the two tell-tales, specified to be located (at 18.6 feet below ground surface) on the top plate of the O-Cell, was successfully welded to the top plate of the O-Cell. The housing for the remaining three tell-tales, specified to be located (at 19.8 feet below ground surface) and welded to the side of the bottom plate of the O-Cell, were welded to the side of the top plate of the O-Cell rather than to the side of the bottom plate. If not identified prior to testing, this crucial error may have resulted in five top plate displacement measurements and no bottom plate displacement measurements. To resolve this problem, 3/8-inch diameter holes were extended through the original three improperly welded mounts using a hammer drill until the depth of the hole was at the top of the to the bottom plate of the O-Cell at 18.9-feet below the ground surface (Figure 5.30a). Each hole extended through the plug at the bottom of the 0.5-inch diameter housing and then through twelve inches of 7500 psi strength concrete (the material surrounding the O-Cell). Due to the torque generated by the hammer drill occasionally shearing the all-thread connections of the drill bit extension within the drill hole (effectively blocking the hole) installation of only one of the three tell-tales was achieved. A new mount was not installed inside the bottom of the successful boring, rather the weight of the telltale itself, and the trimmings surrounding the telltale inside the boring, were utilized to stabilize the assembly. A photograph of the resulting (three total) telltales utilized for testing is presented in Figure 5.30b.

(a) (b)

Figure 5.30. Photographs of (a) telltale depth extension using a 3/8- inch diameter bit hammer drill , and (b) the resulting telltale assemble prior to O-Cell testing of Test Shaft SS-C6.

On September 20, 2013, O-Cell load testing was performed on Test Shaft SS-C6. The shaft was loaded every eight minutes at increments of 500 psi for nine intervals (peaking at 4,500 psi). The shaft was then unloaded using four minute increments, decreasing the pressure by 900 psi for each of the five intervals (reducing pressure back to zero pounds per square inch). Following unloading, the shaft was then monitored at rest for a period of eight minutes. Displacement readings were acquired for the top of the shaft and for the top and bottom of the O-Cell (two within the pipes mounted to the top plate of the O-Cell, and one placed on the bottom plate of the O-Cell after the retrofit). A photograph of the testing setup while the test is in progress is presented in Figure 5.31.

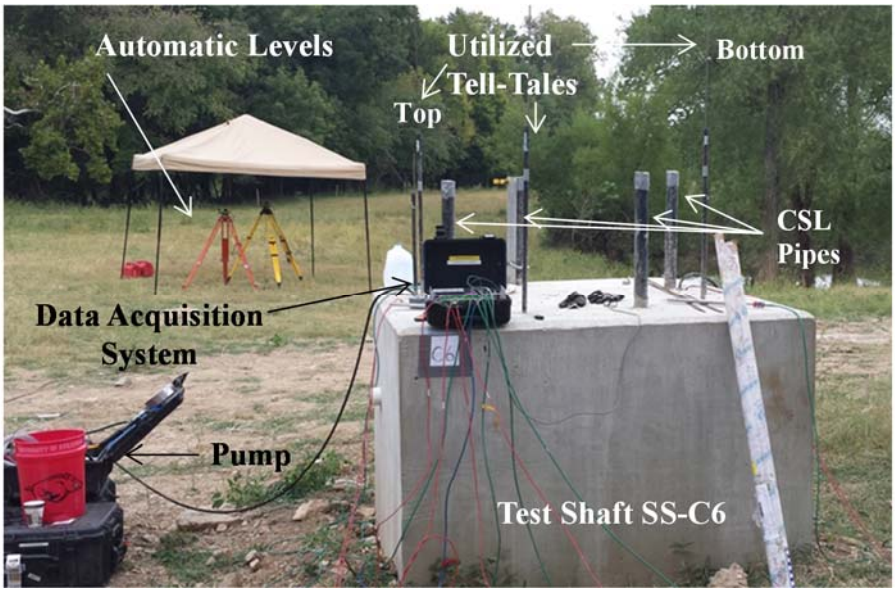

Figure 5.31. Photograph of the Test Shaft SS-C6 O-Cell test in progress.

5.6.3. Test Shaft SS-E4

O-Cell load testing for Test Shaft SS-E4 was originally scheduled to be performed on September 17, 2013 (as described previously in Section 5.3.3.2). However, similar to Test Shaft SS-C6, due to an error occurring during construction, testing was delayed. Although, five (quantity) 0.25-inch diameter telltales were specified to measure O-Cell displacements, the housing for three tell-tales, specified to be located (at 21.5 feet below ground surface) on the bottom plate of the O-Cell, was welded to the side of the top plate of the O-Cell rather than the side of the bottom plate. Like with Test Shaft SS-C6, only one hole was utilized in Test Shaft SS-E4, as only one hole was drilled due to time constraints. A photograph of the resulting (three total) telltales utilized for testing for Test Shaft SS-E4 is presented in Figure 5.32.

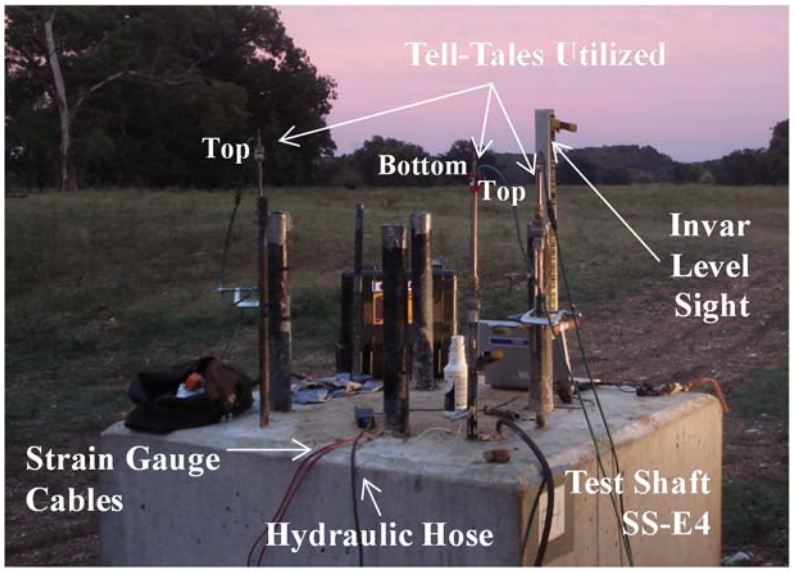

Figure 5.32. Photograph of the resulting telltale assembly in Test Shaft SS-E4 prior to O-Cell testing.

On September 20, 2013, O-Cell load testing was performed on Test Shaft SS-E4. The shaft was loaded every eight minutes at increments of 500 psi for twenty intervals (peaking at 10,000 psi). The shaft was then unloaded using four minute increments, decreasing the pressure by 2000 psi for each of the five intervals (reducing pressure back to zero psi). Following unloading, the shaft was then monitored at rest for a period of eight minutes. Displacement readings were acquired for the top of the shaft and for the top and bottom of the O-Cell (two tell-tales within the pipes mounted to the top plate of the O-Cell, and one tell-tale within the pipe and hole to the bottom plate of the O-Cell). A photograph of the testing setup and the test in progress is presented in Figure 5.33.

Figure 5.33. Photograph of the Test Shaft SS-E4 O-Cell test in progress.

5.7. Interpretation of Load Test Data

After O-Cell testing, data sheets were generated that contained displacement measurements acquired from the LVDTs, automatic levels, survey stations, and strain gauges (in relation to time). These data sheets also contained O-Cell loading information as a function of time. From the data, load displacement curves (Section 5.7.1), load transfer curves (Section 5.7.2), and unit side friction plots were generated (Section 5.7.3).

5.7.1. Load Displacement Curves

From the data collected from each O-Cell test, two load displacement curves were generated. As previously discussed in Chapter 2, the upper curve describes the upward displacement of the top of the cell (skin friction resistance), and the lower curve represents the downward displacement of the bottom of the cell (end bearing resistance). At certain values of displacement, the values of load were added together to generate an equivalent top-down load displacement curve. However, in cases where resistances could not be fully developed, a

hyperbolic extrapolation of the load-displacement curve was performed to complete the equivalent top-down load displacement curve.

5.7.2. Load Transfer (t-z) Curves

Load transfer curves showing the distribution of force along the shaft with depth were obtained from the strain-gauge data. The modulus of elasticity (E_c) of the concrete was determined from one sample from each batch of cylinders cast by UofA personnel. After determining the modulus of elasticity of the concrete, an equivalent shaft modulus was determined by accounting for the contributions of the area of steel and the area of concrete (Equation 5.2).

$$E_{Shaft} = \frac{E_c A_c + E_s A_s}{A_{Shaft}}$$ (modified from Miller, 2003) **Equation 5.2**

Where: E_{Shaft}= equivalent shaft modulus (psi),

E_c = modulus of concrete (psi),

E_s = modulus of steel (psi),

A_c = cross sectional area of concrete (in^2),

A_s = cross sectional area of steel (in^2), and

A_{Shaft} = gross cross sectional area of drilled shaft (in^2).

From the equivalent shaft modulus, the average axial stress at given depths (σ_i) was then calculated (Equation 5.3).

$$\sigma_i = E_{Shaft_i}\ \varepsilon_{axial_i}$$ (modified from Miller, 2003) **Equation 5.3**

Where: σ_i = average axial stress at given depth *i* (psi),

$E_{Shaft\text{-}i}$ = equivalent shaft modulus at depth *i* (psi), and

$\varepsilon_{axial\text{-}i}$ = axial strain within the shaft at depth *i*.

Axial strain within the shaft ($\varepsilon_{axial\text{-}i}$) was determined from the average value of strain from the two strain gauges placed in the shaft at a given elevation. From the average axial stress at a given depth, the axial force (F_i) at a given depth, *i*, was computed (Equation 5.4).

$$F_i = \sigma_i A_{pi} \qquad \text{(Miller, 2003)} \qquad \textbf{Equation 5.4}$$

Where: F_i = axial force within the shaft at depth *i*,

σ_i = average axial stress at given depth *i* (psi), and

A_{pi} = shaft cross sectional area at elevation *i* (in^2).

The distribution of axial force within the shaft at a given elevation was determined upon calculation of the axial force at each strain gauge.

5.7.3. Unit Side Friction Resistance

The determination of average unit side friction resistance for each drilled shaft over a given length was determined from the load distribution along the shaft using Equation 5.5.

$$f_s = \frac{\Delta F_i}{Shaft\ Perimeter * \Delta z_i} \qquad \text{(Miller, 2003)} \qquad \textbf{Equation 5.5}$$

Where: f_s = average unit side friction resistance,

ΔF_i = the change in axial force over a given length of shaft, and

Δz_i = shaft segment length.

The values of the average unit side shear were then plotted as a function of O-Cell displacement to evaluate the amount of attained of maximum unit side friction resistance.

5.8. Summary

The design, construction, testing, and data analysis processes associated with the Siloam Springs Arkansas Test Site were discussed in this Chapter. Design depths for the three drilled shafts (SS-W4, SS-C6, and SS-E4) to be constructed were originally specified to penetrate 25 feet, with percentages of longitudinal steel not exceeding 1.5 percent. The O-Cells for each shaft were designed to be placed within the bottom of the excavation, with two feet of unreinforced concrete separating the bottom plate of the O-Cell from the base of the limestone rock socket. Sonic cross hole logging was performed on each shaft prior to O-Cell testing to ensure the concrete utilized for construction was free from anomalies. The longest rock socket (10.2 feet) was located at Test Shaft SS-W4 (situated furthest West on site and having a diameter of four feet). This socket was the only socket constructed which currently meets AHTD requirements of a minimum of a ten-foot rock socket length. However, due to the depth of the socket, construction time was extenuated, and testing results indicated minimum displacement (suggesting a possible overdesign of the shaft). This resulted in the decision to shorten Test Shafts SS-C6 and SS-E4. During the construction of Test Shafts SS-C6 and SS-E4 however, a construction error was discovered related to the telltale placement of three tell-tales for each shaft. This error further extenuated the testing time, but was resolved by drilling a hole through the original telltale housing location to an appropriate depth of the top of the bottom plate of the O-Cell. Test Shaft SS-C6 was situated centrally between SS-W4 and SS-E4, had a diameter of six feet, and extended to a depth of 21.4 feet. Test Shaft SS-E4 was situated furthest East on site, had a diameter of four feet, and extended to a depth of 23.3 feet. The data from the load tests

performed on each shaft was analyzed, and the procedures for determining load displacement curves, load transfer curves, and unit side friction curves were described.

Chapter 6: Construction and Testing at the Turrell Arkansas Test Site

6.1. Introduction

Osterberg load cell tests (O-Cell) were performed at the Siloam Springs and Turrell Arkansas Test Sites. For the Turrell Site (TATS), the design considerations and construction processes for each shaft are described in Sections 6.2 and 6.3, respectively. Concrete testing (Section 6.4) and cross hole sonic logging (Section 6.5) were performed prior to testing. The testing configuration and testing procedures for each of the shafts at the Turrell Arkansas Test Site are discussed in Section 6.6. An explanation of the data interpretation process for evaluating load transfer characteristics is presented in Section 6.7.

6.2. Foundation Design

Three drilled shaft foundations, two measuring four-feet in diameter, and one measuring six-feet in diameter were designed to support a design load of 987 tons. The North four-foot diameter shaft at the TATS (hereinafter referred to as T-N4), the South four-foot diameter shaft at the TATS (hereinafter referred to as T-S4), and the central six-foot diameter shaft at the TATS (hereinafter referred to as T-C6) were designed using the O'Neill and Reese (1999) methods to predict drilled resistance of the drilled shaft foundation against cohesive and noncohesive materials, as described in AASHTO (2012). The skin friction resistances and end bearing resistances were utilized to determine ultimate shaft capacity. As previously discussed, ultimate side friction resistance was determined using Equations 2.9 through 2.11 and Equations 2.15 through 2.17. Likewise, as previously discussed, ultimate end bearing resistance was determined using Equations 2.12 through 2.14 and Equations 2.18 through 2.19. Based on the geotechnical investigations performed at the TATS (as discussed in Chapter 3) the high plasticity clay present at the ground surface is underlain by 10-feet of a low plasticity silt, which is underlain by poorly

graded sand. Based on the results obtained from the prediction, the design requirements were met when the tips of the four-foot and six-foot diameter shafts reached depths of 86.5 feet (four-foot diameter), and 61.5 feet (six-foot diameter). From the specified depths, additional drilled shaft properties including rebar quantities and configurations, spacer quantities and locations, CSL tubing quantities and locations, and mix design considerations were developed using procedures found in ACI 318 (2008), AASHTO (2012), and O'Neill and Reese (1999). A typical schematic for the four-foot diameter and six-foot diameter test shaft designs is presented in Figure 6.1 and Figure 6.2, respectively.

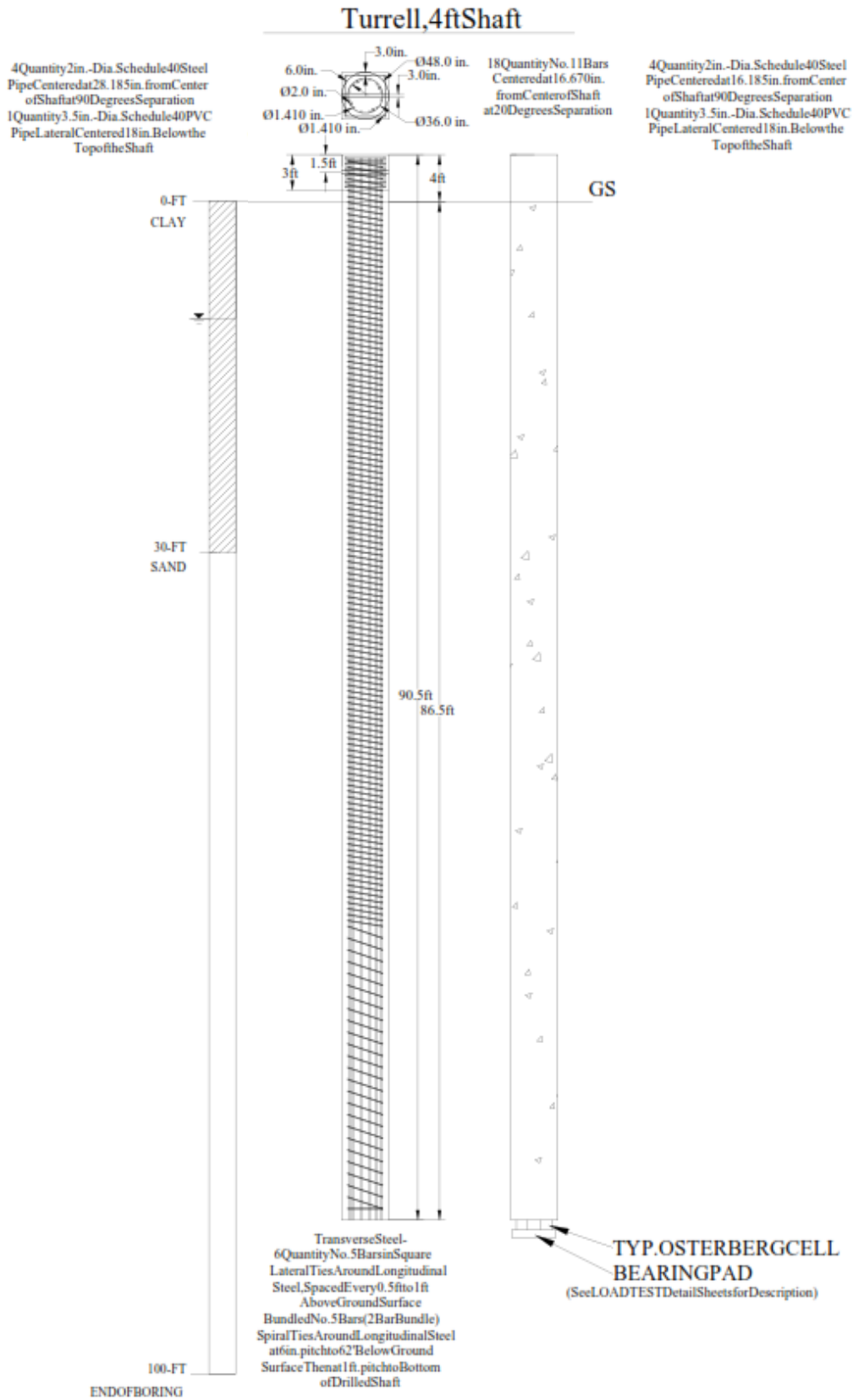

Figure 6.1. Schematic of four-foot diameter shaft design.

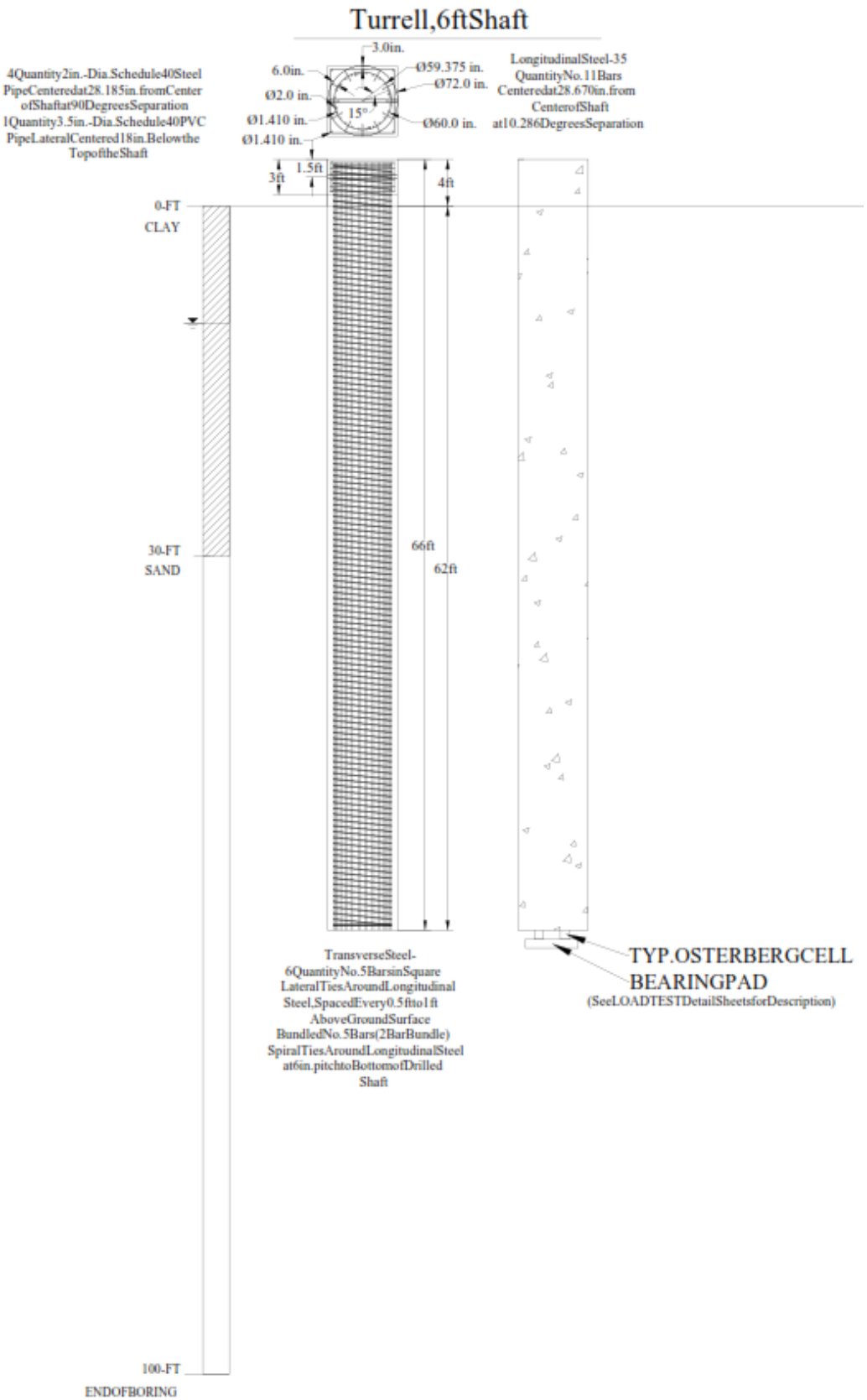

Figure 6.2. Schematic of six-foot diameter shaft design.

6.2.1. Test Shafts T-N4 and T-S4

Test shaft T-N4 (measuring nominally four-feet in diameter and oriented at the furthest North position on the test site) and test shaft T-S4 (measuring nominally four-feet in diameter and oriented at the furthest South position on the test site) were designed to extend 86.5-feet below the ground surface, and have a reveal length of four-feet, equaling a total shaft length of 90.5-feet. The longitudinal steel of each shaft was chosen to equal less than 1.0 percent of the gross cross-sectional area of the shaft with 16 (quantity) Number 11 bars of Grade 60 steel centered at 16.185-inches from the center of the shaft (separated at 30 degrees), as presented in Figure 6.3. Transverse reinforcement within each of the T-N4 and T-S4 shafts included two-bar bundled, Grade 60, Number 5 steel spirals spaced at a 0.5-foot pitch to a depth of 62-feet below ground surface, then spaced at a one-foot pitch to the bottom of the shaft (Figure 6.3). The tubing for cross hole sonic logging consisted of four (quantity), two-inch diameter, Schedule 40 black steel pipe centered 17-inches from the center of the shaft (separated at 90 degrees), as presented in Figure 6.4. One pair of diametrically opposing CSL tubes were also specified to be united at the bottom of each rebar cage using a sleeve fitting to enable future drilled shaft thermal transfer testing.

Figure 6.3. Photograph of a four-foot diameter shaft reinforcement cage from the side view.

Figure 6.4. Photograph of an end view of the four-foot diameter shaft reinforcement cage.

Six-inch diameter plastic spacers, attached to the transverse steel, were specified at eight-foot increments to provide six-inches of clearance between the outer transverse steel and the surrounding soil. The top four-feet of reveal of each shaft consisted of a four-foot cubic block of concrete. This block contained extra reinforcement including four (quantity) Number 11 longitudinal bars and six (quantity) Number 5 transverse bars. A photograph of the reinforcement utilized within the top block is presented in Figure 6.5. A four-foot long piece of 3.5-inch diameter Schedule 40 polyvinylchloride pipe was also specified to be installed across the center of the shaft and located eighteen inches below the top of each block (oriented North to South). This pipe (located at the same vertical elevation in each shaft) was included to enable future lateral testing.

Figure 6.5. Photograph of extra reinforcement for the test shaft T-4N top block reinforcement cage.

Also specified within each shaft for housing telltales were five 0.5-inch diameter Schedule 40 black steel pipes spaced 17.125 inches from the center of the shaft. Specifically, each casing was specified to house a string of 0.125-inch diameter stainless steel telltale rods. Within test shaft T-N4, three telltale casings were specified to rest upon the side of the bottom O-Cell steel plate at a depth of 66.2-feet below ground surface, and two telltale casings were specified to rest upon the side of the top O-Cell plate at a depth of 65.0-feet below ground surface. Within test shaft T-S4, three telltale casings were specified to rest upon the side of the bottom O-Cell steel plate at a depth below ground surface of 66.3-feet, and two telltale casings were specified to rest upon the side of the top O-Cell plate at a depth of 65.25-feet below ground surface. A photograph of the telltale casings that were installed installed is presented in Figure 6.6.

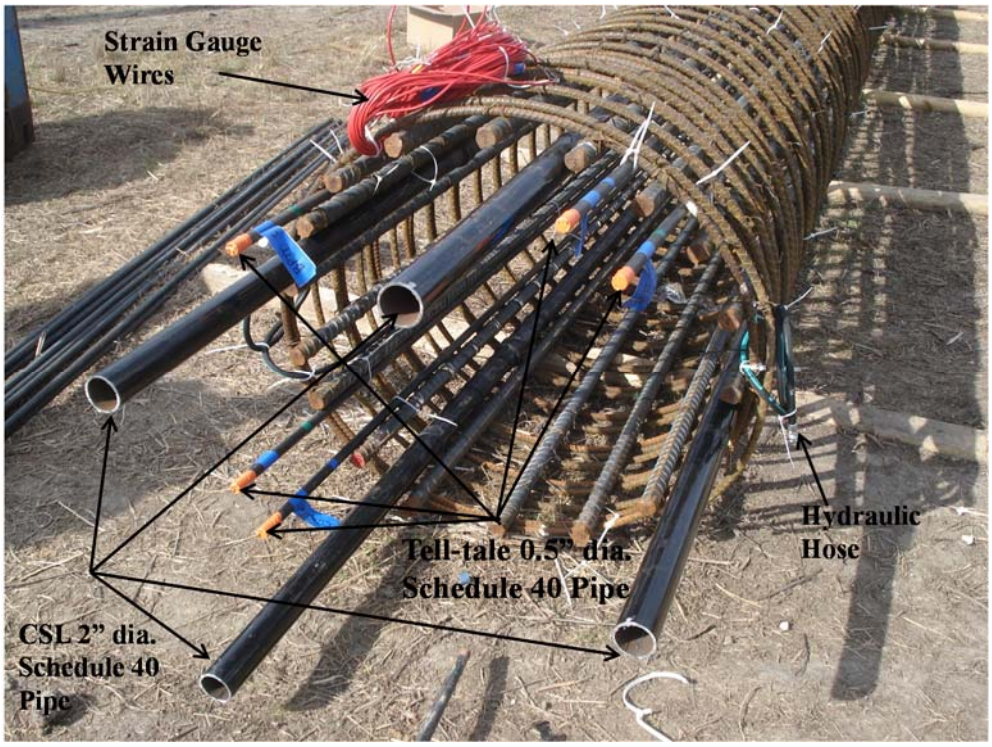

Figure 6.6. Photograph of CSL pipe and telltale casings utilized in each shaft.

Linear vibrating wire strain gauges were specified to monitor strains within the shaft at given locations to better understand the load transfer characteristics. One set of diametrically opposed strain gauges were specified to be installed (utilizing zip ties and welded mounts) within each four-foot diameter shaft at ten locations. Strain gauges were located at depths 12, 19.9, 27.9, 35.9, 43.0, 50.25, 58.0, 71.0, 79.0, and 86.5-feet from the top of the rebar cage of test shaft T-N4. Within test shaft T-S4, displacement transducers were located at depths 12.3, 20.4, 28.3, 36.25, 43.25, 50.3, 58.3, 71.3, 79.3, and 87.25-feet from the top of the rebar cage. A photograph of a linear vibrating wire strain gauge is presented in Figure 6.7.

Figure 6.7. Photograph of the linear vibrating wire strain gauges utilized in each shaft.

6.2.2. Test Shaft T-C6

Test shaft T-C6 (measuring nominally six-feet in diameter and centrally oriented on the test site) was designed to extend 61.5-feet below the ground surface, and have a reveal length of four-feet, equaling a total shaft length of 65.5-feet. The longitudinal steel of the shaft was chosen to equal less than 1 percent of the gross cross-sectional area of the shaft with 35 (quantity) Number 11 bars of Grade 60 steel centered at 28.53 inches from the center of the shaft (separated at 10.3 degrees) [Figure 6.8]. Transverse reinforcement within the T-C6 test shaft included a two-bar bundled Grade 60, Number 5 steel spiral consisting of loops spaced at a 0.5-foot pitch to the bottom of the drilled shaft (Figure 6.8). The tubing for cross hole sonic logging consisted of four (quantity), two-inch diameter, Schedule 40 black steel pipe centered 28.19 inches from the center of the shaft (separated at 90 degrees) [Figure 6.9]. One pair of diametrically opposing CSL tubes were specified to be united at the bottom of the rebar cage using a sleeve fitting to enable future drilled shaft thermal energy transfer testing. Tied, plastic spacers were specified at eight-foot increments to provide six-inches of clearance between the outer transverse steel and

the surrounding soil. The top four-feet of reveal of the shaft consisted of a four-foot high by six-foot by six-foot block of concrete. This block contained extra reinforcement including four (quantity) Number 11 longitudinal bars and 6 (quantity) Number 5 transverse bars. A six-foot long piece of 3.5-inch diameter Schedule 40 polyvinylchloride pipe was also specified to be installed across the center of the shaft and located 18 inches below the top of the block (oriented North to South). This pipe (located at the same vertical elevation as the pipes in test shafts T-N4 and T-S4) was included to enable future lateral testing.

Figure 6.8. Photograph of a side view of the six-foot diameter shaft reinforcement cage.

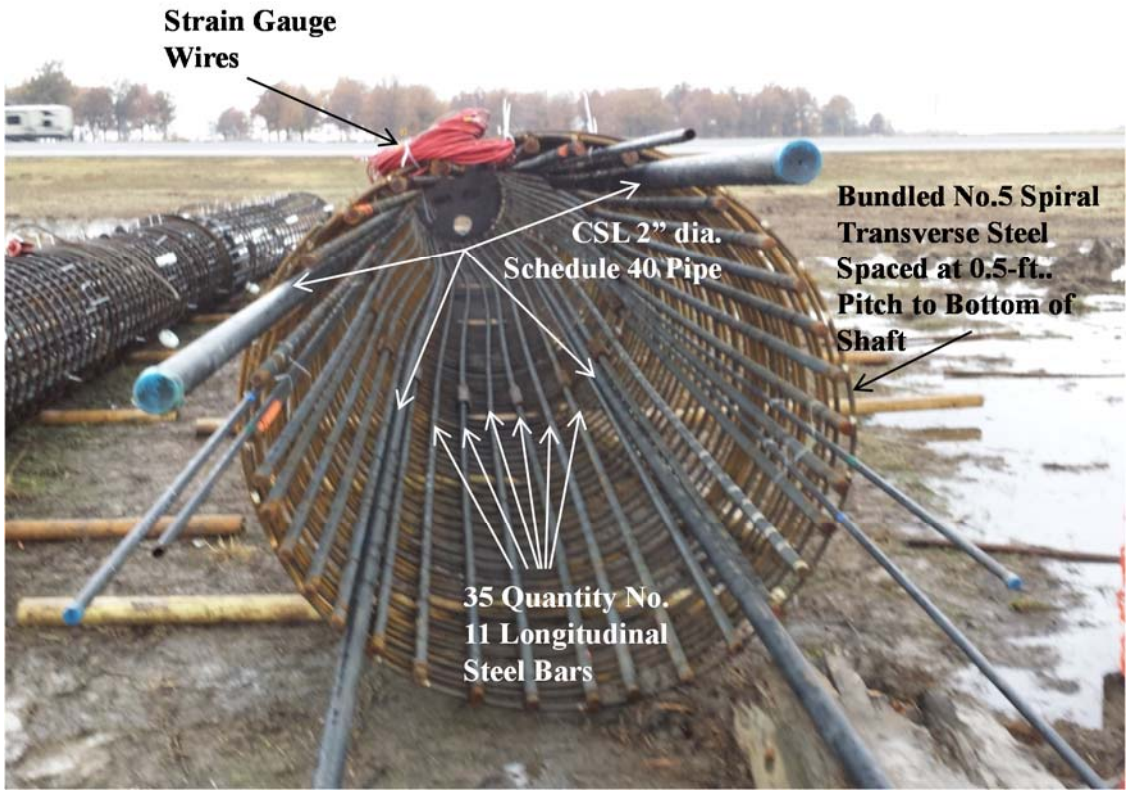

Figure 6.9. Photograph of an end view of the six-foot diameter shaft reinforcement cage.

Linear vibrating wire strain gauges were also specified to monitor strains within test shaft T-C6 at given locations to better understand the load transfer characteristics. One set of diametrically opposed strain gauges were specified to be installed (utilizing zip ties and welded mounts as presented in Figure 6.10) within the six-foot diameter shaft at various locations. Displacement transducers were located at depths below ground surface of 8.0, 16.0, 24.0, 30.0, 35.0, 40.0, 45.0, 50.0, 57.5, and 60.0-feet from the top of the rebar cage. Also specified within this shaft were five 0.5-inch diameter Schedule 40 black steel pipes. Each casing was specified to house a string of 0.125-inch diameter stainless steel telltale rods. Within test shaft T-C6, three telltale casings were specified to rest upon the side of the bottom O-Cell steel plate at a depth of 55.0-feet below ground surface of, and two telltale casings were specified to rest upon the side of the top O-Cell plate at a depth of 53.8-feet below ground surface.

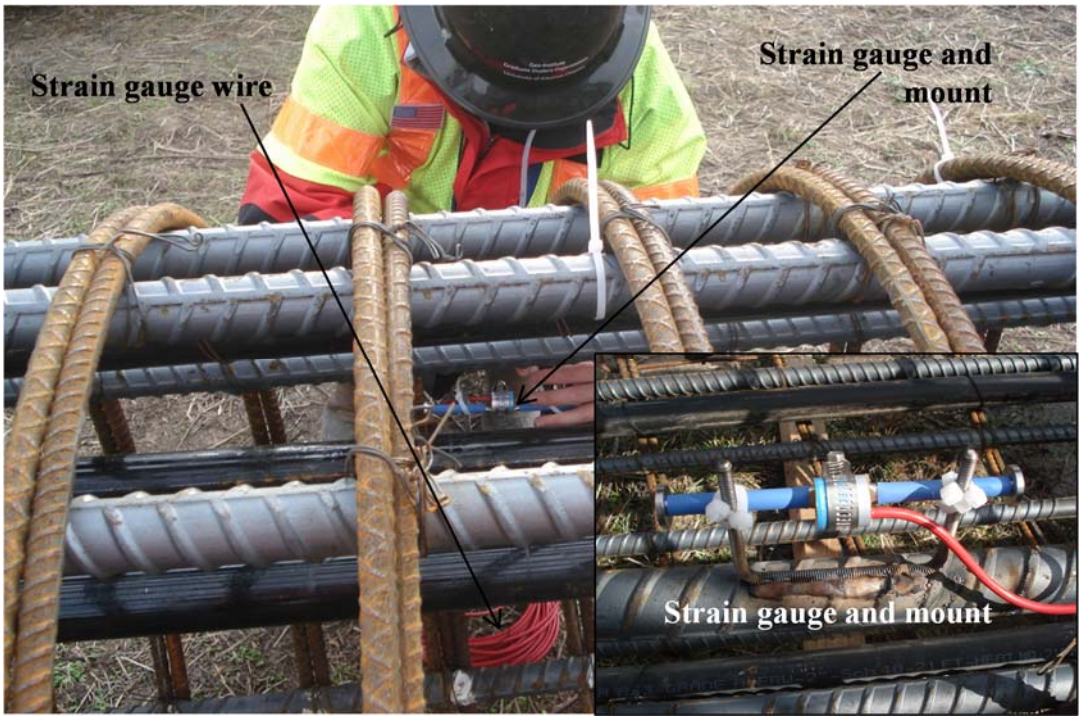

Figure 6.10. Photograph of strain gauge installation utilizing welded bracket and zip ties.

6.3. Construction of Test Shafts

The materials and equipment utilized to construct the test shafts are described in this Section. The construction process of the T-S4 (Section 6.3.1), T-C6 (Section 6.3.2), and T-N4 (Section 6.3.3) drilled shaft foundations are also discussed (including the excavation, reinforcement cage and O-Cell assembly, placement, concrete pouring, and formwork). Each of the test shafts were constructed by personnel from McKinney Drilling. The shafts were constructed on 53-feet center to center spacings. Equipment utilized for the construction of each shaft included a CZM EX125 drill rig (exempting part of the test shaft T-C6 excavation), a TEREX crane, and an American 7260 crane (Figure 6.11). The steel utilized to construct the reinforcement cages for each shaft was provided by West Memphis Steel Corp., while the concrete utilized to pour each shaft was provided by Razorback Concrete Co. Additionally, the spacers utilized to center each shaft were provided by Foundation Technologies.

(a) (b) (c)

Figure 6.11. Photographs of the (a) CZM EX125 drill rig, (b) TEREX crane, and (c) American 7260 crane utilized at the Turrell Arkansas Test Site.

Slurry construction methods were utilized to excavate each shaft. Materials utilized during the slurry construction process included a polymer stabilizer called Super Mud Dry provided by PDS (Figure 6.12a), and light density soda ash provided by DEAL Inc. (Figure 6.12b).

(a) (b)

Figure 6.12. Photographs of (a) polymer stabilizer utilized for slurry construction and (b) light density soda ash at the Turrell Arkansas Test Site.

The concrete mix utilized to pour each shaft was specified to contain a water cement ratio of 0.46 (max of 0.49), a slump of seven-inches (plus or minus one-inch), an entrapped air content of 2 percent, a maximum aggregate size of one-inch, and a unit weight of 136 pounds per cubic foot. Constituents of the concrete mix are presented in Table 6.1. Water reducing admixtures and hydration stabilization admixtures (provided by Razorback Concrete Company) were introduced in accordance with ASTM C494 (2013).

Table 6.1. Concrete mix constituents.

Material Type	Description	Specific Gravity	Design Quantity
Cement	Buzzi Unicem Type I Cement	3.15	489 lb/cy
Fly Ash	Headwaters Resources Class C Fly Ash	2.67	122 lb/cy
Coarse Aggregate	RazorRock Materials #67 Gravel	2.55	1625 lb/cy
Fine Aggregate	RazorRock Materials C-33 Natural Sand	2.64	1433 lb/cy
Water	City Water (34 gal)	1.00	34 gal/cy
Admixture	BASF-Polyheed 900 Mid-Range Water Reducer	-	22 oz/cy
Admixture	Delvo Stabilizer (as required for set control)	-	-

Each shaft was poured utilizing a Putzmeister 52M concrete pump truck (Figure 6.13) along with a 4-inch inner diameter tremie supplied by McKinney Drilling (Figure 6.14). The concrete was poured from the bottom of the shaft with the tremie being moved to maintain approximately 30-feet of head above the bottom of the treime. To ensure concrete quality, the tremie was plugged with a rubber ball.

Figure 6.13. Photograph of the Putzmeister 52M pump truck at the Turrell Arkansas Test Site.

To verify the concrete quality on site, UofA personnel cast four-inch diameter by eight-inch tall cylinders from a portion of the concrete obtained from each concrete truck. The cylinders were later tested to determine values of uniaxial compressive strength and modulus of elasticity. On one truck per shaft (selected towards the middle of the pour), UofA personnel cast 11 cylinders to perform additional testing. UofA personnel also performed slump and air content testing on a portion of the concrete from each truck. Each sample was obtained directly from the concrete mix truck (prior to placing the concrete into the pump truck). An as-built schematic of each test shaft is presented in Figure 6.15.

Figure 6.14. Photograph of installation of the four-inch inner diameter tremie pipe for test shaft T-6C.

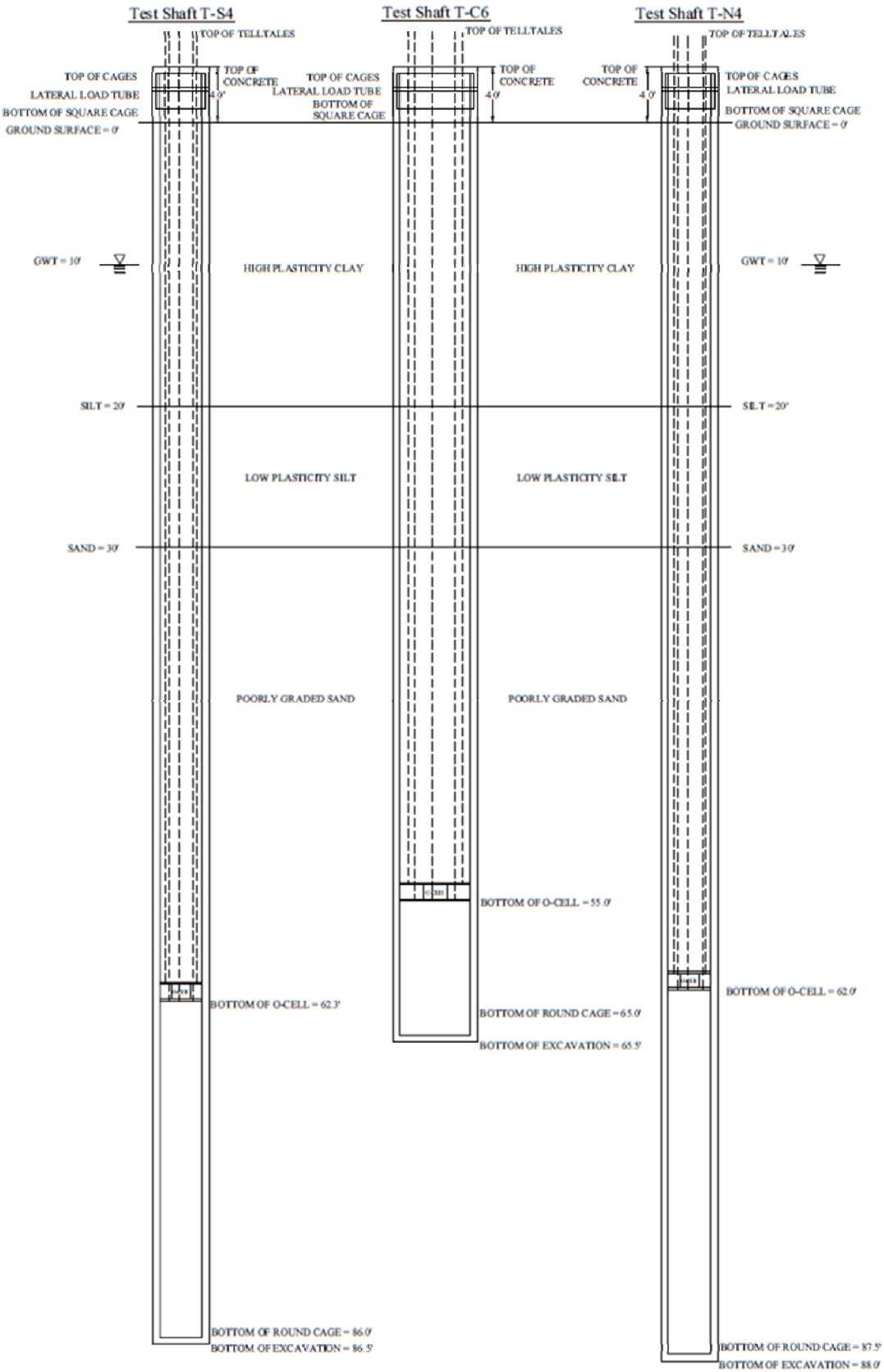

Figure 6.15. As-built schematic of the each test shaft at the TATS.

6.3.1. Test Shaft T-S4

The construction process associated with test shaft T-S4 is described in this section. This shaft, situated furthest South from Interstate 55, had an excavation depth of 86-5 feet below ground surface. The equipment utilized, and the excavation process involved with test shaft T-S4 is described (Section 6.3.1.1). Assembly of the steel reinforcement cage and O-Cell are discussed in Section 6.3.1.2. The placement of the completed cage within the excavation, the concrete placement, and cap formation of test shaft T-S4 are also discussed in Section 6.3.1.2.

6.3.1.1. T-S4 Excavation

Personnel from McKinney Drilling excavated soil at the location of test shaft T-S4 from November 18 through November 21, 2013, using the previously mentioned CZM EX125 drill rig (Figure 6.16a). To prevent caving, a four-foot seven-inch outer diameter, 22.5-foot long temporary steel casing was inserted into the open excavation, reaching a depth of 18.5-feet (Figure 6.16b). Upon installation of the casing and reaching a depth of 20-feet, the excavation was flooded, and four canisters of slurry polymer, and two (quantity) 50-lb bags of soda ash were added (Figure 6.17a). Due to seasonal water table fluctuations, water percolation within the excavation was not observed prior to slurry addition. Silty sand was encountered at a depth of approximately 36-feet (Figure 6.17b).

(a) (b)

Figure 6.16. Photographs of the (a) flight auger, and (b) temporary casing utilized during construction of test shaft T-S4.

(a) b)

Figure 6.17. Photographs of (a) polymer addition, and (b) the resulting silty sand sand slurry obtained from the excavation.

On November 18, at 1:27 p.m. and at a depth of approximately 72-feet below ground surface, the flight auger was exchanged for an excavation bucket (Figure 6.18a). Excavation was continued to a depth of 80.5-feet (2:10 p.m.). The exaction was plugged utilizing the auger

bucket, and left till Novemebr 19th. However, during the final stages of the excavation (at a depth of approximately 82-feet below ground surface), the auger bucket detached from the kelly bar and descended to the bottom of the excavation [due to a defective pin connecting the auger to the sub]. The bucket was retrieved utilizing a hook mounted to the American 7260 crane (Figure 6.18b). Following retrieval of the auger bucket, a new pin was inserted and the excavation was completed to a final depth of 86.5-feet below ground surface. Upon completion of the excavation, the temporary casing was left in place, and the exposed excavation was covered with railroad ties until insertion of the rebar cage on December 4, 2013 (approximately 14 days later).

(a) (b)

Figure 6.18. Photographs of (a) auger bucket during excavation, and (b) auger bucket retrieval.

On November 26 around 8:40 a.m. the CZM EX125 drill rig overturned during the repositioning process. As a result, a new AGBO G150 drill rig was imported to complete the T-C6 excavation while the CZM EX125 drill rig was reoriented and remobilized. Photographs of the overturned CZM EX125 drill rig and of the subsequent replacement rig (Watson AGBO G150) are presented in Figures 6.19 and 6.20, respectively.

Figure 6.19. Photograph of the overturned CZM EX125 drill rig.

Figure 6.20. Photograph of the imported Watson AGBO G150 drill rig.

6.3.1.2. T-S4 Rebar Cage and Concrete Placement

Upon completion of the 86.5-foot deep excavation, the rebar and concrete for test shaft T-S4 were placed on December 4, 2013, by personnel from with McKinney Drilling with oversight by personnel from Loadtest, Inc. and the University of Arkansas. The O-Cell, composed of a 12-

inch tall hydraulic jack encompassed by two-inch thick steel plates mounted on the top and bottom of the jack, was inserted and welded to the reinforcement cage (upon temporary removal of the transverse reinforcement surrounding the area). The O-Cell was centered at approximately 65-feet and one–inch from the top of the rebar cage (Figure 6.21). The assembly was inserted into the rebar cage by cutting away select segments of longitudinal steel to slide the O-Cell and plates into place. The cut pieces were extracted from the shaft, and the remaining pieces were welded to the side of the top and bottom O-Cell plates (Figure 6.21). The lengths of longitudinal steel that were left uncut were also welded to the side of the top and bottom plates of the O-Cell (Figure 6.21). Each of the aforementioned telltale pipes was also welded to the O-Cell. As previously discussed, three telltale pipes were welded to the side of the bottom plate, while two of the telltale pipes were welded to the side of the bottom plate of the O-Cell (Figure 6.21).

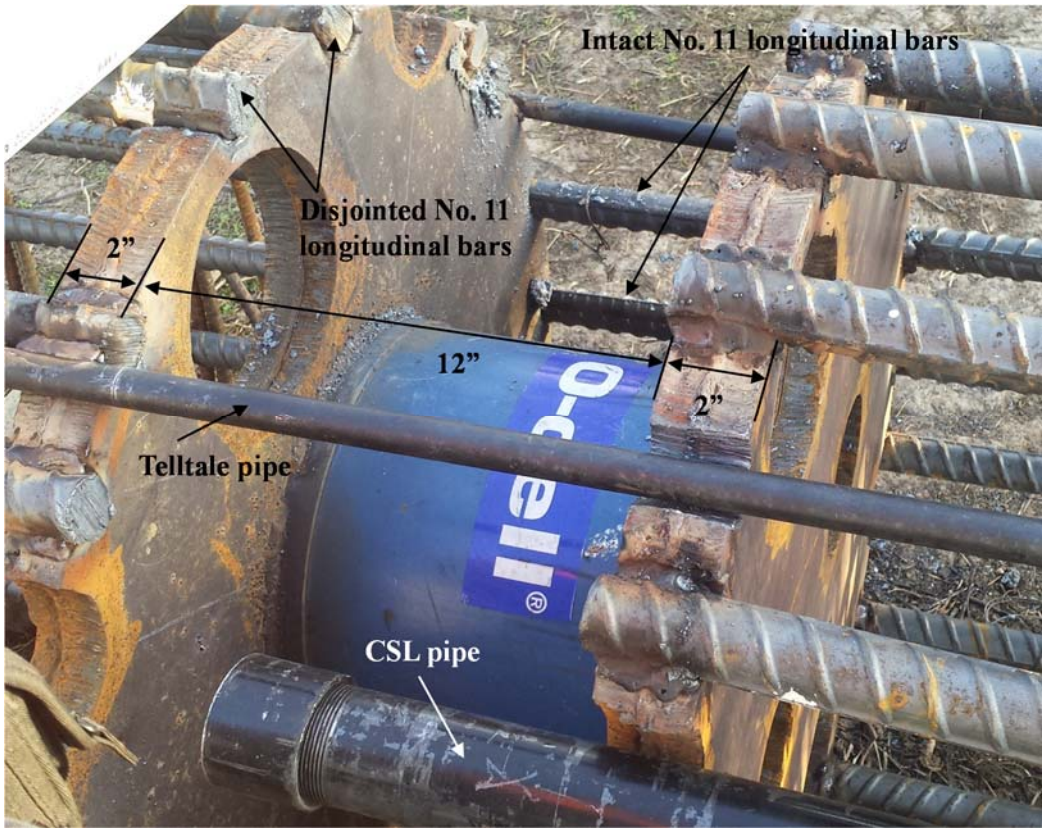

Figure 6.21. Photograph of the installed O-Cell within the reinforcement cage for test shaft T-S4.

Upon placement of the O-Cell within the cage, and placement of the CSL tubes and telltales around the O-Cell, rubber CSL sleeve fittings were secured around each end of the CSL pipes, covering the breaks in the pipes. These fittings were installed to ensure that each pipe remained water tight during the placement of concrete around the CSL pipes (Figure 6.22). Strain gauge wires were also overlaped through a greased 12-inch length of 2-inch inner diameter PVC pipe. This PVC pipe served as a spacer to protect the wires, as well as enable displacement of the O-Cell without damaging the wires (Figure 6.22). Following installation of the strain gauge wire spacer, the hydraulic hoses were installed from the connection on top of the O-Cell to the top of the rebar cage, then the transverse reinforcement was repositioned and tied above and below the O-Cell assembly.

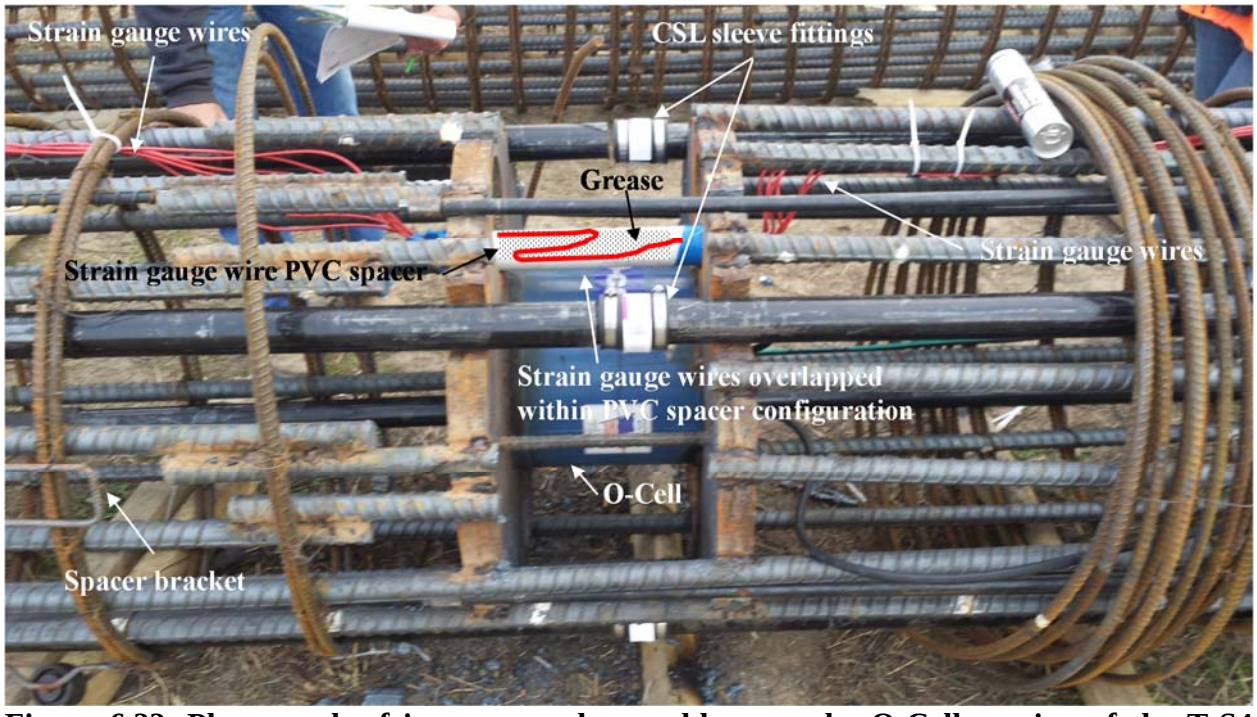

Figure 6.22. Photograph of instrumented assembly near the O-Cell portion of the T-S4 reinforcement cage.

A diagram (Figure 6.23a) of a completed top-down view and a photograph of the instrumented (Figure 6.23b) test shaft T-S4 is presented. Yellow tape on the end of gauge wire indicated the "B" side of the shaft.

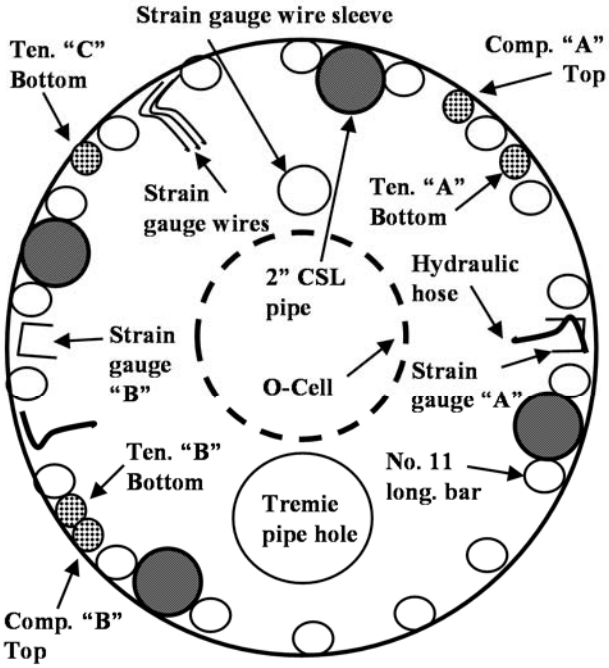

(a)

(b)

Figure 6.23. Schematic of (a) top-down view of test shaft T-4S, and (b) photograph of instrumented assembly.

The total cage, measuring 90-feet and one-inch in length after installation of the O-Cell, was picked up from a horizontal position to a vertical position using the American 7260 crane

and the TEREX crane**.** The American 7260 crane was also utilized to lower the rebar cage into the excavation (Figure 6.24a). During concrete placement within the excavation, the tremie and temporary casing were removed. The aforementioned shaft reveal length of four-feet was formed by placing a pre-constructed four-foot wide by four-foot long wooden form over the poured shaft (Figure 6.24b). Upon lowering the additional reinforcement for the top cap (as outlined in the previous section) and placing the lateral polyvinylchloride pipe at the proscribed elevation, concrete was poured within the assembly. The wooden forms were removed after the concrete within the block was hardened.

(a) (b)

Figure 6.24. Photograph of (a) the placement of the rebar cage for test shaft T-S4 into excavation, and (b) four-foot by four-foot by four-foot reveal form work.

Sixty-three cubic yards of concrete were utilized to complete the construction of the T-S4 shaft. All as-built features met the design specifications outlined in Section 6.2.1, except that the one pair of diametrically opposing CSL pipes at the bottom of the rebar cage were not united, and 18 (instead of 16) No. 11 longitudinal bars were utilized to construct the reinforcement cage.

The total length of test shaft T-S4 measured 90.5-feet from the bottom of the excavation to the top edge of the four-foot tall concrete block reveal. The finished assembly is presented in Figure 6.25.

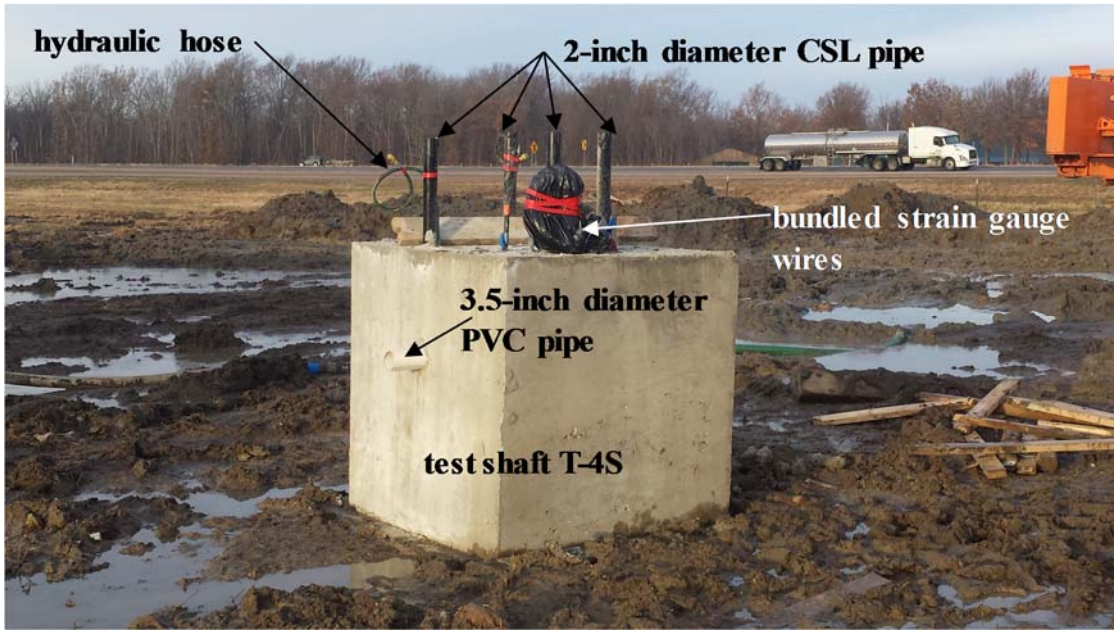

Figure 6.25. Photograph of completed test shaft T-S4.

6.3.2. Test Shaft T-C6

The construction process associated with test shaft T-C6 is described in this Section. Test Shaft T-C6 was constructed from November 26 through December 17, 2013, and was situated centrally between the T-S4 and T-N4 drilled shaft foundations. This shaft was constructed to a depth of 62-feet below ground surface. The equipment utilized and the excavation process involved with test shaft T-C6 is described (Section 6.3.2.1). Assembly of the steel reinforcement cage and O-Cell are discussed in Section 6.3.2.2. Additionally, the placement of the completed cage within the excavation, the concrete placement, and cap formation of test shaft T-C6 are also discussed in Section 6.3.2.2.

6.3.2.1. T-C6 Excavation

Test Shaft T-C6 was excavated by personnel from McKinney Drilling from November 26 through December 17, 2013. To prevent caving, upon reaching an excavation depth of 20-feet, a six-foot outer diameter, 24-foot long temporary steel casing was inserted into the top of the excavation. Upon reaching an excavation depth of 25-feet, the excavation was flooded, and canisters of slurry polymer, and 50-lb bags of soda ash were added. As with test shaft T-S4, water percolation within the excavation was not observed prior to slurry addition. Upon completion of the 62-foot deep excavation, the cased-excavation was covered with railroad ties and left until successful installation of the rebar cage on December 17. Delay for the rebar cage installation was attributed to the previously mentioned overturn of the CZM EX125 drill rig.

6.3.2.2. T-C6 Rebar Cage and Concrete Placement

The rebar and concrete for test shaft T-C6 were placed in the excavation on December 17, 2013 by personnel from McKinney Drilling, with oversight by Loadtest Inc. and University of Arkansas personnel. The O-Cell assembly (O-Cell and plates) was welded to the completely severed reinforcement cage at 53-feet (centered) from the top of the cage. The O-cell assembly was inserted by disjointing each length of longitudinal steel with a welding torch. The cut pieces (forming the intact lower 8.5-feet of the shaft including transverse reinforcement) were welded to the side of the bottom plate of the O-Cell (Figure 6.26). The remaining 54-feet of the upper portion of the shaft was welded to the side of the top plate of the O-Cell (Figure 6.26). Upon placement of the O-Cell within the cage, the CSL tubes and telltales were installed above and below the O-Cell. Rubber sleeve fittings were secured around each end of CSL pipe, covering the breaks in the pipes, to prevent water leakage. All five telltale pipes were welded to the O-

Cell. Three of the telltale pipes welded to the side of the bottom plate, and two of the telltale pipes welded to the side of the bottom plate (Figure 6.26).

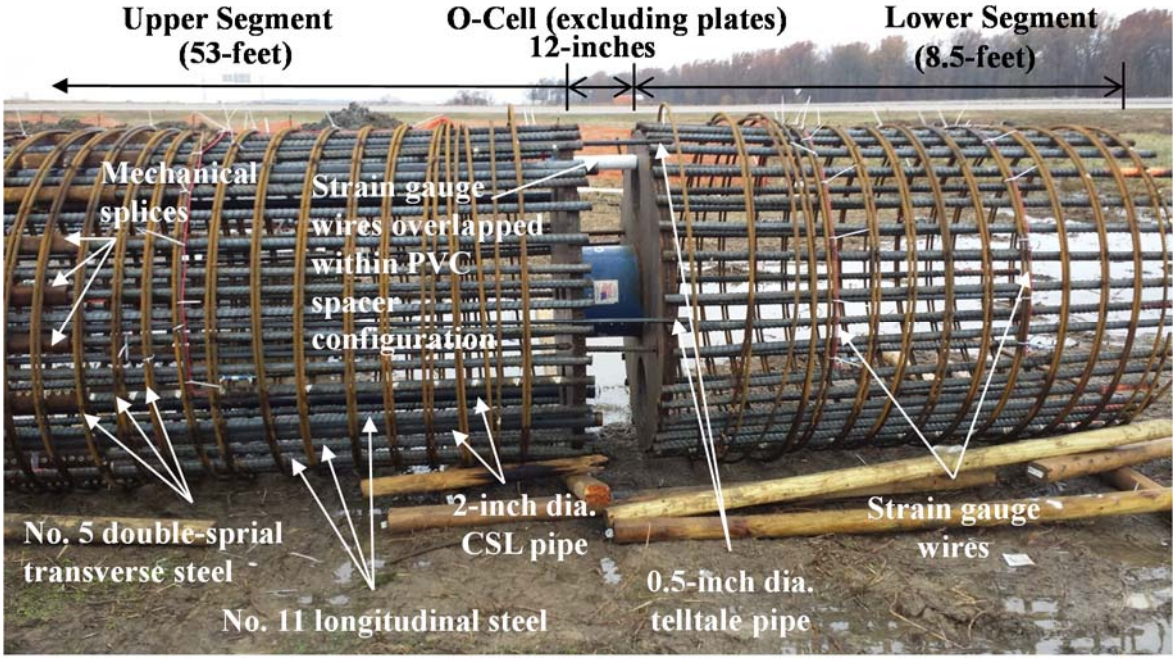

Figure 6.26. Photograph of the lower portion of the test shaft T-C6 instrumented reinforcement cage.

Strain gauge wires were installed throughout the length of the rebar cage using plastic zip ties. Black tape was applied to the end of one of each pair of gauge wires to indicate the "B" side of the shaft. At the location of the O-Cell, the strain gauge wires connected to gauges located below the O-Cell were folded to overlap through a greased 12-inch long of 2-inch inner diameter PVC pipe spanning the height of the O-Cell. This PVC pipe served as a spacer to protect the wires, as well as enable displacement of the O-Cell without damaging the wires. Following installation of the PVC strain gauge wire spacer, hydraulic hoses were installed from the connection on the top of the O-Cell to the top of the rebar cage, and secured with plastic zip ties. During installation of the hydraulic hoses, the transverse reinforcement was repositioned and re-tied above and below the O-Cell assembly. A diagram (Figure 6.27a) of a completed top-down view and a photograph of instrumented rebar cage (Figure 6.27b) for test shaft T-S4 is presented.

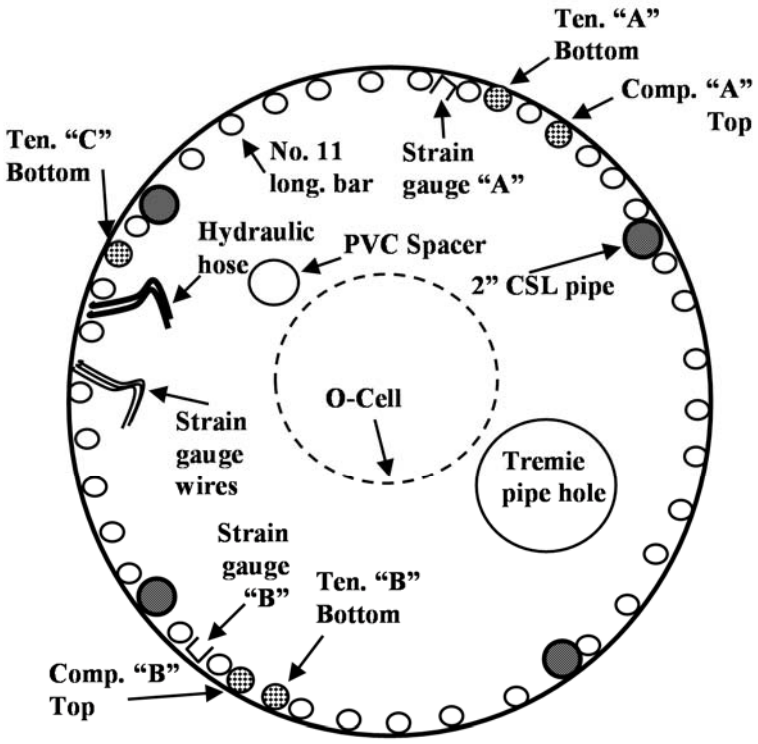

(a)

(b)

Figure 6.27. Schematic of (a) top-down view of test shaft T-C6, and (b) photograph of instrumented assembly.

The instrumented cage, measuring 66-feet and 4-inches in length, was picked using the American 7260 cane and the TEREX crane**.** Two unsuccessful attempts were completed before

the reinforcement cage was left vertically suspended using the American 7260 crane. After the first unsuccessful pick (performed at 8:41 a.m. on December 16), welds connecting the bottom 8.5-ft long segment of the reinforcement cage to the bottom O-Cell plate were severed, and the bottom 8.5-foot cage was racked (Figure 6.28a). As a result, each longitudinal bar connecting the bottom segment to the bottom plate were repositioned and re-welded. Additionally, partial deformations in lengths of the telltale pipe at the location of the O-Cell were observed after the first pick attempt, and were welded (Figure 6.287b).

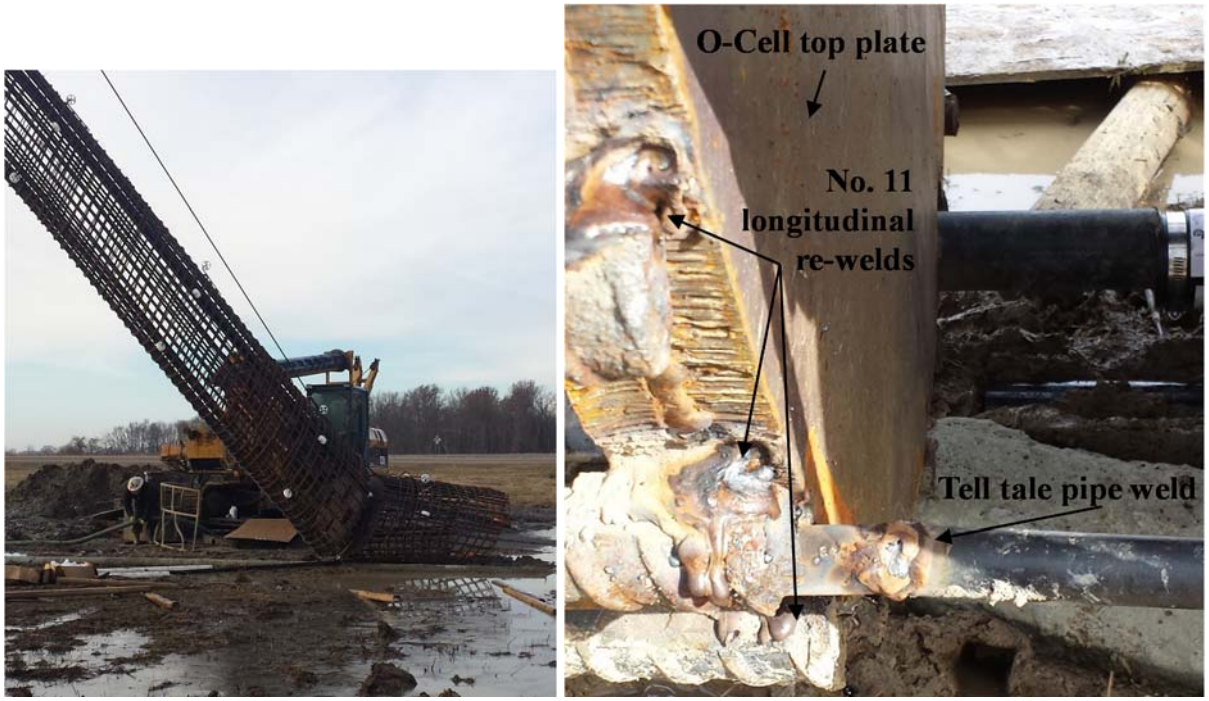

(a) (b)

Figure 6.28. Photograph of the rebar cage for test shaft T-C6 during the (a) first pick attempt, and (b) subsequent CSL pipe damage and longitudinal bar re-welds.

During the second unsuccessful pick (performed at 12:23 p.m. on December 16), the entire bottom segment of the reinforcement cage detached from the bottom plate of the O-Cell and collapsed/pancaked (Figure 6.29a). Despite the collapse, the remainder (top segment and O-Cell) of the cage was further elevated and vertically suspended. The collapsed bottom segment was transported to and positioned within the wooden form of the test shaft T-C6 top cap. After

being lowered into the form, personnel from McKinney Drilling proceeded to realign the longitudinal and transverse steel of the bottom segment in preparation for another re-attachment (Figure 6.29b). The longitudinal steel was then once again welded to the bottom plate of the O-Cell, and the transverse steel was re-tied near the vicinity of the O-Cell. The completed vertical assembly was then transported to hang above the excavation.

(a) (b)

Figure 6.29. Photograph of test shaft T-C6 during the (a) second un-successful pick, and (b) second re-assembly process.

Following the second pick, all previously installed strain gauge wires located within the bottom segment were torn from their original mounts, and replacement of the strain gauges was required. After being positioned above the excavation (Figure 6.31a), four new vibrating wire strain gauges (and their respective wires) were acquired from test shaft T-N4 and installed below the O-Cell (Figure 6.18). A photograph of the suspended instrumented reinforcement cage for test shaft T-C6, prior to concrete placement, is presented in Figure 6.30a.

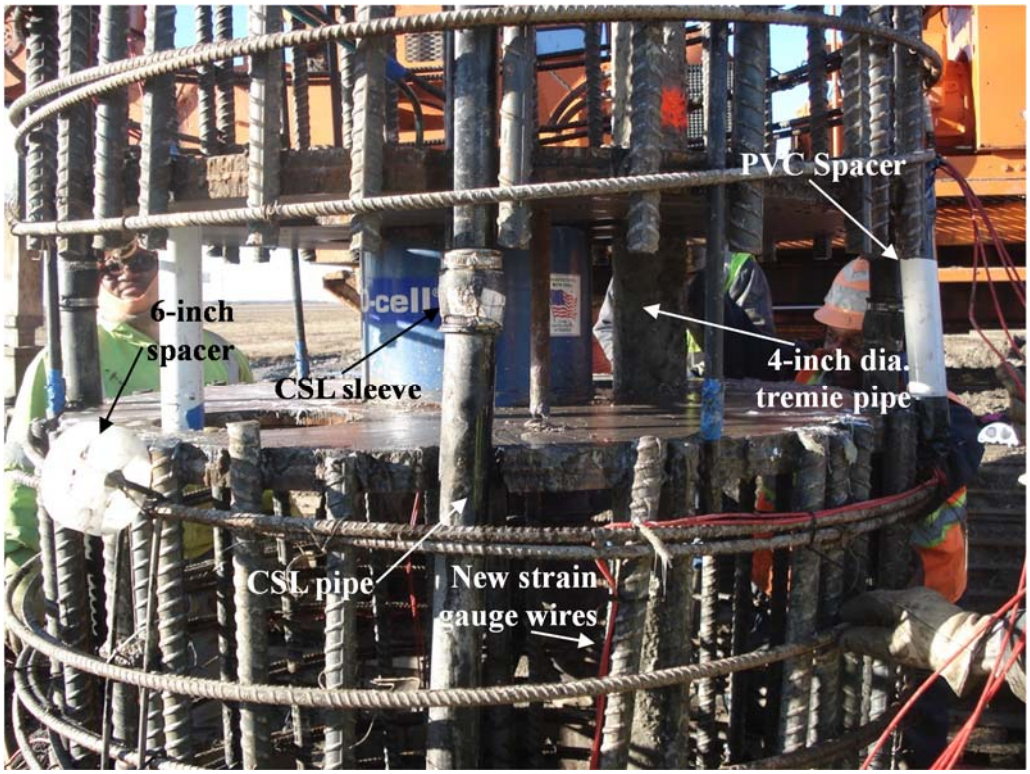

Figure 6.30. Photograph of the lower section of the T-C6 test shaft including segment strain gauge re-installation.

Concrete placement commenced at 10:40 a.m. on December 17, 213. During concrete placement in test shaft T-C6, the reinforcement cage was noted to have raised approximately 1.5-feet after Truck 3, due to uplift from too much concrete being pumped by the pump truck operator. Following concrete placement within the excavation, a shaft reveal length of four-feet was formed by placing a pre-constructed six-foot wide by six-foot long wooden form over the poured shaft (Figure 6.31b). Upon lowering the additional reinforcement for the square cap (as outlined in the previous section), removing the tremie, removing the temporary casing, and placing the lateral polyvinylchloride pipe to elevation, concrete was poured within the assembly. Nine trucks total (each carrying nine cubic yards of concrete) were required to complete the pour. The wooden forms were removed after the concrete within the box was hardened.

(a) (b)

Figure 6.31. Photograph of test shaft T-C6 (a) suspended reinforcement cage prior to concrete placement, and (b) after the four foot reveal construction placement.

Eighty-one cubic yards of concrete were utilized to complete the construction of test shaft T-C6. All as-built features met the design specifications outlined in Section 6.2.2 except that the prescribed one pair of diametrically opposing CSL pipes at the bottom of the rebar cage were not united. Also, due to the uplift observed during concrete placement, the bottom 1.5-feet of the shaft was unreinforced, and the top foot of the reinforcement cage was cut off to encapsulate the top of the rebar in concrete. The total length of test shaft T-C6 measured 65.5-feet from the bottom of the excavation to the top edge of the four-foot tall concrete block reveal. A photograph of the finished shaft is presented in Figure 6.32.

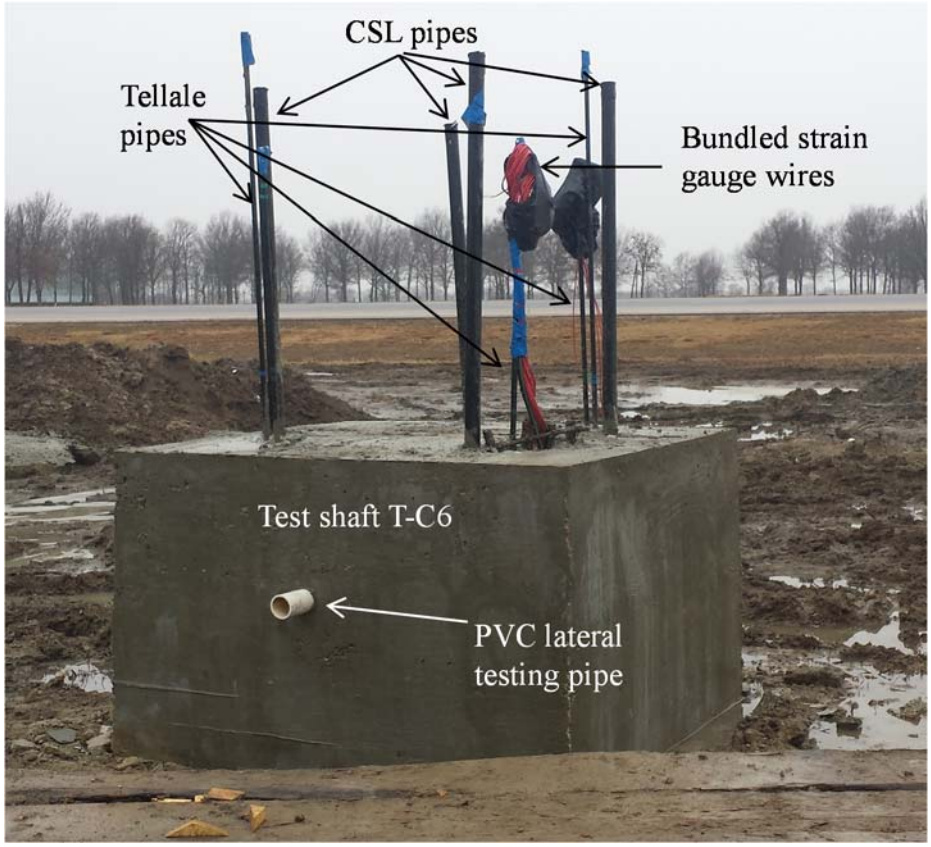

Figure 6.32. Photograph of the test shaft T-C6 finished construction.

6.3.3. Test Shaft T-N4

Test Shaft T-N4 was constructed from November 26 and December 23, 2013. This shaft, located closest to the northbound lanes of Interstate-55, was embedded to a depth of 88-fee. The equipment utilized and the excavation process involved with test shaft T-N4 is described in Section 6.3.3.1. Also discussed in Section 6.3.3.1 is the blowout that occurred within the excavation of test shaft T-N4. Assembly of the steel reinforcement cage and O-Cell are addressed in Section 6.3.3.2. Additionally, the placement of the completed cage within the excavation, the concrete placement, and cap formation of test shaft T-N4 are described in Section 6.3.3.2.

6.3.3.1. T-N4 Excavation

Test shaft T-N4 was excavated by personnel from McKinney Drilling between November 26 and December 23, 2013. To prevent caving, a temporary steel casing with measurements of a four-foot by seven-inch outer diameter by 22.5-foot long was inserted into the top of the excavation. Upon reaching an excavation depth of about 20-feet, the excavation was flooded and slurry polymer and soda ash were added. Due to seasonal water table fluctuations, water percolation within the excavation was not observed prior to slurry addition. Upon completion of the 86.5-foot deep excavation, the cased-excavation was left open until insertion of the rebar cage on December 18. A photograph of the T-N4 excavation process is presented in Figure 6.33.

Figure 6.33. Photograph of the test shaft T-N4 excavation process utilizing the CZM I-25.

Prior to the end of the day on December 18, 2013, the bottom of the rebar cage was lowered to a depth of approximately 35-feet below ground surface into the excavation, and left overnight. On the following morning of December 19, 2013, it was discovered the T-N4 excavation had collapsed, partially embedding the bottom of the rebar cage into soil. Upon retrieval of the reinforcement cage from the excavation (utilizing both cranes), the assembly was

suspended 30-feet away from the shaft, and inspected for damage (Figure 6.34a). No damage to the cage or instrumentation was observed; as a result the silty sand-slurry mixture that was aatached to the rebar cage was removed. During inspection of the rebar cage, the 22.5-foot temporary casing began to sink further into the excavation, from a depth of 1.5-feet above ground surface to a depth of approximately 13-feet below ground surface. As a result, a 39-foot long, 54-inch outer diameter temporary steel casing was imported onto site and installed at the same location. After the 23-foor casing was removed, a safety chain was attached to the 39-foot casing to prevent the casing from descending into the excavation (Figure 6.34b). After installation of the 39-foot casing, the re-excavation process was initialized. At a depth of 22 feet, polymer slurry and soda ash were added to stabilize the excavation (Figure 6.35a) prior to furthering the flight auger (Figure 6.35b) to a final depth of 88-feet. The additional depth was drilled to ensure a competent bottom of the excavation.

(a) (b)

Figure 6.34. Photograph obtained during construction of test shaft T-N4 with (a) the suspended reinforcement cage after collapse, and (b) newly installed 39-foot long casing.

(a) (b)

Figure 6.35. Photograph of test shaft T-N4 (a) soda ash addition for slurry formation, and (b) second excavation process.

6.3.3.2. T-N4 Rebar Cage and Concrete Placement

Upon completion of the 88-foot deep excavation, the rebar and concrete for test shaft T-N4 were placed December 23, 2013, by personnel from McKinney Drilling with oversight from Loadtest, Inc. and University of Arkansas personnel. As with test shaft T-S4, the O-Cell, composed of a 12-inch tall hydraulic jack encompassed by two-inch thick steel plates mounted on the top and bottom of the jack, was inserted and welded to the reinforcement cage (upon partial removal of the transverse reinforcement surrounding the area). The O-Cell was centered at approximately 65-feet and one–inch from the top of the rebar cage (Figure 6.36). The assembly was inserted into the reinforcement cage by cutting away select segments of longitudinal steel to slide the O-Cell and plates into place, similar to test shaft T-S4. The cut pieces were then extracted from the shaft, and the remaining pieces were welded to the side of the top and bottom O-Cell plates (Figure 6.36). The uncut lengths of longitudinal steel were also welded to the side of the top and bottom plates of the O-Cell (Figure 6.36). Five aforementioned telltale pipes were welded to the O-Cell. Three of the previously discussed telltale pipes were

welded to the side of the bottom plate, while two of the telltale pipes were welded to the side of the top plate of the O-Cell. Upon placement of the O-Cell within the cage, and placement of the CSL tubes and telltales around the O-Cell, rubber CSL sleeve fittings were secured around each end of CSL pipe, covering the breaks in the pipes. These fittings were installed to ensure each pipe remained water tight during placement of the concrete (Figure 6.36).

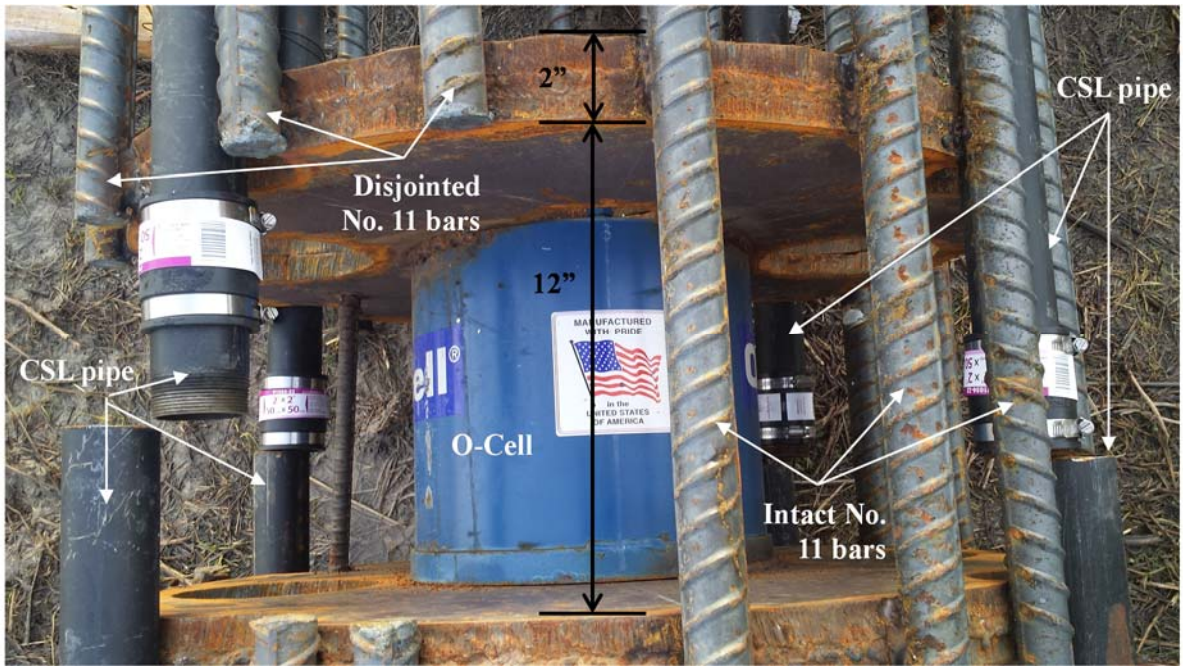

Figure 6.36. Photograph of installed O-Cell to the test shaft T-N4 reinforcement cage.

Four new strain gauge wires (two pairs, located at 58- and 71-feet below the top of the reinforcement cage) were imported to replace those unexpectedly utilized on test shaft T-C6 (Figure 6.37a). These new gauges (as indicated by the blue wires in Figures 6.38 and 6.40b) were installed directly above and beneath the O-Cell. Once bundled, the strain gauge wires were installed to overlap through a greased 12-inch long 2-inch inner diameter PVC pipe. Following installation of the strain gauge wire spacer, hydraulic hoses were installed from the connection on top of the O-Cell to the top of the rebar cage. Then the transverse reinforcement was repositioned and tied in the vicinity of the O-Cell assembly. Unlike test shaft T-4S and T-C6,

one pair of CSL pipes was united at the bottom of test shaft T-4N (Figure 6.38) to enable future temperature studies.

(a) (b)

Figure 6.37. Photograph of the (a) imported sister bar strain gauges, and (b) the mounted gauges upon the test shaft T-N4 reinforcement cage.

Figure 6.38. Photograph of CSL union at the bottom of the T-N4 reinforcement cage.

A diagram of a completed top-down view and a photograph of the instrumented test shaft T-N4 are presented in Figure 6.39. Black tape on the end of the gauge wire indicated the "B" side of the shaft.

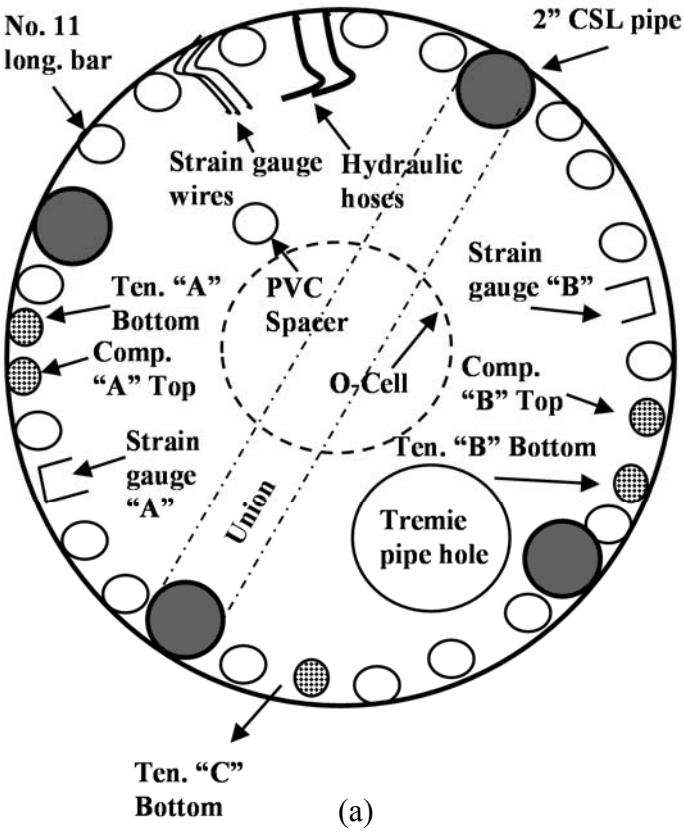

(a)

(b)

Figure 6.39. Schematic of (a) top-down view of test shaft T-N4, and (b) photograph of instrumented assembly.

The total cage, measuring 90-feet and ten-inches in length after installation of the O-Cell, was picked using the American 7260 and the TEREX cranes**.** The American 7260 crane was utilized to lower the rebar cage into the excavation following the blow-out (Figure 6.40a). Concrete placement commenced at 9:31 a.m. on December 23, 2013. During concrete placement in test shaft T-N4, two lengths of the tremie were removed from the excavation at a depth of 38-feet below ground surface (following Truck 4). It was also observed while placing the contents of Truck 7 that five cubic yards of concrete were lost at the sand/clay layer interface at approximately 30-feet below ground surface. During concrete placement, the tremie and temporary casing were removed from the excavation. Following concrete placement, a shaft reveal length of four-feet was formed by reutilizing the pre-constructed four-foot wide by four-foot long by four-foot high wooden form over the poured shaft (Figure 6.40b). Upon lowering the additional reinforcement (as outlined in the previous section) and placing the lateral polyvinylchloride pipe to elevation, concrete was poured within the assembly. Nine trucks were required to complete the pour, with each truck carrying nine cubic yards of concrete (exempting Truck 9, which only carried five cubic yards). The wooden forms were removed after the concrete was hardened.

(a) (b)

Figure 6.40. Photograph of (a) the lifting of the rebar cage for test shaft T-N4, and (b) the four-foot cube reveal form work.

A total of 63 cubic yards of concrete were utilized to complete the construction of test shaft T-N4. All as-built features met the design specifications outlined in Section 6.2.1 except the bulb of concrete developed at a depth of approximately 30-feet below ground surface. The total length of test shaft T-N4 measured 92.5-feet from the bottom of the excavation to the top edge of the four-foot tall concrete block reveal. A photograph of the finished shaft is presented in Figure 6.41.

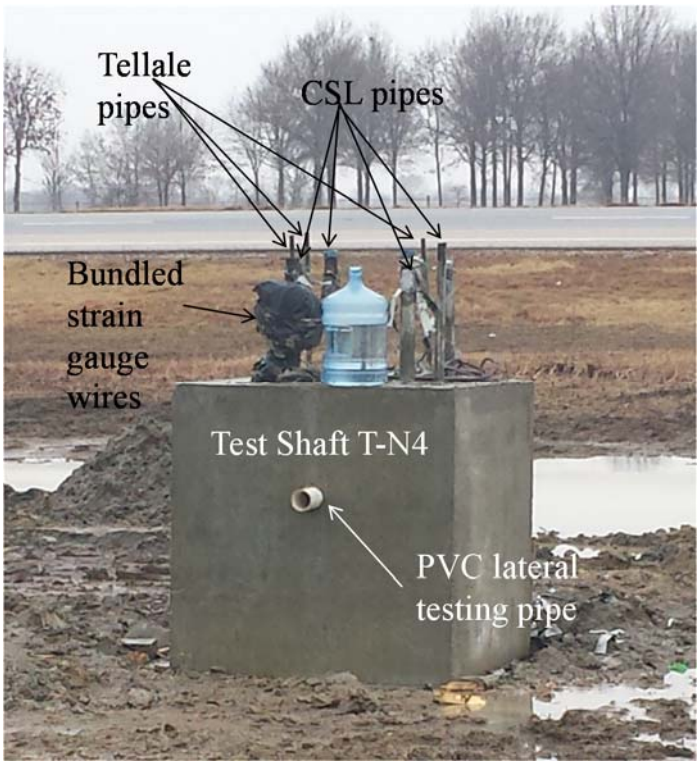

Figure 6.41. Photograph of completed test shaft T-N4.

6.4. Concrete Testing

Concrete testing, including uniaxial compressive strength and modulus of elasticity, were performed on the cylinders that were cast in the field (the sampled were four-inches in diameter and eight-inches in height). Seven trucks of concrete were required for test shaft T-S4 (resulting in six batches of cylinders). Cylinders were not cast for the concrete from Truck 1, and each batch consisted of five cylinders (exempting Truck 5, for which eleven cylinders were cast). A photograph of the test shaft T-S4 cylinders is presented in Figure 6.42. Nine trucks of concrete were required for test shaft T-C6 (resulting in nine batches of cylinders). Each batch consisted of five cylinders (exempting Truck 4, for which eleven cylinders were cast). Nine trucks of concrete were also required for test shaft T-N4 (resulting in nine batches of cylinders). Each batch cast consisted of five cylinders (exempting Truck 5, for which eleven cylinders were cast). The cylinders from every batch were stored on-site (in molds) in a 100-gallon water tank covered

with a plastic tarp. Upon hardening, the molds were removed, and the cylinders were re-submerged until transport to the laboratory at the University of Arkansas (exempting cylinders for test shaft T-N4, which were directly transported). The cylinders were then re-submerged in a water bath until testing was performed. The designated testing regimen for each batch is presented in Table 6.2.

Figure 6.42. Photograph of test shaft T-S4 cylinders prior to transport.

Table 6.2. Designated concrete testing regimen per batch for the Turrell Arkansas Test Site.

Test Performed	No. of Tests per 11-Cylinder Batch			No. of Tests Performed per 5-Cylinder Batch
	T-S4	T-C6	T-N4	
7 Day Uniaxial Compressive Strength	0	0	0	0
13 Day Uniaxial Compressive Strength	0	3	0	0
14 Day Uniaxial Compressive Strength	0	0	0	0
21 Day Uniaxial Compressive Strength	0	0	3	0
28 Day Uniaxial Compressive Strength	3	3	3	3
56 Day Uniaxial Compressive Strength	4	3	3	0
Modulus of Elasticity	1	1	1	1
Date of Testing Uniaxial Compressive Strength	1	1	1	1

6.4.1. Uniaxial Compressive Strength

Prior to compressive strength testing, the ends of each cylinder were ground to ensure even pressure distribution using a Marui Triple Hi Kenma cylinder end grinder. Laboratory uniaxial compressive strength testing was performed in accordance with ASTM C39 (2012). A Forney F Series standard compression machine was utilized to complete the testing (Figure 6.43a). Each batch of cylinders, for each shaft was tested at a rate of 35 +/- 7 pounds per square inch (psi) per second.

6.4.2. Modulus of Elasticity

Modulus of elasticity testing was performed after 28 days in accordance with ASTM 469 (2010). The test was performed on one cylinder per batch using a Forney F Series standard compression machine and a compressometer (Figure 6.43b). Load was applied to each cylinder at a rate of 35 +/- 7 psi per second, and the modulus of elasticity was calculated using Equation 6.1.

$$E = \frac{(S_1 - S_2)}{(\varepsilon_2 - 0.000050)}$$ (ASTM C469, 2010) **Equation 6.1**

Where: E = chord modulus of elasticity of concrete (psi),

S_1 = stress corresponding to a longitudinal strain, ε_1, of 50 millionths (psi),

S_2 = stress corresponding to 40% of ultimate load (psi), and

ε_2 = longitudinal strain produced by stress S_2.

(a) (b)

Figure 6.43. Photographs of (a) uniaxial compression testing, and (b) compressometer used for modulus of elasticity testing.

6.5. Cross-Hole Sonic Logging

On January 9 2014, personnel from GEI performed cross-hole sonic logging on test shafts T-S4 and T-C6. On January 10 2014, personnel from GEI performed cross-hole sonic logging on test shaft T-N4. Two piezoelectric probes were inserted in multiple sequences into the aforementioned two-inch diameter CSL tubes. The sequence utilized on each shaft (composed of six soundings) is presented in Figure 6.44, and commenced from the Northern-most oriented CSL tube (Tube 1).

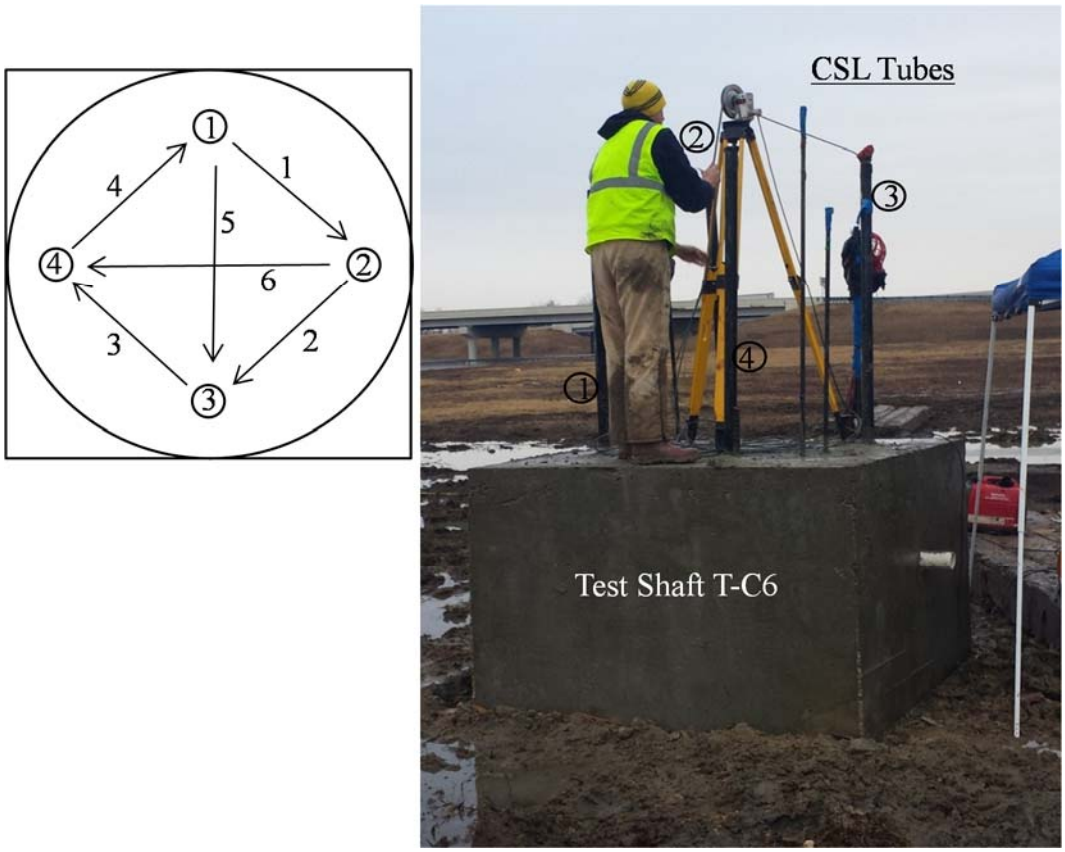

(a) (b)

Figure 6.44. Summary of (a) plan view of six-step CSL testing sequence commencing from the North, and (b) photograph of testing performed on test shaft T-C6.

The probes were lowered to rest upon the bottom cap of the water-filled tubes, located at the bottom of the reinforcement cage of each shaft (exempting test shaft T-N4). Upon commencement of the test, the probes were simultaneously extracted at a rate of about one-foot per second. A photograph of the piezoelectric probes utilized to transmit and receive the sonic waves through the length of the shaft is presented in Figure 6.46a. Prior to CSL testing on test shaft T-N4, it was observed CSL pipes 2, 3, and 4 were clogged below a depth of approximately 67-feet below ground surface. This was due to the CSL tubes detaching and filling with soil when the T-N4 reinforcement cage was lifted from the prior collapse (as discussed in Section 6.6.3). As a result, the pipes were cleaned out using an air compressor attached to a 0.5-inch diameter strung pipe (Figure 6.45), and all CSL testing performed on test shaft T-N4 was

executed from a depth of 67-feet below ground surface. A photograph of the CSL testing in progress for test shaft T-N4 is presented in Figure 6.46b.

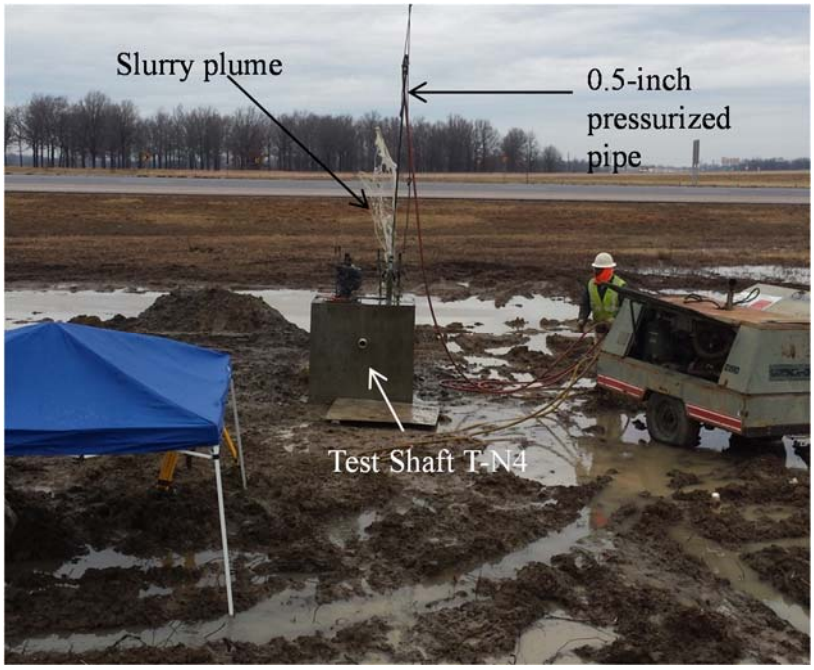

Figure 6.45. Photograph of test shaft T-N4 clean out.

(a) (b)

Figure 6.46. Photograph of (a) piezoelectric probes utilized for CSL testing, and (b) the CSL testing performed on test shaft T-N4.

6.6. Load Test Setup and Procedures

Osterberg load Cell (O-Cell) testing was performed by Loadtest Inc. personnel on each drilled shaft at the TATS with assistance from University of Arkansas personel. Testing on Test shaft T-S4 was performed on January 10, 2013. Testing on test shafts T-C6 and T-N4 was performed on January 11, 2013. Each test consisted of the following general procedure:

6) calibration of the hydraulic pump,
7) separation of O-Cell welds,
8) loading stage,
9) unloading stage, and
10) monitoring of shaft while at rest under no load.

While performing the O-Cell tests, an automatic pressure regulator (Figure 6.48a) was utilized to maintain a constant pressure for each load increment. The displacement of the top of

the shaft was monitored using automated surveying levels and an Invar target that was clamped to one of the cross-hole sonic tubes (Figure 6.47a). Displacement of the 0.125-inch diameter telltale rods that were positioned within the 0.5-inch pipe, connected to the top and bottom plates of the O-Cell, were monitored using linear variable displacement transducers (LVDTs) [Figure 6.47b]. Strain within the strain gauges that were previously attached to the rebar cages were monitored using an automated data acquisition system. All measurements were recorded using the automated data acquisition system (Figure 6.48b).

(a) (b)

Figure 6.47. Photographs of (a) automated survey levels used to record the shaft head displacement, and (b) LVDT displacement instrumentation that was attached to the top of each telltale.

(a) (b)

Figure 6.48. Photographs of (a) automated pressure regulator and hydraulic pump utilized to perform the O-Cell testing, and (b) data acquisition system.

6.6.1. Test Shaft T-S4

On January 10, 2014, full-scale load testing was performed on test shaft T-S4. The shaft was loaded every eight minutes at increments of 1000 psi for thirteen intervals (peaking at 13,000 psi). The shaft was then unloaded ever four-minutes, decreasing the pressure by 2600 psi for each of the five intervals (reducing pressure back to zero psi). Following unloading, the shaft was monitored at rest for a period of eight minutes. Displacement readings were acquired for the top of the shaft and for the top and bottom plates of the O-Cell (two for the compression of the top plate of the O-Cell, and three for tension of the bottom plate of the O-Cell). Due to the weather conditions on site, a rain gazebo was installed above the data acquisition system to prevent electrical shortages. A photograph of the test, while in progress, is presented in Figure 6.49.

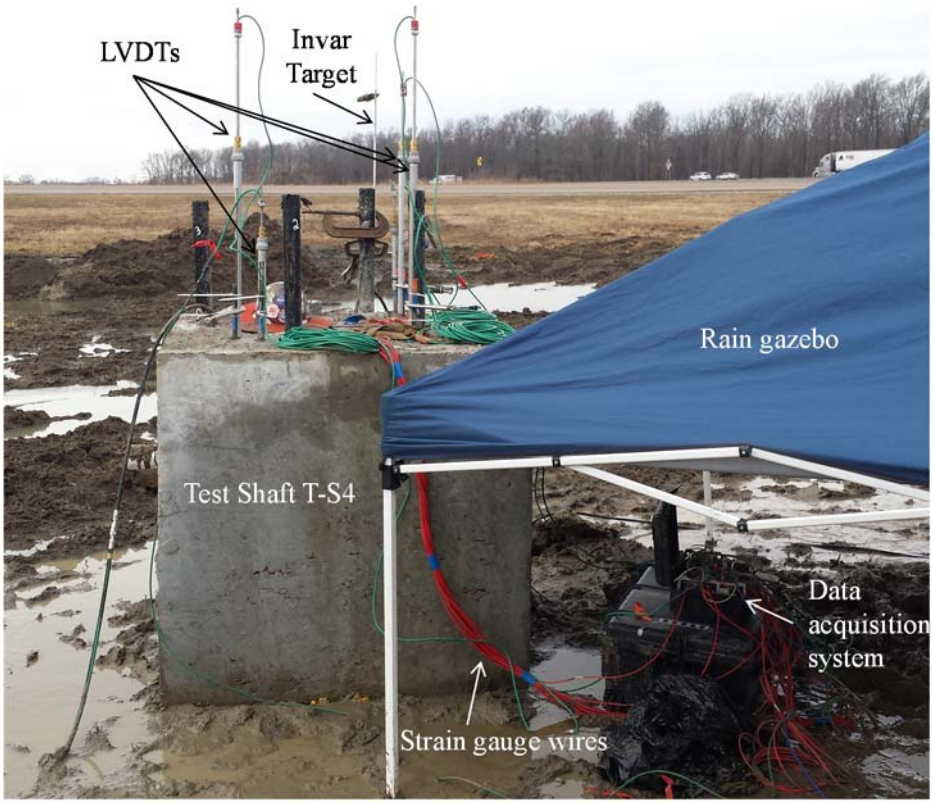

Figure 6.49. Photograph of the test shaft T-S4 O-Cell test in progress.

6.6.2. Test Shaft T-C6

On January 11, 2013, full-scale load testing was performed on test shaft T-C6. The shaft was loaded every eight minutes at increments of 800 psi for twelve intervals (peaking at a pressure of 9600 psi). The shaft was then unloaded at four-minute increments, decreasing the pressure by 3400 psi for each of the five intervals (reducing pressure back to zero psi). Following unloading, the shaft was then monitored at rest for a period of eight minutes. Displacement readings were acquired for the top of the shaft and for the top and bottom plates of the O-Cell (two for the compression of the top plate of the O-Cell, and three for tension of the bottom plate of the O-Cell). It was observed during testing that readings for strain gauge level two fluctuated during the initial load increments (to a pressure of 7000 psi). Pressure gauge problems were also

noted at approximately 10:57 a.m. A photograph of test, while in progress, is presented in Figure 6.50.

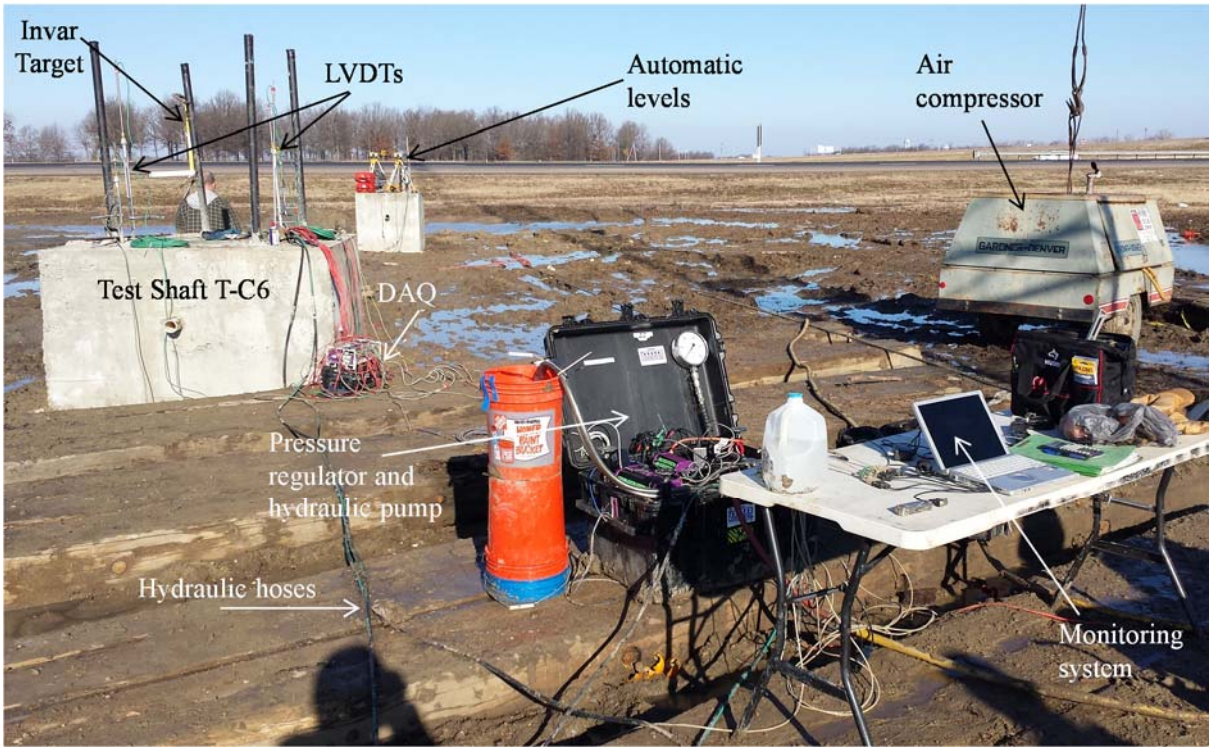

Figure 6.50. Photograph of the test shaft T-C6 O-Cell test in progress.

6.6.3. Test Shaft T-N4

On January 11, 2014, full scale load testing was performed on test shaft T-N4. The shaft was loaded every eight minutes at increments of 1000 psi for thirteen intervals (peaking at 13,000 psi). The shaft was then unloaded using four-minute increments, decreasing the pressure by 2600 psi for each of the five intervals (reducing pressure back to zero psi). Following unloading, the shaft was then monitored at rest for a period of eight minutes. Displacement readings were acquired for the top of the shaft and for the top and bottom plates of the O-Cell (two for the compression of the top plate of the O-Cell, and three for tension of the bottom plate of the O-Cell). A photograph of the test in progress is presented in Figure 6.51.

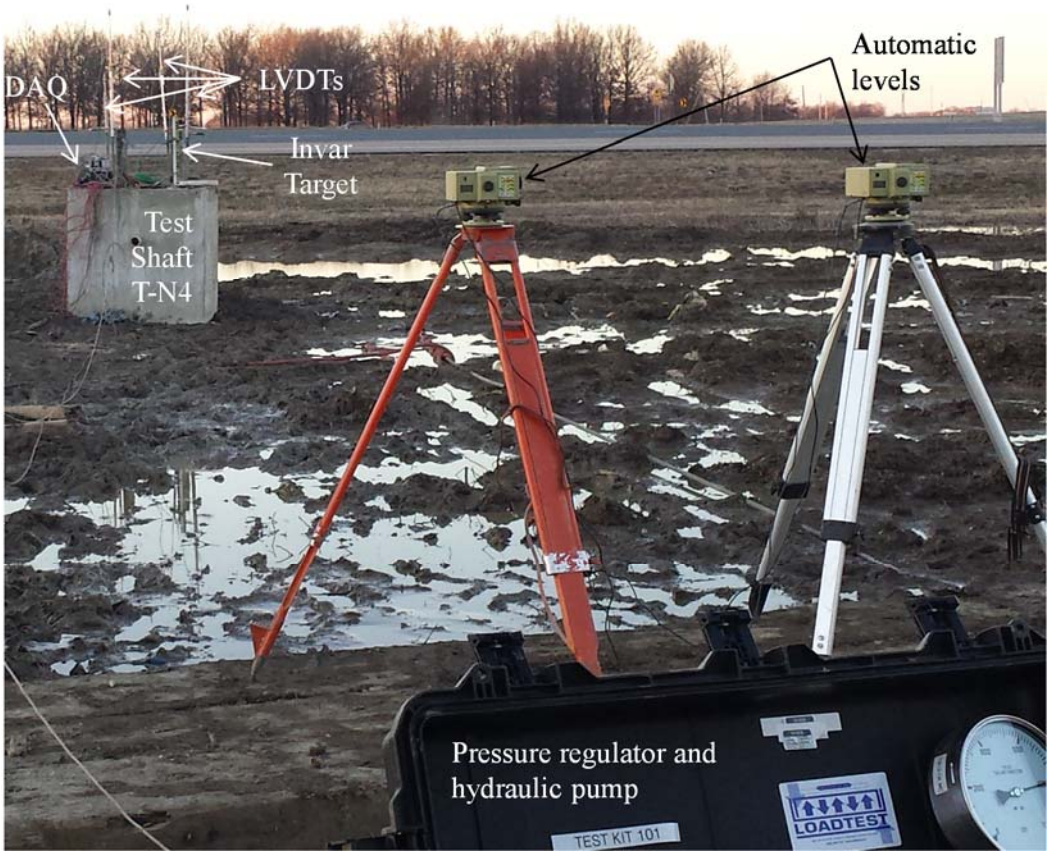

Figure 6.51. Photograph of the test shaft T-N4 O-Cell test in progress.

6.7. Interpretation of Load Test Data

After completion of the full scale O-Cell testing, data sheets were generated. The data sheets contained displacement measurements acquired from the LVDTs, automatic levels, pressure transducers, and strain gauges (as a function of time). From the data, load displacement curves (Section 6.7.1), load transfer curves (Section 6.7.2), and unit side friction plots were generated (Section 6.7.3).

6.7.1. Load Displacement Curves

From the data collected from each O-Cell test, two load displacement curves were generated. As previously discussed in Chapter 2, one upper curve describes the upward displacement of the top of the cell (skin friction resistance), and one lower curve represents the downward displacement of the bottom of the shaft (end bearing resistance). Values of load were

added together at certain values of displacement to generate an equivalent top-down load displacement curve. However, in cases where resistances could not be fully developed, a hyperbolic extrapolation of the load-displacement curve was performed to complete the equivalent top-down load displacement curve.

6.7.2. Load Transfer (t-z) Curves

The distribution of force along the shaft with depth were obtained from the strain-gauge data via load-transfer curves. The modulus of elasticity (E_c) of the concrete was determined from one sample from each batche of cylinders cast by UofA personnel. After determining the modulus of elasticity of the concrete, an equivalent shaft modulus was determined by accounting for the contributions of the area of steel and the area of concrete (Equation 6.2).

$$E_{Shaft} = \frac{E_c A_c + E_s A_s}{A_{Shaft}}$$ (modified from Miller, 2003) **Equation 6.2**

Where: E_{Shaft}= equivalent shaft modulus (psi),

E_c = modulus of concrete (psi),

E_s = modulus of steel (psi),

A_c = cross sectional area of concrete (in^2),

A_s = cross sectional area of steel (in^2), and

A_{Shaft} = gross cross sectional area of drilled shaft (in^2).

From the equivalent shaft modulus, the average axial stress at given depths (σ_i) was then calculated (Equation 6.3).

$$\sigma_i = E_{Shaft_i}\ \varepsilon_{axial_i}$$ (modified from Miller, 2003) **Equation 6.3**

Where: σ_i = average axial stress at given depth *i* (psi),

$E_{Shaft\text{-}i}$ = equivalent shaft modulus at depth *i* (psi), and

$\varepsilon_{axial\text{-}i}$ = axial strain within the shaft at depth *i*.

Axial strain within the shaft ($\varepsilon_{axial\text{-}i}$) was determined from the average value of strain from the two strain gauges placed in the shaft at a given elevation. From the average axial stress at a given depth, the axial force (F_i) at a given depth, *i*, was computed (Equation 6.4).

$$F_i = \sigma_i A_{pi}$$ (Miller, 2003) **Equation 6.4**

Where: F_i = axial force within the shaft at depth *i*,

σ_i = average axial stress at given depth *i* (psi), and

A_{pi} = shaft cross sectional area at elevation *i* (in^2).

The distribution of axial force within the shaft at a given elevation was determined from the calculation of the axial force at each strain gauge.

6.7.3. Unit Side Friction Resistance

The determination of average unit side friction resistance for each drilled shaft over a given length was determined from the load distribution along the shaft using Equation 6.5.

$$f_s = \frac{\Delta F_i}{Shaft\ Perimeter * \Delta z_i}$$ (Miller, 2003) **Equation 6.5**

Where: f_s = average unit side friction resistance,

ΔF_i = the change in axial force over a given length of shaft, and

Δz_i = shaft segment length.

The values of the average unit side shear were then plotted as a function of average upward shaft displacement to evaluate the amount of attained of maximum unit side friction resistance.

6.8. Summary

The site conditions, design, construction, testing, and data analysis processes associated with the TATS were discussed in this chapter. Design depths for test shafts T-S4, T-C6, and T-N4 were specified to penetrate 86.5-, 61.5-, and 86.5-feet, respectively, with percentages of longitudinal steel not exceeding 1.0-percent. These depths were selected to satisfy the required design load of 987 tons. O-Cell assemblies for test shaft T-S4, T-C-6, and T-N4 were placed within the lower segment for each reinforcement cage (at depths of 68.5-, 53-, and 65.6-feet, respectively, from the top of the reinforcement cage). Slurry construction methods were utilized to construct each shaft. Four thousand psi compressive strength concrete was prescribed at the TATS (which contained a mid-range water reducer, 3% by weight Class C fly ash, and an as-required set controller) to fill the excavations.

Test shaft T-S4 was constructed from November 18 to December 4, 2013. During excavation of this shaft, the auger bucket was lost and retrieved from the excavation, and an excavator was tipped over. Upon lowering the instrumented reinforcement cage into the excavation, sixty-three cubic yards of concrete (including placement of a four-foot tall reveal length) were utilized to complete test shaft T-S4. The total length of test shaft T-S4 measured 90.5-feet from the bottom of the excavation to the top of the concrete block.

Test shaft T-C6 was constructed between November 26 and December 4, 2013. During excavation of this shaft, no construction errors were recorded. However, while hoisting the instrumented reinforcement cage, two unsuccessful attempts were made to vertically align the assembly. The first unsuccessful pick resulted in the welds uniting the O-Cell and the lower

segment of the reinforcement cage. The second unsuccessful pick resulted in a total collapse and detachment of the lower segment of the reinforcement cage. Upon reattachment of the lower segment to the already vertically hoisted remainder of the reinforcement cage, the assembly was lowered into the excavation. All strain gauges beneath the O-Cell were replaced with gauges originally intended for test shaft T-N4. Eighty-one cubic yards of concrete (including the placement of a four-foot tall reveal length) were utilized to complete test shaft T-C6. The total length of test shaft T-C6 measured 65.5-feet from the bottom of the excavation to the top of the concrete block.

Test shaft T-N4 was constructed between December 3 and December 23, 2013. Following the excavation of this shaft, the excavation collapsed (with the reinforcement cage partially embedded) the morning prior to anticipated concrete placement. As a result, three of the four CSL tubes mounted to the reinforcement cage were detached during extraction and filled with soil. Although the CSL pipes were unoperational, the strain gauges mounted to the bottom segment of the cage remained operational. As the reinforcement cage was cleaned of soil, the hole was re-excavated. After lowering the instrumented reinforcement cage into the newly re-opened excavation, eighty-one cubic yards of concrete (including placement of a four-foot tall reveal length) were utilized to complete test shaft T-N4. During concrete placement, it was observed the five cubic yards of concrete were lost at the clay interface at a depth of approximately 30-feet below ground surface. The total length of test shat T-N4 measured 92-feet from the bottom of the excavation to the top of the concrete block.

Concrete testing composed of uniaxial compressive strength and modulus of elasticity testing. Uniaxial compressive strength testing was performed at approximately 7, 28, and 56 days following concrete placement for each shaft (or as close as permitted by scheduling and

weather conditions). Testing was performed on sets of three cylinders per batch (i.e. per truck). Modulus of elasticity testing was performed on one cylinder per batch (i.e. per truck).

Cross-hole sonic logging was performed on each shaft prior to O-Cell testing to ensure the concrete utilized for each shaft was free from anomalies. Diametrically opposed probes were inserted and raised at a rate of about one-foot per second. In test shaft T-S4 and test shaft T-C6 probes were raised from the bottom of the reinforcement cage at depths of 86.5- and 61.5-feet below ground surface, respectively to the ground surface. In test shaft T-N4, three of the four CSL tubes were clogged with soil resulting from extraction of the cage after the excavation blow out. As a result, after cleaning, probes were raised from a depth of 67-feet below ground surface to the ground surface.

O-Cell testing was performed in by personnel from Loadtest Inc. from January 10 through January 11, 2013. Test shaft T-S4 was loaded every eight minutes at incremented of 1000 psi to a maximum pressure of 1300 psi. Test shaft T-C6 was loaded every eight minutes at incremented of 800 psi to a maximum pressure of 9600 psi. Test shaft T-N4 was loaded every eight minutes at incremented of 1000 psi to a maximum pressure of 13000 psi. The data from the load test performed on each shaft was analyzed, and the procedures for determining load displacement curves, load transfer curves, and unit side friction resistance curves were described.

Chapter 7: Results from Geotechnical Investigations, Predictive Methods, and Cost-benefit Analyses

7.1. Introduction

The ultimate axial capacity values that were obtained by ingesting the data from the geotechnical investigations into the predictive methods to determine drilled shaft ultimate axial capacity are discussed in this chapter. Specifically, the results obtained from the Siloam Springs, Turrell, and Monticello Arkansas Test Sites are presented in Sections 7.2, 7.3, and 7.4, respectively. The differences between the values by using data obtained from the UofA, AHTD, and MODOT sampling and testing methods, as well as the ranges in data are reported and discussed. The impacts of these data ranges upon the predicted axial capacity, as evaluated utilizing Ensoft SHAFT, Bridge Software Institute FB-Deep, and Microsoft Excel®, are also reported and discussed.

Results of the cost-benefit analyses preformed for the Siloam Springs (Section 7.5) and Turrell (Section 7.6) test sites are presented. Cost-benefit results include a value of unit cost per ton of resistance utilizing the UofA, AHTD, and MODOT sampling and testing methods, and a discussion of the cost implications of UofA, AHTD, and MODOT sampling and testing methods on various types of infrastructure. The results of the fiscal impact of the concrete mix design are also discussed within these sections. Due to the nature of MODOT CPT testing, this method was not included in the Siloam Springs cost-benefit analysis.

7.2. Siloam Springs Arkansas Test Site

As discussed previously in Chapter 3, the Siloam Spring Test Site (SSATS) was underlain by competent limestone. Therefore, the prediction of the ultimate axial capacity for the drilled shaft foundations was predominantly influenced by the presence of competent limestone

below an average depth of 16-feet below ground surface. The comparisons performed were based on the results of predictions of ultimate axial capacity at the SSATS focus below a depth of 16-feet. Results of the geotechnical investigation performed at the SSATS are presented in Section 7.2.1. While comparisons of predicted axial capacity utilizing SHAFT, FB-Deep, and a spreadsheet are discussed in Section 7.2.2.

7.2.1. Siloam Springs Arkansas Test Site Geotechnical Investigation Results

From the geotechnical investigations performed at the SSATS (as previously discussed in Chapter 3), acquired soil properties acquired included moisture content, total unit weight, corrected blow count, undrained shear strength, friction angle, percent fines, rock quality determination (RQD), unconfined compressive strength, and modulus of elasticity. Rock quality designations were performed by AHTD personnel to depths of 38 to 99 feet below ground surface, respectively (Figure 7.1). Exempting the depths to a depth of approximately 20-feet, the ranges of RQD values, to a depth up to 38-feet, as obtained using the UofA method, were observed to be nine-percent lower than those obtained from the AHTD method. Additionally (to a depth of 38-feet), the mean RQD values, as obtained from the UofA procedure, averaged to be nine-percent greater than those obtained from the AHTD method. These differences may be attributed to variations in objective determination or attributed to uncertainties associated with the sampling locations. Both the AHTD and UofA methods utilized double swivel core barrel samplers. In general, values of RQD were observed to increase with depth by about 20-percent until the limestone/shale interface was reached at a depth of 75-feet.

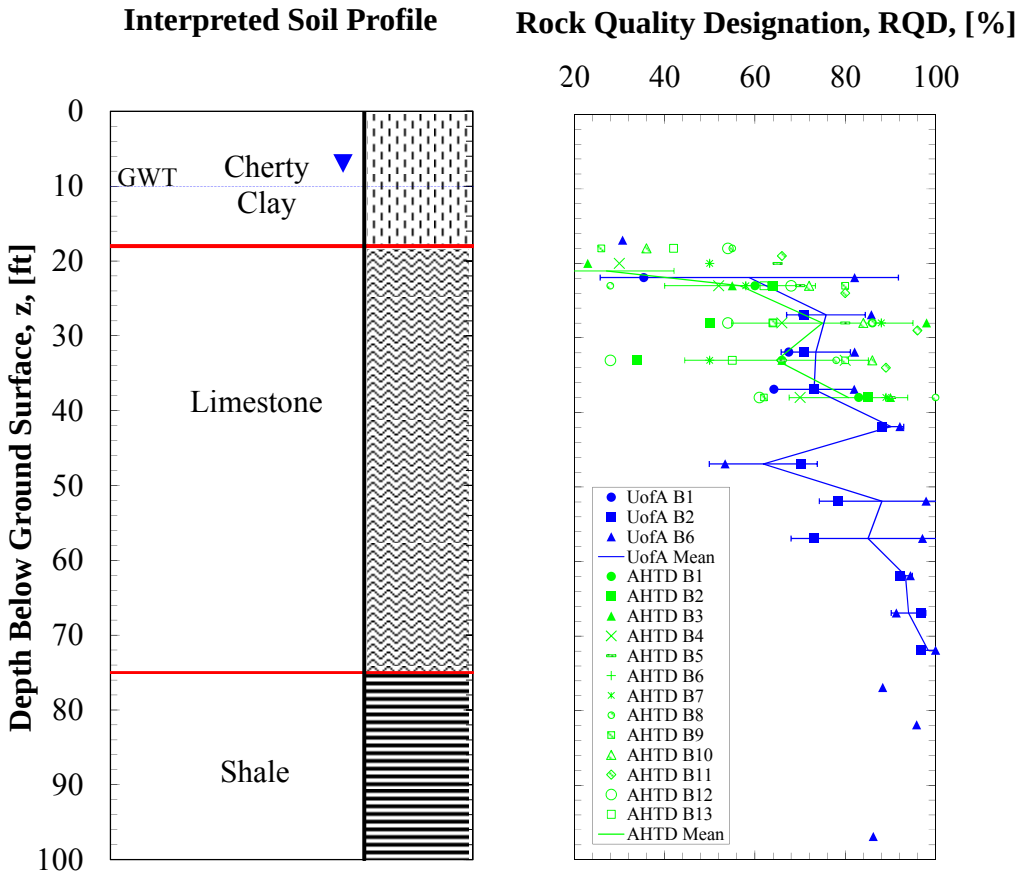

Figure 7.1. Values of RQD as a function of depth for the UofA and AHTD sampling and testing methods.

Values of unconfined compressive strength (q_u) and modulus of elasticity (E_c) encountered at the SSATS, as obtained from the UofA method, are presented in Figure 7.2. As opposed to the increasing values of RQD as a function of depth, the values of unconfined compressive strength were observed to decrease with depth. Although all of the values of unconfined compressive strength in the limestone exceed 11,000-pounds per square inch (psi), the observation contradicts the usually assumed relationship of compressive strength increasing with increasing values of RQD. This observation should be considered when evaluating the effectiveness of only utilizing RQD values to obtain strength estimations within the rock. Average values of modulus of elasticity remained relatively consistent (1900 psi per percent)

within the limestone. For completeness, the additional properties of the soil and rock, as found at the SSATS, are summarized in Appendix A.

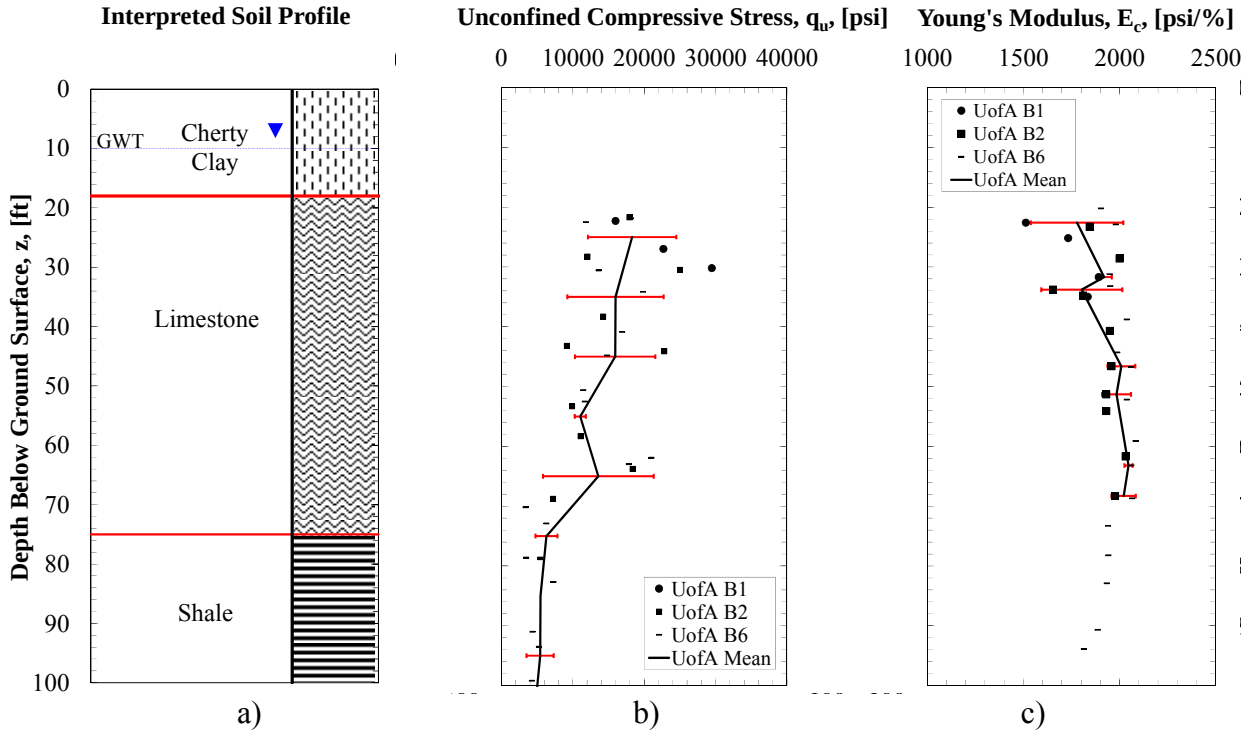

Figure 7.2. Values of a) interpreted soil profile, b) unconfined compressive strength, and c) modulus of elasticity, as a function of depth, as collected by UofA personnel.

Due to current design practices, values of unconfined compressive strength for AHTD were from a correlation with RQD using Table 10.4.6.4-1 from the AASHTO LRFD Bridge Design Manual. The use of this correlation may result in overly-conservative designs.

7.2.2. SSATS Predictive Results

Predictions of the ultimate axial capacity for the drilled shaft foundations were made utilizing three technologies (Ensoft SHAFTv2012, Bridge Software Institute FB-Deep, and Microsoft Excel®) utilizing data collected during the geotechnical investigations at the SSATS. Results obtained from two sensitivity analyses that were performed to better understand rock property inputs are presented in Section 4.2.2.1. Results of the comparisons draw focus upon three characteristics including a) the range in the input data (Section 4.2.2.2), b) the predictive

method utilized to evaluate capacity (4.2.2.3), and c) the testing and sampling method (4.2.2.4). Specifically, various methods for predicting the components of the axial capacity of foundations (end bearing resistance and side friction resistance) were compared (Section 4.2.2.5). The MODOT testing and sampling method was not included in analyses for the SSATS because of the nature of CPT testing is only applicable in sands and clays.

7.2.2.1. Sensitivity Analysis

Two sensitivity analyses were performed to assess the impact of inputting various rock engineering properties from the SSATS. The objective of the first analysis was to distinguish previously unknown a) rock joint discontinuity spacing (s) and b) rock joint discontinuity thickness (t) values. The objective of the second analysis was to determine the engineering property of the rock that had the greatest impact on the predicted load-settlement characteristics for a particular drilled shaft foundation (SS-E4) as situated at the SSATS.

The first analysis, utilizing only SHAFT, was performed to determine the impacts of s- and t-values on axial capacity. These two properties, omitted from the Siloam Springs geotechnical investigations, were required inputs in the SHAFT program and were required to perform an analysis. Results of the sensitivity analysis on the rock joint characteristics are presented in Figure 7.3.

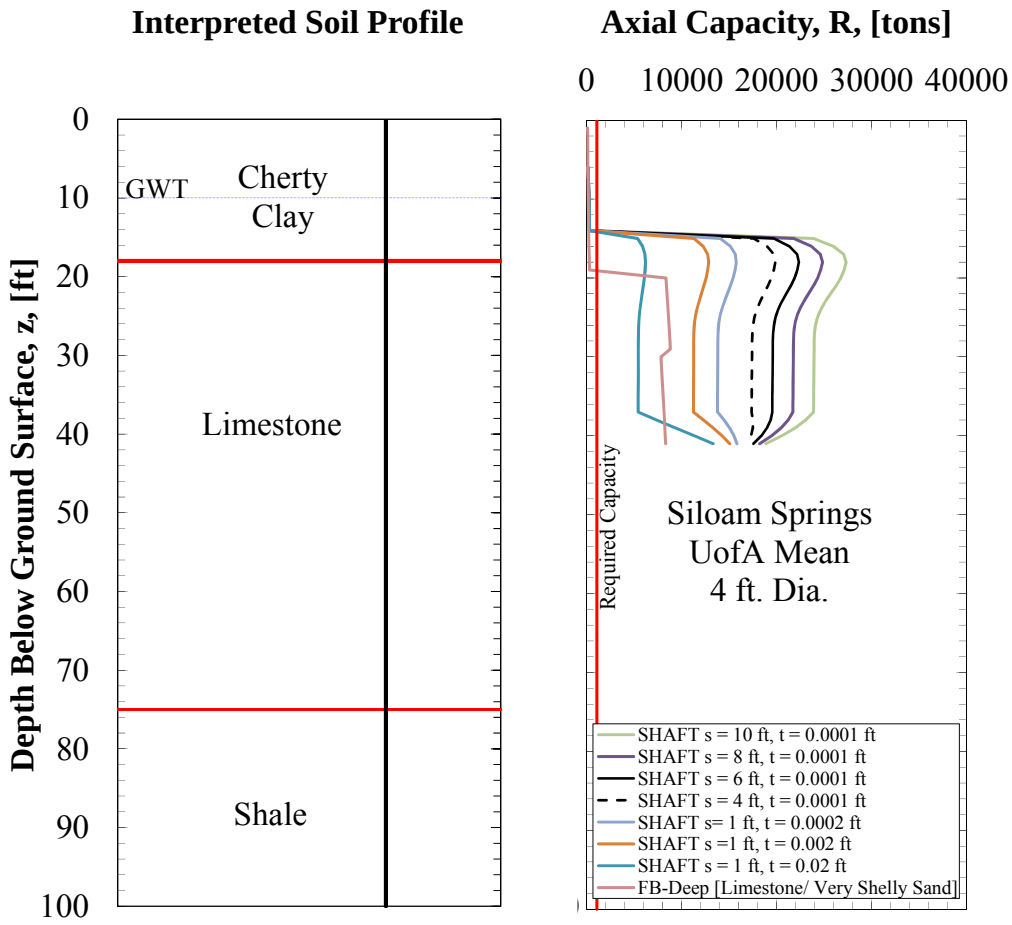

Figure 7.3. Values of axial capacity for a UofA mean four-foot diameter shaft as a function of rock discontinuity spacing and rock discontinuity thickness.

Values evaluated for rock joint discontinuity spacing and rock joint discontinuity thickness ranged from 10-feet to one-foot and 0.02-feet to 0.0001-feet, respectively. As expected, values of axial capacity were observed to be the greatest when the values of joint thickness were minimized and when the values of joint spacing were maximized. From the previously performed geotechnical investigations (as discussed in Chapter 3), the limestone encountered at the SSATS was determined to be "competent" due to the following:

1) inspection of the recovered rock cores,

2) RQD% values generally exceeding 70%, and

3) uniaxial unconfined compressive strength values generally exceeding 10,000 psi.

Because the competent limestone was determined to be “competent”, conservative (regarding end bearing resistance only) values of 6-feet and 0.0001-feet were selected as the appropriate inputs for s- and t-values, respectively. These values were then utilized for all sampling and testing methods (as indicated by the solid black data series presented previously in Figure 7.3). These s- and t- values were also selected based on the guidelines presented in Table 10.4.6.4-1 of AASTHO (2012).

The second sensitivity analysis, utilizing SHAFT and FB-Deep, was performed to determine the engineering property of the rock that had the greatest impact on the predicted load-settlement characteristics (and thus the predicted axial capacity) of drilled shaft foundations at the SSATS. Predicted-settlement curves were generated using the UofA and AHTD sampling and testing methods for the SS-E4 drilled shaft foundation. The rock characteristics were modified within the SHAFT program for the UofA Mean sampling and testing method and compared to the original curves (Figure 7.4). Upon the analyses, it was observed that a 20 percent increase in the RQD values yielded load-settlement curves that were similar to those generated by increasing the RQD values and all other rock characteristics by 20 percent. It was indicated, utilizing SHAFT for the SSATS, that changes in input RQD values had the greatest effect on the shape of the generated load-settlement curve (and thus, the axial capacity). Increasing or decreasing the uniaxial unconfined compressive strength, joint thickness, joint spacing, or the compressive strength of the concrete by 20 percent had negligible effects upon the original curve developed using UofA data in SHAFT. Results of the sensitivity analyses of the engineering properties of the rock are presented in Figure 7.4.

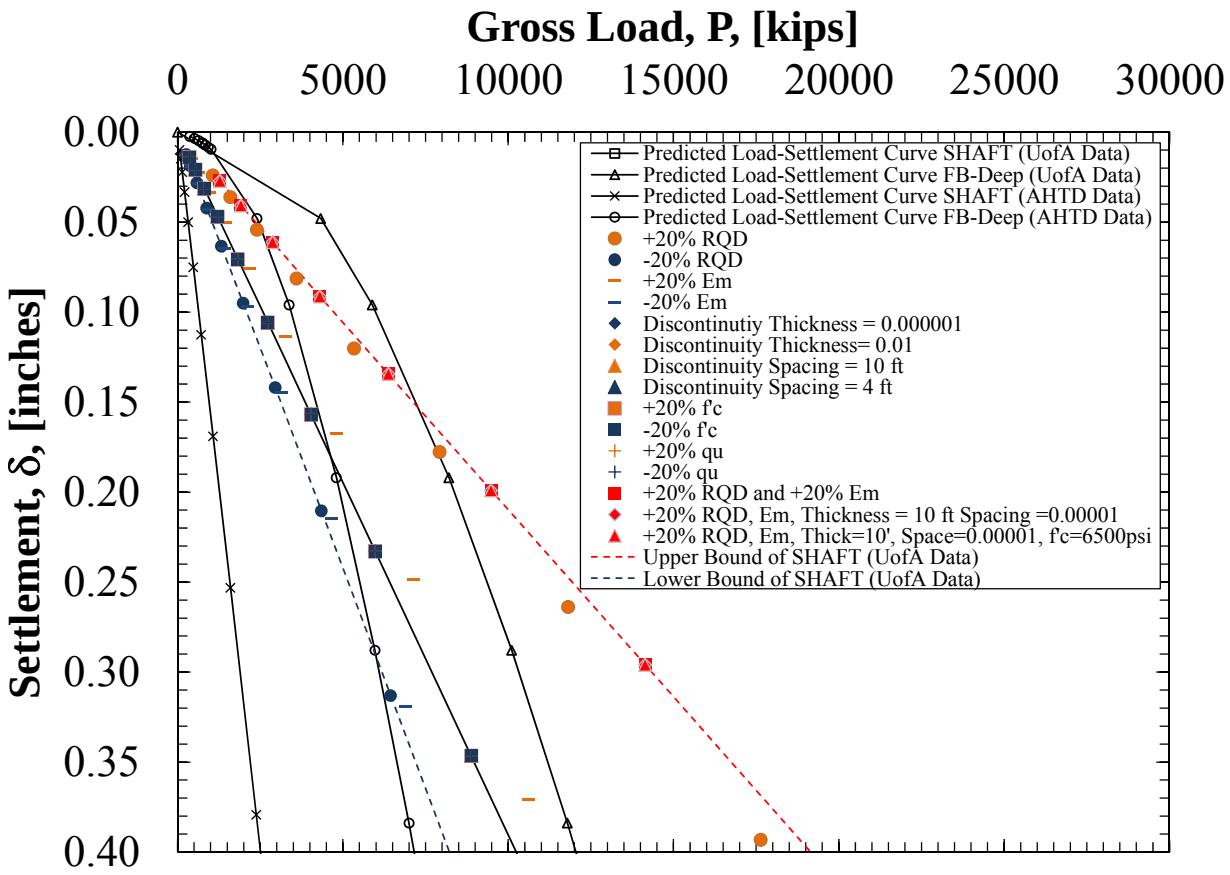

Figure 7.4. Values of predicted gross load, for UofA test shaft SS-E4, as a function of settlement for various combinations of engineering properties of the rock.

7.2.2.2. Data Ranges

Values of ultimate axial capacity were influenced by ranges in data entry for four- and six-foot diameter shafts at given depths. Utilizing SHAFT and the UofA data, an average RQD and q_u value change of 33 percent resulted in an average change in ultimate axial capacity of 39 percent. Utilizing FB Deep, an average RQD and q_u value change of 33 percent resulted in an average change in ultimate axial capacity of 33 percent (Figure 7.5). Larger impacts on the values of axial capacity were noted by deducting (rather than adding) the change in RQD and q_u values in FB Deep. This trend was also observed utilizing a spreadsheet (Figure 7.5). Input data ranges were observed to have the least amount of impact utilizing a spreadsheet; an average

RQD and q_u value change of 33 percent in the spreadsheet resulted in an average change in ultimate axial capacity of only 18 percent (Figure 7.5). The AHTD unconfined compressive strength input data, as determined from AASTHO (2012), resulted in the largest fluctuations in axial load (up to 152 percent). These larger fluctuations are attributed to the conservatism of the correlated unconfined compressive strength values from RQD percentages. Changes in unconfined compressive strength values, for the UofA data, were observed to have the greatest impact on the results from SHAFT and least impact on the results from the spreadsheet.

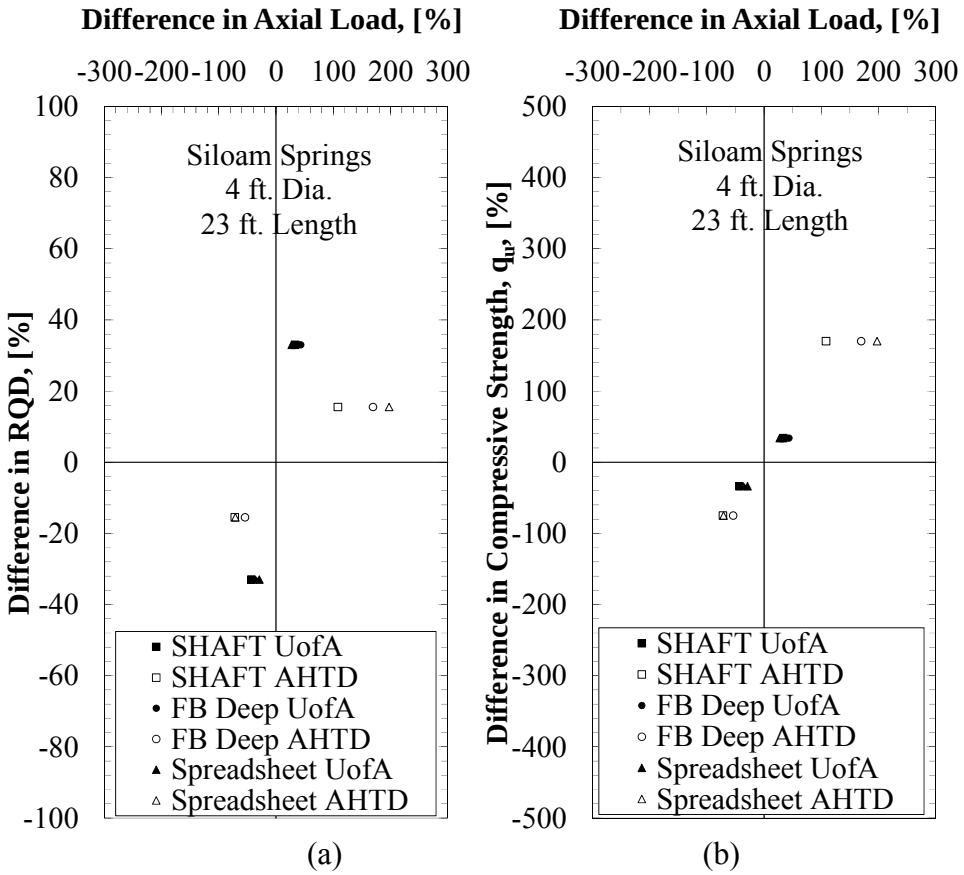

Figure 7.5. Differences in axial load with respect to (a) RQD inputs, (b) unconfined compressive strength inputs.

The effects of the data range within the input values on ultimate axial capacity for four- and six-foot diameter shafts are presented in Figures 7.6, 7.7, and 7.8. Ranges of axial capacities were noted to increase with shaft diameter, as expected. This change in axial capacity is

attributed to the effects of increased levels of side friction resistance and increased base resistance. As a result, the magnitude of the uncertainty associated with increasing shaft diameter increases, but remains proportional, suggesting the possibility of successfully scaling full-scale load tests in Boone Formation limestone by using FB-Deep as a prediction tool.

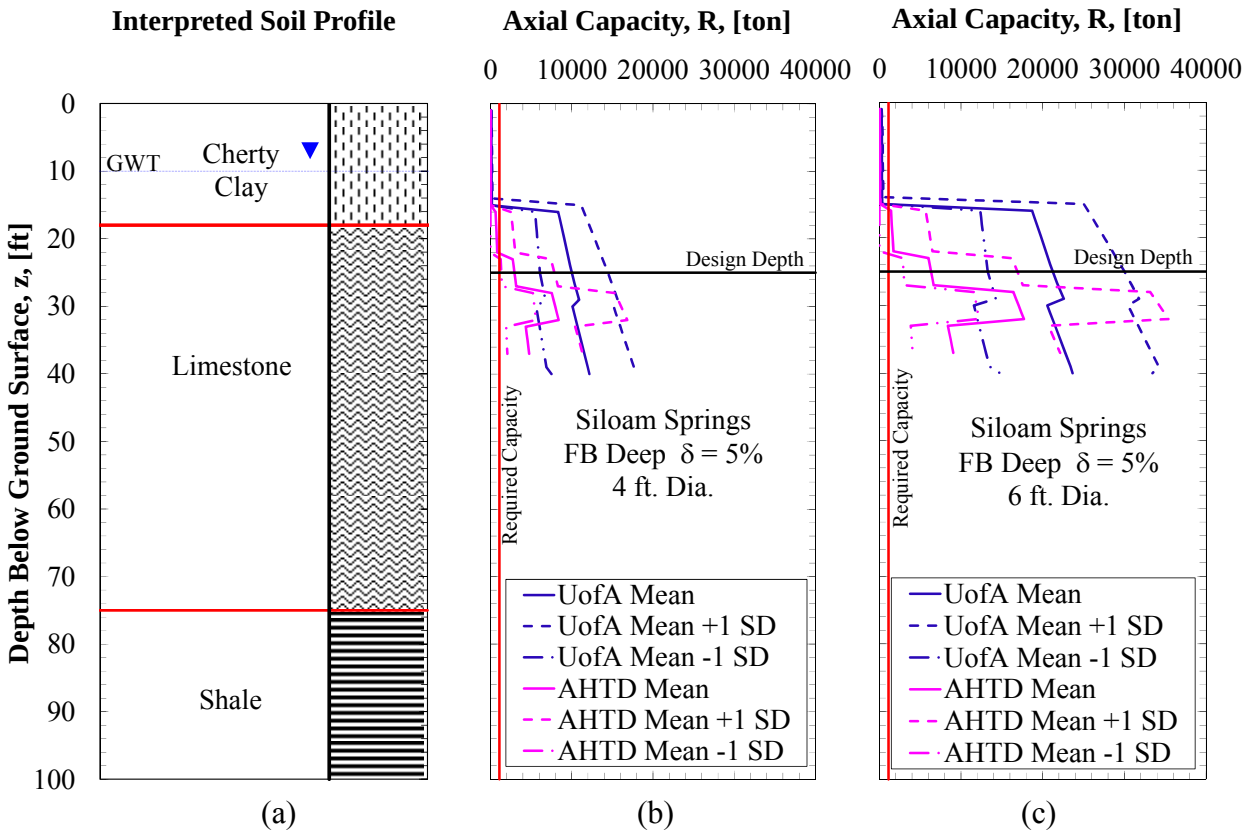

Figure 7.6. Values of (a) interpreted soil profile, and ultimate axial capacity as a function of depth for FB-Deep (b) four-foot and (c) six-foot diameter shafts using the UofA and AHTD testing and sampling methods.

As presented in Figure 7.7, scaling full-scale load tests is also a possibility utilizing a spreadsheet.

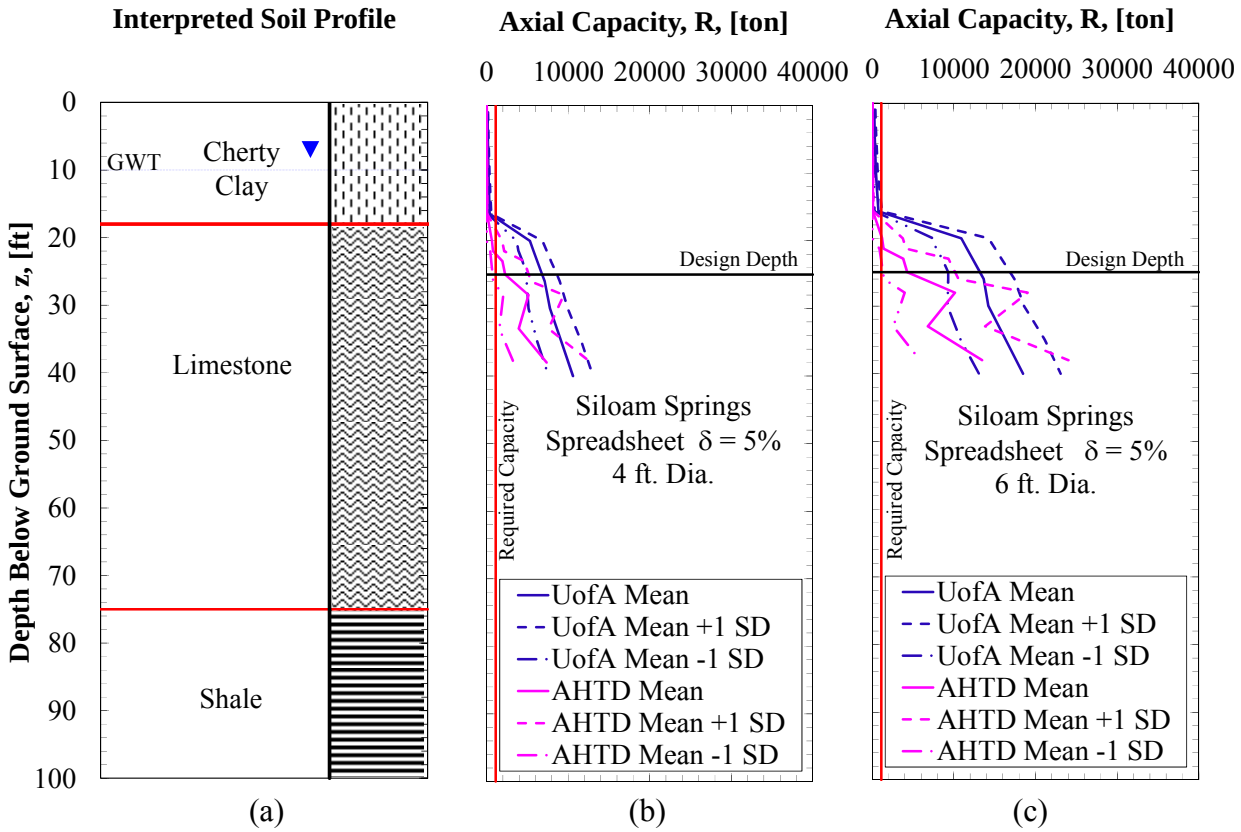

Figure 7.7. Values of (a) interpreted soil profile and ultimate axial capacity with respect to depth for spreadsheet (b) four-foot and (c) six-foot diameter shafts for the UofA and AHTD testing and sampling methods.

No clear relationships were observed between four- and six-foot diameter capacities utilizing the SHAFT predictions for UofA and AHTD sampling and testing methods (Figure 7.8). However, a decrease in capacity around a depth of 25-feet was noted despite an observed increase in RQD and Young's modulus values between depths of 20- and 30-feet for both UofA and AHTD sampling and testing methods. This observation contradicts the results of the second sensitivity analysis that indicated the changes in RQD would more significantly impact axial capacity than the impact from uniaxial unconfined compressive strength. The values of uniaxial unconfined compressive strength were observed to decrease between these depths (20- and 30-feet). As previously stated in Section 4.2.2.2., constant values of joint spacing and joint thickness were utilized. Constant values of concrete compressive strength were also utilized. Therefore,

the decrease in capacity, utilizing SHAFT, at these depths indicates the change in axial capacity is associated with the change in uniaxial compressive strengths. As current AHTD practices do not include the use of uniaxial compressive strength testing data, the uncertainties associated with the ranges of all data outputs are increased.

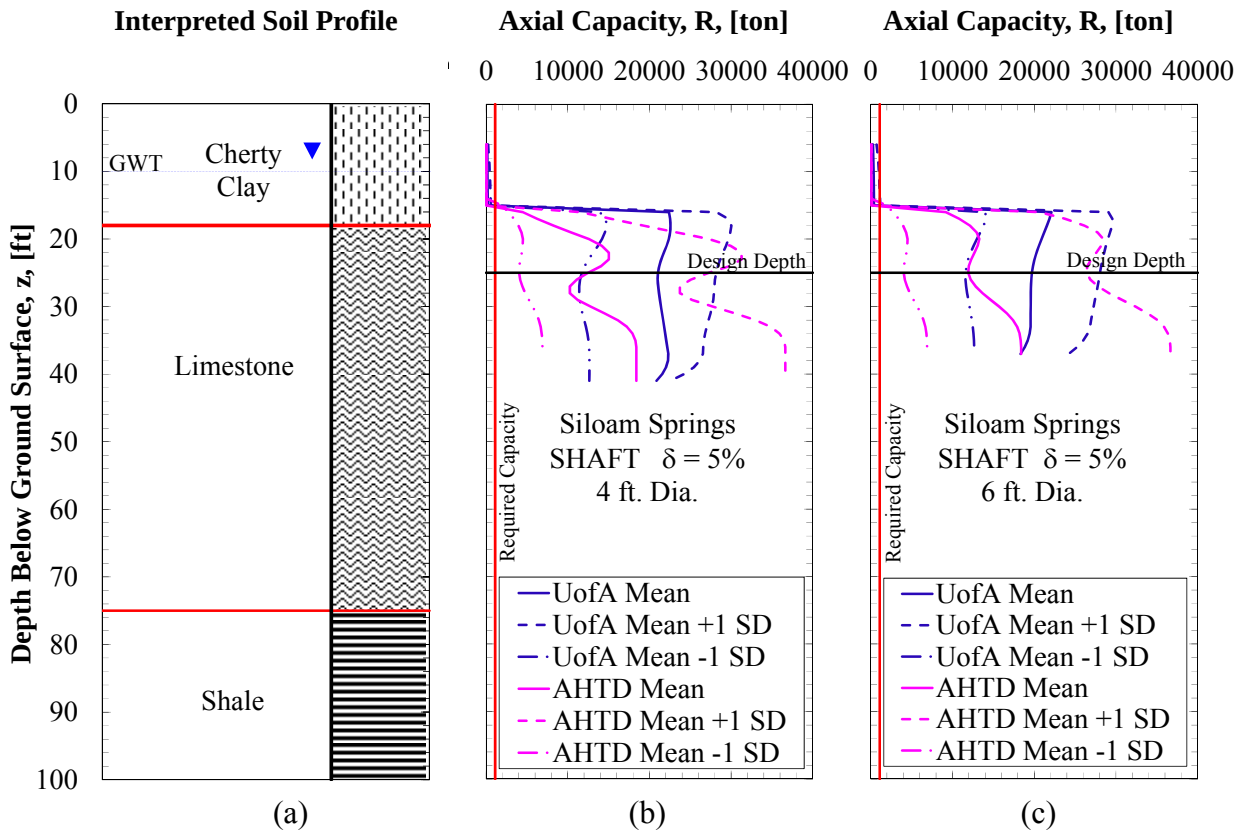

Figure 7.8. Values of (a) interpreted soil profile and ultimate axial capacity as a function of depth for SHAFT (b) four-foot and (c) six-foot diameter shafts for the UofA and AHTD testing and sampling methods.

7.2.2.3. Predictive Technologies

The effects of the predictive technologies (SHAFT, FB-Deep, and a spreadsheet) utilized to predict ultimate axial capacities at the SSATS were compared (Figure 7.9 and 7.10). For four-foot diameter shafts, outputs generated by SHAFT were observed to be less conservative. This may be due to proprietary reasons only understood by Ensoft. Specifically, the analytical methods utilized to develop SHAFT capacity predictions in rock were based on regional load-

test data associated with the regional geology of Texas. This regional geology exhibits rock with more competent characteristics than that of the Floridian limestone associated with the load-test database for which of FB-Deep was developed. The outputs generated utilizing a spreadsheet were observed to be the most conservative. This may be a result of the method utilized in AASHTO (2012) because the axial capacity is predicted as a function of rock mass quality material constants *m* and *s*. For this study, the predictions were based on values of the constants that were indicative of good quality jointed rock masses. For the six-foot diameter shafts, the outputs generated by SHAFT were observed to be more consistent with outputs generated utilizing FB-Deep (Figure 7.10). However, the values predicted using a spreadsheet were still longer than those obtained from SHAFT and FB-Deep.

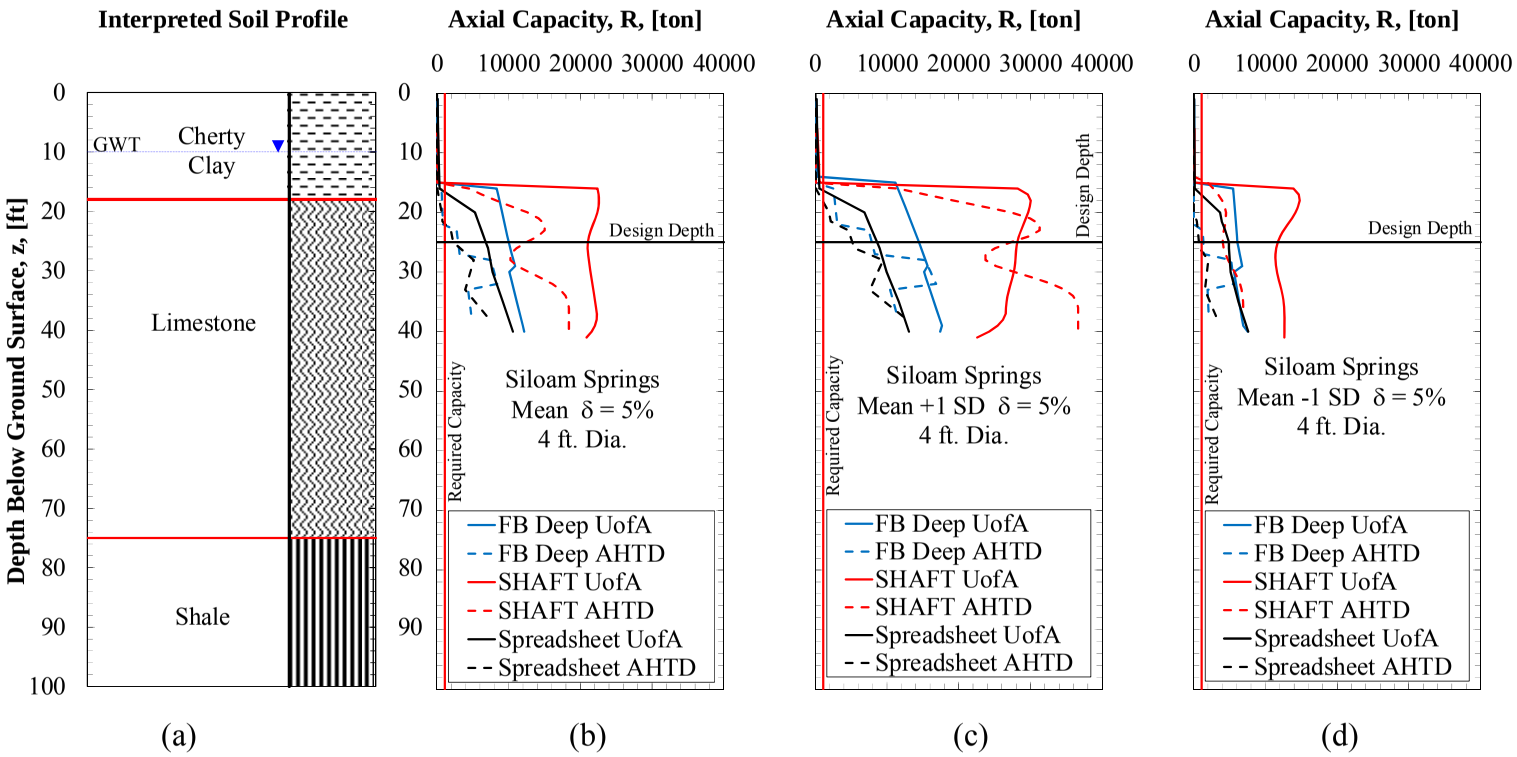

Figure 7.9. Values of (a) interpreted soil profile and axial capacity using the (b) mean, (c) mean plus one standard deviation, and (d) mean minus one standard deviation data values as a function of depth for four-foot diameter shafts utilizing FB-Deep, SHAFT, and a spreadsheet.

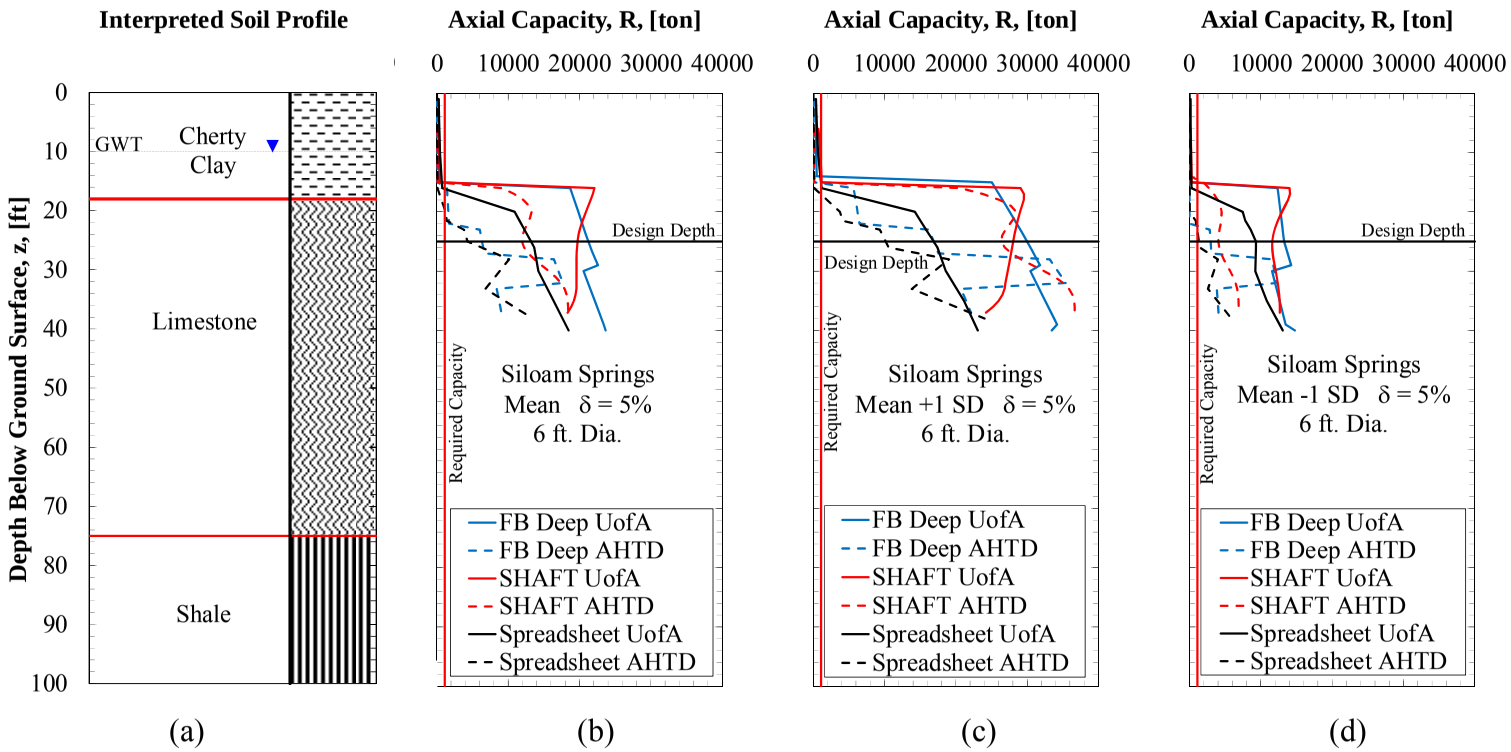

Figure 7.10. Values of (a) interpreted soil profile and axial capacity using the (b) mean, (c) mean plus one standard deviation, and (d) mean minus one standard deviation data values as a function of depth for six-foot diameter shafts utilizing FB-Deep, SHAFT, and a spreadsheet.

7.2.2.4. Sampling and Testing Methods

The effects of the sampling and testing methods including (UofA, AHTD) utilized to predict ultimate axial capacities at the SSATS were compared. The capacities generated using the data from the AHTD method were observed to fluctuate more than for those generated by using UofA obtained data (Figure 7.11). This increased fluctuation is attributed to the large range in uniaxial unconfined compressive strength values input that were utilized within each method because of the correlations from AASHTO (2012). The UofA generated capacities were observed to be generally greater than those generated by AHTD. This increase may be accounted for again by the direct input of the values of measured uniaxial unconfined compressive strength.

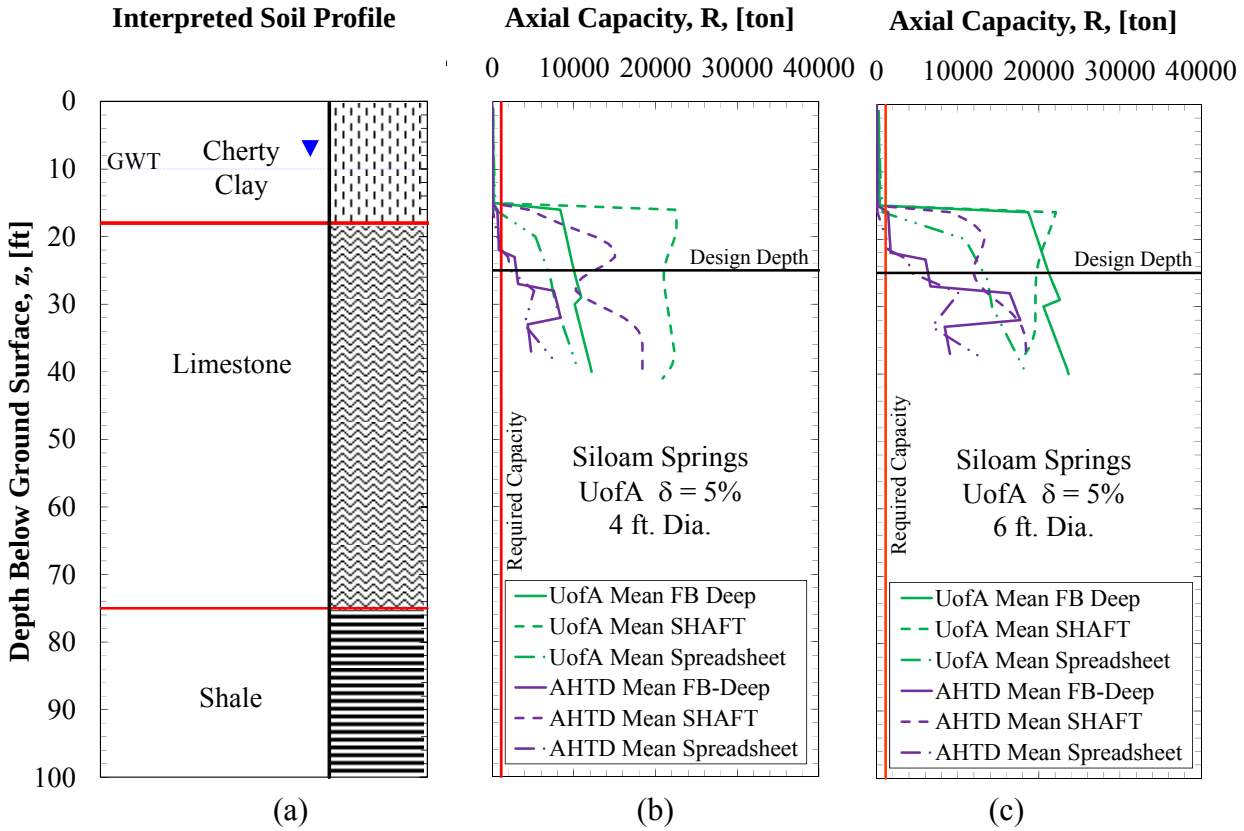

Figure 7.11. Values of (a) interpreted soil profile and ultimate axial capacity as a function of depth for (b) four-foot and (c) six-foot diameter shafts for the UofA and AHTD testing/sampling methods.

7.2.2.5. Methodology Predictions for Rock

Various methods for predicting the components of rock-socketed drilled shaft axial capacity were compared at the SSATS utilizing a spreadsheet for UofA data. Methods for predicting side friction resistance are presented in Section 4.2.2.5.1. Methods for predicting end bearing resistance are presented in Section 4.2.2.5.2. Upon acquisition of full-scale load test data, a best-fitting method for both side friction and end bearing resistance shall be chosen to develop a more accurate rock-socketed drilled shaft design process for the state of Arkansas. All predicted capacities were calculated utilizing The uniaxial unconfined compressive strength data obtained from the UofA sampling method. A five-percent displacement failure criterion was also utilized. Summarizing figures for additional predictive results as presented in Appendix A.

7.2.2.5.1. Side Friction Resistance

Seven methods were selected to compare side friction resistance based on criteria previously discussed in Chapter 4. All methods assumed a smooth rock socket and intact rock mass. Results of the comparison between methods of predicting unit side friction resistance are presented in Figure 7.12. The Reynolds and Kaderabek (1980) method was observed to predict the largest amount of unit side friction resistance. The values predicted utilizing the Gupton and Logan (1984) method provided a unit side friction resistance equivalent to 66.7-percent of the Reynolds and Kaderabek (1980) method. Compared to previous estimations for ultimate axial capacity utilizing FB-Deep, SHAFT, and a spreadsheet, (all of which fail to exceed 38,000 tons) these methods generate a significantly higher amount of unit side friction resistance. However, (as previously stated in Chapter 4) the side friction capacities generated utilizing FB-Deep, SHAFT, and a spreadsheet all utilized more conservative prediction methods such as O'Neill and Reese (1999) and Reese and O'Neill (1988). The AASHTO (2012) method was observed as the

most conservative method of predicting unit side shear resistance. This AASTHO (2012) method was developed from Horvath and Kenney (1979) and includes a reduction factor (α) from O'Neill and Reese (1999) method.

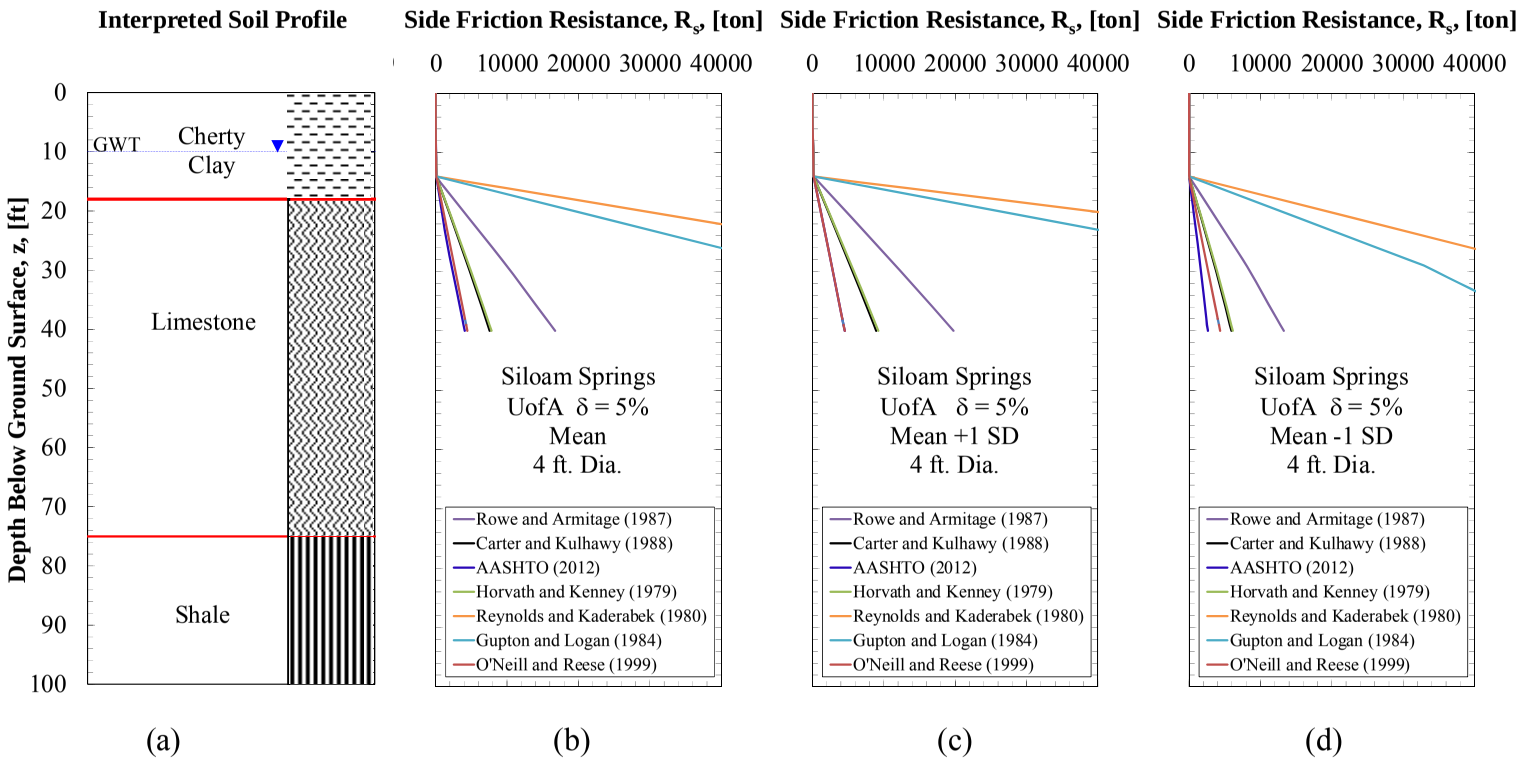

Figure 7.12. Values of (a) interpreted soil profile (b) mean, (c) mean plus one standard deviation, and (d) mean minus one standard deviation side friction resistance as a function of depth for a four-foot diameter shaft utilizing a spreadsheet.

Differences in side friction resistance, with respect to differences in uniaxial unconfined compressive strength, for a 23-foot long, four-foot diameter shaft (SS-E4) are presented in Figure 7.13. As predicted, results obtained using the Reynolds and Kaderabek (1980) and Gupton and Logan (1984) methods tended to be the most sensitive to changes in rock compressive strength values. These methods are utilized to calculate side friction resistance as a linear function of unconfined compressive strength. The O'Neill and Reese (1999) method was observed to be the least sensitive to changes in values of rock compressive strength, with only a 5.8 percent change in side friction resistance calculated from a change in rock compressive strength values of 33.8 percent.

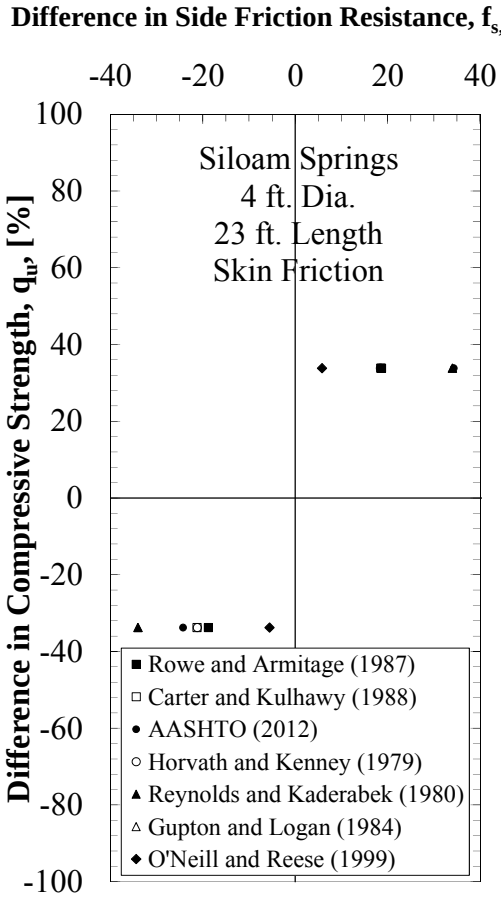

Figure 7.13. Differences in side friction resistance with respect to differences in unconfined compressive strength.

7.2.2.5.2. End Bearing Resistance

Five methods were utilized to compare values of end bearing resistance based on criteria previously discussed in Chapter 4. All methods, exempting those associated with AASTO (2012), assumed an intact rock mass up to depths greater than two diameters below the base of the shaft. The O'Neill and Reese (1999) methodology (and therefore one of the AASHTO [2012] methodologies for predicting end bearing resistance) was omitted from this comparison, as it refers to Rowe and Armitage (1987). However, two additional methods were included from AASHTO (2012) to account for a jointed rock mass up to depths that were greater than two diameters below the base of the shaft. The first additional method accounted for very good quality jointed rock, and the second accounted for good quality jointed rock. Results of the comparison between methods of predicting end bearing resistance are presented in Figure 7.14.

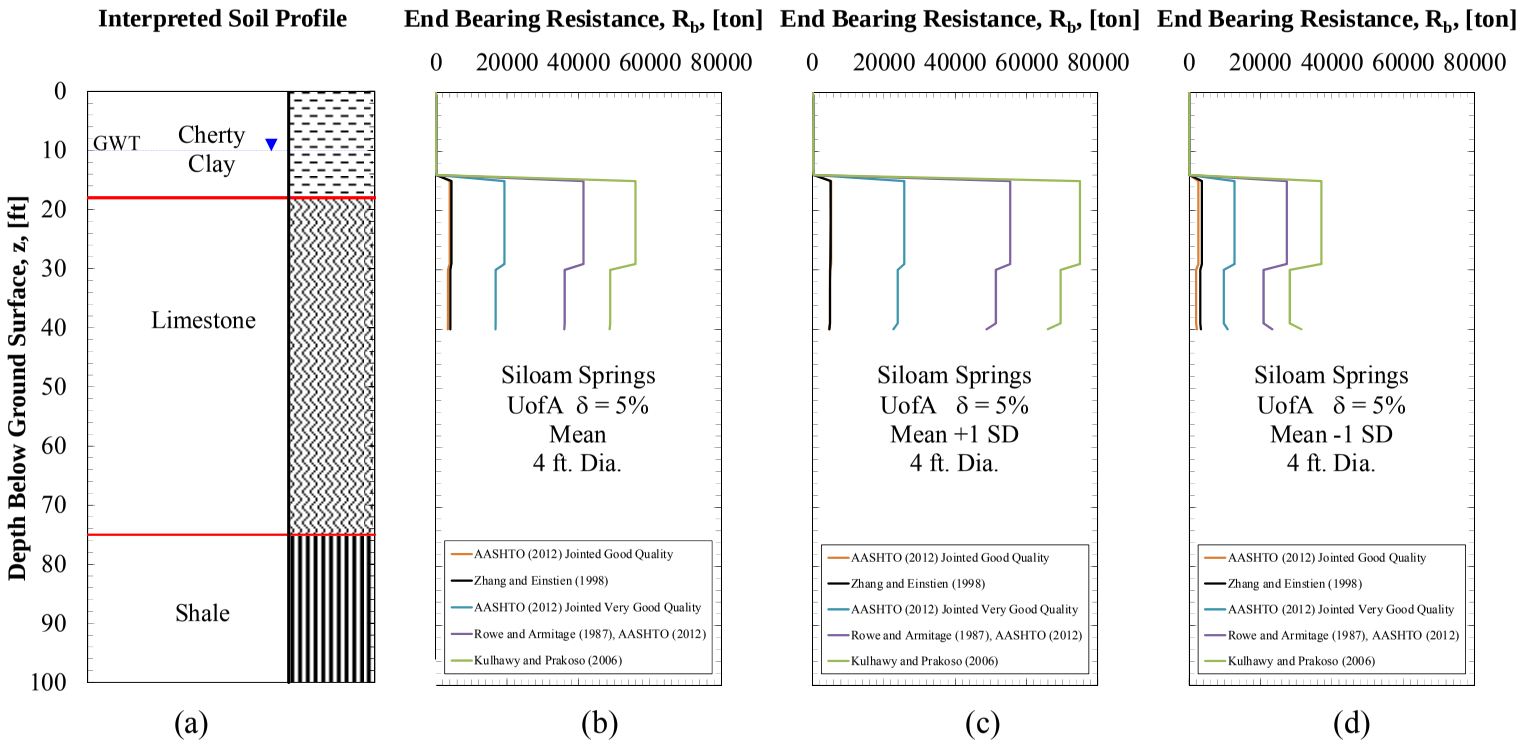

Figure 7.14. Values of (a) interpreted soil profile (b) mean, (c) mean plus one standard deviation, and (d) mean minus one standard deviation end bearing resistance as a function of depth for a four-foot diameter shaft utilizing a spreadsheet.

The Kulhawy and Prakaso (2006) method was observed to have the largest values of predicted end bearing resistance, with the Rowe and Armitage (1987) method being used to predict end bearing resistance values that were equivalent to 74 percent of the Kulhawy and Prakaso (2006) method. Compared to previous estimations for ultimate axial capacity that utilized a spreadsheet and the AASHTO (2012) "jointed good quality rock" method, these methods generate a significantly higher amount of end bearing resistance. The capacities generated utilizing SHAFT also utilized more conservative prediction methods such as and O'Neill and Reese (1999). The capacities generated utilizing FB-Deep were produced utilizing a proprietary method in which unit end bearing resistance is defaulted to equal one-half of the value of input uniaxial unconfined compressive strength. The AASHTO (2012) "jointed good quality rock" method was observed to produce the smallest values of end bearing resistance. Differences in end bearing resistance, with respect to differences in uniaxial unconfined compressive strength, for a 23-foot long, four-foot diameter shaft (SS-E4) are presented in Figure 7.15.

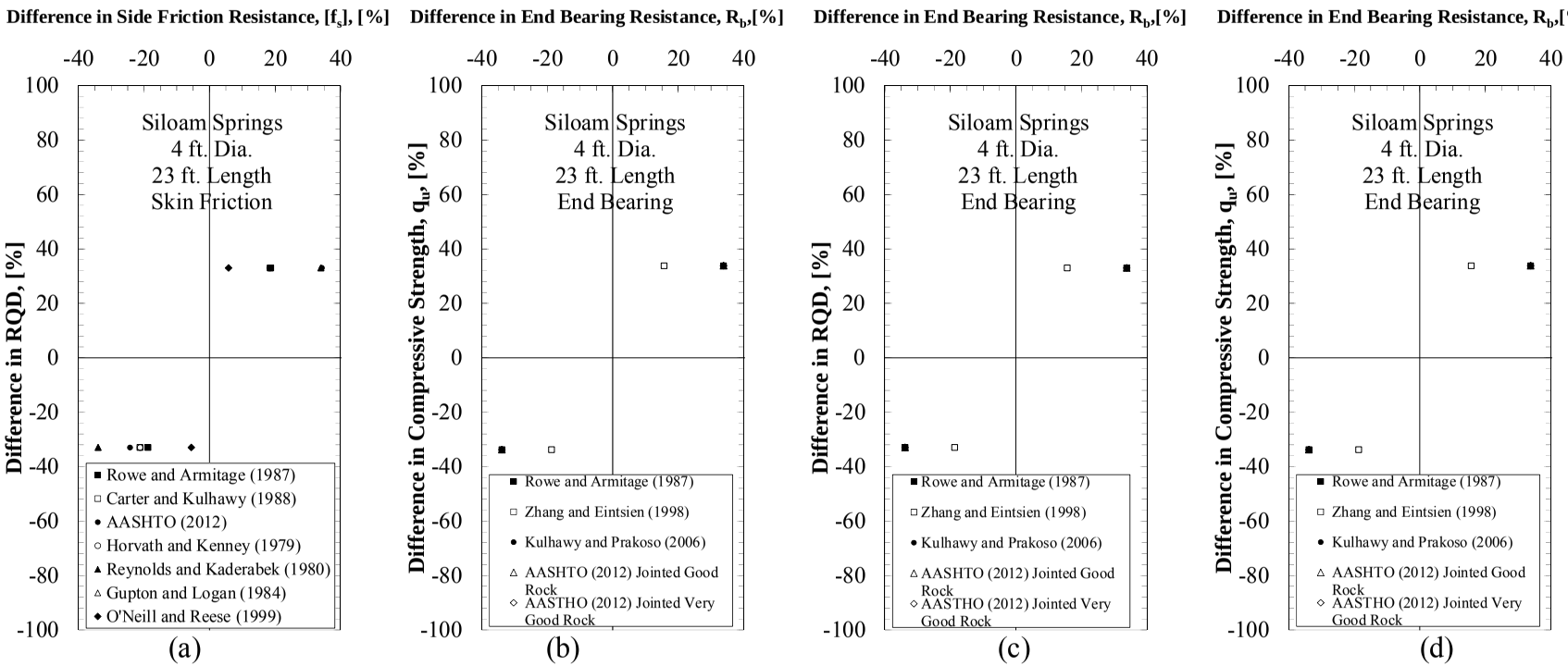

Figure 7.15. Differences in values of (a) & (b) side friction resistances, and (c) & (d) end bearing resistances with respect to differences in RQD% and uniaxial unconfined compressive strength input values, respectively.

7.3. Turrell Arkansas Test Site

At the Turrell Arkansas Test Site (TATS), the prediction of the ultimate axial capacity of the drilled shaft foundations was predominantly influenced by the presence of poorly graded sand at an average depth of 32-feet below ground surface. Comparisons performed upon the predicted values of ultimate axial capacity at the TATS focus on differences between inputs. Results of the geotechnical investigation performed at the TATS are presented (Section 4.3.1). Comparisons of the predicted axial capacity values, as obtained by utilizing SHAFT, FB-Deep, and a spreadsheet, are also discussed (Section 4.3.2).

7.3.1. Turrell Arkansas Test Site Geotechnical Investigation Results

From the geotechnical investigations performed at the TATS, the acquired soil properties included the following: moisture content, total unit weight, plastic limit, liquid limit, corrected blow count, undrained shear strength, friction angle, percent fines, CPT tip resistance, CPT side friction resistance, and shear wave velocity. Comparisons between the UofA, AHTD, and MODOT sampling and testing methods are presented in Figure 7.16, as a function of depth, for the engineering properties of corrected blow count, total unit weight, undrained shear strength, and correlated friction angle.

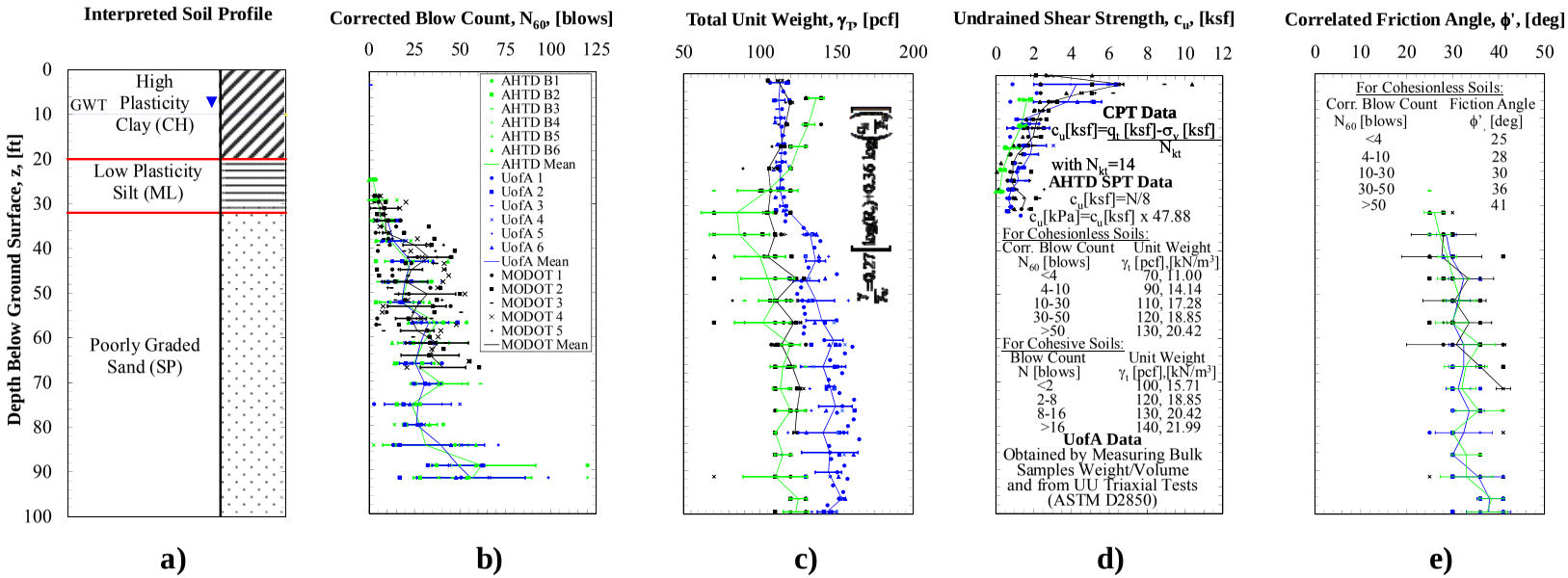

Figure 7.16. (a) interpreted soil profile and differences in values of (b) corrected blow count,(c) total unit weight, (d) undrained shear strength, and (e) correlated friction angle, as a function of depth, as gathered during the UofA, AHTD, and MODOT geotechnical investigations at the Turrell Arkansas Test Site (modified from Race and Coffman, 2013).

Values of UofA and AHTD corrected blow count coincide well with each other (Figure 7.16b), which affirms the empirical transfer function that was previously discussed in Chapter 3 applied to UofA raw blow count values to obtain a standard blow count (Figure 7.17). Compared to the UofA obtained unit weight from bulk samples, the AHTD values of total unit weight (obtained through corrected blow count correlations) were determined to be over-conservative in clays and under-conservative in sands by approximately 13 and 21 percent, respectively (Figure 7.16c). This observation indicates the possibility of cost savings through measured rather than blow count-correlated total unit weight values in clay (as discussed in Chapter 9). Correlated MODOT CPT values of total unit weight were observed to coincide well with UofA values in clay. In sand, the correlated MODOT CPT total unit weight values were observed to consistently plot between the correlated AHTD and the measured UofA values.

Values of undrained shear strength were generally observed to decrease with depth (especially at depths lower than 10-feet below the ground surface near the location of the ground water table). The AHTD method (also correlated from corrected blow count values) was observed to produce values of undrained shear strength not exceeding 0.6-kips per square foot (ksf), nearly 77-percent less than average values obtained by UofA UU triaxial testing. MODOT CPT undrained shear strength values were observed to plot between the values obtained from the UofA and AHTD methods (Figure 7.16d). As all values of friction angle were correlated from blow count (Figure 7.16e), these values coincided well with each other as a function of depth. Values of correlated friction angle for the MODOT sampling and testing regime were plotted to a depth of approximately 71.5-feet below ground surface due to refusal of the cone in the dense

sand at this depth (as previously discussed in Chapter 4). For completeness, summarizing figures for additional soil properties are presented in Appendix A.

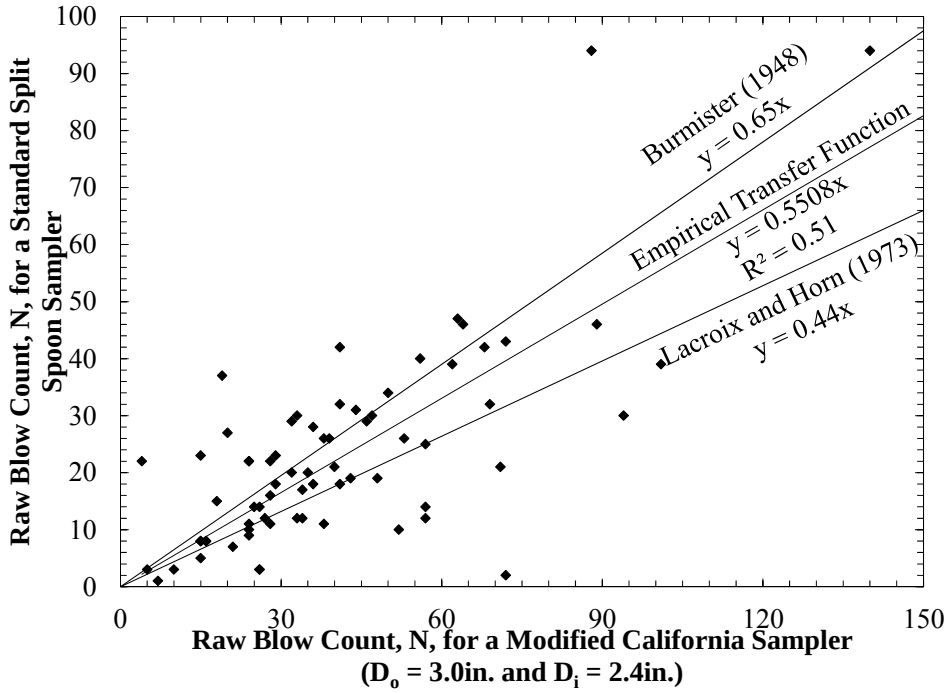

Figure 7.17. Comparison of values from a standard split spoon sampler and a California split spoon sampler in adjacent boreholes at the TATS, from Race and Coffman (2013).

7.3.2. Turrell Arkansas Test Site Predictive Results

From data collected during the geotechnical investigations at the TATS, the ultimate axial capacity of drilled shaft foundations were predicted utilizing three technologies (Ensoft SHAFTv2012, Bridge Software Institute FB-Deep, and Microsoft Excel®). Comparisons of the results draw focus upon three characteristics including a) the range in input data (Section 7.3.2.1), b) the method utilized to evaluate capacity (7.3.2.2), and c) the testing and sampling regime conducted (7.3.2.3). For the clay at the TATS, the FB-Deep predictions utilized correlated blow count values (N_{60}) or CPT tip resistance (q_c) values. For sand at the TATS, the SHAFT predictions utilized blow count values, or correlated effective friction angles (ϕ') values.

7.3.2.1. Data Ranges

Values of ultimate axial capacity were influenced by ranges in the ingested data for the four- and six-foot diameter shafts at given depths (Figure 7.18). Utilizing the FB-Deep program, the UofA shear strength (c_u) data ranges had a greater influence on the axial capacity than the ranges in the AHTD and MODOT c_u values. This phenomenon is expected, as UofA c_u values were directly measured, rather than being correlated values from N_{60} vales or calculated values from CPT tip resistance (q_c) and sleeve friction resistance (f_s). However, it was noted that a large decrease in c_u does not equate to a large decrease in axial capacity (approximately 34 percent) despite a large increase in c_u significantly increasing axial capacity (approximately 71 percent). It was further observed that for data obtained from the MODOT method, utilizing c_u values calculated from f_s and q_c values, rather than directly inputting values of q_c had little effect on capacity. Changes in the values of ultimate axial capacity utilizing SHAFT and the spreadsheet were consistent (exempting changes in MODOT input data from Mean to Mean +1 SD) with the SHAFT obtained axial capacity differences generally exceeding those of the spreadsheet by approximately 15 percent.

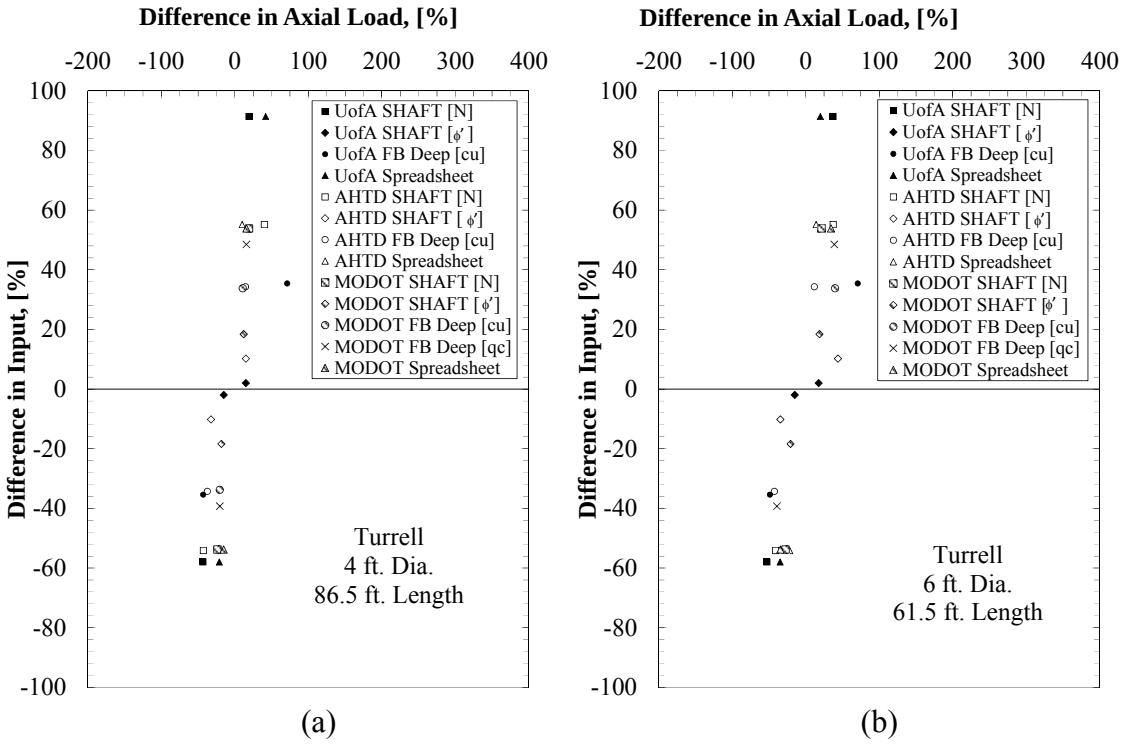

Figure 7.18. Differences in axial load with respect to various soil engineering properties inputs for (a) four-foot diameter and (b) six-foot diameter shafts at the TATS.

The effects of the range in the data inputs on the ultimate axial capacity, as a function of depth for the four- and six-foot diameter shafts are presented in Figures 7.19, 7.20, and 7.21. As with the SSATS, ranges of axial capacities in FB-Deep were noted to increase with shaft diameter, however not as linearly. Within the clay and silt strata, capacity values predicted utilizing the UofA [c_u] and MODOT [q_c] data were noted to be the largest and have the greatest ranges, as expected. The smaller capacity values predicted utilizing AHTD and MODOT [c_u] data had much smaller ranges in the data due to the input values for these methods being developed from correlations or calculations. Within the sand stratum, capacity value ranges increased for all methods, with the greatest ranges observed within predictions obtained using the UofA [c_u] and MODOT [q_c] data.

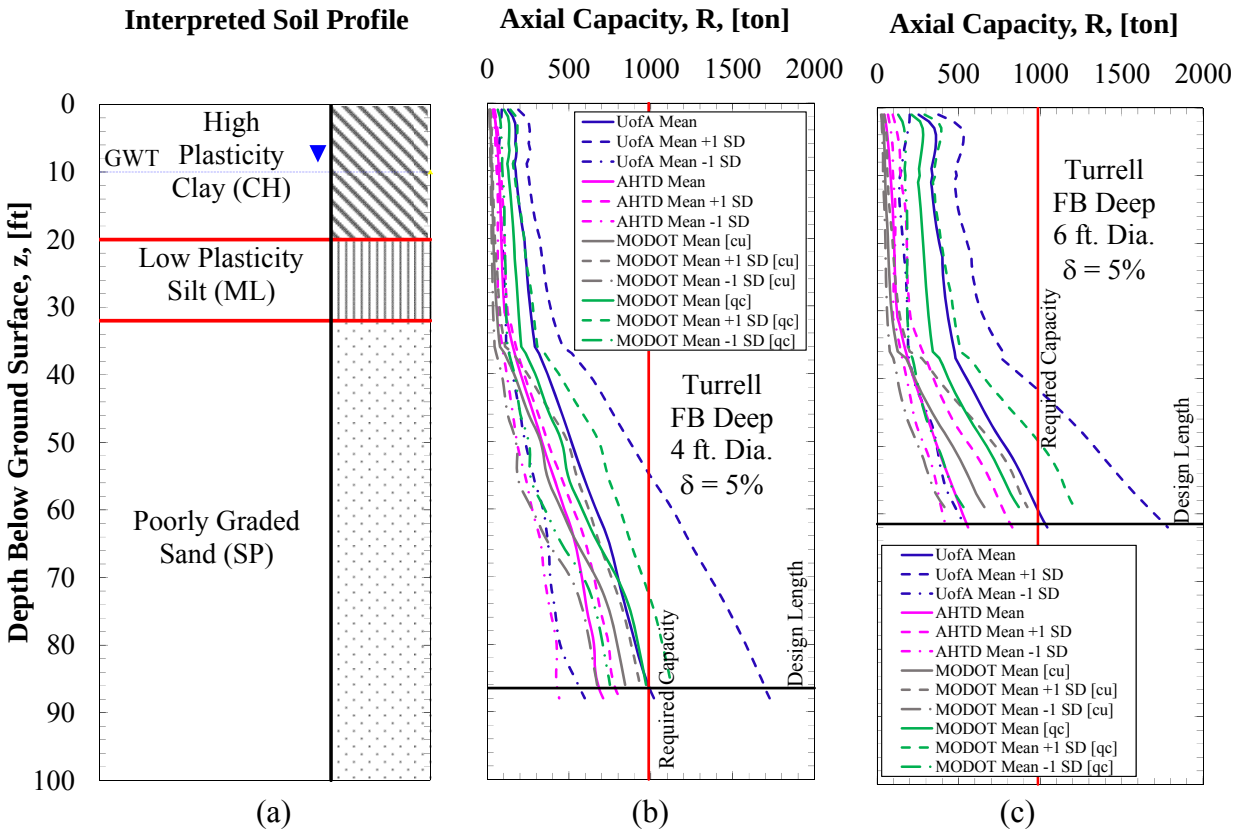

Figure 7.19. Values of (a) interpreted soil profile and ultimate axial capacity as a function of depth for FB-Deep (b) four-foot, and (c) six-foot diameter shafts for various testing and sampling methods.

As presented in Figure 7.20, the predicted values of axial capacity as obtained from the spreadsheet were noted to have larger variations of mean values, yet overall decreased ranges within the data for the MODOT and AHTD methods. This observation was expected within the clay and silt strata. However within the sand stratum, the ranges of capacity between UofA and AHTD were expected to be similar to the UofA and AHTD corrected blow count profiles were not observed.

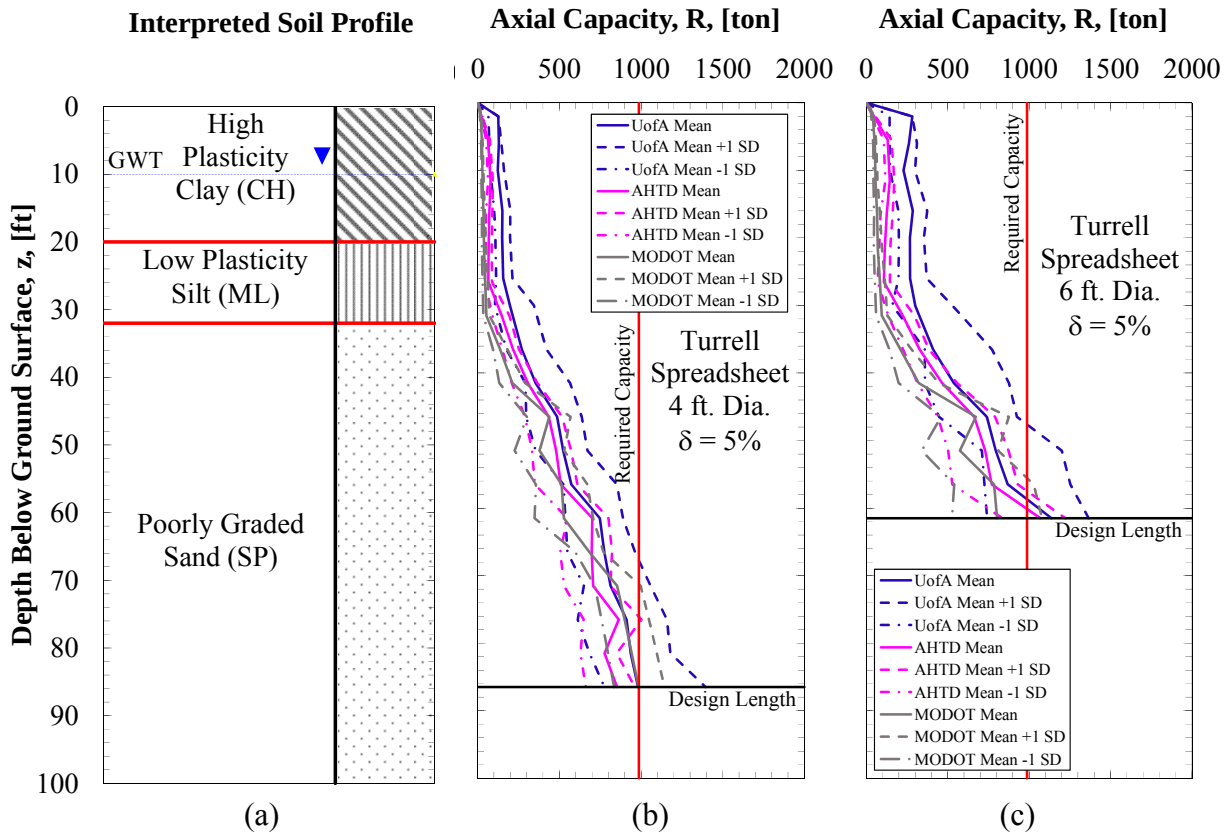

Figure 7.20. Values of (a) interpreted soil profile and ultimate axial capacity as a function of depth using a spreadsheet b) four-foot and (c) six-foot diameter shafts for the various testing and sampling methods.

Utilizing the SHAFT software, comparisons of the values of axial capacity, as obtained using blow count and friction angle inputs, were performed (Figure 7.21). For four-foot diameter UofA shafts, capacity ranges from the friction angle inputs were observed to be 36.2 percent less than those obtained from blow count inputs. This result was expected, as all input friction angles were correlated from corrected blow count values. This trend was also observed for the AHTD regime, suggesting the precedence of measured blow count input data when utilizing SHAFT. However, utilizing the MODOT CPT data, correlated friction angle capacities were observed to be greater (especially in dense sands) and exhibit larger amounts of uncertainty than capacities generated from the calculated blow count inputs. Less variation was observed

within the mean AHTD capacities than within the UofA capacities was noted. This may be due to the correlation of unit weight from correct blow count values.

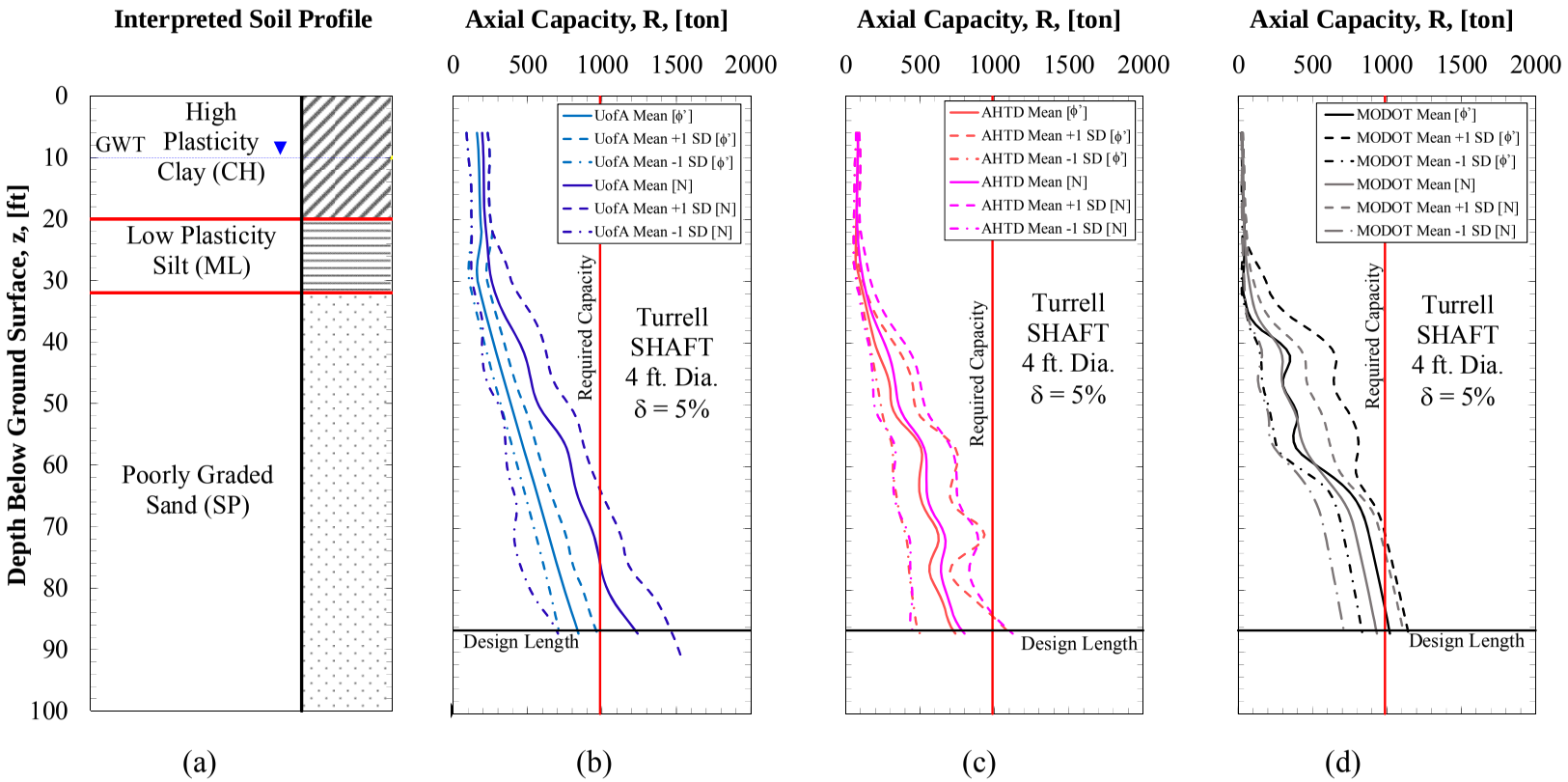

Figure 7.21. Values of (a) interpreted soil profile and ultimate axial capacity as a function of depth for SHAFT four-foot diameter shafts for (b) UofA, (c) AHTD, and (d) MODOT sampling and testing methods.

7.3.2.2. Predictive Technologies

The results obtained from the predictive methods (SHAFT, FB-Deep, and a spreadsheet) that were utilized to predict the ultimate axial capacity for drilled shaft foundations at the TATS were compared (Figure 7.22 and 7.23). For the four-foot diameter shafts, the outputs for the UofA drilling and sampling method were observed to display a pattern (Figure 7.22a). Although the mean values of axial capacity (as a function of depth) for the UofA showed little distinction between technologies (with SHAFT capacity values plotting 10.6 percent greater than FB-Deep or spreadsheet capacities, on average, for depths below 32-feet below the ground surface), the range of capacities generated by each technology were distinctive. Utilizing the same (measured) UofA input data within each method, the FB-Deep generated capacities were observed to have the largest range (spread) within the results, followed by SHAFT, followed by the spreadsheet.

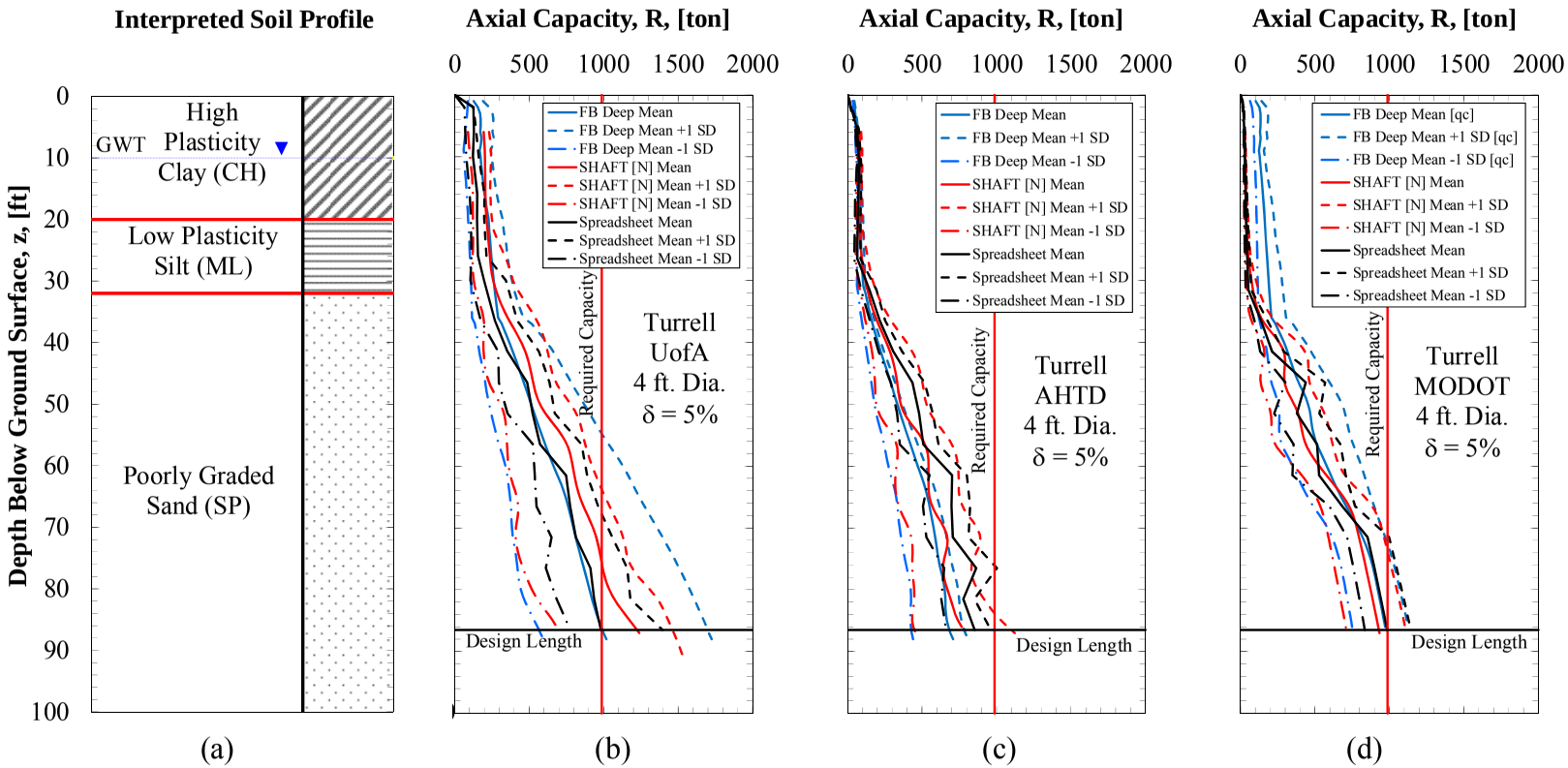

Figure 7.22. Values of (a) interpreted soil profile and axial capacity as a function of depth for four-foot diameter shafts utilizing various technologies for (b) UofA, (c) AHTD, and (d) MODOT methods.

Significantly smaller ranges within the results, at respective depths, were generated by utilizing the values obtained from the AHTD method without any observed pattern (Figure 7.22b). This is attributed to all of the AHTD values being correlated from the corrected blow count values. The axial capacity outputs that were obtained using the MODOT method were also noted to display smaller ranges within the results; however less distribution between values of mean predictions than those for the AHTD regime were observed (Figure 7.22c). Within the clay and silt strata, the MODOT predicted capacities were notably larger as predicted using FB-Deep [q_c] than those predicted utilizing SHAFT or the spreadsheet. The MODOT FB-Deep [q_c] predictions display larger ranges of uncertainty than those generated using SHAFT or the spreadsheet, however these values are still greater (by approximately 74-percent) than the others.

For six-foot diameter shaft, the outputs obtained using the UofA method were observed to display a similar trend to outputs generated for four-foot diameter drilled shafts below a depth of 32 feet below ground surface (Figure 7.23a). Above this depth, the mean capacity values as obtained from FB-Deep were observed to be greater (by approximately 18 percent). Utilizing the same (measured) input data into each method, the FB-Deep generated capacities were observed to have the largest range within the results, followed by SHAFT, followed by the spreadsheet. As with the four-foot diameter shafts, smaller ranges of results were generated by utilizing each of the prediction techniques for the AHTD method, as well as an increased range between mean predictions (Figure 7.23b). Outputs obtained utilizing results from the MODOT method were noted to display smaller ranges within the results (Figure 7.23c). Within the clay and silt strata, FB-Deep [q_c] predictions were notably larger for MODOT than those utilizing SHAFT or the spreadsheet. This trend also supports the precedence of utilizing measured

property input values instead of correlated property values. A table comparing the overall differences between each of the prediction programs is presented in Table 7.1.

Table 7.1. Summary of differences between each axial capacity prediction program.

Program	Pros	Cons
FB-Deep	user friendly interface	enables only one diameter per output
	enables a user-defined displacment input	
	values of side friction resistance and end bearing resistance at user-defined settlements are seperated	utilizes only input values of q_u (not RQD)
	enables a range of lengths per output	
SHAFT	utilizes input values of q_u and RQD	requires values of rock joint spacing and rock joint length
		inefficent soil property input inerface
	computes a range of diameters per output	requires the use of itterations to produce values of capacity at a given displacement
		values of side friction resistance and end bearing resistance at user-defined settlements are not seperated
		enables only one length per output
Spreadsheet	easy to edit input values	based on AASHTO (2012) for prediction of capacity values only at 5 percent displacments
	program versitility	

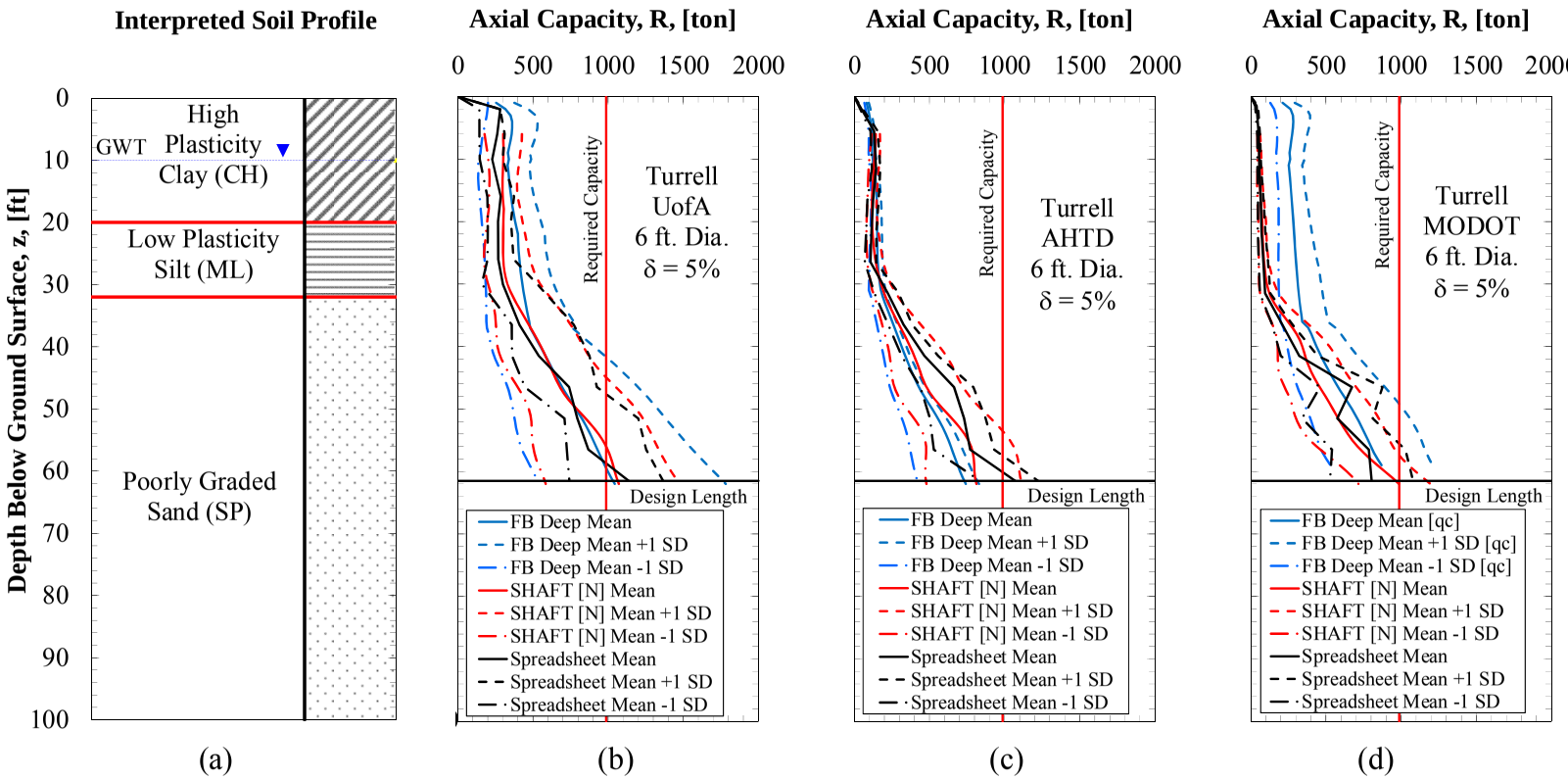

Figure 7.23. Values of (a) interpreted soil profile and axial capacity as a function of depth for six-foot diameter shafts utilizing various technologies for (b) UofA, (c) AHTD, and (d) MODOT methods.

7.3.2.3. Sampling and Testing Methods

The effects of the sampling and testing methods (UofA, AHTD, and MODOT) that were utilized to predict the ultimate axial capacity values for the drilled shaft foudnations at the TATS were compared (Figure 7.24). It was observed that the predicted capacities (as obtained from FB-Deep, SHAFT, and the spreadsheet) utilizing the UofA data were greatest. Again, the difference between the direct input of measured values rather than correlations is the cause for the discrepancy. The AHTD capacities obtained using the AHTD drilling and sampling data within all three of the predictive programs were observed to be greater than the MODOT generated capacities in clay (exempting MODOT FB-Deep [q_c]). However, below a depth of 32-feet, the MODOT data generated capacity values were observed to surpass those generated using the AHTD data. Summarizing figures for additional predictive results were generated are presented in Appendix B.

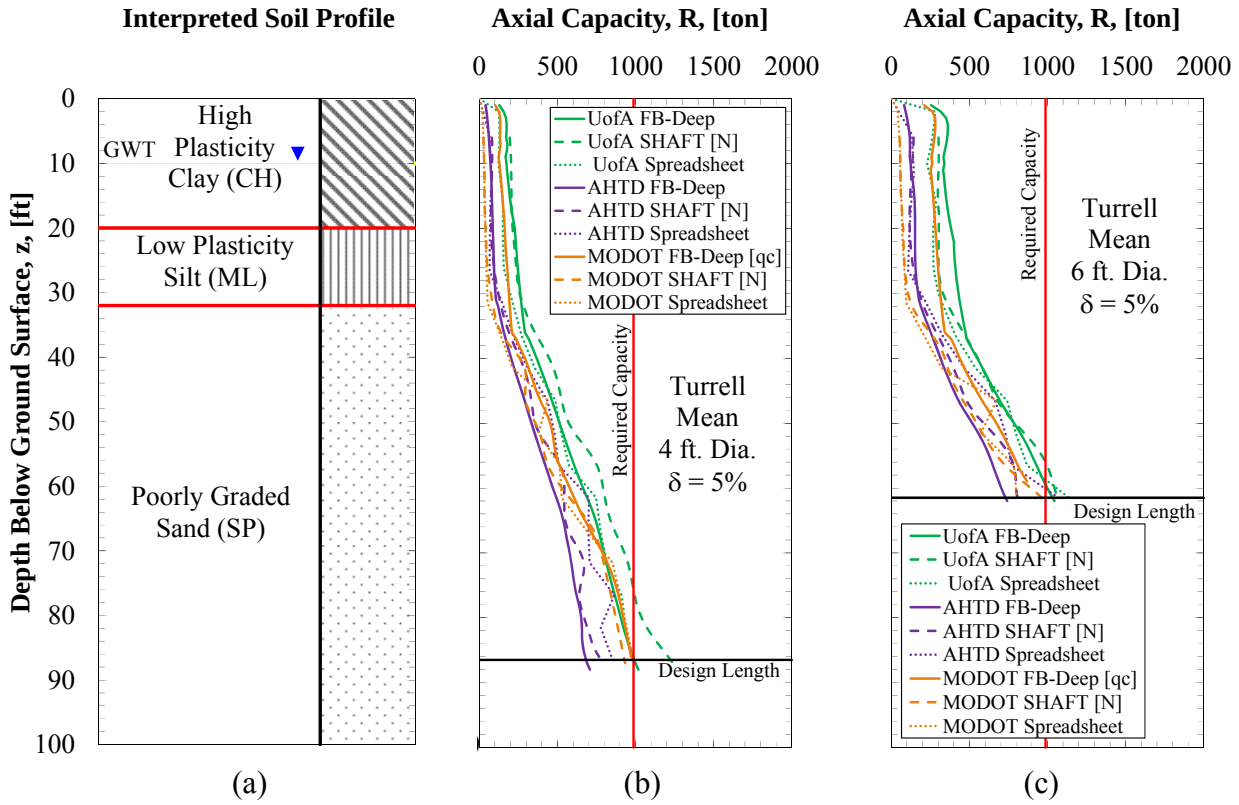

Figure 7.24. Mean values of (a) the interpreted soil profile and of ultimate axial capacity as a function of depth for (b) four-foot and (c) six-foot diameter shafts for the UofA, AHTD, and MODOT testing and sampling methods.

7.4. Monticello Arkansas Test Site

At the Monticello Arkansas Test Site (MATS), the prediction of the ultimate axial capacity for the drilled shaft foundations was attributed to by the presence of poorly graded sand between depths of 27- and 42-feet below ground surface and beneath 60-feet below ground surface. Comparisons between the predicted ultimate axial capacity values at the MATS focus on the amount of difference within the input values. Results of the geotechnical investigation performed at the MATS are presented (Section 7.4.1). Comparisons of the predicted axial capacity, as obtained utilizing SHAFT, FB-Deep, and a spreadsheet, are also discussed (Section 7.4.2).

7.4.1. Monticello Arkansas Test Site Geotechnical Investigation Results

From the geotechnical investigations performed at the MATS, the acquired soil properties included the following: moisture content, total unit weight, plastic limit, liquid limit, corrected blow count, undrained shear strength, friction angle, percent fines, CPT tip resistance, CPT side friction resistance, and shear wave velocity. Comparisons between the UofA, AHTD, and MODOT sampling and testing methods are presented in Figure 7.25, as a function of depth, for the engineering properties of corrected blow count, total unit weight, undrained shear strength, and correlated friction angle. For the respective depths, values of AHTD corrected blow count averaged 36.0 percent greater than the values calculated from the correlated MODOT CPT data (Figure 7.25a). Below a depth of 60-feet below the ground surface, the values of UofA corrected blow count averaged 12 percent greater than those obtained from the AHTD method (Figure 7.25b). This increase is the result of the empirical transfer function being applied to the raw blow count values that were obtained with a modified California split spoon sampler (Figure 7.26).

As observed at the TATS, the AHTD values of total unit weight (obtained through corrected blow count correlations) were determined to be under-conservative in clays and over-conservative in sands by approximately 15 percent and 8 percent, respectively, as compared to the UofA measured bulk sample values (Figure 7.25c). This observation also indicates the possibility of cost savings through measured rather than blow count-correlated total unit weight values in sand (as discussed in Chapter 9). Correlated MODOT CPT values of total unit weight were observed to coincide well with UofA values in clay (exempting one outlier at a depth of approximately 51.5-feet below the ground surface). In sand, the correlated MODOT CPT total unit weight values were observed to consistently plot between the correlated AHTD and the measured UofA values.

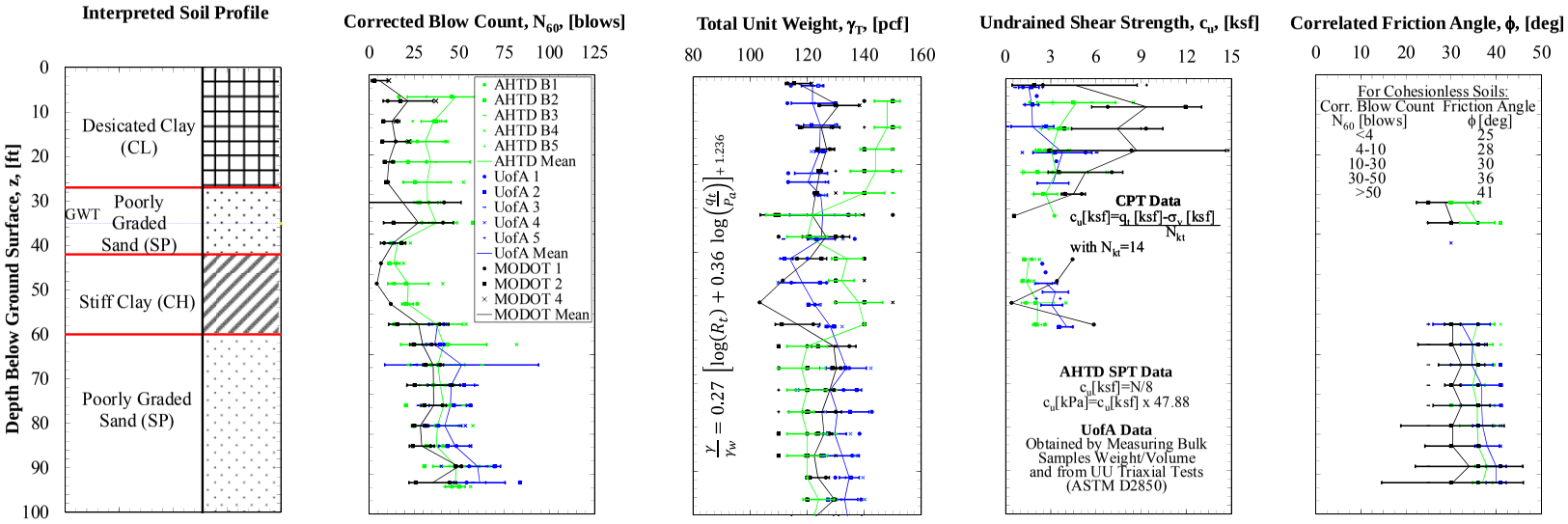

a) **b)** **c)** **d)** **e)**

Figure 7.25. The (a) interpreted soil profile with differences in values of a) corrected blow count, (b) total unit weight, (c) undrained shear strength, and (d) correlated friction angle as gathered from UofA, AHTD, and MODOT geotechnical investigations at the MATS.

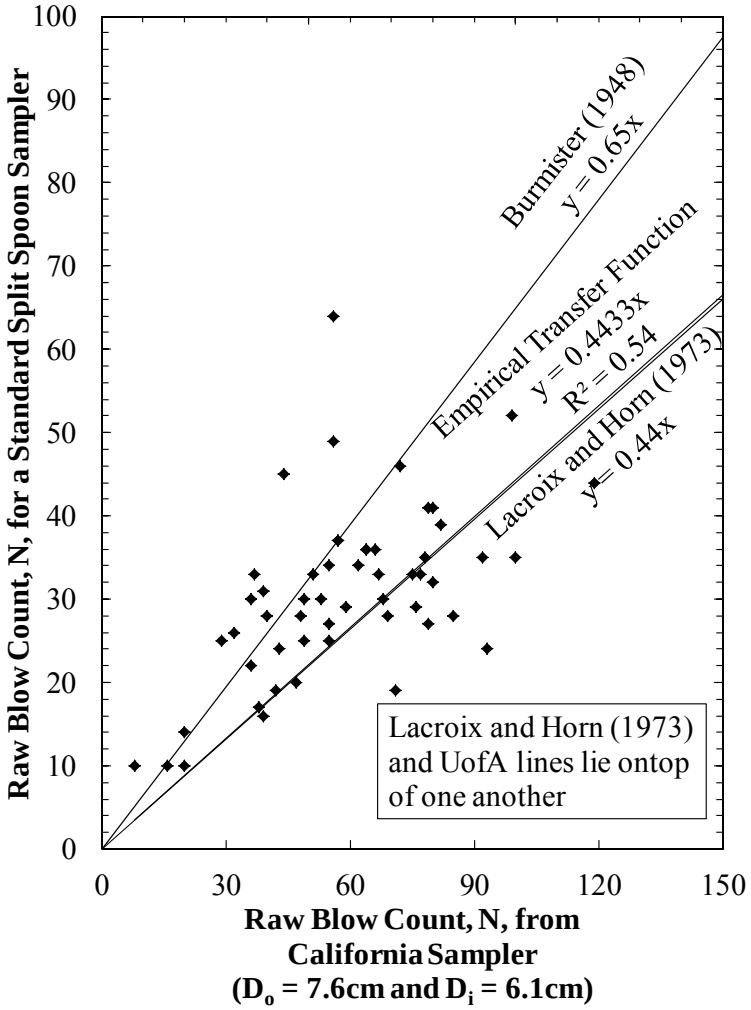

Figure 7.26. Comparison of values from a standard split spoon sampler and a California split spoon sampler in adjacent boreholes at the MATS, from Race and Coffman, (2013).

Values of undrained shear strength were generally observed to decrease with depth for the MODOT CPT sampling and testing method. Additionally, the MODOT method was observed to yield the greatest values within the topmost clay stratum, with mean values of undrained shear strength peaking at 8.7 ksf (nearly 61 percent greater than the average values obtained by UofA UU triaxial testing). The AHTD undrained shear strength values (as correlated from corrected blow count values) were observed to be the smallest within the lower clay stratum, with AHTD values plotting an average 44.7 percent less than those obtained from the UofA method (Figure 7.25d). As all values of friction angle were correlated from corrected

blow count (Figure 7.25e), the arrangement of values of correlated friction angle is similar to the arrangement of the values plotted in corrected blow count. The MODOT method was observed to yeild the smallest values of correlated friction angle, plotting an average 13.0 and 15.8 percent lower than the values obtained from the AHTD and UofA methods, respectively. Summarizing Additional soil properties, as a function of depth, are presented in Appendix A.

7.4.2. Monticello Arkansas Test Site Predictive Results

From data collected during the geotechnical investigations at the MATS, the ultimate axial capacity of the drilled shaft foundations were predicted utilizing three technologies (Ensoft SHAFTv2012, Bridge Software Institute FB-Deep, and Microsoft Excel®). Comparisons of the results draw focus upon three characteristics including a) the range in input data (Section 7.4.2.1), b) the method utilized to evaluate capacity (7.4.2.2), and c) the testing and sampling method conducted (7.4.2.3). As with the TATS, for the clay at the MATS, the FB-Deep predictions utilized correlated blow count values (N_{60}), or CPT tip resistance values (q_c). For the sand at the MATS, the SHAFT predictions utilized blow count values, or correlated effective friction angle (ϕ') values.

7.4.2.1. Data Ranges

Values of ultimate axial capacity were influenced by ranges in the ingested data for the four- and six-foot diameter shafts at given depths (Figure 7.27). Utilizing the FB-Deep program, the UofA c_u data ranges had little effect on axial capacity. Little effect was observed by using the c_u values calculated from CPT f_s and q_c values rather than directly inputting values of q_c. Changes in ultimate axial capacity values as obtained from SHAFT [ϕ'] were consistent among the input parameters, with smaller changes in the AHTD inputs (9 percent) having larger effects on capacity (22 percent) than larger changes in the UofA inputs (15 percent). This phenomenon

was not expected, as UofA and AHTD correlated friction angle inputs had similar ranges within the data. Changes in axial capacity between SHAFT [N] and the spreadsheet were observed to be similar to those at the TATS. Although there were similar changes in the input values, the output from the SHAFT program was observed to exhibit larger changes in axial capacity (by about 22.5 percent) with the exception of the MODOT Spreadsheet.

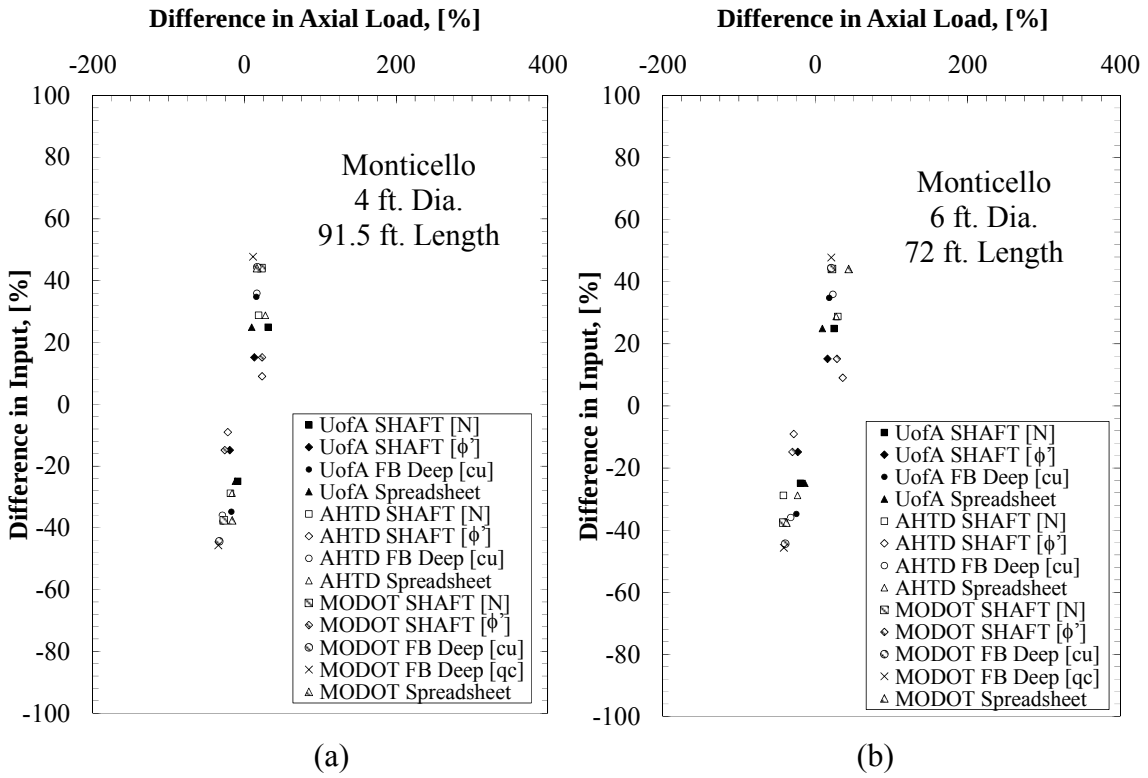

Figure 7.27. Differences in axial load with respect to various soil engineering properties inputs for (a) four-foot diameter and (b) six-foot diameter shafts at the MATS.

The effects of rang in the data inputs on the ultimate axial capacity, as a function of depth for the four- and six-foot diameter shafts, are presented in Figures 7.28, 7.29, and 7.30. Utilizing the FB-Deep program, the predicted capacity values from the MODOT [c_u] and MODOT [q_c] data were noted to be the largest and have the greatest ranges. Smaller capacity values were predicted utilizing AHTD and UofA data, and also were observed to have smaller ranges in the capacity values. Offset decreases in axial capacity were observed within sand strata for the six-

foot diameter shafts. This is a result of an end bearing reduction factor being applied, as discussed in Reese and O'Neill (1988).

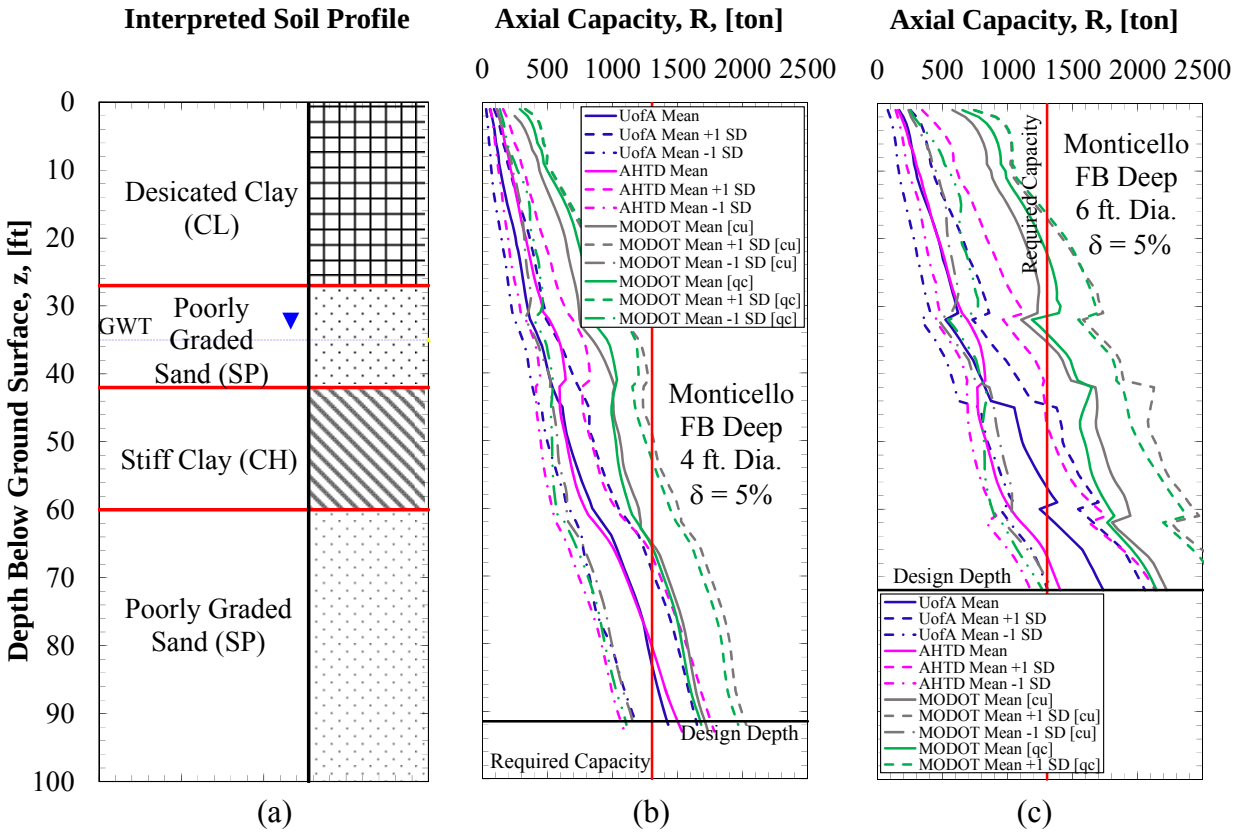

Figure 7.28. Values of (a) the interpreted soil profile and ultimate axial capacity as a function of depth for FB-Deep (b) four-foot and (c) six-foot diameter shafts for various testing and sampling methods.

As presented in Figure 7.29, the predicted values of axial capacity as obtained from the spreadsheet were noted to be the smallest when the MODOT inputs were utilized. The MODOT inputs also resulted in the largest ranges of capacities (exempting depths below ground surface between 42- and 52-feet on the four-foot diameter shaft and the outlier encountered at 52-feet on the six-foot diameter shaft). Unlike the TATS, the UofA data inputs resulted in the smallest ranges of output capacities.

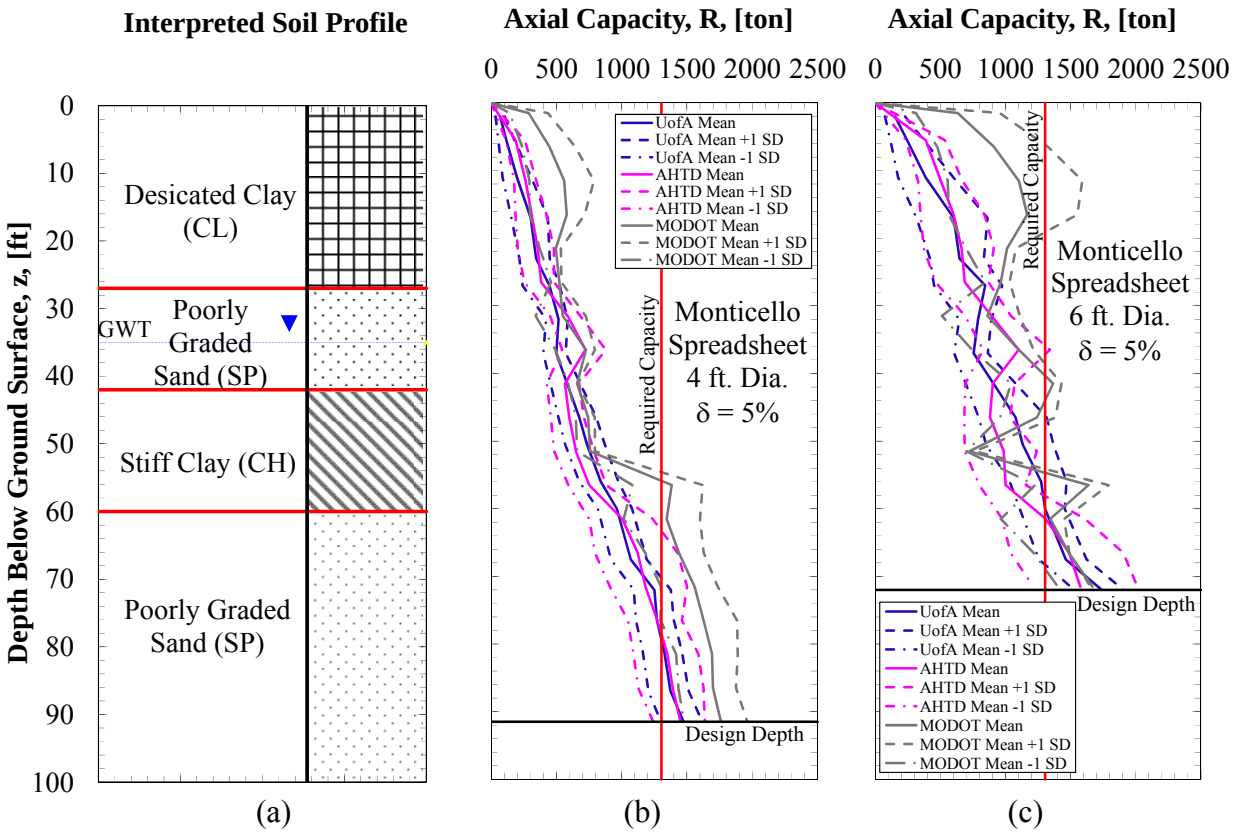

Figure 7.29. Values of (a) the interpreted soil profile and ultimate axial capacity as a function of depth for spreadsheet (b) four-foot and (c) six-foot diameter shafts for various testing and sampling methods.

Utilizing the SHAFT predictive software, comparisons of the values of axial capacity between blow count and friction angle inputs were performed (Figure 7.30). For four-foot diameter shafts, the ranges in the values of capacity from the friction angle inputs (UofA) were observed to be similar, with output capacities generated from blow count values (UofA) exceeding the output capacities generated from friction values (UofA) by 10.3 percent. For four-foot diameter AHTD and MODOT shafts, capacity ranges from the friction angle inputs (AHTD and MODOT) were also observed to be comparable, with output capacities generated from blow count values (AHTD and MODOT) exceeding those from friction values by 7.1 percent and 5.4 percent, respectively. It was further observed between depths of 6- and 18-feet and 35- and 59-

feet below ground surface, the capacity values for all the methods coincided. This is believed to be attributed to the presence of water at these depths.

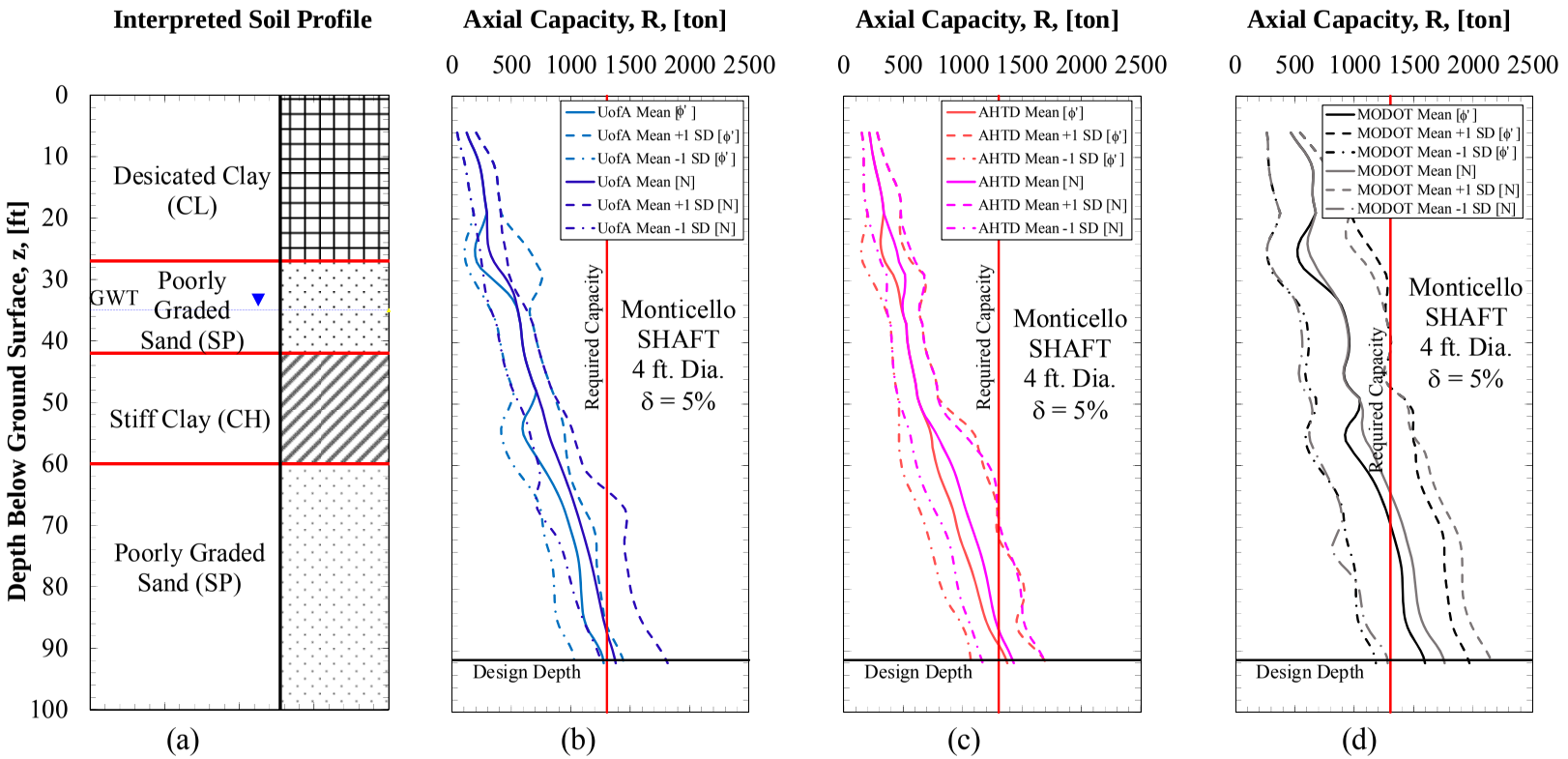

Figure 7.30. Values of (a) the interpreted soil profile and ultimate axial capacity as a function of depth for SHAFT four-foot diameter shafts for (b) UofA, (c) AHTD, and (d) MODOT sampling and testing methods.

7.4.2.2. Predictive Technologies

The results obtained from the predictive methods (SHAFT, FB-Deep, and a spreadsheet) that were utilized to predict the ultimate axial capacity for the drilled shaft foundations at the MATS were compared (Figure 7.31 and 7.32). For the four-foot diameter shafts, mean capacity values obtained using the UofA method showed little difference between software programs. Utilizing the same (AHTD) input data into each software program, the FB-Deep software program generated capacities that were observed to have the largest range of results, followed by the spreadsheet.

Larger ranges within the capacity values were generated by each software program using the AHTD data, as well as an increased variation between mean predictions (Figure 7.31c). Outputs from the AHTD method were noted to display larger ranges of results; however the ranges were smaller than the ranges observed for the capacity values obtained using MODOT data (Figure 7.31d). The capacity values from the MODOT data also exhibited the largest deviation between mean values; particularly for those capacities predicted utilizing the spreadsheet. Within the lower sand stratum, the capacity values that were obtained utilizing the spreadsheet were 9.9 percent greater than capacities generated from FB-Deep or SHAFT (Figure 7.31d).

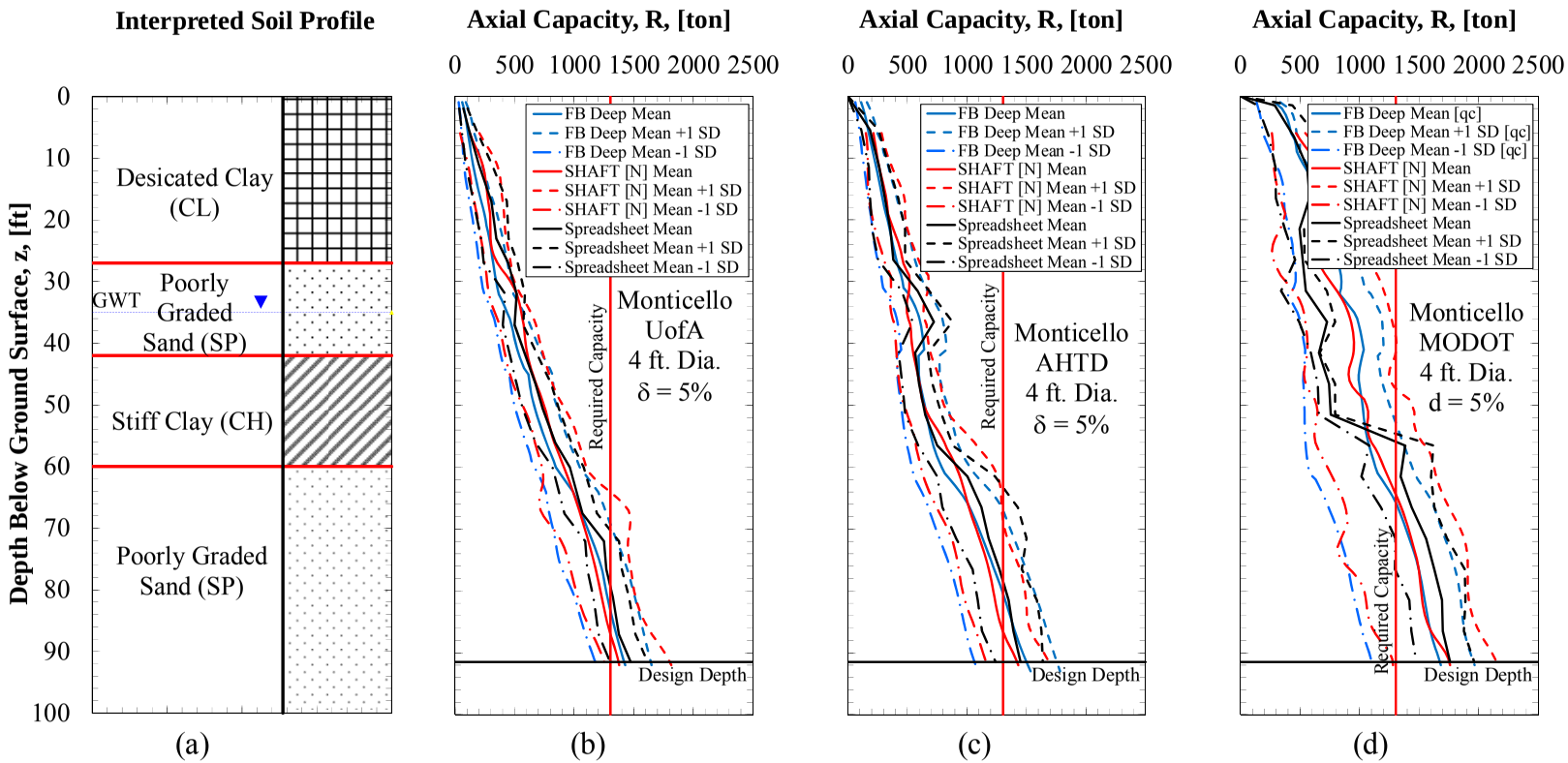

Figure 7.31. Values of (a) the interpreted soil profile and axial capacity as a function of depth for four-foot diameter shafts utilizing various technologies for (b) UofA, (c) AHTD, and (d) MODOT methods.

For the six-foot diameter shaft, output values obtained by using the UofA drilling and sampling method were not observed to display a similar trend to outputs generated for four-foot diameter drilled shafts (Figure 7.32b). However, utilizing the data from the AHTD drilling and sampling method, more consistency between mean capacity values was observed (Figure 7.32c). The largest ranges within the results was observed for the MODOT drilling and sampling method (Figure 7.32d).

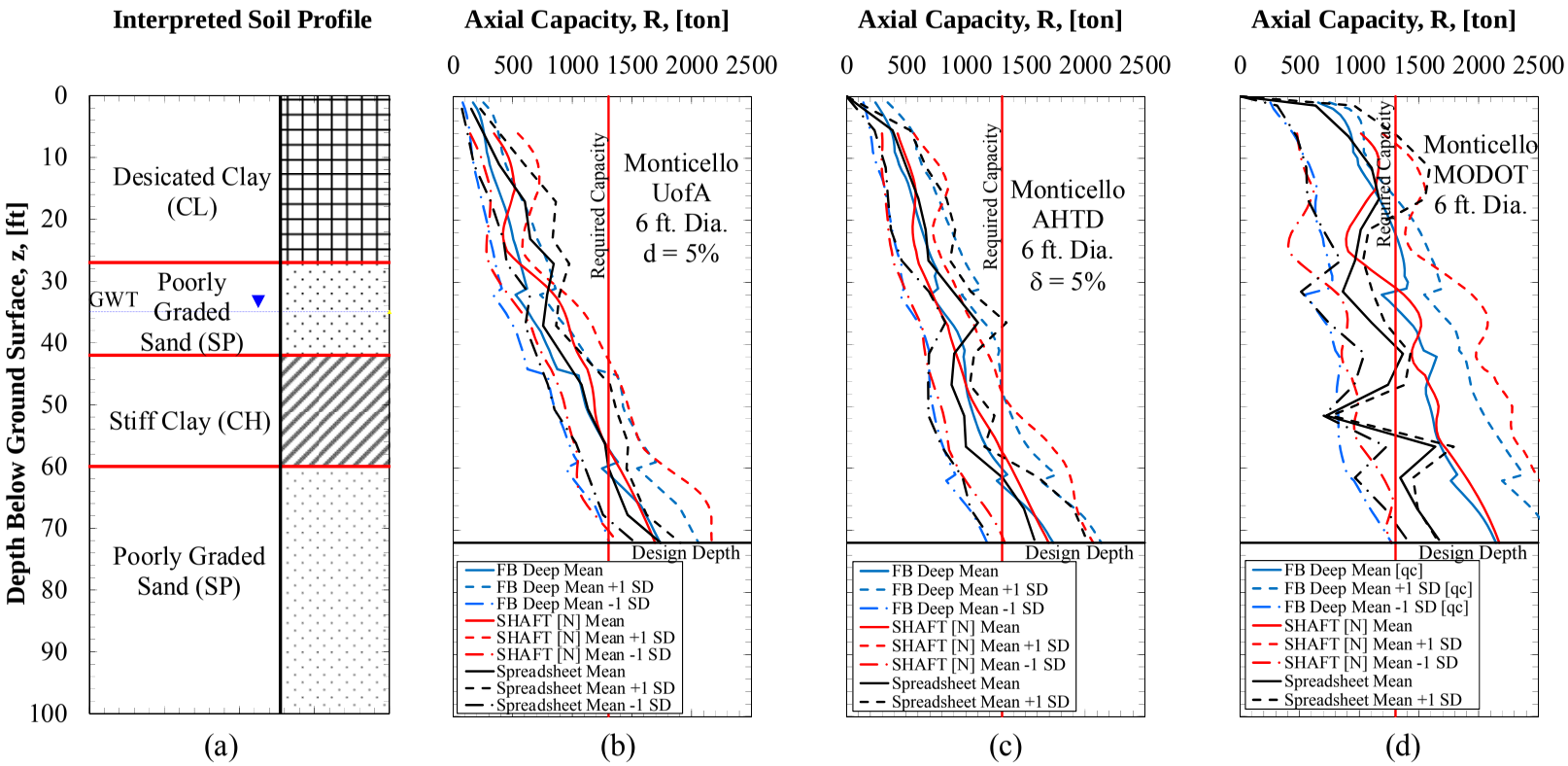

Figure 7.32. Values of (a) the interpreted soil profile and axial capacity as a function of depth for six-foot diameter shafts utilizing various technologies for (b) UofA, (c) AHTD, and (d) MODOT methods.

7.4.2.3. Sampling and Testing Methods

The effects of the sampling and testing methods (UofA, AHTD, and MODOT) that were utilized to predict the ultimate axial capacity values for drilled haft foundations at the MATS were compared (Figure 7.33). It was observed that the predicted capacity values (as obtained from FB-Deep, SAHFT, and the spreadsheet) [exempting the 6-foot diameter spreadsheet anomaly at 51-ft] were the greatest by utilizing the MODOT data. This may be attributed to the advantages of continuous in-situ testing (as exemplified with MODOT CTP data) at sites featuring high soil variability. At the MATS, the predicted capacities (UofA and AHTD) for all three of the software programs were observed to be more consistent than the capacities generated at the TATS. This may also be attributed to the high amount of soil variability as the MATS. Capacity predictions for all methods were observed to stabilize below a depth of 60-feet below ground surface (the location of the final sand stratum). Summarizing figures for additional predictive results are presented in Appendix B.

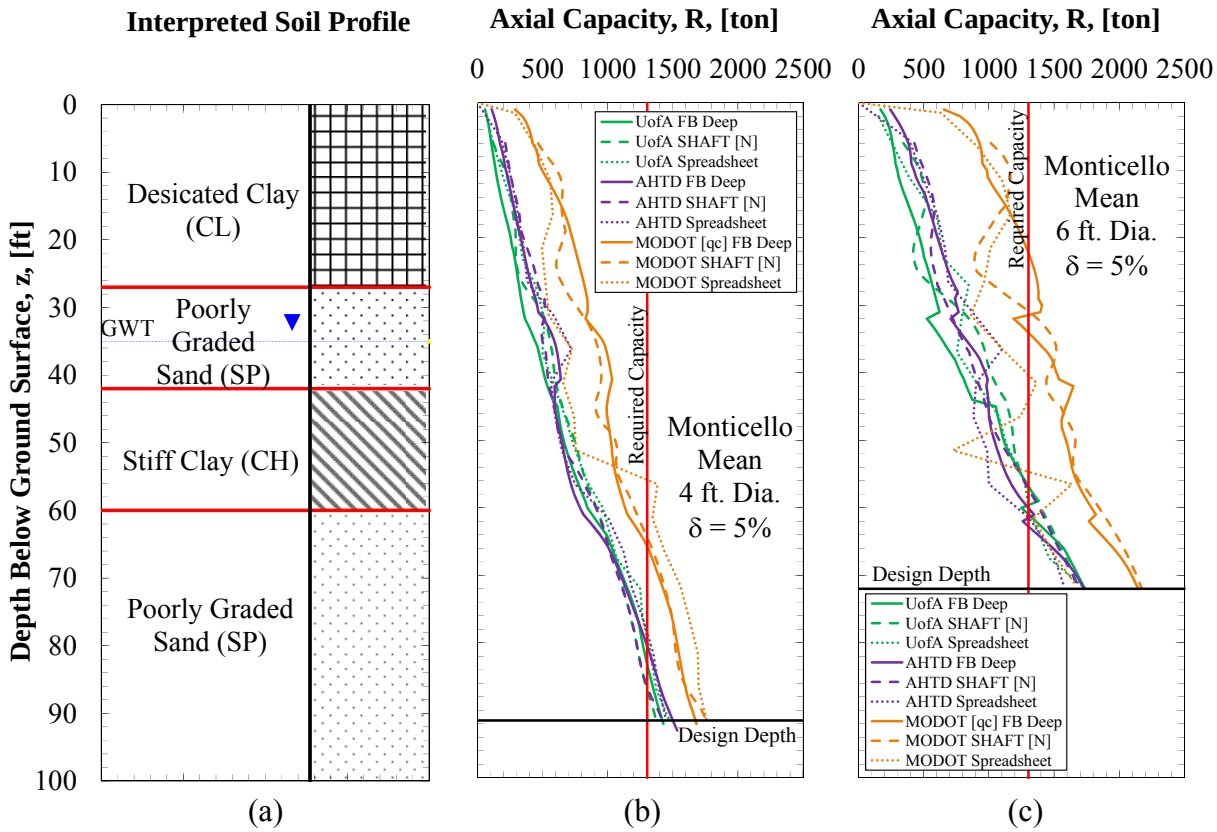

Figure 7.33. Mean values of (a) the interpreted soil profile and ultimate axial capacity with respect to depth for (b) four-foot and (c) six-foot diameter shafts for the UofA, AHTD, and MODOT testing and sampling methods.

7.5. Siloam Springs Arkansas Test Site Cost-benefit Results

From the cost-benefit analyses performed at the Siloam Springs Arkansas Test Site (SSATS), results regarding the unit cost per ton of resistance for AHTD and UofA sampling and testing methods are presented in Section 7.5.1. Results of cost implications of UofA and AHTD sampling and testing methods at the Siloam Springs Site are also discussed (Section 7.5.2.). Results of the cost implications of using fly ash supplemented concrete are presented in Section 7.5.3. It is important to again note that values of maximum measured capacity were intended to be reported at settlements of five percent, however due to scheduled lateral load testing, displacements during testing were minimalized. Instead, results of the SSATS cost-benefit analysis for the UofA sampling and testing method were developed utilizing measured load test

values ranging between 0.02 and 0.18 percent. As a result, the cost savings associated with the SSATS are conservative estimates.

7.5.1. Unit Cost of UofA and AHTD Sampling and Testing Methods in Rock

The unit costs per ton of resistance utilizing the UofA and AHTD testing and sampling methods of the SSATS are presented in this Section. Overall, values of unit cost per ton of axial capacity for the UofA and AHTD testing and sampling methods were found to equal $24.11 and $82.70, respectively (Table 7.2). This large difference in values is due to multiple reasons. First, the shaft selected to represent the entire SSATS for the UofA sampling and testing method was SS-E4, which had a seven-foot rock socket. The typical shaft for the AHTD sampling and testing method had a ten-foot rock socket. It was observed concrete costs for the ten-foot rock socketed shaft were $590.4 greater than that of the seven-foot rock socketed shaft. More noticeably, costs associated with the drilling of the ten-foot rock socket were observed to be $14,582 greater for the ten-foot socket, compared to the seven-foot rock socket. Additionally, the measured capacity of test shaft SS-E4 was observed to be 2.0 times greater than the design capacity of the AHTD shaft.

It was also noted that despite the UofA geotechnical investigation including uniaxial compressive strength testing, costs associated with this investigation were $4,011 less than that of the AHTD geotechnical investigation. This may be attributed to the time spent on site acquiring RQD values. The AHTD geotechnical investigation included at least 13 boreholes extending an average of 38-feet. The UofA geotechnical investigation included only six boreholes (three extending less than 17 feet, two extending less than 69 feet, and one extending 116.9 feet). As a result, the AHTD geotechnical investigation logged approximately 1.8 times

more linear feet of geomaterial than the UofA geotechnical investigation. However, as no values of compressive strength were measured, cost surfeits were still observed (Table 7.2).

The fiscal advantage of performing full-scale load testing was observed to equal a cost savings of approximately $15,173 per shaft or $8.97 per ton of resistance. This difference is contributed to the difference in rock socket depths (the UofA originally designed 10-foot socket and the UofA load tested seven-foot socket). However, the design capacity for the 10-foot socketed shaft was observed to be greater than that of the seven-foot socketed shaft by 215.5 tons, indicating the potential for an even greater amount of cost savings (Table 7.2).

Table 7.2. Unit cost per ton of resistance and overall SSATS fiscal summary.

SSATS		ID	Dia. [ft]	Design Capacity [tons]	Measured Capacity [tons]	Depth of Shaft [ft]	Total Cost of Shaft	Cost/ton	Total Cost of Drilled Shaft Project
Measured	UofA	W4	4	1112.5	1271	26	$ 36,800	$ 28.95	$ 890,776
		E4	4	1112.5	897	23	$ 21,628	$ 24.11	$ 556,983
		C6	6	1112.5	500	21	$ 32,635	$ 65.27	$ 799,137
Designed	AHTD	N/A	4	445	N/A	26	$ 36,800	$ 82.70	$ 819,789
	UofA	N/A	4	1112.5	N/A	26	$ 36,800	$ 33.08	$ 815,778

7.5.2. Cost Implications for Infrastructure in Rock

Utilizing the unit cost per ton of resistance factors (as previously discussed in Section 7.5.1.) generated for the UofA and AHTD sampling and testing method, the total project

foundation cost of each load condition was calculated and compared. Results of the fiscal infrastructure impact analysis are presented in Table 7.3. Overall, the UofA Measured method (which utilizes the benefits of advanced sampling and testing and advanced full-scale load testing) was observed to be the least expensive method, saving an average of 47 and 46 percent more than the AHTD and UofA Designed methods, respectively, for the original load condition.

Utilizing unit cost per ton values for each method in hypothetical situations, the degree of potential savings using the UofA Measured Method was noted to increase compared to the AHTD method and decrease compared to the UofA Designed method. The UofA Measured method averaged a savings of 220 percent and 28 percent, compared to the AHTD and UofA Designed methods, respectively. These fluctuations were a result of two factors. First, values of unit cost per ton of resistance values for the AHTD sampling and testing method were based upon provided design loads that were conservative. Additionally, although UofA Designed values of unit cost per ton of resistance utilized larger values of capacity than those from the UofA Measured method, the labor costs associated with the excavation of the UofA Designed shaft were also significantly larger. As a result, the UofA designed unit cost per ton or resistance value was noted to exceed the UofA measured value. This result verifies the advantage of full-scale load testing, even at small settlements.

Table 7.3. Summary of the cost implications of UofA, MODOT, and AHTD sampling and testing methods on various types of infrastructure at the SSATS.

Load Condition	Description	Project Cost		
		UofA Measured	AHTD	UofA Designed
AHTD - Provided	Single-lane Bridge Superstructure	$ 556,983	$ 819,789	$ 815,778
Hypothetical 1*	Heavy Building with Concentrated Loads	$ 2,130,618	$ 7,039,419	$ 2,817,869
Hypothetical 2*	Large Stucture with Less Concentrated Loads	$ 3,155,339	$ 10,554,036	$ 4,223,715
Hypothetical 3*	Medium Structure with Moderate Loads	$ 563,397	$ 1,664,124	$ 667,750

* Evaluated utilizing cost/ton values

7.5.3. Concrete Cost-benefit Results at the SSATS

From the cost-benefit analyses performed on the concrete utilized at the Siloam Springs Arkansas Test Site (SSATS), results regarding the costs of the traditional AHTD Class S (containing 20 percent fly ash) and the Mid Continent/GCC Concrete (containing 30 percent fly ash) concrete mixtures are presented in this Section. Current specifications for AHTD Class S concrete allow a maximum Class C fly ash replacement of 20 percent in rock socketed drilled shafts. The fiscal benefits of 30 percent fly ash replacement were investigated by UofA researchers (in conjunction with Mid Continent/GCC Concrete) at the SSATS. Performance characteristics of the Mid Continent/GCC mix are discussed in Chapter 8. Results of the cost implications of using 30 percent fly ash supplemented concrete are presented in Tables 7.4 through 7.5.

On a mix design level, cost savings between the AHTD and Mid Continent/GCC are primarily realized through the 10 percent additional fly ash replacement. Savings equal to $1.85 and $1.40 per cubic yard of cement were observed for concrete and fly ash components, respectively (Table 7.4). However, savings were also realized through reduced portions of aggregate, and the use of a water reducer rather than a high range water reducer. Overall, using a 30 percent fly ash substitution, a savings of $2.66 per cubic yard of concrete was observed, compared to the traditional 20 percent fly ash substitution currently utilized by AHTD.

Table 7.4. Summary of the costs associated with AHTD Class S concrete and GCC concrete utilized at the SSATS.

Material	Traditional AHTD Class S	Mid Continent GCC Concrete	Difference in Cost Per Cubic
Cement [lb/cyd]	489	452	$ 1.85
Fly Ash [lb/cyd]	122	192	$ 1.40
Rock [lb/cyd]	1850	1765	$ 0.51
Sand [lb/cyd]	1320	1260	$ 0.36
Water [gal/cyd]	31	35	$ -
Admixture	High Range Water Reducer	Water Reducer	$ 1.34
Admixture	Retarder	Retarder	$ -
Total [lb/cyd]	3812	3704	$ 2.66

At the SSATS, cost savings between the AHTD and Mid Continent/GCC mixes were calculated for each of the test shafts on site (Table 7.5). As expected, cost savings were observed to increase with shaft size, with test shaft SS-C6 incurring approximately 56.8 percent greater savings. An average cost savings of $2.7 and $5.57 per linear foot were calculated for the four-foot and six-foot diameter shafts, respectively.

Table 7.5. Summary of the costs associated with AHTD Class S concrete and GCC concrete utilized at for each test shaft.

Test Shaft	Cubic Yards Purchased	Cost of Traditional AHTD Class S	Cost of GCC Concrete Drilled Shaft	Difference in Cost
SS-W4	27	$ 3,144.88	$ 3,073.06	$ 71.82
SS-C6	44	$ 5,125.00	$ 5,007.96	$ 117.04
SS-E4	23	$ 2,678.97	$ 2,617.79	$ 61.18
Total	94	$ 10,948.85	$ 10,698.81	$ 250.04

Although the magnitude of savings observed at the SSATS may seem small, the potential cost savings associated with the concrete utilized for an entire level of foundation infrastructure is significant. Utilizing the UofA (Mid Continental/GCC Concrete) mix design alone, a cost savings of $680 was observed at the SSATS for the AHTD originally planned single-lane bridge (Table 7.6). Pairing the UofA design methodology with this mix increases these savings to $4176. As the level of infrastructure associated with a project increased, cost savings were observed to reach a potential of $28,476 for large structures with less concentrated loads.

Table 7.6. Summary of the costs associated with AHTD Class S concrete and GCC concrete for various levels of infrastructure at the SSATS.

Load Condition	Description	Concrete Cost		
		UofA [Mix Only]	UofA [Mix + Design]	AHTD
AHTD - Provided	Single-lane Bridge Superstructure	$ 29,135	$ 25,640	$ 29,816
Hypothetical 1	Heavy Building with Concentrated Loads	$ 66,216	$ 58,272	$ 67,764
Hypothetical 2	Large Stucture with Less Concentrated Loads	$ 198,648	$ 174,815	$ 203,291
Hypothetical 3	Medium Structure with Moderate Loads	$ 52,973	$ 46,617	$ 54,211

7.6. Turrell Arkansas Test Site Cost-benefit Results

From the cost-benefit analyses performed at the Turrell Arkansas Test Site (TATS), results regarding the unit cost per ton of resistance for UofA, MODOT, and AHTD sampling and testing methods are presented in Section 7.6.1. Results of the cost implications of the UofA, MODOT, and AHTD sampling and testing methods upon various levels of infrastructure at the TATS are also discussed (Section 7.6.2.). Results of the TATS cost-benefit analysis for the UofA and MODOT sampling and testing methods were developed utilizing measured load test values, the proposed cost savings associated with the TATS are conservative estimates. A cost-benefit analysis of the concrete utilized at the TATS was not performed, as the concrete utilized was within specifications for AHTD Type S concrete (20 percent fly as substitution). Values of maximum measured capacity were intended to be reported at settlements of five percent, however due to scheduled lateral load testing, displacements during testing were minimalized (between 1.02 and 3.06 percent).

7.6.1. Unit Cost of UofA and AHTD Sampling and Testing Methods in Soil

The unit costs per ton of resistance utilizing the UofA, MODOT, and AHTD testing and sampling methods of the TATS are presented in this Section. The costs associated with the construction of each UofA (MODOT) shaft, as well as a typical AHTD constructed pile group are presented in Table 7.7. Overall, values of unit cost per ton of axial capacity for the UofA, MODOT, and AHTD testing and sampling methods were found to equal $75.47, $75.47, and

$141.57, respectively (Table 7.7). This difference in values was due to the measured capacity of test shaft T-S4, which was observed to be about 2.1 times greater than the design capacity of the AHTD pile group.

The UofA (MODOT) shaft selected to best represent the test site was test shaft T-S4. Although this shaft was not observed to reach the required design strength, the maximum measured capacity of 818 tons was recorded at a settlement of 1.19 percent. UofA geotechnical investigation costs were observed to be $1,913 greater than AHTD geotechnical investigation costs (Table 7.7). This was attributed to the time spent recovering the crushed Shelby tube during the UofA investigation. MODOT geotechnical investigation costs were observed to be the most costly, with fees exceeding those of the UofA and AHTD sampling and testing methods by $5,133 and $7,046.

AHTD total costs for the foundation project were observed to be $137,398 (8.78%) and 142,263 (9.11%) less than costs for the selected UofA and MODOT methods, respectively. This may be due to the unexpected cost incurred with the extended labor schedule from McKinney Drilling Co. constructing UofA shafts. Despite the AHTD piling method being less expensive, a benefit of constructing drilled shafts utilizing the UofA design method includes the increased lateral stability of the construction. Given the seismic hazards associated with the TATS, this benefit is considerable.

Table 7.7. Unit cost per ton of resistance and overall TATS fiscal summary.

TATS		ID	Dia. [ft]	Depth of Shaft [ft]	Cost of Concrete	Cost of Steel	Cost of Labor / Equiptment	Cost of Mobilization	Cost of Geotechnical	Cost of Load Test
Measured	UofA	S4	4	86.5	$ 5,903.87	$ 12,330.06	$ 99,483.51	$ -	$ 8,927.98	$ 75,000.00
		N4	4	88	$ 7,590.69	$ 11,910.54	$ -	$ -	$ 8,928.98	$ 75,000.00
		C6	6	62.5	$ 7,590.69	$ 15,878.27	$ -	$ -	$ 8,929.98	$ 75,000.00
	MODOT	S4	4	86.5	$ 5,903.87	$ 12,330.06	$ -	$ -	$ 14,060.63	$ 75,000.00
Designed	AHTDa	N/A	1.5	85	Not Available	Not Available	Not Available	Not Available	$ 7,014.84	$ -
	AHTDb	N/A	1.5	85	Not Available	Not Available	Not Available	Not Available		
	AHTDc	N/A	1.5	85	Not Available	Not Available	Not Available	Not Available		
	UofA	N/A	4	86.5	$ 653.70	$ 41,925.00	$ 7,656.54	$ -	$ 8,927.98	$ -

*Load test cost based upon Brown (2008)

7.6.2. Cost Implications for Infrastructure in Soil

Utilizing the unit cost per ton of resistance factors (as previously discussed in Section 7.6.1.) generated for the UofA, MODOT, and AHTD sampling and testing methods, the total project foundation cost of each load condition was calculated and compared. Results of the fiscal infrastructure impact analysis are presented in Table 7.8. Overall, the MODOT method (which utilized the benefits of MODOT CPT testing and UofA advanced full-scale load testing) was observed to be the most expensive method, costing an average of 9.1, 5.1, and 0.3 percent more than the AHTD, UofA Designed, and UofA Measured methods, respectively, for the original load condition.

Utilizing unit cost per ton values for each method in hypothetical situations, the degree of potential savings using the UofA Measured Method was noted to increase compared to the AHTD method and decrease compared to the UofA Designed method. The UofA Measured method averaged a savings of 83 percent compared to the AHTD method, a savings of 0.15 percent compared to the MODOT method, and a surfeit of 18.9 percent compared to the UofA Design method (Table 7.8). Savings compared to the AHTD method can be attributed to the fact that values of unit cost per ton of resistance values for the AHTD sampling and testing method were based upon provided design loads that were conservative. Savings compared to the MODOT method can be attributed to the increase in MODOT geotechnical investigation costs. Surfeits compared to the UofA Design method can be attributed to two factors. First, unit cost per ton values for the UofA Design method were calculated utilizing a design load that measured 169 tons greater than that of the UofA Measured Method. Also, (as previously stated in Section 7.6.1) labor costs associated with the construction of each test shaft were unexpectedly greater than those estimated due to an extended construction schedule.

Table 7.8. Summary of the cost implications of UofA, MODOT, and AHTD sampling and testing methods on various types of infrastructure at the TATS.

TATS		ID	Dia. [ft]	Design Capacity	Measured Capacity	Depth of Shaft [ft]	Total Cost of Shaft	Cost/ton	No. of Shafts	Total Cost of Drilled Shaft
Measured	UofA	S4	4	987	818	86.5	$ 61,735.37	$ 75.47	24	$ 1,565,576.85
		N4	4	987	1065	88	$ 75,239.14	$ 70.65	24	$ 1,889,668.37
		C6	6	987	1050	62.5	$ 106,297.37	$ 101.24	24	$ 2,635,066.91
	MODOT	S4	4	987	818	86.5	$ 61,735.37	$ 75.47	24	$ 1,570,709.50
Designed	AHTDa	N/A	1.5	395	N/A	85	$ 52,632.00	$ 133.25	14	$ 1,428,078.84
	AHTDb	N/A	1.5	395	N/A	85	$ 65,790.00	$ 166.56	8	
	AHTDc	N/A	1.5	395	N/A	85	$ 78,948.00	$ 199.87	2	
	UofA	N/A	4	987	N/A	86.5	$ 61,735.37	$ 62.55	24	$ 1,490,576.85

*Load test cost based upon Brown (2008) AHTD Avg $ 141.57

7.7. Conclusion

Predicted results as obtained from software programs utilizing soil properties obtained from geotechnical investigations preformed to estimate drilled shaft ultimate axial capacity at the Siloam Springs, Turrell, and Monticello Arkansas Test Sites were discussed herein Chapter 7. From each geotechnical investigation, the differences between UofA, AHTD, and MODOT sampling and testing methods, as well as ranges in data were compared. Utilizing the results from the geotechnical investigation, the impacts of the data on predicted axial capacity of drilled shaft foundations were evaluated utilizing Ensoft SHAFT, Bridge Software Institute FB-Deep, and Microsoft Excel®.

At the SSATS, the predicted ultimate axial capacity of drilled shaft foundations (only predicted using data from the UofA and AHTD methods) was predominantly influenced by the presence of competent limestone at an average depth of 16-feet below ground surface. As a result, the geotechnical investigation soil properties of interest, at the SSATS, were focused on rock quality properties such as RQD, E_m and q_u. RQD values were observed to increase with depth and in depths up to 38-feet below ground surface, the difference in the range of values were observed to be nine percent lower, as obtained by the UofA, than the values obtained by AHTD. Additionally the mean RQD values averaged nine percent greater for UofA data than the

AHTD data. Values of unconfined compressive strength and modulus of elasticity were only tested for the UofA method. The values of unconfined compressive strength were observed to decrease with depth.

Two sensitivity analyses were performed to understand the dominant rock quality inputs utilized to predict axial capacities within the SHAFT software program. From the first analysis, s- and t-values of 6- and 0.0001-feet were selected as the rock joint inputs. From the second analysis, comparing load-settlement behavior with various changes in input data, values of RQD were determined to have the largest impact on the predicted axial capacity (although these results contradict the results generated by utilizing the program at the SSATS).

The values of the ultimate axial capacity were influenced by ranges in in input data, at given depths, for the four- and six-foot diameter shafts. The AHTD unconfined compressive strength input data was determined from AASTHO (2012), and resulted in larger fluctuations in the predicted axial capacity as compared to the measured UofA data. These larger fluctuations are attributed to the correlation function between unconfined compressive strength values and RQD percentages. Changes in unconfined compressive strength values for the UofA were observed to have the greatest impact on the SHAFT obtained results and the least impact on spreadsheet obtained results.

Utilizing a spreadsheet and the UofA rock data, seven methods for predicting side friction resistance and five methods for predicting end bearing resistance were compared. For side friction resistance, the results obtained using the Reynolds and Kaderabek (1980) and Gupton and Logan (1984) methods were the most sensitive to changes in rock compressive strength values. Although values of capacity obtained using the AASTHO (2012) method were observed to be the smallest, the O'Neill and Reese (1999) method was observed to be the least sensitive to

changes in values of rock compressive strength. For end bearing resistance, the Kulhawy and Prakaso (2006) method was observed to yield the highest values, and the AASHTO (2012) Jointed Good rock method was observed to yield the lowest values.

At the TATS, the prediction of drilled shaft ultimate axial capacity was predominantly influenced by the presence of poorly graded sand below an average depth of 32 feet below ground surface. From the geotechnical investigations performed at the TATS, comparisons between the UofA, AHTD, and MODOT sampling and testing methods for major soil engineering properties indicated AHTD values of total unit weight (obtained through corrected blow count correlations) were determined to be under-conservative in clays and over-conservative in sands, compared to UofA measured properties. The values of undrained shear strength, within the clay layer, were generally observed to decrease with depth. Values of correlated friction angle for the MODOT sampling and testing regime plot to a depth of approximately 71.5-feet below ground surface due to practical refusal within the dense sand at this location.

The values of ultimate axial capacity, at given depths, were influenced by ranges in data entry for the four- and six-foot diameter shafts. The ranges within the UofA c_u data were observed to affect the axial capacity more than the ranges of the AHTD and MODOT shear strength values. This phenomenon is expected, as UofA c_u values were directly measured, rather than correlated from N60-vales or calculated from CPT q_c and f_s values. For the MODOT obtained data, utilizing the c_u values calculated from CPT f_s and q_c values, rather than directly inputting values of q_c had little effect on the predicted capacity values. Within the clay and silt strata, the predicted capacity values that were obtained by using the UofA and MODOT [q_c] data were noted to be the highest and have the largest ranges. Within the sand stratum, the ranges in

the capacity values increased for all of the drilling and sampling methods, with the greatest ranges being observed for the UofA and MODOT [q_c] methods.

Although the mean capacity values as obtained using UofA drilling and sampling methods showed little difference between software programs (with SHAFT capacity values plotting an average 10.6 percent greater than FB-Deep or spreadsheet capacities below a depth of 32-feet below ground surface), the range of capacities generated by each technology was unique. Using the same (measured) input data in each software program, the FB-Deep generated capacities were observed to have the largest range within the results, followed by SHAFT, followed by the spreadsheet. Smaller ranges of results were generated by each software program within the data using the AHTD data, as well as an increased difference between mean predictions. Capacity predictions from the MODOT method were also noted to display smaller ranges of results; however less difference between the mean predictions was observed, as compared to the results obtained using the AHTD data. Within the clay and silt strata at the TATS, the predictions using the MODOT data were notably larger from FB-Deep [q_c] than those from SHAFT or the spreadsheet. The predictions from MODOT FB-Deep [qc] data displayed larger ranges of uncertainty than those generated using SHAFT or the spreadsheet, however these values are still higher than either (shaft and the spreadsheet). The UofA generated capacities obtained from all three software programs were observed to be the highest. This is attributed to the direct input of measured values rather than the input of correlated values. The generated capacities, in clay, for all three software programs, using the AHTD data, were observed to be higher than generated capacities obtained using the MODOT data (exempting FB-Deep MODOT [q_c]).

At the MATS, the predicted ultimate axial capacity values for drilled shaft foundations was attributed to the presence of poorly graded sand between depths, below ground surface, of 27- and 42-feet and below 60-feet. From the geotechnical investigation, the values of the AHTD corrected blow count averaged 36.0 percent larger than those correct blow count values calculated from MODOT CPT data. Below a depth of 60-feet, the values of the UofA corrected blow count averaged 12 percent larger than those measured from the AHTD data. As was observed at the TATS, AHTD values of total unit weight (obtained through corrected blow count correlations) were determined to be under-conservative in clays and over-conservative in sands by approximately 15 and 8 percent, respectively, as compared to UofA measured bulk sample values. Values of undrained shear strength obtained from the MODOT method were observed to be the highest within the topmost clay stratum, with mean values of undrained shear strength peaking at 8.7 ksf (nearly 61 percent larger than the average values obtained from the UofA UU triaxial testing).

Values of ultimate axial capacity at the MATS were influenced by ranges in the input data, at given depths, for four- and six-foot diameter shafts. For FB-Deep MODOT method, utilization of c_u values calculated from CPT f_s and q_c values, rather than directly inputting values of q_c, had little effect on the capacity. Changes in values of ultimate axial capacity for the SHAFT [ϕ'] method were consistent, with smaller changes in AHTD inputs (9 percent) having larger effects on capacity (22 percent) than changes in UofA inputs (15 percent). This phenomenon was not expected, as the UofA and AHTD correlated friction angle inputs had similar ranges. For the four-and six-foot diameter shaft utilizing the SHAFT program , it was observed that between depths of 6- and 18-feet and 35- and 59-feet below ground surface, the

predicted capacity values for all methods coincided. This coincidence is attributed to the presence of water at these depths.

The effects of the predictive software programs (SHAFT, FB-Deep, and a spreadsheet) that were utilized to predict ultimate axial capacities at the MATS were compared. The outputs for the UofA method were observed to display similar patterns to those exhibited at the TATS. utilizing the same (measured) input data into each technology, the FB-Deep program using the AHTD data generated capacity values were observed to have the largest range within the results, followed by the spreadsheet. Larger ranges of results were generated by each software program using the AHTD data, as well as an increased difference between mean predictions. The MODOT method exhibited the largest deviation between mean values, as obtained from the different programs; particularly for those capacities predicted utilizing the spreadsheet.

The effects of the sampling and testing methods (UofA, AHTD, and FB-Deep) utilized to predict ultimate axial capacities at the MATS were compared. The MODOT generated capacities (exempting the 6-foot diameter spreadsheet anomaly at 51-ft) from all three software programs were observed to be the highest. This is attributed to the advantages of continuous in-situ testing (as exemplified with MODOT CTP data) at sites featuring high soil variability. The capacity predictions for all drilling and sampling methods were observed to stabilize below depths of 60-feet below ground surface (the location of the final sand stratum).

Results of the cost-benefit analyses performed for the constructed drilled shafts at the SSATS indicated the UofA sampling and testing method to be 47 percent less expensive than the AHTD sampling and testing method. Results not only confirmed the fiscal benefits of performing advanced sampling and testing techniques, but also advanced full-scale load testing (even at small values of settlement). Unit costs per ton of resistance for the UofA and AHTD

sampling and testing methods were calculated to be $24.11 and $82.70, respectively. Results of the infrastructure cost analyses indicated the UofA sampling and testing method had the potential to save (conservatively) an average of 220 percent. A savings of $2.66 per cubic yard of concrete was observed utilizing a 30 percent fly ash replacement, rather than the current standard (AHTD Class S) of 20 percent fly ash replacement. Potential total savings associated with the concrete utilized for the originally planned construction at the SSATS utilizing the UofA design methodology amounted to $4176, and increased with the scale of infrastructure (to a potential savings of $28,476).

Results of the cost-benefit analyses performed for the constructed drilled shafts at the TATS indicated the UofA sampling and testing method to be 8.8 percent more expensive than the pilings associated with AHTD sampling and testing method. This was attributed to the unexpected labor costs associated with the extended construction of the TATS test shafts. Although more expensive, drilled shafts at the TATS offer more lateral support in the event of a seismic event. Unit costs per ton of resistance for the UofA and AHTD sampling and testing methods were calculated to be $75.47 and $141.57, respectively. Results of the infrastructure cost analyses indicated the UofA sampling and testing method had the potential to save an average of 83 percent.

Chapter 8: Measured Results

8.1. Introduction

Comparisons between the predicted and measured resistance values for the drilled shaft foundations at the Siloam Springs and Turrell Arkansas Test Sites are presented in Sections 8.2 and 8.3, respectively. Due to time limitations, the comparisons between predicted and measured values of resistance for the foundations at the Monticello Arkansas Test Site (MATS) are not discussed because the full-scale load tests at the MATS have not yet been completed. For completeness, additional information is presented in Appendix C. This additional information, from Loadtest Inc., includes the formal reports for each of the O-Cell load tests.

8.2. Siloam Springs Arkansas Test Site

Comparisons between the predicted and measured resistances at the Siloam Springs Arkansas Test Site (SSATS) are presented in this section. Interpretations of the obtained results from the O-cell tests, as performed on the western most four-foot diameter drilled shaft foundations (SS-W4), the centrally oriented six-foot diameter drilled shaft foundation (SS-C6), and eastern oriented four-foot diameter drilled shaft foundation (SS-E4) are discussed in Section 8.2.1. Results of the concrete testing that was performed for each drilled shaft are also presented and discussed (Section 8.2.2). The comparisons between the predicted and measured axial capacities, the side friction resistance in rock, and the end bearing resistance are presented in Sections 8.2.3 through 8.2.5, respectively.

8.2.1. Interpretations of O-Cell Tests at SSATS

An interpretation of the results obtained from the O-cell testing performed at the SSATS is presented in this section. Specifically, results from the tests performed on SS-W4 (Section 8.2.1.1), SS-E4 (Section 8.2.1.2), and SS-C6 (Section 8.2.1.3) drilled shaft foundations are

presented and discussed. As previously mentioned, additional information that may have influenced the results of the O-cell testing (including the site conditions and construction practices) was presented in Chapters 3 (Test Sites and Investigations) and 5 (Construction and Testing at the Siloam Springs Arkansas Test Site), respectively.

8.2.1.1. Test Shaft SS-W4

Test shaft SS-W4, the first shaft that was constructed and the first shaft tested at the SSATS, extended to a depth of 26 feet below the ground surface and was constructed with the longest rock socket length (10.2 feet). This shaft, the only shaft that met the current AHTD design requirement of a 10-foot rock socket, was observed to exhibit the least amount of side friction displacement (less than 0.03 inches). Test shaft SS-W4 was also the only shaft on site to displace more in end bearing than side shear (Figure 8.1a). This was attributed to concrete placement practices, which were subsequently modified to improve the quality of concrete placement for test shafts SS-C6 and SS-E4. Based on the developed equivalent top-down load-displacement curve, the elastic limit of the limestone was not exceeded during the loading of SS-W4, as the curve was observed to return along the loading line during unloading (Figure 8.1b). The required axial capacity of 1112.5 tons was attained at a top-down vertical displacement of 0.065 inches (equal to 0.135 percent of shaft diameter). The creep limit for test shaft SS-W4 was defined as a load in which the observed displacements between four and eight minute increments of loading become non-linear. No creep limit values for test shaft SS-W4 were observed to develop at the tested loads (Figure 8.1c). As presented in Figure 8.1d, significant load transfer for test shaft SS-W4 was observed below a depth of sixteen-feet below the ground surface (the location of the cherty-clay/limestone interface), as presented in Figure 8.1d. Compared to SS-E4, reduced amounts of load transfer were exhibited between depths of 16- and 20-feet below ground

surface for SS-W4. This was attributed to strain gauge placement, and the presence of weathered limestone within the top five-feet of the stratum. Test was halted after the pump stroke for the O-Cell was maximized. Testing was also halted after the required design capacity had been achieved to limit upward movement of the drilled shaft foundation to facilitate future lateral load testing.

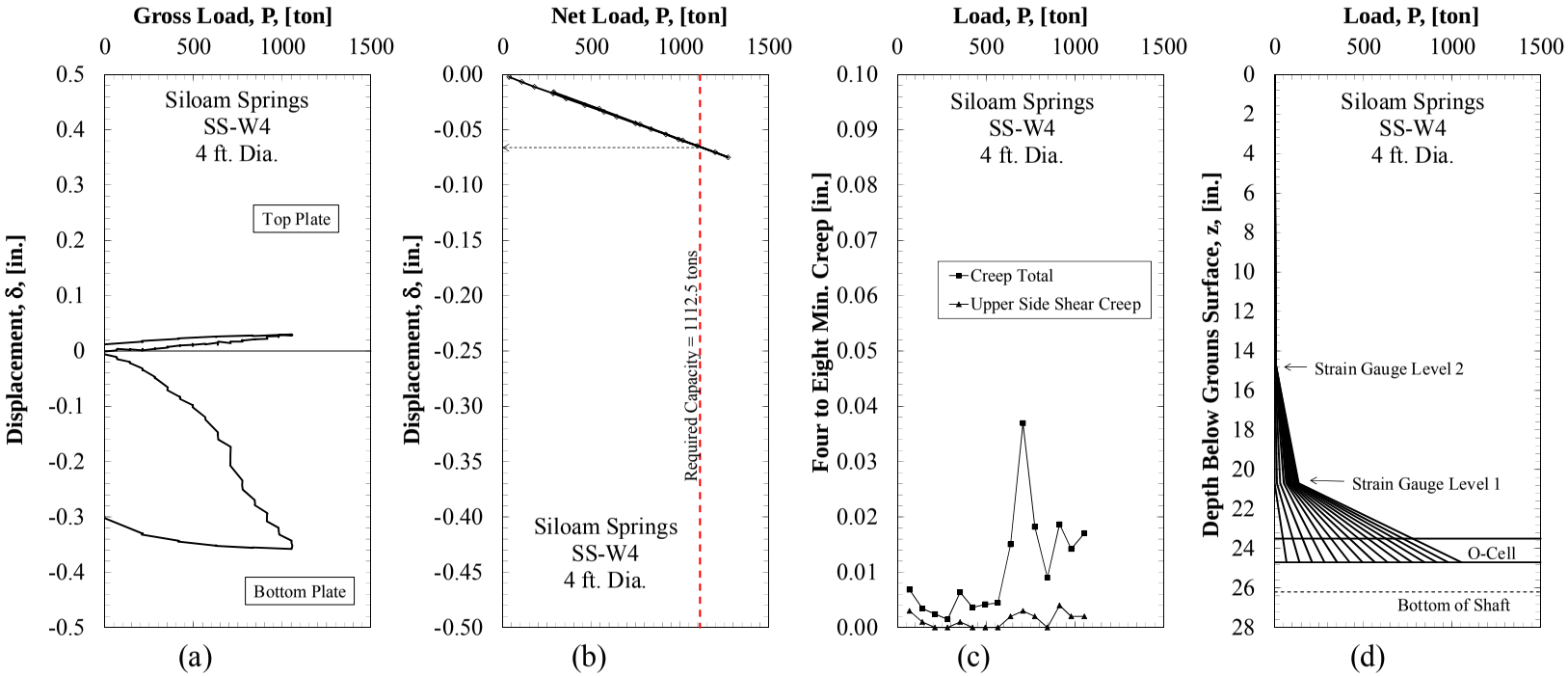

Figure 8.1. Test Shaft SS-W4 (a) O-cell load displacement curve, (b) equivalent top-down load displacement curve, (c) creep limit, and (d) load transfer characteristics.

8.2.1.2. Test Shaft SS-C6

Test shaft SS-C6 extended to a depth of 21.5 feet below ground surface, and was constructed with the shortest rock-socket length (5.4 feet). This shaft was observed to exhibit the greatest amount of displacement in the upward direction (0.47 inches) and negligibly displaced in the downward direction, resulting in the most rapid mobilization of axial capacity (Figure 8.2a). Based on the equivalent top-down load-displacement curve for test shaft SS-C6, the elastic limit of the limestone was not exceeded, as the curve was observed to return along the loading line during unloading (Figure 8.2b). The required design axial capacity of 1112.5 tons was not attained, with a maximum recorded top-down displacement of 0.012-inches at 500.12 tons (equal to 0.017 percent of the shaft diameter). Based upon the creep limit curve that appears to go non-linear, an upper side shear creep limit of 250 tons was determined for test shaft SS-C6 (Figure 8.2c). Significant load transfer for test shaft SS-C6 was observed below a depth of 16-feet (2.7-feet below the location of SG-1), as presented in Figure 8.2d. Testing was halted at a displacement of 0.01 inches due to maximization of the pump stroke for the O-Cell and to limit upward movement of the drilled shaft foundation to facilitate future lateral load testing.

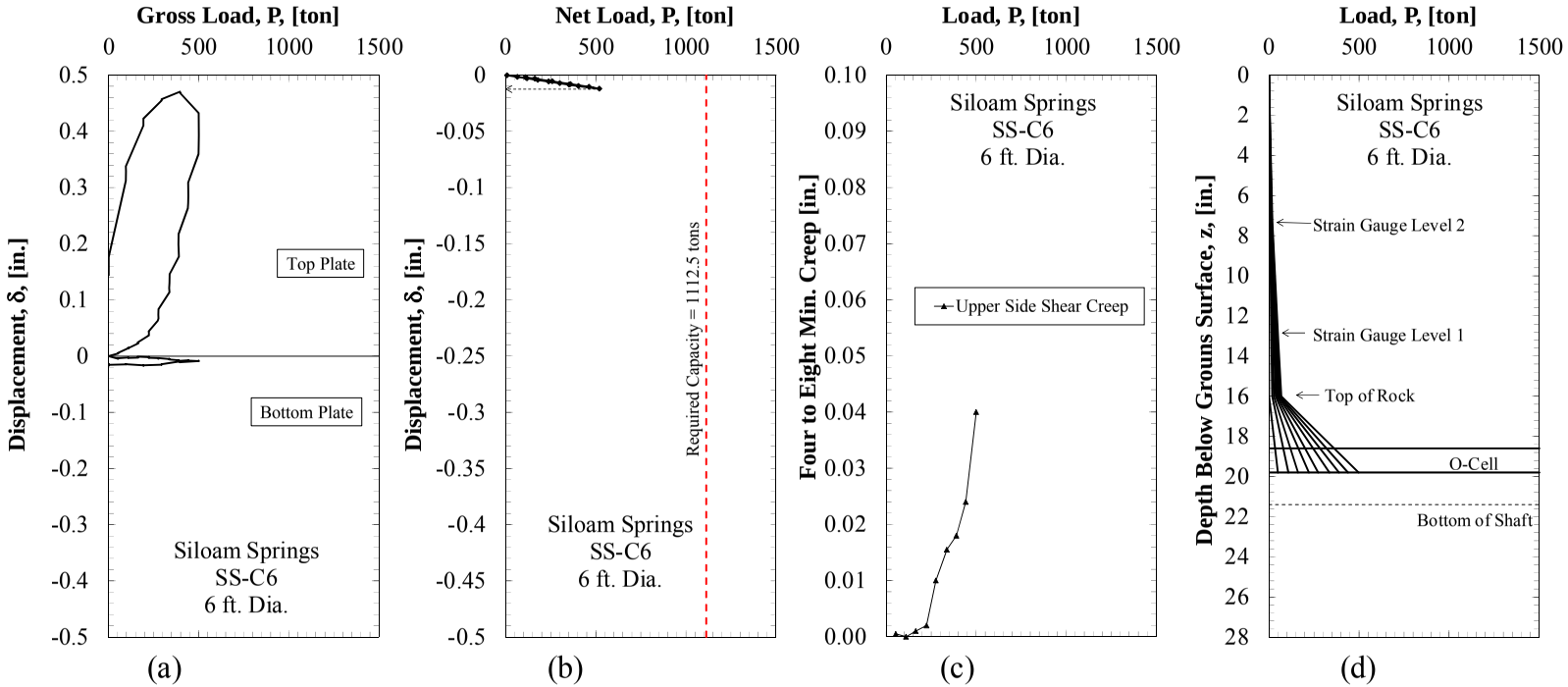

Figure 8.2. Test Shaft SS-C6 (a) O-cell load displacement curve, (b) equivalent top-down load displacement curve, (c) creep limit, and (d) load transfer characteristics.

8.2.1.3. Test Shaft SS-E4

Test shaft SS-E4 extended to a depth of 23.3 feet below the ground surface and was constructed with a rock-socket length of 7.3 feet. Test shaft SS-E4 was observed to displace more in the upward direction than the downward direction, with 0.307 inches of top plate displacement (Figure 8.3a). This displacement was noted to be 0.16-inches less that that measured for test shaft SS-C6, despite a 63.77 square foot (ft^2) decrease in rock socket surface area. Based on the equivalent top-down load-displacement curve for test shaft SS-E4, the elastic limit of the limestone was not exceeded, as the curve was observed to return along the loading line during unloading (Figure 8.3b). The required axial capacity of 1112.5 tons was not attained, with a maximum recorded top-down displacement of 0.07 inches at 897 tons recorded (equal to 0.15 percent of the shaft diameter). Based upon the creep limit curve that appears to go non-linear, an upper side shear creep limit of 615 tons was determined for test shaft SS-E4 (Figure 8.3c). Significant load transfer for test shaft SS-E4 was observed below 17 feet below ground surface, as presented in Figure 8.2d. Testing was halted at a displacement of 0.07 inches due to a lack of daylight remaining to properly perform testing, a maximization of the O-Cell pump stroke, and intent to limit the upward movement of the shaft to enable future lateral load testing.

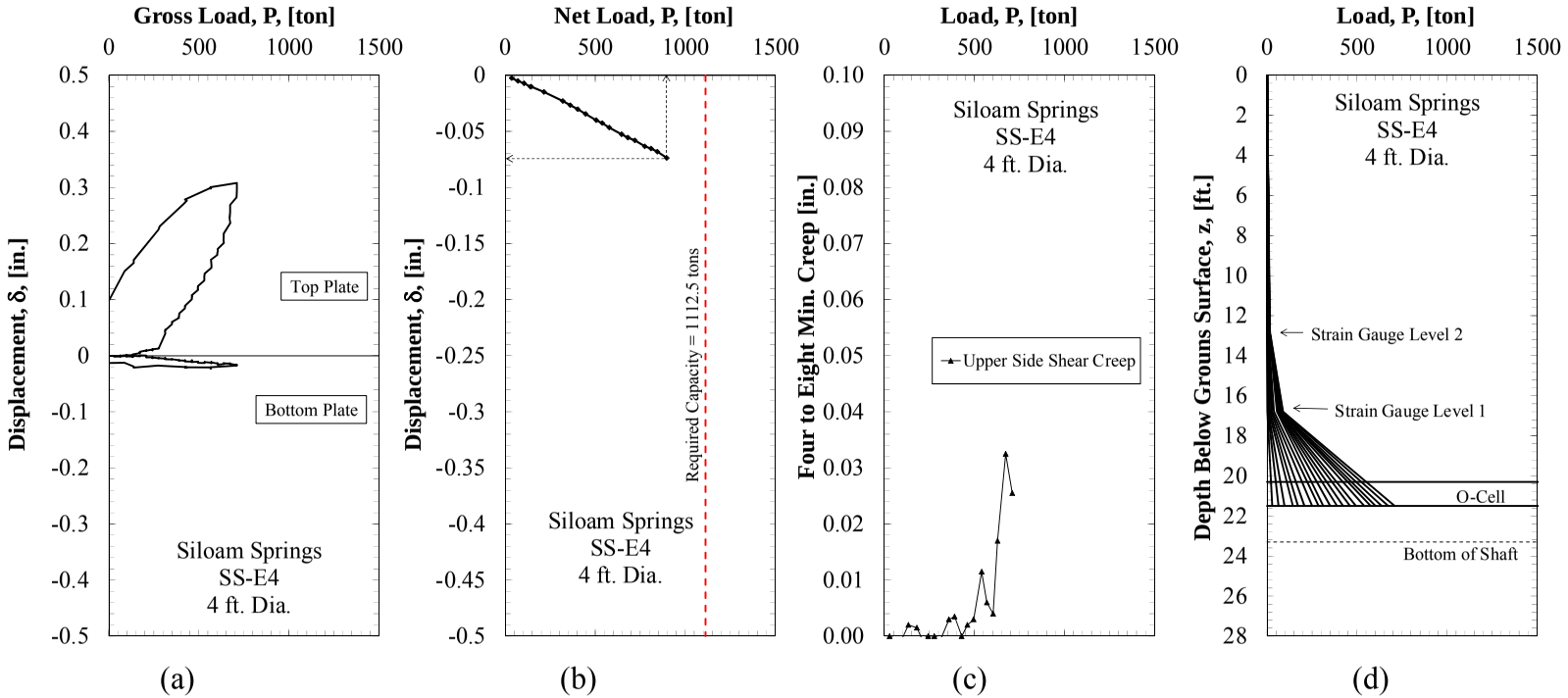

Figure 8.3. Test Shaft SS-E4 (a) O-cell load displacement curve, (b) equivalent top-down load displacement curve, (c) creep limit, and (d) load transfer characteristics.

8.2.2. Concrete Testing Results

A compressive strength of 4500 pounds per square inch (psi) was specified for the concrete that was utilized in drilled shaft foundations constructed at the SSATS. Unconfined uniaxial compressive strength and modulus of elasticity testing was performed on selected cylinders from the cylinders that were cast in the field on the date of construction (as discussed previously in Chapter 5). The results of these tests are presented in Table 8.1. Although 30 percent fly ash was used within the concrete, the concrete that was utilized for the drilled shaft foundations met the design specifications, with the compressive strength values for all shafts exceeding the required strength by over 1700 psi. The concrete within these shafts also exceeded the minimum design requirement for concrete compressive strength, as required by the state of Arkansas, by over 2700 psi. Concrete compressive strength for each drilled shaft foundation as a function of depth is presented in Figure 8.4. As aforementioned in Chapter 7, cost-benefits were achieved with the concrete utilized at the SSATS.

Table 8.1. Average unconfined uniaxial compressive strength and Young's modulus testing results.

Shaft	28 Day Unconfined Unaxial Compressive Strength	28 Day Modulus of Elasticity
	[psi]	[ksi]
SS-W4	6,900	5,637
SS-C6	6,932	5,560
SS-E4	6,228	4,700

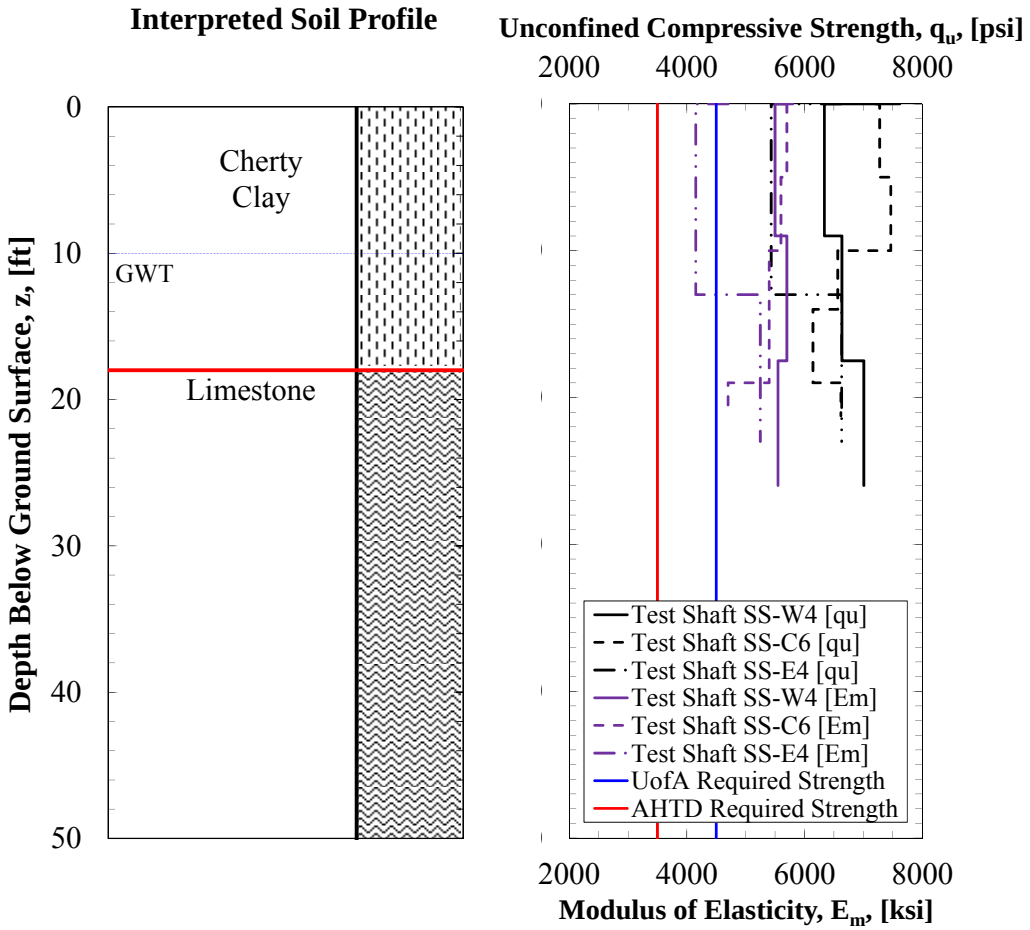

Figure 8.4. Average unconfined uniaxial compressive strength and modulus of elasticity as a function of depth for the drilled shaft foundations at the SSATS.

8.2.3. Predicted and Measured Axial Capacity

Axial capacity predictions for drilled shafts at the SSATS were determined at a five-percent displacement criterion. However upon testing, the top-down displacement values were not observed to exceed 0.15 percent. As a result, only eh results obtained from the software programs were utilized to compare the predicted and measured results (FB-Deep and SHAFT). To ensure adequate comparisons, these programs were utilized to generate predicted capacity values at the measured settlements. The spreadsheet was not utilized due to the nature of the analysis methods within the program. Specifically, the axial capacity at a user defined settlement value is not enabled using the AASTHO method that was within the spreadsheet. The predicted

mean values of axial capacity (at the actual measured values of displacement) were compared utilizing FB-Deep, and SHAFT. Comparisons between predicted and measured axial capacities for the UofA and AHTD testing and sampling methods are presented in Tables 8.2 through 8.4.

Table 8.2. Comparisons between the predicted capacity values utilizing FB-Deep and measured axial capacity values at the SSATS.

							Prediction Software Program			
							FB-Deep			
Required Axial Capacity [ton]	Dia. [ft]	SHAFT I.D.	As-Constructed Length [ft]	Measured axial Capacity [ton]	Measured Displacement [% Dia.]	Sampling/Testing Method	Predicted Axial Capacity at Measured Displacement [ton]	Percent Difference [%]	Predicted Ultimate Axial Capacity at 5% Displacement	Percent Difference [%]
1112.5	4	SS-W4	26.2	1271	0.156	UofA Mean	6294	-395.20	10226	-704.56
				1271	0.156	AHTD Mean	1882	-48.07	10866	-754.92
	6	SS-C6	21.4	520	0.017	UofA Mean	3315	-537.50	20395	-3822.12
				520	0.017	AHTD Mean	344	33.85	5491	-955.96
	4	SS-E4	23.3	710	0.181	UofA Mean	5631	-693.10	9635	-1257.04
				710	0.181	AHTD Mean	1382	-94.65	8595	-1110.56

Table 8.3. Comparisons between predicted capacity values utilizing SHAFT and the measured axial capacity values at the SSATS.

						Prediction Software Program			
						SHAFT			
Dia. [ft]	SHAFT I.D.	As-Constructed	Measured axial Capacity	Measured Displacement [% Dia.]	Sampling/Testing Method	Predicted Axial Capacity at Measured Displacement [ton]	Percent Difference [%]	Predicted Ultimate Axial Capacity [ton]	Percent Difference [%]
4	SS-W4	26.2	1271	0.156	UofA Mean	884	30.45	21011	-1553.11
			1271	0.156	AHTD Mean	273	78.52	12135	-854.76
6	SS-C6	21.4	520	0.017	UofA Mean	N/A	N/A	41635	-7906.73
			520	0.017	AHTD Mean	N/A	N/A	26062	-4911.92
4	SS-E4	23.3	710	0.181	UofA Mean	1122	-58.03	21451	-2921.27
			710	0.181	AHTD Mean	186	73.80	15646	-2103.66

Table 8.4. Comparisons between predicted capacity values utilizing the spreadsheet and the measured axial capacity values at the SSATS.

						Prediction Software Program	
						Spreadsheet	
Dia. [ft]	SHAFT I.D.	As-Constructed	Measured axial Capacity	Measured Displacement [% Dia.]	Sampling/Testing Method	Predicted Ultiamte Axial Capacity at 5% Displacement [ton]	Percent Difference [%]
4	SS-W4	26.2	1271	0.156	UofA Mean	7126	-460.66
			1271	0.156	AHTD Mean	2272	-78.76
6	SS-C6	21.4	520	0.017	UofA Mean	11594	-2129.62
			520	0.017	AHTD Mean	1401	-169.42
4	SS-E4	23.3	710	0.181	UofA Mean	6211	-774.79
			710	0.181	AHTD Mean	1936	-172.68

The predicted capacities values at a displacement of five percent of the shaft diameter were observed to be significantly greater than those generated for the measured settlement. This difference was expected, as the shafts tested in the field were not loaded to failure (5% D) to enable the shafts to be used again for future lateral load testing. Also, the O-Cells were not large enough to develop the required load, and values of side shear were not great enough to develop the required load. All of the shafts were expected to exceed the required axial capacity, although only test shaft SS-W4 was observed to do so because of the field changes. At least 46 percent of the required capacity was generated in vertical movements that were less than 0.181 percent of the respective shaft diameter.

The predicted capacities, as obtained from the FB-Deep software program at the measured value of maximum displacement, were observed to be 289 percent greater than the measured capacity (Table 8.2). This large difference is attributed to the load-transfer database, for Floridian limestone, that was used to develop the FB-Deep software program. Capacities predicted utilizing SHAFT at measured values of maximum displacemet were generally observed to be closer to measured capacities, and less than axial capacity values that were predicted using the FB-Deep program (Tables 8.2 and 8.3). The predicted capacity values, as obtained by using the SHAFT software program at the measured values of maximum displacements, were observed to be 32 percent less than the measured capacities (Table 8.3). Predictions obtained using the mean values of the UofA sampling and testing data were closer to the measured values than the predicted capacity values obtained using the mean values of the AHTD sampling and testing data (Tables 8.2 through 8.4).

Comparisons between the measured capacity values and predicted capacity values, at the measured displacements are presented in Figures 8.5 and 8.6. As previously discussed in Chapter

7, utilizing the SHAFT and FB-Deep predictive programs, the magnitude of he predicted values using the UofA testing and sampling method were greater than those for the predicted values using the AHTD sampling and testing method (Figure 8.5). However, unlike the predictions from Chapter 7, the values of predicted capacity at the measured displacements as obtained using FB-Deep were observed to be greater than those obtained using SHAFT. While values of q_u and RQD were ingested into FB-Deep, only values of q_u were observed to impact the output results. Conversely, ingested values of q_u and RQD were both observed to impact predicted axial capacity values from SHAFT. Other input values ingested into SHAFT, which may have impacted the predicted capacity values were either kept constant, or shown to have little impact on the predicted capacity (as previously discussed based on the results of the sensitivity analysis that were reported in Chapter 7). Therefore, the differences between predicted and measured observations were attributed to proprietary methods and the differences in measured displacements (less than 0.2 percent of the shaft diameter to 5 percent of the shaft diameter).

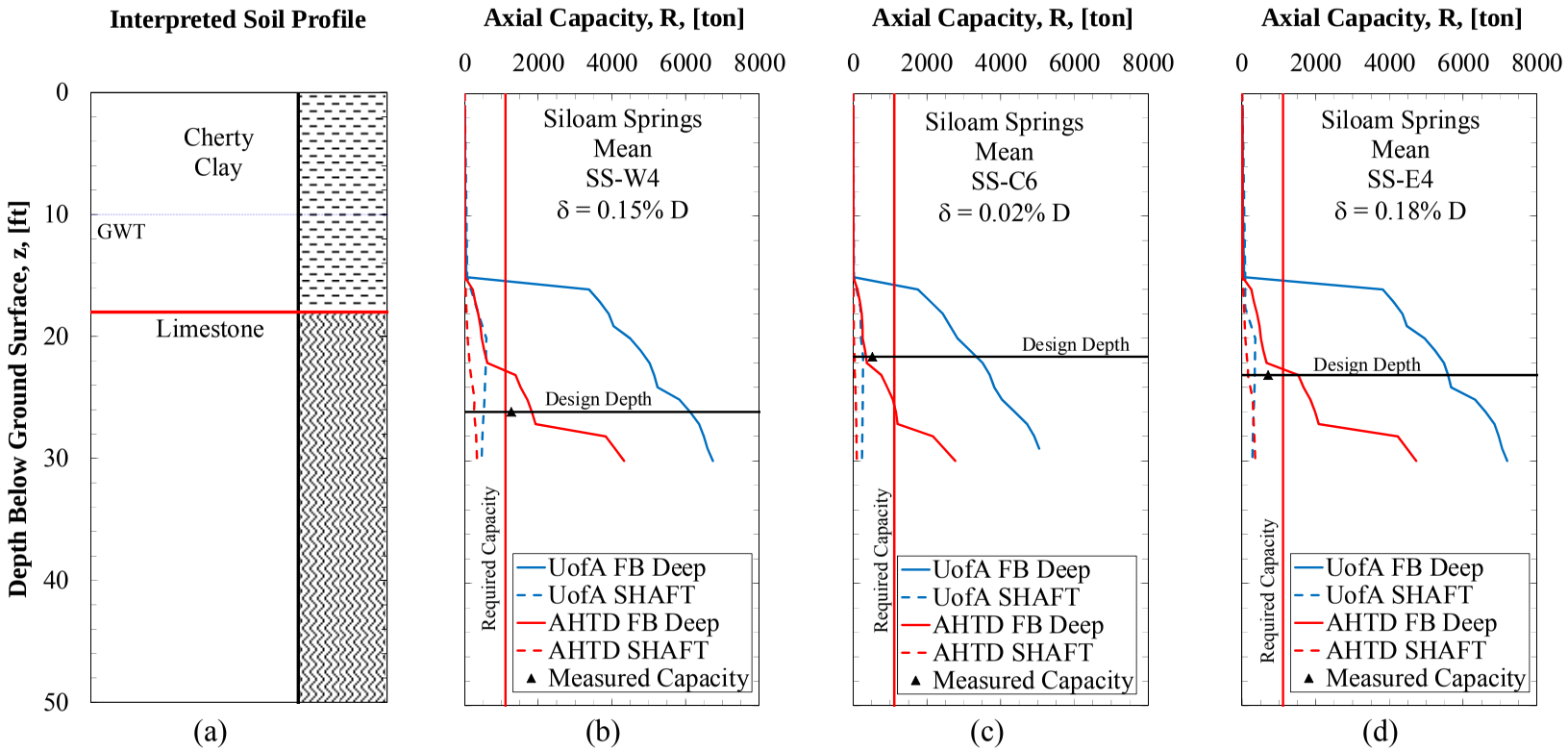

Figure 8.5. Predicted and measured axial capacities as a function of depth for the (a) interpreted soil profile at the SSATS for (b) test shaft SS-W4, (c) test shaft SS-C6, and (d) test shaft SS-E4.

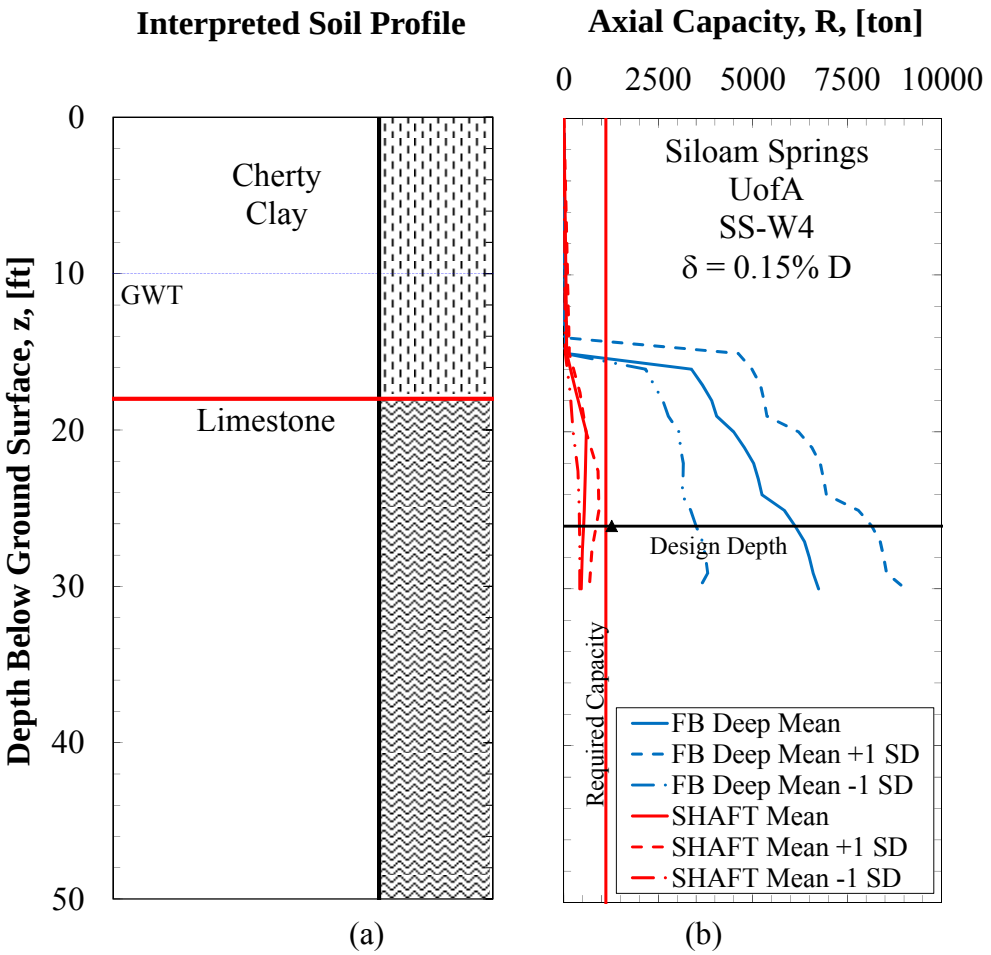

Figure 8.6. Predicted ranges of axial capacities and measured axial capacity for (a) the interpreted soil profile using UofA sampling and testing data for (b) test shaft SS-W4.

The measured capacity value (1271 tons) for test shaft SS-W4 was observed to be less than the predicted capacity values obtained from FB-Deep (by approximately 381 and 43.9 percent for the UofA and AHTD sampling and testing methods, respectively), as presented in Figure 8.5b. However, this measured value was observed to be greater than the predicted capacity values obtained from SHAFT (by approximately 58.6 and 87.25 percent for the UofA and AHTD sampling and testing methods, respectively). The measured capacity value (520 tons) for test shaft SS-C6 was observed to be less than the predicted axial capacity values obtained from FB-Deep (by approximately 542 and 33.9 percent for the UofA and AHTD

sampling and testing methods, respectively), as presented in Figure 8.5c. However, this measured value was also observed to be greater than the predicted axial capacity values obtained from SHAFT (by approximately 48.8 and 93.4 percent for the UofA and AHTD sampling and testing methods, respectively). The measured capacity value (897 tons) for test shaft SS-E4 was observed to be less than the predicted capacity values obtained from FB-Deep (by approximately 523 and 70.3 percent for the UofA and AHTD sampling and testing methods, respectively), as presented in Figure 8.5d. However, this measured value was also observed to be greater than the predicted capacity values obtained from SHAFT (by approximately 61.4 and 80.6 percent for the UofA and AHTD sampling and testing methods, respectively).

A comparison between the ranges values of measured capacities and predicted capacities at measured settlements for the UofA sampling and testing method is presented in Figure 8.6. Ranges of predicted axial capacity values for the UofA data were observed to be significantly greater when using the FB-Deep program than when using the SHAFT program. Furthermore, the SHAFT obtained values of predicted capacity for UofA data were observed to be closer to the value of measured axial capacity, with values produced from FB-Deep software overestimating the axial capacity by 831 percent. This result opposes the results of the predictions made in Chapter 7, where values of predicted axial capacity for SHAFT data were observed to be significantly greater than those using FB-Deep. This is believed to be attributed to the influence of the amount of displacement (δ = 0.15% D instead of δ = 5% D), and lack of end bearing resistance utilization.

A comparison between the ranges values of measured capacities and predicted capacities at the constructed depth and at measured displacements for each test shaft, using each of sampling and testing methods, is presented in Table 8.5. As with the UofA testing method,

ranges of predicted axial capacity values obtained using the AHTD data were observed to be significantly greater when using the FB-Deep program than the SHAFT program. Unlike the UofA testing method, the FB-Deep values of predicted capacity for AHTD data were observed to be closer to the value of measured axial capacity, with values produced using SHAFT software underestimating the measured axial capacity by an average of 87 percent. This result also opposes the results of the predictions made in Chapter 7, where values of predicted axial capacity for SHAFT data were observed to be significantly greater than those using FB-Deep. This again is believed to be attributed to the influence of the amount of displacement (δ = 0.15% D instead of δ = 5% D). Overall, the AHTD method utilizing FB-Deep was observed to produce values of axial capacity closest to the measured values. Although the method over predicted values of axial capacity for the four-foot diameter shafts, these predictions were still the closest by comparison. Overall, AHTD data using the FB-Deep predictive program was observed to best predict values of axial capacity at the SSATS. Although the method over predicted values of axial capacity for the four-foot diameter shafts, these predictions were still the closest by comparison (Table 8.5). Predicted values, as obtained by averaging the AHTD/FB-Deep data and the UofA/SHAFT data, were within 41.3 percent of the measured capacity and typically under predicted the capacity (with the exception of SS-E4, which was 4.4 percent greater than the measured capacity).

Table 8.5. Comparisons between mean predicted and measured axial capacities and subsequent data ranges at the given constructed depth of each test shaft.

		Test Shaft SS-W4		Test Shaft SS-C6		Test Shaft SS-E4	
		Depth = 26 ft, δ = 0.15% D		Depth = 21.5 ft, δ = 0.017% D		Depth = 23 ft, δ = 0.18% D	
		Mean [μ]	Range [Δ R]	Mean [μ]	Range [Δ R]	Mean [μ]	Range [Δ R]
FB-Deep	UofA	6122.1	4649.0	3342.8	4015.3	5590.7	4032.3
	AHTD	1829.0	3919.0	343.6	1170.4	1528.0	3843.1
SHAFT	UofA	525.7	441.2	266.3	148.1	345.5	202.5
	AHTD	256.0	605.9	34.2	138.5	157.4	212.9
Actual	UofA / AHTD	1271.0	-	520.0	-	897.0	-
	Average	1177.3		305.0		936.8	

8.2.4. Predicted and Measured Side Friction Resistances in Rock

Measured unit side friction resistances for test shafts SS-W4, SS-E4, and SS-C6 are presented in Figure 8.7. As previously discussed, the rock socket depths for test shafts SS-W4, SS-E4, and SS-C6 were 10, 7.3, and 5.5 feet, respectively. Accordingly, the unit side friction resistances, at the base of the shafts, were observed to increase with rock socket length. Test shaft SS-W4, was observed to exhibit over 14 tons per square foot (tsf) of unit side shear resistance at an average upward movement of less than 0.03 inches. Values of unit side friction resistance for test shaft SS-E4, which were generated at ten times the amount of upward average movement than SS-W4, were observed to reach a maximum value of 10.5 tsf. Because all of the strain gauges within test shaft SS-C6 were placed at depths above rock, and because the rock socket was the shortest, the values of unit side friction resistance for this shaft were observed to be the smallest, with an observed maximum unit side shear resistance of 6.0 tsf.

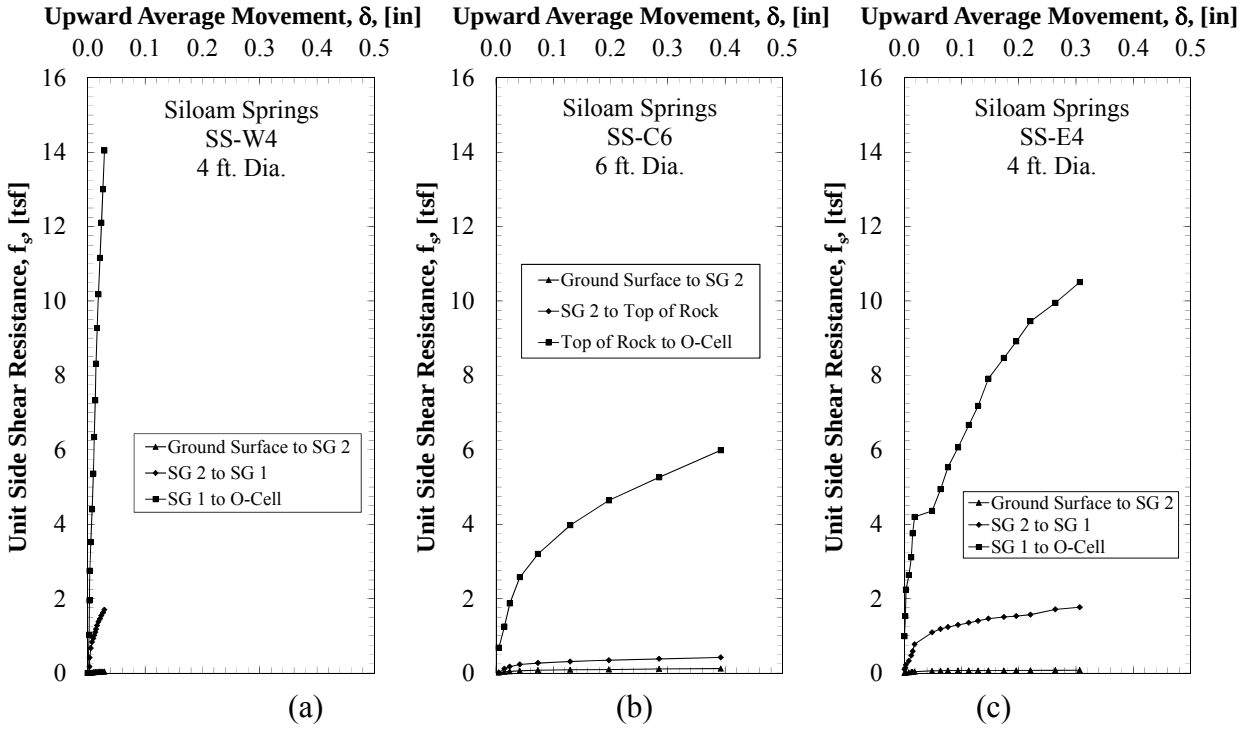

Figure 8.7. Measured unit side friction resistances as a function of displacement for test shafts (a) SS-W4, (b) SS-C6, and (c) SS-E4.

The amount of side friction resistance was predicted for drilled shaft foundations at the SSATS for the largest common vertical displacement (0.012 inches) using the FB-Deep program. Results of the comparisons between the predicted and measured side friction resistance values for the four-foot and six-foot diameter shafts, using data from the UofA and AHTD testing and sampling methods, are presented in Figure 8.8. All comparisons were made utilizing the FB-Deep program, because it was the only program that enabled the determination of the side friction resistance at user defined settlement. Compared to the values obtained from the side friction predictions at the measured displacement and the design length, the side friction values for the SS-W4 and SS-E4 drilled shaft foundations were observed to be an average of -117 and 67 percent different than the measured values, when using the data from the UofA and AHTD sampling and testing methods, respectively (Figure 8.8b). The measured side friction value for

SS-C6 was observed to be an average of 744 and 19 percent less than the predicted values that were obtained using the UofA and AHTD sampling and testing methods, respectively (Figure 8.8c). Overall, the measured values of side friction resistance for the six-foot diameter drilled shaft foundation were observed to compare most closely with predicted values generated utilizing the AHTD sampling and testing method. Measured values of side friction resistance for the four-foot diameter drilled shaft foundations were observed to compare almost equally with predicted values generated utilizing the AHTD and UofA sampling and testing methods.

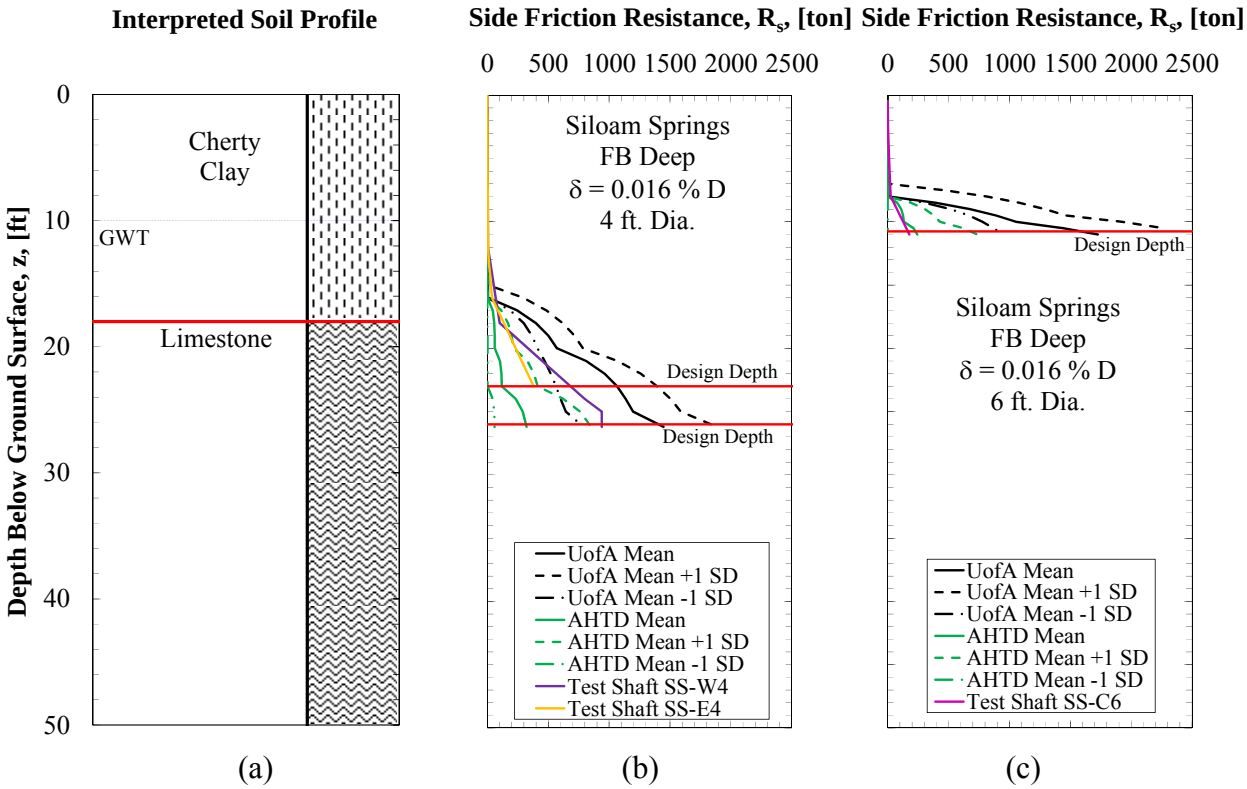

Figure 8.8. Measured and predicted side friction resistances for (a) a given interpreted soil profile for (b) four-foot diameter and (c) six-foot diameter shafts utilizing FB-Deep (at 0.016% settlement).

8.2.5. Predicted and Measured End Bearing Resistance in Rock

Measured unit end bearing resistances for the SS-W4, SS-C6, and SS-E4 drilled shaft foundations are presented in Figure 8.9. The SS-W4 drilled shaft foundation was the only shaft

to mobilize significant displacement at the end of the shaft. Although more displacement was observed for the SS-W4 shaft, the unit end bearing resistances that were developed at the base of each of the shafts were observed to increase with rock socket depth. Test shaft SS-W4 was observed to exhibit over 69 tsf in unit end bearing resistance at an average downward movement of less than 0.35 inches. The value of unit end bearing resistance for test shaft SS-C6 was observed to be the smallest, with an observed maximum unit end bearing resistance of 17.6 tsf. The value of unit end bearing resistance for test shaft SS-E4, which was generated at a movement of 0.025 inches, (14 times less downward average movement than SS-W4) was observed to reach a maximum value of 48 tsf.

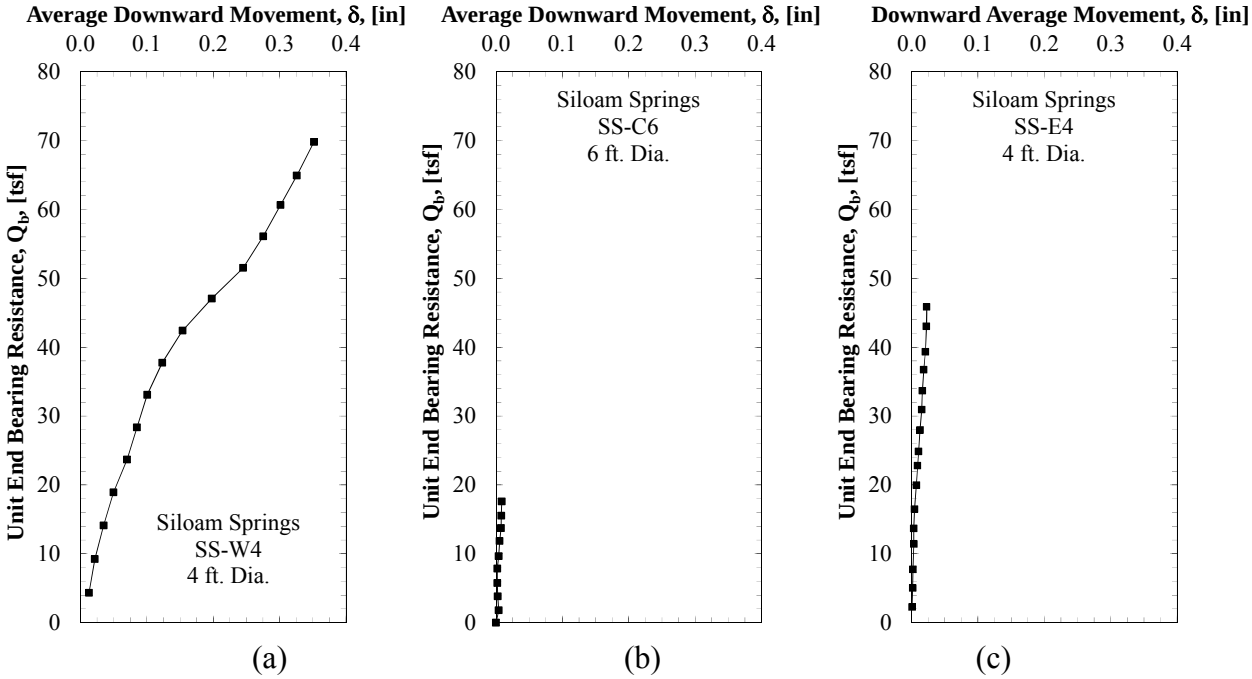

Figure 8.9. Measured unit end bearing resistance, as a function of displacement, for test shafts (a) SS-W4, (b) SS-C6, and (c) SS-E4.

Predicted values of end bearing resistance were determined at the largest common value of measured vertical displacement (0.009 inches) for the drilled shaft foundations at the SSATS. Comparisons between predicted and measured values of end bearing resistance, using the data obtained from the UofA and AHTD testing and sampling methods for the four-foot and six-foot

diameter drilled shaft foundations, are presented in Figure 8.10. The measured values of end bearing resistance the SS-W4 and SS-E4 drilled shaft foundations were observed to be an average of -31 and 61 percent different than the predicted values that were obtained using the UofA and AHTD sampling and testing methods, respectively (Figure 8.10b). The measured values of end bearing resistance for test shaft SS-C6 were observed to be an average of -720 and 47 percent different than the predicted values that were obtained using the UofA and AHTD sampling and testing methods, respectively (Figure 8.10c). Overall, measured values of end bearing resistance were observed to most closely compare with the predicted values generated utilizing the AHTD sampling and testing method.

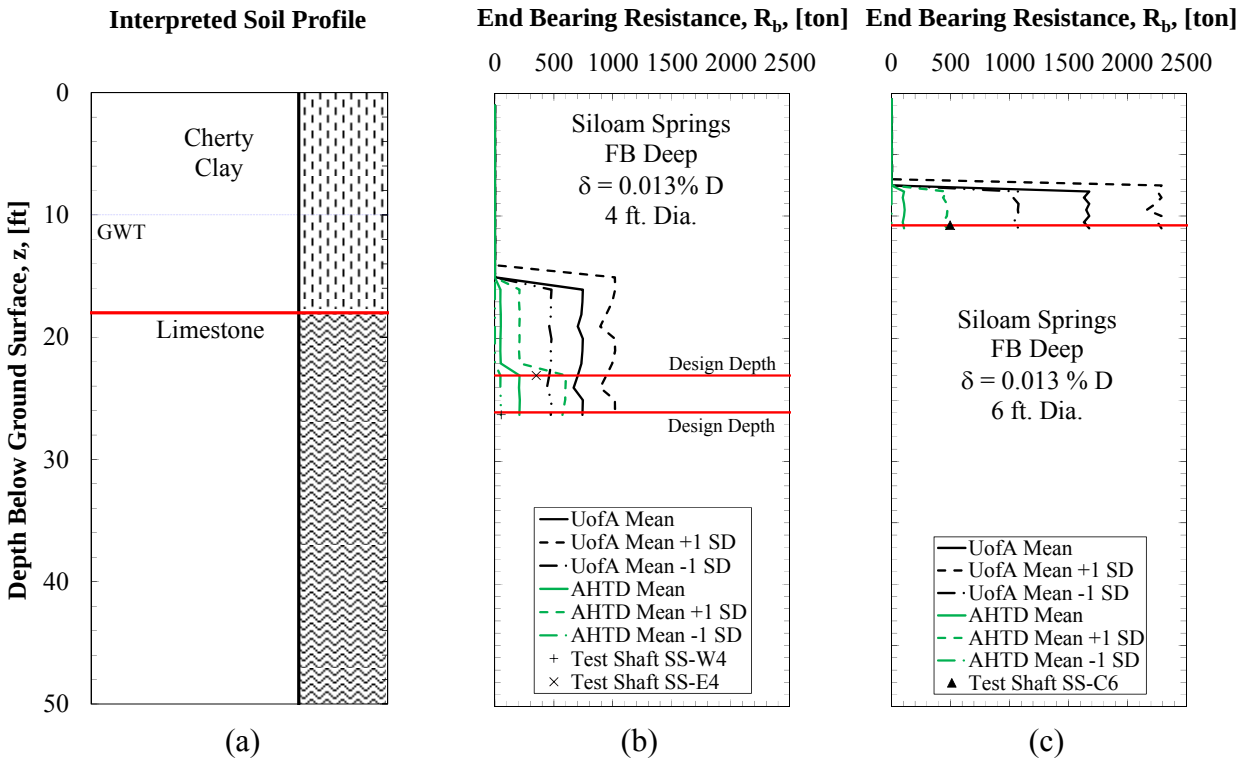

Figure 8.10. Measured and predicted end bearing resistances given the (a) interpreted soil profile for (b) four-foot and (c) diameter shafts utilizing FB-Deep (at 0.013% settlement).

8.3. Turrell Arkansas Test Site

Comparisons between the predicted and measured resistances at the Turrell Arkansas Test Site (TATS) are presented in this section. Interpretations of the obtained results from the O-cell testing performed on the southernmost four-foot diameter drilled shaft foundation (T-S4), the central six-foot diameter drilled shaft foundation (T-C6), and the northern most four-foot diameter drilled shaft foundation (T-N4) are discussed in Section 8.3.1. Results of the concrete testing that was performed for each drilled shaft are also presented and discussed (Section 8.3.2). The comparisons between the predicted and measured axial capacities, the side friction resistance, and the end bearing resistance are presented in Sections 8.3.3 through 8.3.5, respectively.

8.3.1. Basic Interpretation of O-Cell Tests at the TATS

An interpretation of the results obtained from the O-cell testing performed at the TATS is presented in this section. Specifically, the results from the tests performed on the T-S4 (Section 8.3.1.1), T-N4 (Section 8.3.1.2), and T-C6 (Section 8.3.1.3) drilled shaft foundations are presented and discussed. As previously mentioned, additional information that may have influenced the results of the O-cell testing (including the site conditions and construction practices) was presented in Chapters 3 (Test Sites and Investigations) and 6 (Construction and Testing at the Turrell Arkansas Test Site), respectively.

8.3.1.1. Test Shaft T-S4

Test shaft T-S4, the first shaft at that was constructed and the first shaft that was tested at the TATS extended a depth of 86.5-feet below the ground surface. Construction errors associated with the excavation of this shaft included hole size irregularity from a lost excavation bucket and the excavation being open an extended period of time. Despite these errors, the least amount of upward displacement (less than 0.47 inches) was observed for the T-S4 drilled shaft foundation (Figure 8.11a). Based on the developed equivalent top-down load-displacement curve, the elastic limit of the soil was exceeded during loading of the T-S4 drilled shaft foundation, as the curve was observed to exhibit a displaced regression during the unloading stages of the testing program (Figure 8.11b). The required design axial capacity of 987 tons was not attained due to limitations with the pump at 13,000 psi, however a top-down vertical displacement of 0.62 in (equal to 1.29 percent of the shaft diameter) was observed at an axial load of 818 tons. The creep limit for test shaft T-S4 was defined as a load in which the observed displacements between four and eight minute increments of loading become non-linear. Creep limits for test shaft T-S4 were observed to develop at loads equal to 400 tons and 500 tons for

total creep and side shear creep, respectively (Figure 8.11c). The load transfer for T-S4 was observed to increase with depth to the location of the O-Cell (62.3-feet below ground surface), as presented in Figure 8.11d.

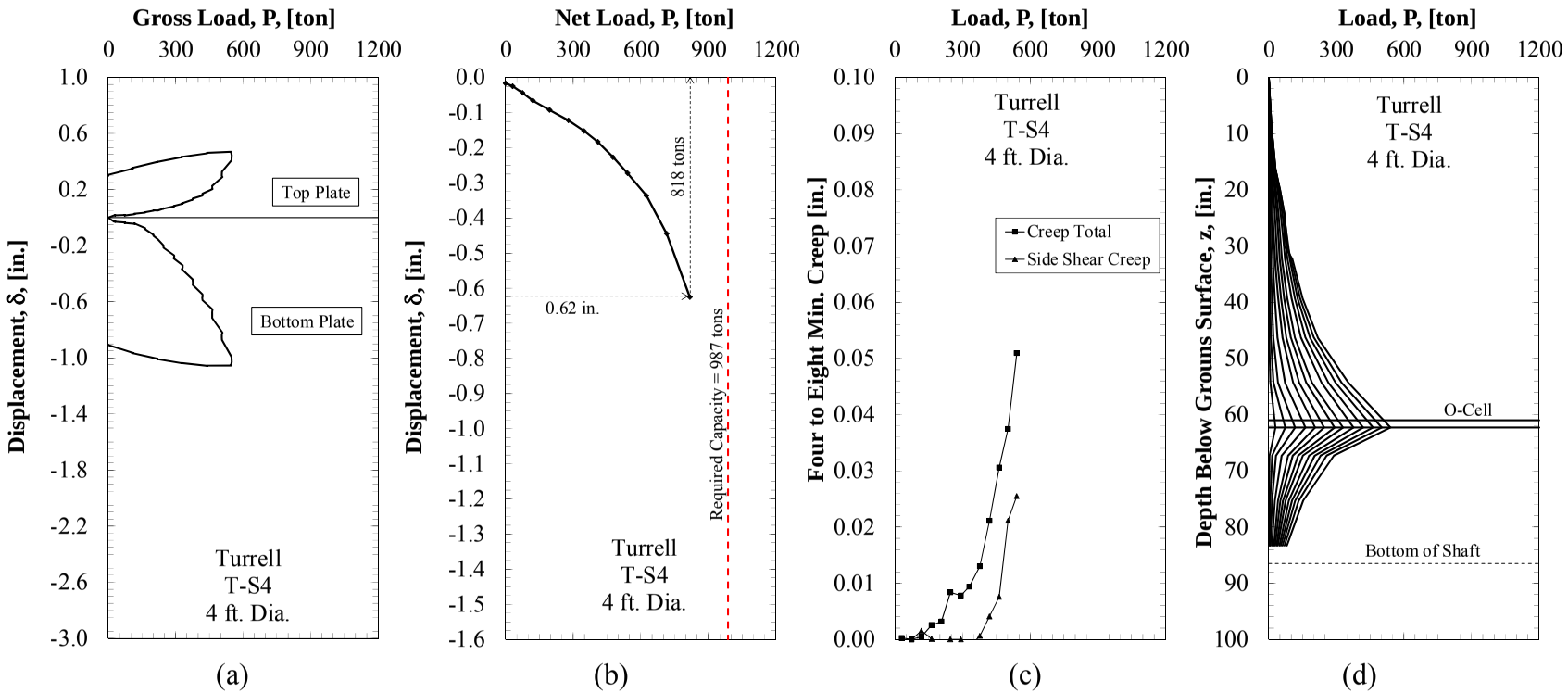

Figure 8.11. Test Shaft T-S4 (a) O-cell load displacement curve, (b) equivalent top-down load displacement curve, (c) creep limit, and (d) load transfer characteristics.

8.3.1.2. Test Shaft T-C6

Test shaft T-C6 extended to a depth of 65.5-feet below the ground surface. No known construction errors were associated with the excavation of this shaft. A maximum nominal load within the O-Cell of 638 tons (with a side friction displacement of 0.64 inches), was observed (Figure 8.12a). Based on the developed equivalent top-down load-displacement curve, the elastic limit of the soil was exceeded during loading of the T-C6 drilled shaft foundation, as the curve was observed to exhibit a displaced regression during the unloading stages of testing (Figure 8.12b). The required design axial capacity of 987 tons was attained at a top-down vertical displacement of 0.65-inches (equal to 0.902 percent of the shaft diameter). Creep limits for test shaft T-C6 were observed to develop at loads equal to 500 tons for both total and side shear creep (Figure 8.12c). The load transfer for T-C6 was observed to increase with depth to the location of the O-Cell (55 feet below ground surface), as presented in Figure 8.12d.

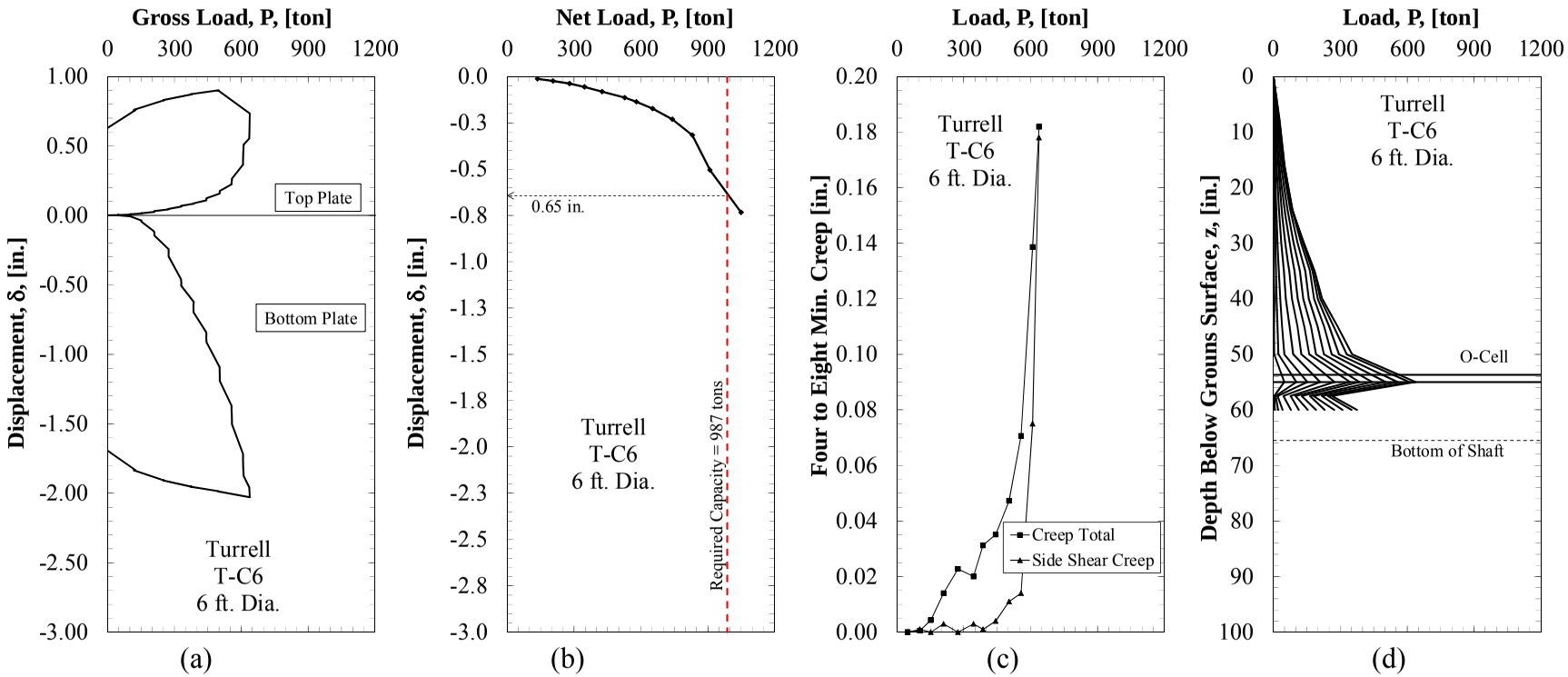

Figure 8.12. Test Shaft T-C6 (a) O-cell load displacement curve, (b) equivalent top-down load displacement curve, (c) creep limit, and (d) load transfer characteristics.

8.3.1.3. Test Shaft T-N4

Test shaft T-N4 extended to a depth of 88-feet below ground surface. Construction errors associated with the excavation of this shaft included a blowout within the silt stratum. As a result of the incident, the side walls of the excavation were coated/smeared with a thin layer of silt below a depth of approximately 20 feet below ground surface and the effective stress within these stratum were also reduced. Test shaft T-N4 was observed to exhibit a maximum nominal top plate load of 562.8 tons at an upward displacement of 1.31 inches (Figure 8.13a). Based on the equivalent top-down load-displacement curve, the elastic limit of the soil was exceeded during loading of the T-N4 drilled shaft foundation, as the curve was observed to exhibit a displaced regression during the unloading stages of testing (Figure 8.13b). The required design axial capacity of 987 tons was attained at a top-down vertical displacement of 1.05-inches (equal to 2.18 percent of the shaft diameter). Creep limits for test shaft T-N4 were observed to develop at loads equal to 425 tons and 450 tons for total and side shear creep, respectively (Figure 8.13c). The load transfer for test shaft T-N4 was observed to increase with depth to the location of the O-Cell (61.6 feet below ground surface), as presented in Figure 8.13d.

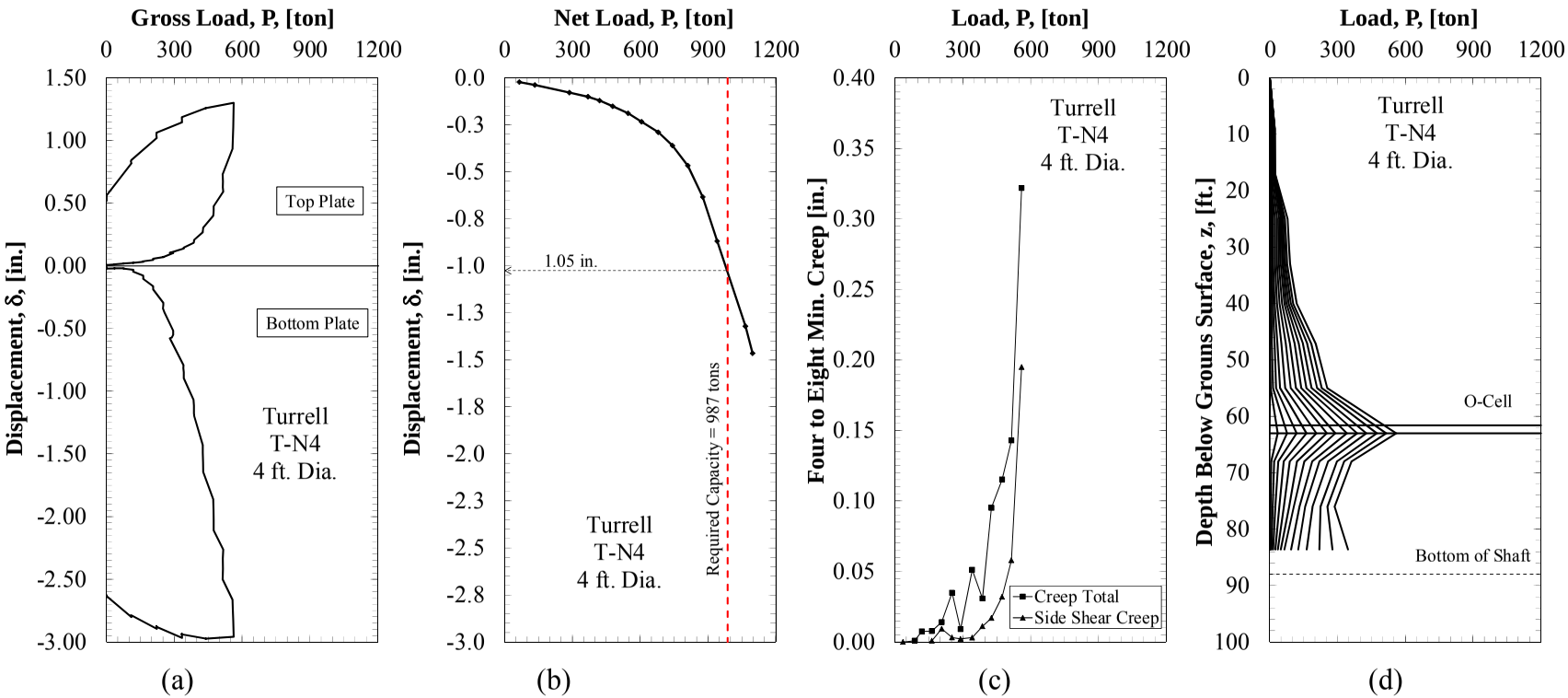

Figure 8.13. Test Shaft T-N4 (a) O-cell load displacement curve, (b) equivalent top-down load displacement curve, (c) creep limit, and (d) load transfer characteristics.

8.3.2. Concrete Testing Results

The design compressive strength was specified to be 4000 psi for the concrete utilized in the drilled shaft foundations constructed at the TATS. Unconfined uniaxial compressive strength and modulus of elasticity testing was performed on selected cylinders from the cylinders that were cast in the field on the date of construction (as discussed previously in Chapter 6). The results of these tests are presented in Table 8.6. Although 20% fly ash was used within the concrete, the concrete that was utilized for the drilled shaft foundations met the design specifications, with the compressive strength values for all shafts exceeding the required strength by over 1700 psi. The concrete within these shafts also exceeded the minimum design requirement for concrete compressive strength, as required by the state of Arkansas, by over 2200 psi. As concrete with 20% fly ash replacement is included within the specifications for AHTD Class S concrete, no cost savings due to fly ash replacement were realized. Concrete compressive strength for each drilled shaft foundation as a function of depth is presented in Figure 8.14.

Table 8.6. Average unconfined uniaxial compressive strength and Young's modulus testing results.

Shaft	28 Day Unconfined Unaxial Compressive Strength	Modulus of Elasticity
	[psi]	[ksi]
T-S4	5,739	4,983
T-N4	6,642	4,913
T-C6	6,673	5,522

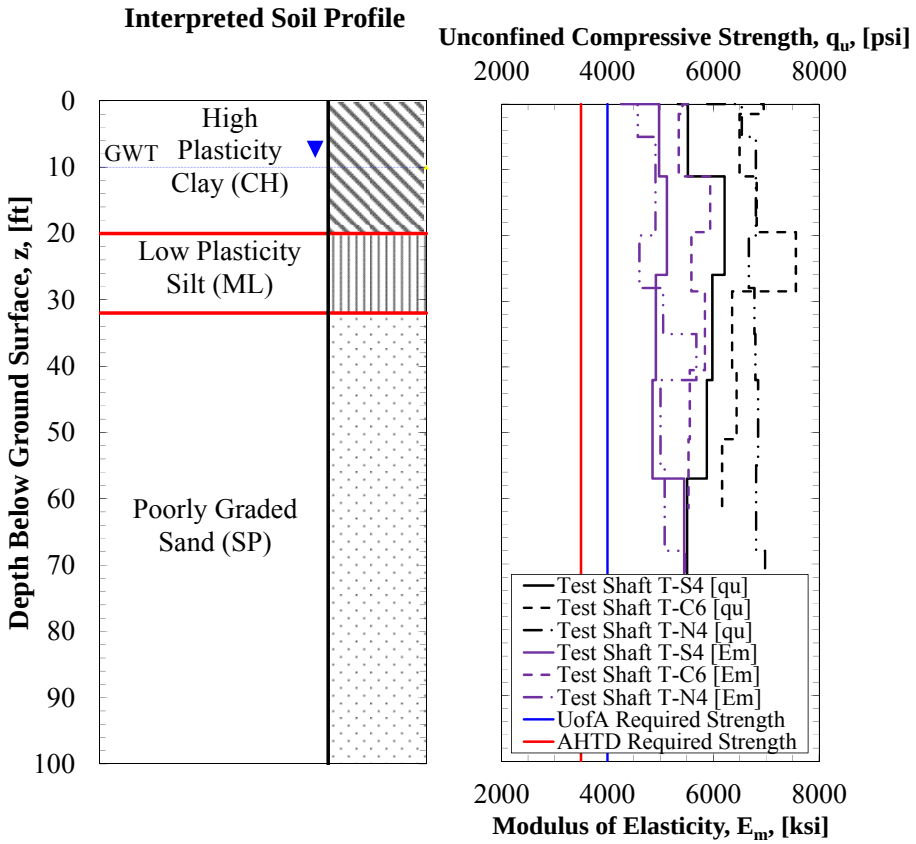

Figure 8.14. Average unconfined uniaxial compressive strength and modulus of elasticity as a function of depth for the drilled shaft foundations at the TATS.

8.3.3. Predicted and Measured Axial Capacity

Axial capacity predictions for drilled shafts at the TATS were determined at a five-percent displacement criterion. However upon testing, none of the top-down load-displacement values were not observed to exceed 3.06 percent. To ensure adequate comparisons between the measured and predicted values, the measured axial capacity values were compared to the predicted mean axial capacity values, at the actual measured displacement, as obatined utilizing the FB-Deep and SHAFT software programs.

Comparisons between measured and predicted axial capacity values, as obtained for the UofA, AHTD, and MODOT testing and sampling methods, are presented in Tables 8.7 through 8.9, respectively. The predicted capacity values, at a displacement of 5 percent of the shaft

diameter, were observed to be an average of 25 percent greater than those generated at the measured settlement. This difference was expected, as the shafts tested in the field were not loaded to failure (5% D) to enable the shafts to be used again for future axial and lateral load tests. However, the T-S4 drilled shaft foundation was observed to generate 82.8 percent of the required resistance at a vertical displacement of less than 1.19 percent of the shaft diameter. Likewise, the T-N4 drilled shaft foundation was observed to generate 108 percent of the required resistance at a vertical displacement of less than 3.06 percent of the shaft diameter. Furthermore, the T-C6 drilled shaft foundation was observed to generate 106 percent of the required resistance at a vertical displacement of 1.02 percent of the shaft diameter. The capacity values that were predicted utilizing the spreadsheet were calculated at displacement values of 5 percent of the diameter of the drilled shaft (following the AASHTO recommendations), and were therefore considered not to be comparable with the measured results (Table 8.9).

Table 8.7. Comparisons between the predicted capacity values utilizing FB-Deep and measured axial capacity values at the TATS.

								Prediction Software Program			
								FB-Deep			
Site	Required Axial Capacity [ton]	Dia. [ft]	SHAFT I.D.	As-Constructed Length [ft]	Measured axial Capacity [ton]	Measured Displacement [% Dia.]	Sampling/Testing Method	Predicted Axial Capacity at Measured Displacement [ton]	Percent Difference [%]	Predicted Ultimate Axial Capacity at 5% Displacement [ton]	Percent Difference [%]
Turrell	987	4	T-S4	86.5	818	1.188	UofA Mean	810	0.98	984	-20.34
					818	1.188	AHTD Mean	528	35.43	684	16.42
					818	1.188	MODOT Mean	590	27.88	843	-3.07
		6	T-C6	61.5	1050	1.019	UofA Mean	798	23.97	1032	1.70
					1050	1.019	AHTD Mean	500	52.37	732	30.32
					1050	1.019	MODOT Mean	479	54.39	738	29.70
		4	T-N4	88	1065	3.063	UofA Mean	902	15.32	1019	4.33
					1065	3.063	AHTD Mean	625	41.32	708	33.49
					1065	3.063	MODOT Mean	741	30.38	859	19.35

Table 8.8. Comparisons between the predicted capacity values utilizing SHAFT and measured axial capacity values at the TATS.

						Prediction Software Program			
						SHAFT			
Dia. [ft]	SHAFT I.D.	As-Constructed Length [ft]	Measured axial Capacity [ton]	Measured Displacement [% Dia.]	Sampling/Testing Method	Predicted Axial Capacity at Measured Displacment [ton]	Percent Difference [%]	Predicted Ultimate Axial Capacity [ton]	Percent Difference [%]
4	T-S4	86.5	818	1.188	UofA Mean	838	-2.46	1066	-30.33
			818	1.188	AHTD Mean	570	30.29	783	4.31
			818	1.188	MODOT Mean	615	24.77	929	-13.56
6	T-C6	61.5	1050	1.019	UofA Mean	850	19.02	1064	-1.36
			1050	1.019	AHTD Mean	551	47.53	808	23.01
			1050	1.019	MODOT Mean	597	43.11	963	8.32
4	T-N4	88	1065	3.063	UofA Mean	956	10.23	1107	-3.91
			1065	3.063	AHTD Mean	699	34.33	841	21.08
			1065	3.063	MODOT Mean	776	27.18	941	11.60

Table 8.9. Comparisons between the predicted capacity values utilizing a spreadsheet and measured axial capacity values at the TATS.

						Prediction Software Program	
						Spreadsheet	
Dia. [ft]	SHAFT I.D.	As-Constructed Length [ft]	Measured axial Capacity [ton]	Measured Displacement [% Dia.]	Sampling/Testing Method	Predicted Ultiamte Axial Capacity at 5% Displacement [ton]	Percent Difference [%]
4	T-S4	86.5	818	1.188	UofA Mean	982	-20.04
			818	1.188	AHTD Mean	853	-4.33
			818	1.188	MODOT Mean	985	-20.43
6	T-C6	61.5	1050	1.019	UofA Mean	1137	-8.30
			1050	1.019	AHTD Mean	1070	-1.91
			1050	1.019	MODOT Mean	803	23.54
4	T-N4	88	1065	3.063	UofA Mean	1029	3.41
			1065	3.063	AHTD Mean	872	18.08
			1065	3.063	MODOT Mean	998	6.26

The predicted capacity values, as obtained from the FB-Deep software program at the measured value of maximum displacement using the UofA, AHTD, and MODOT testing and sampling methods, respectively, were observed to be 13, 43, and 38 percent less than measured axial capacity values (Figure 8.15). The Capacity values that were predicted using SHAFT at the measured values of displacement for UofA, AHTD, and MODOT testing and sampling methods, respectively, were observed to be similar to those predicted using FB-Deep, and were observed to be 9, 37, and 32 percent less than values of measured capacity (Figure 8.15). Overall, values of predicted capacity for the UofA sampling and testing method were observed to be the closest to the measured values, being closer than the values obtained when using the data obtained from the AHTD and MODOT sampling and testing methods (Tables 8.5 through 8.7).

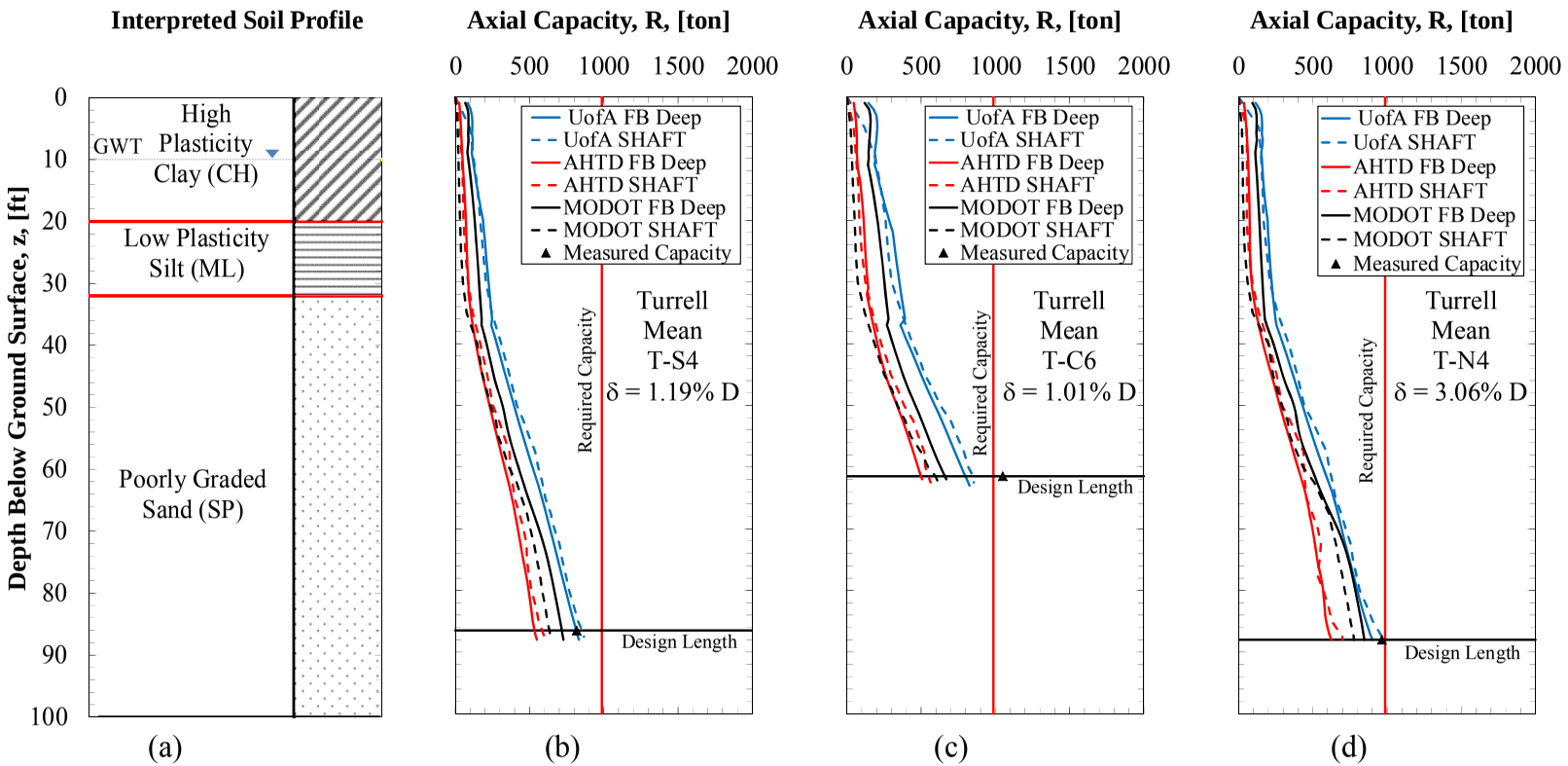

Figure 8.15. Predicted and measured axial capacities as a function of depth for the (a) interpreted soil profile at the TATS for (b) test shaft T-S4, (c) test shaft T-C6, and (d) test shaft T-N4.

As previously discussed in Chapter 7, although UofA capacities were observed to exhibit increased ranges in capacities for all programs, the magnitudes of these predictions were greater than those for either AHTD or MODOT sampling and testing methods. A comparison between the ranges values of measured capacities and predicted capacities at measured displacements for the UofA sampling and testing method is presented in Figure 8.16. Ranges of predicted axial capacity values when using the UofA data were observed to be greater when using the FB-Deep program than when using the SHAFT program. Although the mean values of predicted axial capacity for both programs were very close to the measured value of axial capacity, the SHAFT obtained values of predicted capacity for UofA data were observed to be generally closer (due to the decreased range in values) to the value of measured axial capacity.

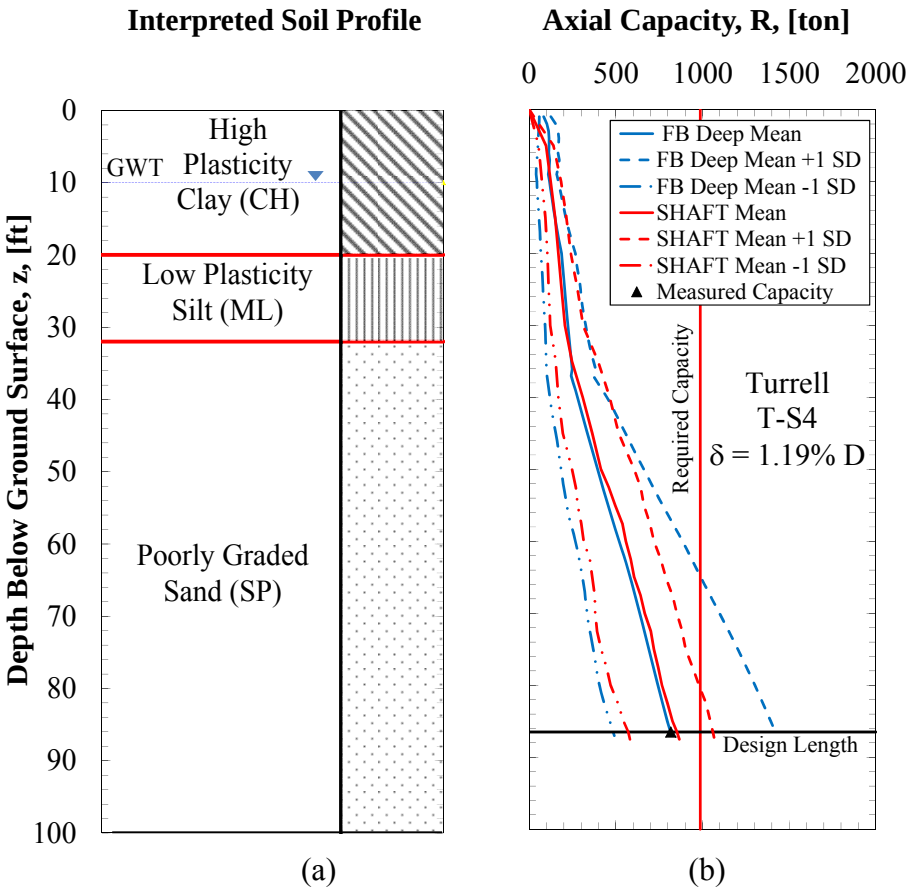

Figure 8.16. Predicted ranges of axial capacities and measured axial capacity for (a) the interpreted soil profile using UofA sampling and testing data for (b) test shaft T-S4.

Comparisons between the ranges values of measured capacities and predicted capacities at the measured settlement values and the design lengths, for each drilled shaft foundation when using each of sampling and testing methods is presented in Table 8.10. Ranges of predicted axial capacity values for UofA data were observed to be greater when using the FB-Deep program than when using the SHAFT program. Ranges of predicted axial capacity values for AHTD data were observed to be greater when using the SHAFT program than when using the FB-Deep program. Furthermore, ranges of predicted axial capacity values for MODOT data were observed to be greater when using the FB-Deep program than when using the SHAFT program. Overall, the UofA method, utilizing SHAFT or FB-Deep, was observed to produce values of

axial capacity that closely matched the measured values. Due to the increased ranges of predicted capacity values using FB-Deep, the SHAFT program was selected as the overall best. However, difficulties producing values of predicted capacity using the SHAFT program were encountered. To generate values of predicted axial capacity using SHAFT, interpolations of load-displacement curves at various depths had to be generated, which proved time-costly. Furthermore, at these user-interpolated displacement values of predicted capacity, end bearing and side friction resistance could not be separated.

Table 8.10. Comparisons between mean predicted and measured axial capacities and subsequent data ranges at the given constructed depth of each test shaft.

		Test Shaft T-S4		Test Shaft T-C6		Test Shaft T-N4	
		Depth = 86.5 ft, δ = 1.19%		Depth = 61.5 ft, δ = 1.01%		Depth = 88 ft, δ = 3.06%	
		Mean [μ]	Range [Δ R]	Mean [μ]	Range [Δ R]	Mean [μ]	Range [Δ R]
FB-Deep	UofA	814.2	926.5	798.0	962.3	901.8	1010.4
	AHTD	533.9	287.4	499.5	293.7	624.8	330.5
	MODOT	717.6	327.7	660.3	456.8	848.1	337.3
SHAFT	UofA	853.1	597.9	849.6	608.1	965.8	624.2
	AHTD	584.5	393.8	549.9	408.1	699.5	528.9
	MODOT	634.0	257.3	596.6	310.7	776.0	322.3
Actual		818.0		1050.0		1065.0	

8.3.4. Predicted and Measured Side Friction Resistance

Measured unit side friction resistances for the T-S4, T-N4, and T-C6 drilled shaft foundations are presented in Figure 8.17. The bottom depths for T-S4, T-N4, and T-C6 were recorded at 86.5, 88, and 61.5 feet, respectively. Unit side friction resistances within each stratum were observed to increase with upward average movement (exempting the lower sand stratum for T-N4, and the silt stratum for T-S4). This decreased unit side friction resistance within the lower sand stratum for T-N4, as previously discussed in Chapter 6, was believed to be due to a thin silt film coating the wall of the excavation. For T-S4, 1.7 tsf of unit side shear

resistance was observed within the lower sand stratum at an average upward movement of less than 0.47 inches (Figure 8.17a). Values of unit side friction resistance for T-N4 were observed to be generally less than those for test shaft T-S4, as expected due to the collapse, with the maximum recorded value within the lower sand stratum being 1.0 tsf (Figure 8.17b). The T-N4 drilled shaft foundation was also observed to be the only shaft which mobilized side friction resistance (based on the regression of side friction values with increased values of displacement). Values of unit side friction resistance for test shaft T-C6 were observed to be greater, with an observed maximum unit side shear resistance value of 2.8 tsf occurring within the lower sand stratum (Figure 8.17c).

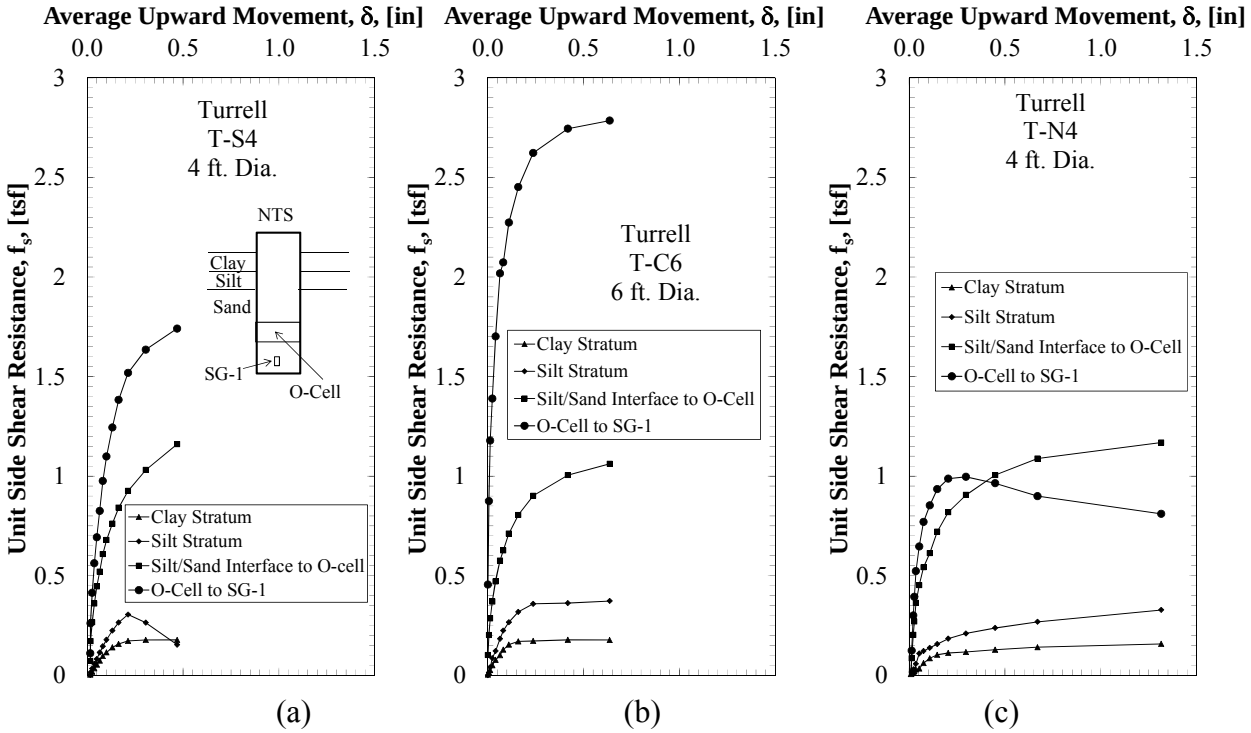

Figure 8.17. Measured unit side friction resistances for (a) T-S4, (b) T-C6, and (c) T-N4 drilled shaft foundations.

Side friction resistance predictions for drilled shaft foundations at the TATS were determined at the measured largest common displacement (0.5 inches) using the FB-Deep program. Results of the comparisons between the predicted and measured side friction resistance

values for the four-foot and six-foot diameter shafts, using the data from the UofA, AHTD, and MODOT testing and sampling methods, are presented in Figure 8.18. All comparisons were made utilizing the FB-Deep program, because it was the only program that enabled the determination of the side friction resistance at user defined settlement. Compared to the values obtained from the side friction predictions, at the measured displacement and design length of the drilled shaft foundation, the side friction resistance values for the T-S4 and T-N4 drilled shaft foundations were observed to be an average of 30, 57, and 56 percent different than the measured values, when using the data obtained from the UofA, AHTD, and MODOT sampling and testing methods, respectively (Figure 8.18b). The measured side resistance values for the T-C6 drilled shaft foundation was observed to be an average of 12, 50, and 55 percent greater than the predicted values that were obtained using the UofA, AHTD, and MODOT sampling and testing methods, respectively (Figure 8.18c). Overall, the measured values of side friction resistance were observed to compare most closely with predicted values generated utilizing the UofA sampling and testing method, but were still significantly different for the four-foot diameter shafts.

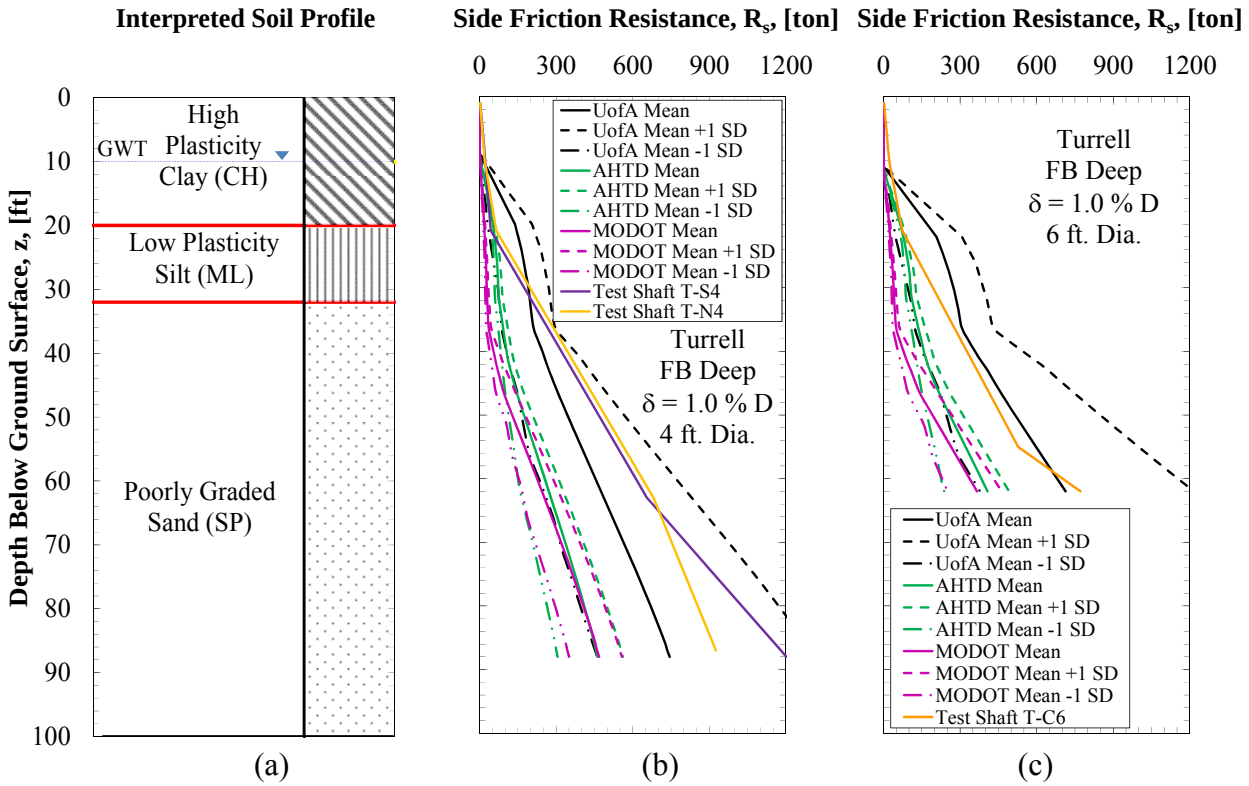

Figure 8.18. Measured and predicted side friction resistances for (a) a given interpreted soil profile for (b) four-foot diameter and (c) six-foot diameter shafts utilizing FB-Deep (at 1.0% D).

8.3.5. Predicted and Measured End Bearing Resistance

Measured unit end bearing resistances for the T-S4, T-N4, and T-C6 drilled shaft foundations are presented in Figure 8.19. Unit end bearing resistances, within the sand stratum, were observed to increase with increased amounts of average downward movement, as expected. The amount of unit end bearing resistance observed for the T-S4 drilled shaft foundation was 4.7 tsf at an average upward movement of one inch (Figure 8.19a). Values of unit end bearing resistance for the T-N4 drilled shaft foundation were observed to be greater than those for the T-S4 drilled shaft foundation, with a maximum recorded value at 26.7 tsf (Figure 8.19b). This was attributed to the excavation being extended an additional 1.5 feet due to the blowout at T-N4. The values of unit end bearing resistance for the T-C6 drilled shaft foundation were observed to reach a maximum value of 10.4 tsf (Figure 8.19c).

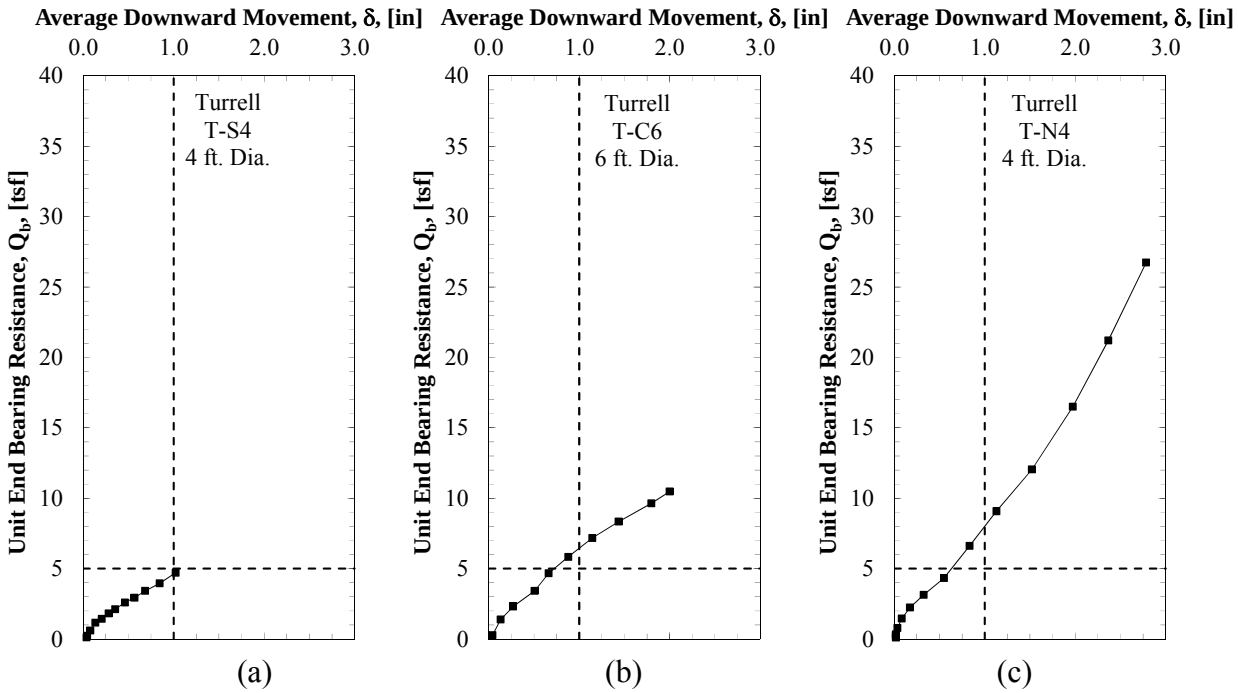

Figure 8.19. Measured unit end bearing resistances for test shafts (a) T-S4, (b) T-C6, and (c) T-N4.

The amount of end bearing resistance was predicted for the drilled shaft foundations at the TATS for the measured largest common vertical displacement (1.02 inches). Results of the comparisons between predicted and measured end bearing resisance values for the four-foot and six-foot diameter shafts using the data from the UofA, AHTD, and MODOT testing and sampling methods, are presented in Figure 8.20. When compared to end bearing prediction values that were predicted at the measured displacements generated utilizing the UofA, AHTD, and MODOT sampling and testing methods, respectively, the T-S4 and T-N4 drilled shaft foundations were observed to be an average of 83, 69, and 183 percent less than the measured values (Figure 8.20a). The measured axial capacity value for the T-C6 drilled shaft foundation was observed to be an average of 31, 26, and 10 percent greater than values generated utilizing the UofA, AHTD, and MODOT sampling and testing methods, respectively (Figure 8.20b). Overall, the measured values of end bearing resistance were observed to most closely compare

with the predicted values generated utilizing the AHTD sampling and testing method (again only for FB-Deep daa).

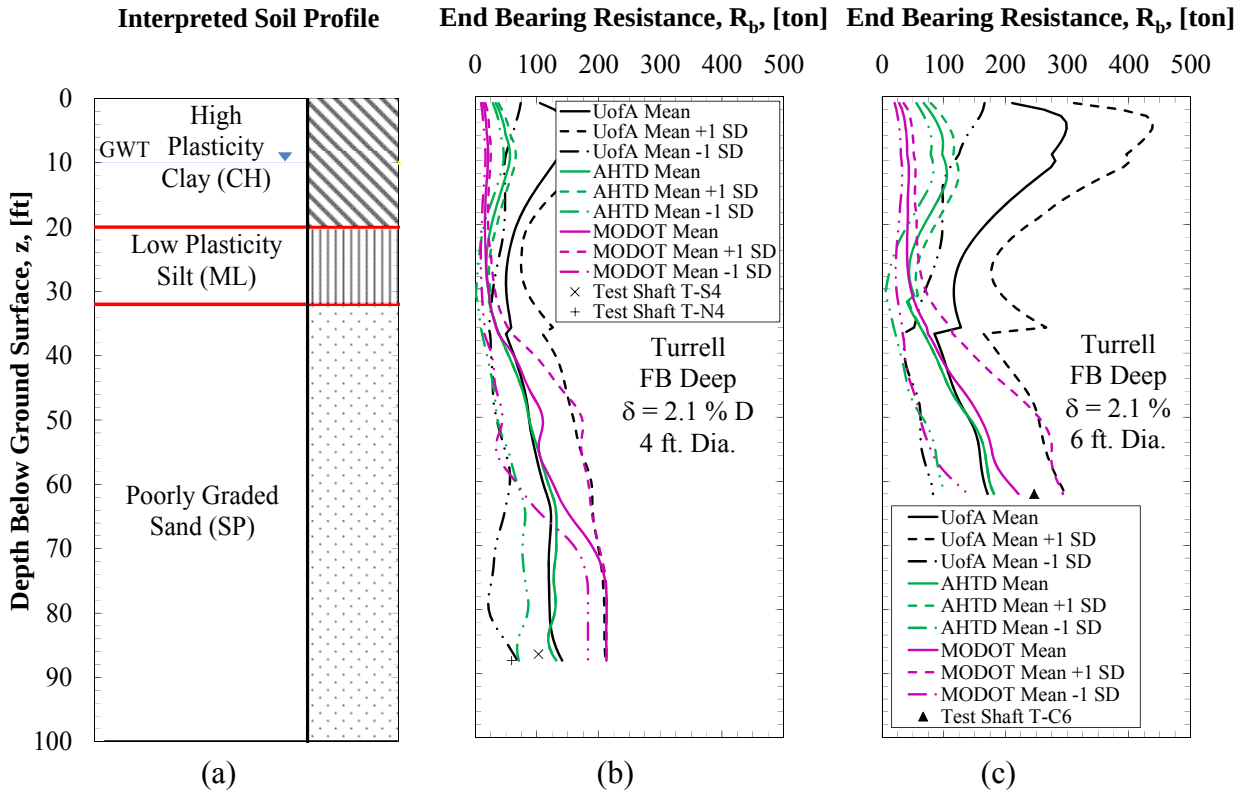

Figure 8.20. Measured and predicted side friction resistances for (a) a given interpreted soil profile for (b) four-foot diameter and (c) six-foot diameter shafts utilizing FB-Deep (at displacements of 2.1% D).

8.4. Conclusion

Comparisons between the values of predicted and measured drilled shaft resistances at the SSATS and TATS were presented in this chapter. Greater gross loads could have been applied to each shaft, but were not, due to scheduled future lateral load testing, pump capacity limits, or shorted uplift resistances. As a result, the measured values of axial capacity, side shear resistance, and end bearing resistance for displacements less than 0.3 inches were not compared with the original predictions performed at displacements equal to five percent of the diameter of the shaft. Instead, predictions of shaft capacity were conducted for the displacement values utilizing FB-Deep and SHAFT. However, difficulties producing values of predicted capacity

using the SHAFT program were encountered. To generate values of predicted axial capacity using SHAFT, interpolations of load-displacement curves at various depths had to be generated, which proved time-costly. Furthermore, at these user-interpolated displacement values of predicted capacity, end bearing and side friction resistance could not be separated. Based on the predictions, at measured displacements, more reliable comparisons were evaluated.

Based on the available data at the SSATS, the FB-Deep program utilizing the data from the AHTD sampling and testing method was observed to best predict overall shaft axial capacity. The SS-W4 drilled shaft foundation was the only foundation that met the required design load of 1112.5 tons at a displacement value equal to 0.065 inches. The overall capacity was more heavily impacted by the amount of rock side friction resistance than initially anticipated. The FB-Deep program utilizing the data from the AHTD sampling and testing method was observed to best predict side friction resistance. The overall capacity was significantly less impacted by the amount of end bearing resistance than initially anticipated. However, this under-development of end bearing resistance is attributed to the previously stated under-mobilization of load during testing. As with the side friction, the FB-Deep program utilizing the data from the AHTD sampling and testing method was observed to best predict overall end bearing resistance.

As with the SSATS (however not to the same degree of severity), greater gross loads should have been applied to each shaft, but were not, due to scheduled future axial and lateral load testing and maximization of the pump. Predictions of shaft capacity, at the measured displacement values, were performed utilizing the FB-Deep and SHAFT programs. Based on the predictions, at the measured displacements, more reliable comparisons were evaluated.

Based on the available data, the SHAFT program utilizing the data from the UofA sampling and testing method was observed to best predict overall shaft axial capacity. However,

it should be noted the FB-Deep program utilizing the UofA sampling and testing method may also be utilized. The T-C6 and T-N4 drilled shaft foundations met the required design load of 987 tons at displacement values equal to 0.65 and 1.05 inches, respectively. The FB-Deep program utilizing data from the UofA sampling and testing method was observed to best predict values of unit side friction resistance. Furthermore, the FB-Deep program utilizing the data from the AHTD sampling and testing method was observed to best predict the values of unit end bearing resistance.

Chapter 9: Conclusions and Recommendations

9.1. Introduction

Conclusions and recommendations, based on the results from the preformed predections and cost-benefit analyses (Chapter 7) and the results from full-scale field testing (Chapter 8), are presented in his chapter. Conclusions for the Siloam Springs, Turrell, and Monticello Arkansas Test Sites are presented in Sections 9.2., 9.3., and 9.4., respectively. Finally, a global conclusion highlighting the overall "take-aways" from this document and recommendations for future research are discussed in Section 9.5.

9.2. Siloam Springs Arkansas Test Site

Conclusions and recommendations, based on the Siloam Springs Arkansas Test Site (SSATS) are presented in this section. Predictive results from the SSATS illustrated the need for measured unconfined compressive strength data, as this parameter is just as important as RQD and has a significant impact on the predicted on axial capacity value for sites that contain rock. The FB-Deep program actually uses values of q_u instead of RQD to generate values of predicted axial capacity. The UofA sampling and testing method produced the highest predicted values for axial capacity, as well as the smallest range in values. This was attributed to the range of input q_u values. The range of the correlated q_u values, as utilized for the AHTD sampling and testing method was greater than the range in the measured q_u values obtained from the UofA method, and resulted in more sporadic predictions. At displacements that correspond to five percent of the shaft diameter, the SHAFT program utilizing the UofA sampling and testing method produced the highest values of predicted axial capacity, and the FB-Deep program utilizing the data from the AHTD sampling and testing method produced the lowest values of predicted axial capacity. Conversely, when predictions were modified to better represent actual displacements

at the SSATS, the FB-Deep program utilizing data from the UofA sampling and testing method produced the highest values of predicted axial capacity, and the SHAFT program utilizing data from the AHTD sampling and testing method produced the lowest values of predicted axial capacity.

Full-scale load testing at the SSATS was not performed to the full potential for multiple reasons. First, not enough side resistance was generated due to difficult drilling, not enough pump capacity was available to optimize displacements, and displacements at the SSATS were controlled to enable future lateral load testing. Although predictions of ultimate axial capacity were performed at displacement values equal to five percent of the diameter for the drilled shaft (which assumed an unreasonable amount of displacement for rock geology), measured displacement values for the SSATS did not exceed 0.18 percent of the diameter of the drilled shaft foundations. From the full-scale load testing performed at the SSATS, the SS-E4 drilled shaft foundation (that had a rock socket length of 7.0-feet) and the SS-C6 drilled shaft foundation (that had a rock socket length of 5.0-feet) displaced upward in side friction before displacing downward to generate enough resistance to engage full end bearing resistances. As a result, the top five-feet of limestone at the SSATS were determined to be weathered limestone. From the data gathered from test Shaft SS-W4 (that had a rock socket length of 10-feet), values of unit end bearing resistance reached 70 tsf before testing was halted, and were not observed to exhibit any signs of mobilization (or non-linearity). Current MODOT (2011) regulations allow a maximum design unit end bearing resistance of 50 tsf, while current AHTD regulations require a minimum rock socket length of ten feet. Based on the results of the O-Cell testing, a ten-foot rock socket length is recommended for data acquisition when conducting an O-Cell test to develop enough side resistance to balance the end bearing resistance, thereby utilizing the full capacity of the O-

Cell; or additional weight should be added to the top of the shaft to counter balance the end bearing force to utilize the full capacity of the O-Cell. However, a 10-foot long rock socket is not necessary for production shafts constructed within this moderately strong to strong limestone.

Compared to values of predicted axial capacity at measured displacements at the SSATS, measured values of axial capacity were smaller than anticipated. The FB-Deep program utilizing data from the AHTD sampling and testing method best predicted values of axial capacity. However, this conclusion was generated using the available data. As previously mentioned, the full-scale load tests failed to fully illustrate the potential of the strength associated with the end bearing resistance of the Boone Formation. Additional load-displacement information may lead to different conclusions. Therefore, additional load tests, specifically modified O-Cell/top down load tests are recommended for the current shafts at the SSATS (Section 9.5).

Based on the results of the concrete testing performed on concrete samples obtained from the SSATS, the concrete utilized at the SSATS (which contained 30 percent fly ash replacement) met all the strength requirements set forth by UofA researchers and AHTD regulations. Therefore, concrete containing up to 30 percent fly ash replacement may be utilized for drilled shaft foundations within the state of Arkansas, instead of the standard AHTD Class S concrete (which contains up to 20 percent fly ash replacement). Using this additional fly ash replacement, a cost savings of $2.66 per cubic yard was achieved. The savings associated with the use of additional fly ash replacement was equivalent to a site savings of $4,176, and can be increased to $28,476 depending upon the scale of the planned infrastructure.

In consideration to the construction practices and testing performed at the SSATS, the SS-E4 drilled shaft foundation was selected as the most appropriate shaft to perform the cost-

benefit analysis. Although the AHTD method was selected as the most appropriate method to predict values of resistance at displacements less than 0.18 percent, by utilizing the UofA sampling and testing method (which is believed to better portray the strength, specifically end bearing, characteristics of the limestone present at the SSATS upon top-down load testing), a minimum potential savings of $327,800 (32 percent of the cost associated with the planned foundation systems) may be achieved using a 7.0-foot rock socket length instead of a 10-foot rock socket length at the SSATS. This savings includes the additional costs associated with the full-scale load testing and the additional effort involved with the geotechnical investigation. By simply performing a full-scale load test, a minimum potential savings of $323,800 may be achieved. This large sum is attributed to the time and labor required to bore excessive depths through competent limestone. Actually knowing how much a foundation will hold is a significant additional benefit associated with full-scale load testing. The unit cost per ton of resistance for the UofA and AHTD sampling and testing methods were found to equal $24.11 and $82.70, respectively. When related to the costs associated with various scales of infrastructure, a savings of 67 percent may be realized for the foundation systems by employing the UofA method (full-scale load tests, uniaxial unconfined compression testing of rock, and 30 percent fly ash replacement).

9.3. Turrell Arkansas Test Site

Conclusions and recommendations, based on the testing performed at the Turrell Arkansas Test Site (SSATS), are presented in this section. From soil property results at the TAS, the UofA and AHTD methods for determining values of N_{60} were similar, indicating the validity of using the empirical transfer function for the UofA sampling and testing method to obtain blow count values while using a modified California split spoon sampler instead of a split spoon

sampler. Predictive results from the TATS illustrated that the current AHTD sampling and testing practices of correlating soil properties using blow count data may prove costly. The AHTD testing and sampling method (a method that is used to correlate all soil property values from corrected blow count values) that was utilized to obtain values of unit weight was deemed to be under-conservative for clay stratigraphy by 13 percent when compared to the UofA testing and sampling method. The possibility of current AHTD design practices being inadequate for clay stratigraphy may be indicated by these under-conservative values. The same AHTD testing and sampling method was deemed over-conservative in sand stratigraphy, by 21 percent, when compared to the UofA testing and sampling method. Therefore, cost savings may be obtained by implementing UofA testing and sampling methods.

For the predicted values of axial capacity at movement corresponding to five percent of the shaft diameter, the same measured UofA testing and sampling method data was input data into each program/spreadsheet. The capacity values that were generated at a depth of 86.5-feet below ground surface utilizing FB-Deep had a range of 103 percent. The capacity values that were generated utilizing SHAFT and the spreadsheet had ranges of 62.7 and 63 percent, respectively. Likewise, the same correlated AHTD testing and sampling method data was input into each program/spreadsheet. The capacity values generated had smaller ranges than those produced utilizing the UofA method. Although the ranges in the capacity data were larger for the UofA method, mean values of axial capacities, using the UofA data, still averaged 44, 43.9, and 23.9 percent greater than AHTD method generated capacities for SHAFT, FB-Deep, and the spreadsheet, respectively. Although measured input values produce a larger range within the values of the predicted capacity, than those generated using correlated values, these predicted capacity values are still greater than the “correlated” predicted values.

For the predicted values of axial capacity at movements corresponding to the measured displacements, the capacity values generated at a depth of 86.5-feet below ground surface, as obtained utilizing FB-Deep, also had the largest range of results when using the UofA and MODOT sampling and testing methods (approximately 35.7 and 21.4 percent greater than than those values obtained from SHAFT, respectively). However, ranges of capacity values generated at a depth of 86.5-feet below ground surface, as obtained from FB-Deep, when using the AHTD sampling and testing method were 37 percent less than those generated using SAHFT. Mean values of predicted axial capacity, as obtained from the UofA method, averaged 32.9 and 18.7 percent greater than AHTD and MODOT method values of predicted capacity, respectively. As with the predicted results for movements corresponding to displacements of the diameter of the drilled shaft foundation at five percent, although the "measured" input values produce a larger range of predicted capacity values than those generated from "correlated" input values, these "measured" capacity predictions are still greater than "correlated" capacity predictions.

Full-scale load testing at the TATS was not performed to the full potential extent. Although predictions of ultimate axial capacity were performed at displacement values that were equal to five-percent of the diameter of the drilled shaft foundations, measured displacement values for the TATS did not exceed 3.06 percent. As with the SSATS, the amount of displacement at the TATS was limited due to pump difficulties, and to enable future axial and lateral load testing. From the full-scale load testing performed at the TATS, the T-N4 drilled shaft foundation exhibited the most displacement due to a collapse and redrilling during construction. The T-N4 and T-C6 drilled shaft foundations were the only shafts observed to mobilize (or go non-linear) side friction resistances, however, values of side friction resistance for T-N4 were observed to be lower than those of T-C6 (also attributed to the collapsed

excavation/re-drilling during construction of the T-N4 drilled shaft foundation). Values of end bearing resistance for each shaft were similar, with approximately 5 tsf of resistance observed at displacement values of one-inch.

Compared to the predicted axial capacity values, at the measured displacements recorded for the drilled shaft foundations at the TATS, the measured axial capacity values were larger than anticipated. The SHAFT program utilizing the UofA sampling and testing method best predicted the axial capacity values. However, the values of predicted axial capacity using FB-Deep and the UofA testing and sampling method were very similar to the as obtained using SHAFT and the UofA sampling and testing method, and therefore may also be utilized. Due to the more user friendly interface of FB-Deep, the capability of the program to generate predicted values of capacity based on user-specified values of settlement, and the capability of the program to separate values of end bearing and side friction resistance at a user-defined value of settlement, FB-Deep was selected as the preferred prediction program (as previously presented in Table 7.1).

In consideration of the construction practices and testing performed at the TATS, the T-S4 drilled shaft foundation was selected as the most appropriate shaft to perform the cost-benefit analysis. The drilled shaft foundations that were designed using the UofA testing and sampling method, for the TATS, were 8.8 percent ($137,500) more expensive than the driven piles that were designed using the AHTD method. This estimate includes the additional costs associated with the full-scale load testing and the additional effort involved with the geotechnical investigation. However, this estimate does not account for the additional lateral support provided by utilizing drilled shaft foundations instead of driven pile foundations. As the TATS is located in a region prone to seismic activity, this benefit may be considerable. A unit cost per ton of resistance for the UofA and AHTD sampling and testing methods were found to equal

$75.47 and $141.57, respectively. It is interesting to note that although it is cheaper to construct drilled shaft foundations at the Turrell Arkansas Test Site from a design standpoint, the expertise of the contractor also plays an important role in the costs incurred. When related to the costs associated with increasing scales of infrastructure, a cost savings of 86 percent can be obtained for the foundations system by employing the UofA method (utilizing unit cost per ton of resistance values).

9.4. Monticello Arkansas Test Site

At this time, only predicted results are available for conclusion for the Monticello Arkansas Test Site (MATS). Based on the predicted results from the MATS, it is hypothesized that the MODOT CPT testing method is an effective method for gathering soil properties in areas with highly variable soil profiles. Utilizing FB-Deep, SHAFT, and the spreadsheet fpr displacements corresponding to five percent of the diameter of the drilled shaft foundations, the MODOT method predicted the highest values of axial capacity, followed by the UofA and AHTD methods.

9.5. Global Conclusion

Overall, the use of full-scale load testing, within the state of Arkansas, can and will produce cost savings based on the following recommendations:

a) utilizing the UofA testing and sampling methods that were described in Chapter 3,
b) utilizing the FB-Deep program to estimate the values of axial capacity (as described in Chapter 4),
c) utilizing 30% fly ash replacement in drilled shafts,
d) the performance of hybrid top-down/O-Cell load testing on the SS-E4 and SS-C6 drilled shaft foundations, and
e) further development of a full-scale load test database for the state of Arkansas, by conducting more full-scale load tests.

Though the UofA testing and sampling method involves more up-front expenditures, it has been proven to benefit the overall cost of construction (assuming the use of a qualified and experienced contractor). This method also encourages the continual development of a load-test database, in which soil properties and the predicted and measured performances for foundations, for the various regions of the state, can be referred to by designers, aiding in the design process. To further aid in the design process, researchers at the University of Arkansas advocate the use of FB-Deep as a prediction tool for estimating drilled shaft axial capacity due to the following:

a) the performance of the program in predicting capacity compared to SHAFT and a spreadsheet,
b) the user-friendly interface of the program, and
c) the capability of the program to separate the end bearing and side friction resistance components at a given settlement value.

Future top-down load testing on these shafts is recommended to fully gauge the potential of end bearing resistance in the Boone Formation. Top-down load testing on test shafts SS-E4 and SS-C6 may help to determine a maximum unit end bearing resistance value for geological regions of the state that are similar to the geologic conditions at the SSATS, and help to better understand the necessity of using a ten-foot length rock socket length. It is recommended for future research to be performed which enables the impact of load settlement on the prediction of capacity to be incorporated into the AASHTO design regulations.

Given the time scope of the research project, measured friction angle capacity values were not entered into the input database, as the testing was still in progress. Upon acquisition of this data, to fully utilize SHAFT predictions utilizing the UofA data, it is suggested that the estimated capacity values obtained by measured friction angle values (rather than correlated friction angle values) be compared to the capacity values as obtained using the measured blow

count values. Further, to fully utilize SHAFT predictions utilizing the MODOT data, it is suggested that eh estimated capacity values obtained by using calculated friction angle values (rather than correlated friction angle values) be compared to the capacity values as obtained using the measured blot count values.

References

AASHTO (1997). *Standard Specification for Highway Bridges*. American Association of State Highway and Transportation Officials, Washington, D.C. 17th Ed.

AASHTO (2007). *LRFD Bridge Design Specifications,* American Association of State Highway and Transportation Officials, Washington, D.C.4th Ed.

AASHTO (2012). *LRFD Bridge Design Specifications,* American Association of State Highway and Transportation Officials, Washington, D.C.5th Ed.

ACI 318 (2008). *Building Code Requirements for Structural Concrete and Commentary*. American Concrete Institute, Detroit, MI, pp. 473.

AGS (2013). "Geologic Stratigraphy of the Ozark Plateaus." Arkansas Geological Survey. <http://www.geology.ar.gov/geology/ozark_mississippian.htm>. (Oct 3, 2013)

Allen, T.M., Nowak, A.S., Bathurst, R.J. (2005). "Calibration to Determine Load and Resistance Factors for Geotechnical and Structural Design." Circular E-C079, Transportation Research Board, Washington, D.C., pp. 83.

ASTM C39/C39M. (2012). "Standard Test method for Compressive Strength of Cylindrical Concrete Specimens." Annual Book of ASTM Standards, Vol. 4.02, ASTM International, West Conshohocken, PA.

ASTM C260. (2010). "Standard Specification for Air-Entraining Admixtures for Concrete." Annual Book of ASTM Standards, Vol. 4.02, ASTM International, West Conshohocken, PA.

ASTM C469/469M. (2010). "Standard Test Method for Static Modulus of Elasticity and Poisson's Ratio of Concrete in Compression." Annual Book of ASTM Standards, Vol. 4.02, ASTM International, West Conshohocken, PA.

ASTM C494. (2013). "Standard Specification for Chemical Admixtures in Concrete." Annual Book of ASTM Standards, Vol. 4.02, ASTM International, West Conshohocken, PA.

ASTM C618. (2012). "Standard Specification for Coal Fly Ash and Raw or Calcined Natural Pozzolan for Use in Concrete." Annual Book of ASTM Standards, Vol. 4.02, ASTM International, West Conshohocken, PA.

ASTM C989. (2012). "Standard Specification for Slag Cement for Use in Concrete and Mortars." Annual Book of ASTM Standards, Vol. 4.02, ASTM International, West Conshohocken, PA.

ASTM C1240. (2012). "Standard Specification for Silica Fume Use in Cementitious Mixtures." Annual Book of ASTM Standards, Vol. 4.02, ASTM International, West Conshohocken, PA.

ASTM D1143. (2013). "Standard Test Method for Piles Under Static Axial Compression Load." Annual Book of ASTM Standards, Vol. 4.08, ASTM International, West Conshohocken, PA.

Barker, R M, Duncan, J. M., Rojiani, K. B., Ooi, P. S. K., Tan, C. K. Kim, S. G. (1991). Manuals for Design of Bridge Foundations, NCHRP Report 343, Transportation Research Board, Washington D.C.

Bieniawski, Z. (1984). Rock Mechanics Design in Mining and Tunneling, Pennsylvania State University, College of Earth and Mineral Sciences, Boston, pp. 272.

Bloomquist, D., McVay, M., Hu, Z. (1992). "Updating Florida Department of Transportation's (FDOT) Pile. Shaft Design Procedures Based on CPT & DTP Data." Florida Department of Transportation, BD-545, RPWO No. 43, MF Project 00005780, pp. 199.

Bowles, J.E. (1977). *Foundation Analysis and Design*. 2nd Ed., McGraw-Hill, New York.

Brown, D. (2008). "Load Testing of Drilles Shaft Foundations in Limestone, Nashville, TN." Research report for ADSC-Southeastern Chapter. pp. 103.

Brown, D., Turner, J., Castelli, R. (2010). "Drilled Shafts: Construction Procedures and LRFD Design Methods." *FHWA Publication No. NHI-10-016,* Federal Highway Administration, Washington, D.C., pp. 970.

Burmister, D. M., (1948). “The Importance and Practical use of Relative Density in Soil Mechanics.” Proceedings ASTM, Vol. 48. pp. 1249.

Bustamante, M. , Gianeselli, L. (1982). “Pile Bearing Capacity Prediction by Means of Static Penetrometer CPT.” Proceedings of the 2nd European Symposium on Penetration Testing Vol. 2, pp. 493-500.

Canadian Geotechnical Society (1978). Canadian Foundation Engineering Manual (CFEM). BiTech Publishers Ltd., Vancouver, B.C.

Canadian Geotechnical Society. (1985). Canadian Foundation Engineering Manual (CFEM). 2nd Ed. BiTech Publishers, Vancouver, B.C.

Canadian Geotechnical Society (1992). Canadian Foundation Engineering Manual (CFEM), 3rd Ed., Richmond.

Carter, J. P., Kulhawy, F. H. (1988). "Analysis and Design of Drilled Shaft Foundations Socketed into Rock." Report EL-5918, Electric Power Research Institute, Palo Alto, Calif.

Chernauskas, L. R., Paikowsky, S. G. (2000). “Defect Detection and Examination of Large Drilled Shafts Using a New Cross-Hole Sonic Logging System.” Proceedings, Performance Conformation of Constructed Geotechnical Facilities, ASCE, Reston, VA, pp. 66–83.

Coffman, R. A. (2013). Personal Correspondence, September 23.

Coffman, R., Race, M. (2013). “Statistical Analysis of Arkansas Soil Parameters as used in Deep Foundation Design.” Proc. Deep Foundations Institute 38th Annual Conference on Deep Foundations, Phoenix, AZ. Submitted for Review.

Cornell, C. A. (1969). "A Probability-Based Structural Code." Journal of the American Concrete Institute, Vol. 66, No. 12.

Danish Geotechnical Institute.(1985).‘‘Code of Practice for Foundation Engineering.’’ Bulletin 36, DGI, Copenhagen.

Davis , R.E., Carlson, R.W., Kelly, J.W., Davis H.E. (1937). "Properties of Cements and Concrete Containing Flyash." ACI Journal. Vol. 33, pp. 577-612.

Ding, Dan. (2013). "Uncertainty and Variability Analysis in Load and Resistace Factor Design on Spread Footing Foudations – Considering the Effect of Number of Samples." doctoral dissertation. University of Missouri, Columbia, pp. 36-144.

Edmeades, R. M., Hewlett P. C. (1986). "Admixtures—Present and Future Trends." Concrete, Vol. 20, No.8, pp.4-7.

FB-Deep (2012). Bridge Software Institute, Gainesville, FL. Ver. 2.04.

FHWA. (2011). "Admixtures." Infrastructure Materials Group. U.S Department of Transportation. Federal Highway Administration. <http://www.fhwa.dot.gov/infrastructure/materialsgrp/admixture.html>. (Sept. 23, 2013)

Freudenthal, A. M. (1956). "Safety and the Probability of Structural Failure." Transactions, ASCE, Vol. 121, 1956, pp. 1337-1397.

Gupton, C., Logan, T. (1984). "Design Guidelines for Drilled Shafts in Weak Rock in South Florida." Preprint, Annual Meeting of South Florida Branch of the American Society of Civil Engineers, Miami, FL.

Halstead, W. J. (1986). "Use of Fly Ash in Concrete." National Cooperative Highway Research Program (NCHRP), Transportation Research Board, National Research Council, Washington, D.C.

Hansen, J. B. (1965). ''Philosophy of foundation design: design criteria, safety factors and settlement limits.'' Proceedings, Symposium on Bearing Capacity and Settlement of Foundations, Duke University, Durham, N.C., pp. 1–13.

Hasofer, A. M., Lind, N. (1974). "An Exact and Invariant First-Order Reliability Format." Journal of Mechanical Engineering, ASCE, Vol. 100, No. 1, pp.111-121.

Hoek, E. Brown.E., T. (1988). "The Hoek-Brown Failure Criterion – A 1988 Update." Proceedings from 15th Canadian Rock Mechanics Symposium, Toronto Canada.

Horvath, R., Kenney, T. (1979). "Shaft Resistance of Rock-Socketed Drilled Piers." Proceedings of Symposium on Deep Foundations, American Society of Civil Engineers, pp. 182-214.

Kulhawy, F.H., Prakoso, W.A., Akbas, S.O. (2005). "Evaluation of Capacity of Rock Foundation Sockets." Proceedings 40th U.S. Symposium of Rock Mechanics, Anchorage, AK. pp. 5-767.

Kuo, C.L., McVay, M. C., Birgisson, B. (2002). "Calibration of Load and Resistance Factor Design: Resistance Factors for Drilled Shaft Design." Transportation Research Record: Journal of the Transportation Research Board, Vol. 18, No. 8, Soil Mechanics 2002, pp. 108-111.

Lacroix, Y., Horn, H. (1973). "Direct Determination and Indirect Evaluation of Relative Density and its Use on Earthwork Construction Projects." In *Evaluation of Relative Density and Its Role in Geotechnical Projects Involving Cohesionless Soils*: ASTM Special Technical Publication 523, pp. 251–280.

Lai, Peter. (2012). "An Introduction to the Design methodology of FB-Deep." Florida Department of Transportation Structures Design Office State Geotechnical Engineering Section. <http://www.dot.state.fl.us/geotechnical/documents/fb-deep.pdf>. (May 30, 2013).

Lewis, D. W. (1981). "History of Slag Cements." Proceedings of University of Alabama Slag Cement Seminar, American Slag Association. Paper No. 186-6.

Li, D.Q., Zhang, L.M., Tang, W.H. (2005). ''Reliability Evaluation of Cross-Hole Sonic Logging for Bored Pile Integrity,'' Journal of Geotechnical and Geoenvironmental Engineering, Vol. 131, No. 9, pp. 1130–1138.

Lind, N. C., (1971). "Consistent Partial Safety Factors." Journal of the Structural Engineering Division, ASCE, Vol. 97, pp. 1651-1670.

Lwin, M.M. (2007). "Clarification of LRFD Policy Memorandum." US Department of Transportation, Federal Highway Administration. <http://www.fhwa.dot.gov/bridge/012207.cfm>. (Aug 26, 2013)

Luther, M.D. (1989). “Silica Fume (Microsilica): Production, Materials, and Actions in Concrete.” Proceedings in Advancements in Concrete Materials Seminar, Peoria, IL, pp. 18.1-18.21.

Luther, M.D. (1990). “High-Performance Silica Fume (Microsilica): Modified Cementitious Repair Materials.” Proceedings of 69th Annual Meeting of the Transportation Research Board, Paper No. 890448.

Malhotra, V. M., (1989). “Superplasticizers and Other Chemical Admixtures in Concrete.” American Concrete Institute. SP-119: Detroit, MI.

Mayne, P., Harris, D. (1993). “Axial Load-Displacement Behavior of Drilled Shaft Foundations in Piedmont Residuum.” *FHWA Publication No. 41-30-2175*, Georgia Tech Research Corporation, Georgia Institute of Technology, Atlanta, GA, pp. 162.

McFarland, J. D. (2004). “Stratigraphic Summary of Arkansas.” Arkansas Geologic Commission Information Circular 36. University of Arkansas Geosciences Department. Little Rock, Arkansas.

McVay, M. C., Townsend, F. C., Williams, R. C. (1992). "Design of Socketed Drilled Shafts in Limestone." Journal of Geotechnical Engineering, ASCE, Vol. 118, No. 10, pp. 1626-1637.

Meyerhof, G. (1976) .“Bearing Capacity and Settlement of Pile Foundations.” Journal of Geotechnical Engineering, Vol. 102, No. 63, pp. 195-228.

Miller, A. D. (2003). “Prediction of Ultimate Side Shear for Drilled Shafts in Missouri Shales.” MS Thesis. University of Missouri, Columbia, pp. 30-53.

Mindess, S., Young, J. F. (1981). *Concrete*. Prentice-Hall, Englewood Cliffs, N.J.

Missouri Department of Transportation. (2011). *Engineering Policy Guidelines for Design of Drilled Shafts.* Report No. CMR12003.US. Department of Transportation (FHWA). Washington, D.C.

Nowak, A.S. (1999). "Calibration of LRFD Bridge Design Code." NCHRP Report 368, National Cooperative Highway Research Program, Transportation Research Board, Washington, D.C.

O'Neill, M., Reese, L. (1999). "Drilled shafts: Construction Procedures and Design Methods." *FHWA Publication No. IF-99-025*, Federal Highway Administration, Washington, D.C., pp. 537.

O'Neill, M., Townsend, F., Hassan, K., Buller, A., Chan, P. (1996). "Load transfer for drilled shafts in intermediate geomaterials." *FHWA Publication No. RD-95-172*, Federal Highway Administration, Washington, D.C., pp. 196.

Osterberg, J. O. (1984). "A New Simplified Method for Load Testing Drilled Shafts." Foundation Drilling, Vol. XXIII, No. 6 (July/August, 1984), International Association of Foundation Drilling (ADSC), p.9.

Osterberg, J. O. (1998). ''The Osterberg Load Test Method for Bored and Driven Piles. The First Ten Years.'' Proc., 7th Int. Conf. and Exhibition on Piling and Deep Foundations. Vienna, Austria, (June 15–17, 1998), Deep Foundation Institute, Englewood Cliffs, N.J.

Paikowsky, S. G. (2002). "Load and Resistance Factor Design (LRFD) for Deep Foundations." NCHRP Project 24-17, Transportation Research Board, National Research Council, Washington, D.C.

Paikowsky, S.G. (2004). "Load and Resistance Factor Design (LRFD) for Deep Foundations." NCHRP Report 507, National Cooperative Highway Research Program, Transportation Research Board of the National Academies, Washington, D.C., pp. 126.

Paikowsky, S. G., Stenersen, K. L. (2000). ''The Performance of the Dynamic Methods, Their Controlling Parameters and Deep Foundation Specifications.'' Proc., 6th Int. Conf. on Application of Stress-Wave Theory to Piles, S. Niyama and J. Beim, eds., Balkema, Rotterdam, The Netherlands, pp. 281–304.

Phoon, K. K. (2004). "Towards Reliability-Based Design for Geotechnical Engineering." Lecture for Korean Geotechnical Society, Seoul, July 2004.

Pugsley, A. (1955). ‘‘Report on Structural Safety.’’ Journal of Structural Engineering, Vol. 33, No.5, pp.141–149.

Quiros, G., Reese, L. (1977). “Design Procedures for Axially Loaded Drilled Shafts” *FHWA Publication No. TX78-1765F*; Federal Highway Administration Final Report, Washington, D.C., pp. 176.

Race, M.L., Bey, S.M., Coffman, R.A., (2013). “Discussion of Implementation of LRFD of Drilled Shafts in Louisiana” by Xinbao Yu, Murad Y. Abu-Farsakh, Sungmin Yoon, Ching Tsai, and Zhongjie Zhang” Journal of Infrastructure Systems, Vol. 19, No. 3, pp. 351-353.

Ramachandran, V. S. (1984a). *Accelerators. In Concrete Admixtures Handbook: Properties, Science, and Technology*. Noyes Publications. Park Ridge, NJ.

Ramachandran, V. S., Malhotra V. M. (1984b). Superplasticizers in Concrete Admixtures Handbook: Properties, Science, and Technology, Noyes Publications. Park Ridge, NJ. pp. 211-68.

Ravindra, M. K., Galambos, T. V. (1978). "Load and Resistance Factor Design for Steel," Journal of the Structural Division, ASCE, Vol. 104, No. ST9, pp. 1337-1353.

Reese, L. C., O’Neill, M. W. (1988). ‘‘Drilled shafts; Construction Procedures and Design Methods.’’ Rep. No. FHWA-HI-88-42, U.S. Dept. of Transp., Federal Highway Administration, Washington, D.C.

Reese, L., Wang, S., Arrellaga, J., Vasquez, L. (2012a). “SHAFT v2012- User’s Manual: A Program for the Study of Drilled Shafts Under Axial Loads.” ENSOFT, INC. Austin, TX, pp. 186.

Reese, L., Wang, S., Arrellaga, J., Vasquez, L. (2012b). “SHAFT v2012- Technical Manual: A Program for the Study of Drilled Shafts Under Axial Loads.” ENSOFT, INC. Austin, TX, pp. 76.

Reese, L. C , Wright, S. J. (1977). “Drilled Shaft Design and Construction Guidelines Manual." Implementation Package 77-21, U.S. Department of Transportation., Washington, D.C.

Reynolds, R.T., Kaderbeck, T.J. (1980). "Miami Limestone Foundation Design and Construction." Preprint 80-546, Annual Meeting of South Florida Branch of the American Society of Civil Engineers, Miami, FL.

Rixom, M. R., N. P. Mailvaganam. (1986). *Chemical Admixtures for Concrete*. Cambridge, England: The University Press.

Rojiani, K. B., Ooi, P. S. K. & Tan, C. K. (1991). "Calibration of Load Factor Design Code for Highway Bridge Foundations." Proceedings of Geotechnical Engineering Congress (GSP27), ASCE, New York, NY, pp. 1353-1364.

Rollins, K., Clayton, R., Mikesell, R., Blaise, B. (2005). "Drilled Shaft Side Friction in Gravelly Soils." Journal of Geotechnical and Geoenvironmental Engineering, Vol. 131, No. 8, pp. 987-1003.

Rowe, R.K., Armitage, H.H. (1987). "A Design Method for Drilled Piers in Soft Rock." Canadian Geotechnical Journal, Vol. 24, pp. 114–125.

Schmertmann, J. H. (1967). "Guidelines for Use in the Soils Investigation and Design of Foundations for Bridge Structures in the State of Florida." Research Bulletin 121 (RB-121), Report Prepared for the FDOT by the Univ. of Florida, Gainesville, Fla.

Schmertmann, J.H. (1978). "Guidelines for Cone Test, Performance, and Design." *FHWA Publication No. TS-78209*, Federal Highway Administration, Washington, D.C., pp. 145.

Schmertmann, J.H. and Hayes, J.A. (1997). "The Osterberg Cell and Bored Pile Testing – A symbiosis." *3rd Int. Geot. Eng. Conf.*, Cairo University.

SHAFT (2012). ENSOFT, INC. Austin, TX. Ver. 2012.

Sheikh, S., O'Neill, M. (1986). "Long-Term Behavior of Expansive Concrete Drilled Shafts". Canadian Journal of Civil Engineering, Vol. 13, No. 2, pp. 213-217.

Skempton, A. (1951). "The Bearing Capacity of Clays." Proceedings from Building Research Congress, London, Vol. 1, pp. 180-189.

Townsend, F. (2003a). “SHAFT-Spt Validation Problems.” Bridge Software Institute. Gainesville, FL, pp. 91.

Townsend, F. (2003b). “User’s Guide for SHAFT-SPT.” Bridge Software Institute. Gainesville, FL, pp. 16.

U.S. Department of Transportation. Federal Highway Administration. (1990). *Portland Cement Concrete Materials Manual*. Report No. FHWA-Ed-89-006. Washington D.C.

Vu, Thanh. (2013). “Load and Resistance Factor Design of Drilled Shafts at Service Limit State.” doctoral dissertation. University of Missouri, Columbia, pp. 283-295.

Williams, A.F., Johnston, I.W., Donald, I.B. (1980). “The Design of Socketed Piles in Weak Rock.” In Proceedings of the International Conference on Structural Foundations on Rock. A.A. Balkema, Sydney, pp. 327–347.

Withiam, J.L., Voytko, E.P., Barker, R.M., Duncan, J.M., Kelly, B.C., Musser, S.C., Elias, V. (1998). Load and Resistance Factor Design (LRFD) for Highway Bridge Substructures. Report FHWA HI-98-032. Federal Highway Administration, Washington, D.C.

Yang, X., Han, J., Parsons, R. L., and Henthorne, R. W. (2008). “Resistance Factors for Drilled Shafts in Weak Rock Based on O-Cell Test Data.” Journal of the Transportation Research Board, No. 2045, pp. 62-67.

Yoon, G. L., O'Neill, M. W. (1997). “Resistance Factors for Single Driven Piles from Experiments.” Research Record 1569, Transportation Research Board, Washington, 47-54.

Yu, X., Abu-Farsakh, M., Yoon. S., Tsai, C., Zhang, Z. (2012). “Implementation of LRFD of Drilled Shafts in Louisiana.” Journal of Infrastructure Systems, ASCE, Vol. 8, No.2, pp.103-112.

Zhang, L., Einstein, H.H. (1998). “Estimating the Mean Trace Length of Rock Discontinuities.” Journal of Rock Mechanics and Rock Engineering, Vol. 31, No.4, pp. 217–235.

Zhang, L., Tang, W.H., Ng, C.W.W. (2001). "Reliability of Axially Loaded Driven Pile Groups." Journal of Geotechnical and Environmental Engineering, ASCE, Vol. 127, pp.1051–1060.

Zhang, L. (2004). *Drilled shafts in rock—Analysis and design*, Balkema, Rotterdam, The Netherlands, pp. 189-222.